

Federal University of Paraíba

Centre of Technology

GRADUATE PROGRAMME OF CIVIL

AND ENVIRONMENT ENGINEERING

-DOCTORATE -

_

EVALUATION OF BIODYNAMIC MODELS FROM WALKING TESTS FOR CIVIL ENGINEERING APPLICATIONS

By

Rafaela Lopes da Silva, MSc.

Thesis submitted to the Federal University of Paraíba for the Degree of Doctor

João Pessoa - Paraíba

April 2025



Federal University of Paraíba

Centre of Technology

GRADUATE PROGRAMME OF CIVIL

AND ENVIRONMENT ENGINEERING

-DOCTORATE -

_

EVALUATION OF BIODYNAMIC MODELS FROM WALKING TESTS FOR CIVIL ENGINEERING APPLICATIONS

Thesis submitted to the Postgraduate Programme in Civil and Environment Engineering of the Federal University of Paraíba as a part of the requirements to get the Degree of Doctor.

Rafaela Lopes da Silva

Supervisor: Prof. Roberto Leal Pimentel, Ph.D.

João Pessoa - Paraíba

April 2025

Catalogação na publicação Seção de Catalogação e Classificação

S586e Silva, Rafaela Lopes da.

Evaluation of biodynamic models from walking tests for civil engineering applications / Rafaela Lopes da Silva. - João Pessoa, 2025.

206 f.: il.

Orientação: Roberto Leal Pimentel.
Tese (Doutorado) - UFPB/CT.

1. Engenharia civil. 2. Vibrações estruturais. 3.
Interação humano-estrutura. 4. Modelos biodinâmicos. I. Pimentel, Roberto Leal. II. Título.

UFPB/BC CDU 624(043)



EVALUATION OF BIODYNAMIC MODELS FROM WALKING TESTS FOR CIVIL ENGINEERING APPLICATIONS

RAFAELA LOPES DA SILVA

Thesis approved on April 29, 2025 Academic Term: 2025.1

Documento assinado digitalmente

ROBERTO LEAL PIMENTEL
Data: 12/05/2025 21:32:00-0300
Verifique em https://validar.iti.gov.br

Prof. Roberto Leal Pimentel, Ph.D. – UFPB Supervisor

Documento assinado digitalmente

HIDELBRANDO JOSE FARKAT DIOGENES
Data: 13/05/2025 08:25:06-0300

Verifique em https://validar.iti.gov.br

Prof. Dr. Hidelbrando José Farkat Diógenes – UFPB Internal Member

Documento assinado digitalmente

FELIPE TAVARES DA SILVA
Data: 13/05/2025 10:08:08-0300
Verifique em https://validar.iti.gov.br

Prof. Dr. Felipe Tavares da Silva – UFPB Internal Member

Prof. Aleksandar Pavic, Ph.D. – University of Exeter External Member

Documento assinado digitalmente

FLAVIO DE SOUZA BARBOSA

Data: 13/05/2025 10:50:56-0300

Verifique em https://validar.iti.gov.br

Prof. Dr. Flávio de Souza Barbosa - UFJF External Member

> João Pessoa/PB 2025

The author informs that part of the text, figures and tables herein presented have already been published or submitted in four papers:

a) Conference Paper (published):

Silva, R.L. Pimentel, R.L., Pavic, A. (2020). *Performance of biodynamic models to represent the action of a pedestrian in the vertical direction*. In Proceedings of the 11th International Conference on Structural Dynamics (EURODYN'20), v 1, p 1824–1834, Athens, Greece.

b) Journal Paper (published):

Hawryszków P., Pimentel R., Silva R., Silva F. (2021). Vertical vibrations of footbridges due to group loading: effect of pedestrian structure interaction. Applied Sciences, MDPI 2021, v11(4), p 1355.

c) Conference Paper (published):

Silva, R.L. Pimentel, R.L., Pavic, A., Hawryszków P. (2024). *Influence of Ground Reaction Force Prediction on the Human Interaction Phenomenon: An application of a Bipedal Model*. In Proceedings of the 42nd International Modal Analysis Conference (IMAC XLII), Orlando, USA.

d) Journal Paper (submitted in March 2025 to Structures Elsevier – in peer review status):

Silva, R.L. Pimentel, R.L., Pavic, A. (2025). *Evaluating SDOF and 2DOF bipedal models from walking tests on rigid surfaces*. Submitted to Structures (Elsevier).

To my family and friends,

for their unconditional love, support, and encouragement throughout every step of this journey. And to everyone who believed in me, even when I doubted myself.

AKNOWLEDGEMENTS

First and foremost, I thank God for granting me the strength and health to face this journey.

To my father, José Jorge, and my mothers, Maria Gorette and Ana Lúcia, thank you for all the love, dedication, patience, understanding, education, and support you have given me throughout my life. Without the values and principles you instilled in me, I would not have achieved this professional and personal growth.

To my siblings, for their friendship and encouragement – especially to Victória Lopes and Isabela Lopes, who never stopped believing in me. I deeply appreciate every word of support you offered.

To all my family members who helped and encouraged me in any way – especially my grandmother, Alice.

To the friendships I've cultivated over the years: I am particularly grateful for the invaluable support of Kamilla Mendonça, Wênia Cristina, Lucélia Araújo, Tamáris Brasileiro, Danielle Conceição, and Márcio Gonçalves. Your friendship and companionship uplifted me in moments of doubt and difficulty, both in this work and in life. You have been pillars of support throughout this PhD journey.

To the friends I made in Exeter, who I will carry in my heart – especially Ellie Brown and Beatriz Arellano – you made me feel at home.

To my love, Dan – your belief in me and your constant encouragement carried me through the most challenging moments of this journey.

To the friends I made during the doctorate – Lays Raianne, João Paulo, and Ronald Lopes – thank you for the joyful moments, which were undoubtedly crucial throughout this journey. I especially thank those who became close to my heart: Camilla Nunes, Erika Lorena, and Aldilene Pinheiro.

To my advisor, Prof. Roberto Leal Pimentel, thank you not only for your outstanding guidance and patience throughout this work but also for your friendship, dedication, motivation, teachings, and availability – without which this thesis would not have been possible.

To Prof. Aleksandar Pavic, thank you for welcoming me to Exeter. Your support was immensely valuable to the development of this research.

To all my teachers – not only from the doctoral program but also from my undergraduate and high school years – who contributed to my ethical, moral, and professional development. A special thanks to Prof. Andrea Brasiliano, whose words of support were essential to overcoming the challenges of this PhD.

To Dianelys Vega Ruiz, for your invaluable technical and emotional support.

To the entire staff of the Graduate Program in Civil and Environmental Engineering at UFPB, especially the secretary Diandra, for her efficiency and dedication. I also thank the program coordinators, Prof. Davi Carvalho and Prof. Hidelbrando Diógenes, for their excellent leadership.

To the team from the VSimulator Facilities at the University of Exeter – a special thanks to Katy Manning and James Bassit.

To the members of the examination board for their time and valuable contributions to the improvement of this study.

Lastly, I am grateful to the Coordination for the Improvement of Higher Education Personnel of Brasil (CAPES-BR) for the scholarship granted, which made this work possible; to the National Council for Scientific and Technological Development (CNPq-BR) and the Research Support Foundation of the State of Paraíba (FAPESQ-PB) for the financial support provided during this research; and to the University of Exeter for hosting me during the experimental campaign.

ABSTRACT

Structural vibrations induced by human activities, such as walking, have become a significant concern from a design perspective, especially due to modern structures featuring low natural frequencies. A key aspect of this field in dynamics is the Human-Structure Interaction (HSI) phenomenon, which refers to the feedback loop between occupants and pedestrian structures, such as footbridges and floors. In this context, human walking models designed to simulate HSI have gained interest for civil engineering applications. Focusing on walking in the vertical direction, so-called biodynamic models have been introduced to represent pedestrians, with approaches ranging from mathematical assumptions to kinematic representations of the body. Among the simplest biodynamic models, two approaches stand out in HSI investigations: the single-degree-of-freedom (SDOF) spring-mass-damper (SMD) model and the damped bipedal inverted pendulum (DBIP) model. While the SMD model approximates the ground reaction force (GRF) transmitted to the structure as a coupled moving force acting at a single contact point, the DBIP model calculates GRFs based on selected parameters and the model's motion, transmitting them to the ground while accounting for the relative position of both feet during walking. Despite both models being capable of reproducing interaction forces, DBIP models, unlike SMD models, have the potential to capture changes in walking patterns due to surface vibrations. This is because, in DBIP models, the step frequency is not an input parameter but rather a consequence of the model's motion. In this context, this study aimed to evaluate both models for civil engineering applications based on walking tests. The performance of SMD and DBIP models was initially analysed by applying an HSI formulation using experimental structural acceleration time-history data from two lively footbridges. While SMD models performed well, DBIP models tended to overestimate the structural response due to the high values of dynamic load factors (DLFs) produced, even while accurately reproducing the walking speed and step frequency pairs. Further investigations of DBIP models were conducted using kinetic and kinematic data from experimental walking tests performed on a moving platform equipped with force plates. In rigid surface scenarios, results from three test subjects confirmed that DBIP models tend to overestimate DLFs while simultaneously reproducing experimental walking speeds and step frequencies. However, these models could qualitatively predict trends in variations of applied forces due to surface vibrations – something not possible with SMD models, as their GRFs are predefined inputs. Additionally, experimental insights from moving surface scenarios highlighted that significant changes in applied forces can occur, depending on the surface's vertical displacement levels and its vertical position at the moment of foot contact – factors neglected by existing guidelines and standards adopted for the design of structures.

Keywords: Structural vibrations; Human-structure Interaction; Biodynamic Models.

RESUMO

As vibrações estruturais provocadas por atividades humanas, como a caminhada, tornaram-se uma preocupação relevante no projeto estrutural, especialmente devido às baixas frequências naturais das estruturas modernas. Um aspecto central da dinâmica estrutural é a Interação Humano-Estrutura (IHS), que descreve os efeitos mútuos entre ocupantes e estruturas para pedestres, como passarelas e lajes. Nesse cenário, modelos de caminhada foram desenvolvidos para simular a IHS, atraindo interesse na Engenharia Civil. Focando no movimento vertical, surgiram os chamados modelos biodinâmicos para representar pedestres, variando de formulações matemáticas a representações cinemáticas do corpo. Entre os mais simples, destacam-se dois na investigação da IHS: o modelo de mola-massa-amortecedor (SMD) de um grau de liberdade (SDOF) e o modelo de pêndulo invertido bípede amortecido (DBIP). O modelo SMD representa a força de reação de piso (FRP) como uma força móvel acoplada em um único ponto de contato, enquanto o modelo DBIP calcula as FRPs a partir de parâmetros específicos e do movimento do modelo, considerando a posição relativa dos pés. Apesar de ambos reproduzirem forças de interação, os modelos DBIP, diferentemente dos modelos SMD, conseguem captar alterações no padrão da marcha induzidas por vibrações da superfície. Isso ocorre porque, nos modelos DBIP, a frequência de passo emerge do movimento, e não como dado de entrada. Nesse contexto, este estudo buscou avaliar ambos os modelos em aplicações na Engenharia Civil com base em testes de caminhada. A performance dos modelos SMD e DBIP foi inicialmente analisada por meio de uma formulação de IHS aplicada a dados experimentais de aceleração estrutural de duas passarelas flexíveis. Enquanto os modelos SMD apresentaram um bom desempenho, os modelos DBIP tenderam a superestimar a resposta estrutural devido aos altos valores dos fatores dinâmicos de carga (DLFs), mesmo reproduzindo corretamente velocidades e frequências dos passos. Estudos adicionais com os modelos DBIP foram conduzidos com dados cinéticos e cinemáticos obtidos em testes de caminhada sobre uma plataforma móvel com placas de força. Em superfícies rígidas, os resultados de três participantes confirmaram que os modelos DBIP superestimam os DLFs, ainda que representem bem as velocidades e frequências experimentais. Contudo, esses modelos conseguem prever variações nas forças aplicadas em função das vibrações - o que não ocorre nos modelos SMD, pois suas FRPs são definidas previamente. Além disso, análises experimentais em superfície móvel mostraram que alterações significativas nas forças aplicadas podem ocorrer, dependendo dos níveis de deslocamento vertical e da posição da superfície no instante do contato do pé – fatores ignorados por normas e diretrizes atuais de projeto estrutural.

Palavras-chave: Vibrações Estruturais; Interação Humano-Estrutura; Modelos Biodinâmicos.

TABLE OF CONTENTS

L	IST OI	F FIGURES	11
L	IST OI	F TABLES	19
N	OMEN	CLATURE	22
1	INT	RODUCTION	25
	1.1	CONTEXT AND QUESTIONS	25
	1.2	OBJECTIVE	29
	1.3	JUSTIFICATIVE AND SIGNIFICANCE	30
	1.4	THESIS STRUCTURE	33
2	TH	EORETICAL BACKGROUND	34
	2.1	EXCESSIVE VIBRATIONS DUE TO HUMAN LOADS	34
	2.2	GUIDELINE'S APPROACH	37
	2.3	HUMAN INDUCED LOADS	45
	2.4	HUMAN STRUCTURE INTERACTION AND HUMAN WALKING MODELS	48
	2.4.	l SMD models	56
	2.4	2 Damped Bipedal Models	62
	2.5	CONCLUDING REMARKS	78
3	MA	TERIAL AND METHODS	81
	3.1	INVESTIGATION OF THE HUMAN WALKING MODELS	82
	3.2	BIODYNAMIC MODELS APPLICATION FROM A HSI PERSPECTIVE	82
	3.2.	l Aberfeldy Footbridge	84
	3.2	2 Złotnicka Footbridge	86
	3.3	EXPERIMENTAL CAMPAIGN – VSIMULATOR	89
	3.3.	l Test program	89
	3.3	2 Data Processing	94
	3.4	EVALUATION OF DBIP MODELS	101

	3.4.1	Procedure for parameters calibration	3
4	RESU	LTS AND DISCUSSIONS104	4
	4.1 P	ERFORMANCE OF BIODYNAMIC MODELS FROM A HSI PERSPECTIVE 104	1
	4.1.1	SMD models	5
	4.1.2	SDOF DBIP model versus SMD model	3
	4.1.3	Concluding Remarks	0
	4.2 P	ERFORMANCE OF DBIP MODELS FROM THE S2HI PERSPECTIVE 122	2
	4.2.1	Rigid surface scenarios	2
	4.2.2	Moving floor scenarios	7
	4.2.3	Concluding Remarks	2
	4.3 A	NALYSIS OF DBIP MODELS AFTER CALIBRATION: ACCOUNTING FOR HSI1	74
	4.3.1	2DOF DBIP model (BM ₂)	5
	4.3.2	SDOF DBIP model (BM ₁)	8
	4.3.3	Concluding Remarks	2
5	CONC	CLUSIONS	3
	5.1 G	GENERAL CONCLUSIONS	3
	5.2 R	LECOMMENDATIONS FOR FUTURE RESEARCH	5
R	EFEREN	ICES187	7
A	PPENDE	X A197	7
A	PPENDE	X B203	3

LIST OF FIGURES

Figure 1 – (a) Millenium Bridge, London, UK (Geograph, 2025); and (b) Solferino Bridge Paris, France (Wikipedia, 2025).
Figure 2 - Frequency ranges (Hz) of the vertical vibrations and associated risk of resonance level (After Sétra, 2006).
Figure 3 - Reduction coefficient Ψ (After Hivoss, 2008)
Figure 4 - Graphic to determine Combined Factor $k(f_v)$ (After UK NA to BS, 2008)44
Figure 5 - Reduction factor, γ , to allow for the unsynchronized combination of pedestrian actions within groups and crowds (each curve represent effective span S_{eff}) (After UK NA to BS, 2008).
Figure 6 – Representation of a gait cycle with respective typical GRFs for each footfall (After Pirker & Katzenschlager, 2017; and Ruiz, 2021)
Figure 7 – Representation of MF model applied on a structure (After Caprani & Ahmadi, 2016)
Figure 8 – Representation of MF model coupled with inertial mass applied on a structure (After Caprani & Ahmadi, 2016)
Figure 9 – SMD biodynamic model (After Caprani et al., 2011)
Figure 10 – 3DOF biodynamic model (Miyamori <i>et al.</i> , 2001)52
Figure 11 – Biodynamics models with (a) 2DOF (After ISO 5982, 1981), (b) 9DOF and (c) 34DOF (Maca & Valasek, 2011)
Figure 12 - SMDA biodynamic model (Toso & Gomes, 2018)54
Figure 13 – Inverted pendulum biodynamic models with (a) mass concentrated on rigid legs (b) mass and legs' stiffness; (c) mass, legs' stiffness, and damping; (d) mass, legs stiffness, and damping with roller feet. (After Shahabpoor <i>et al.</i> , 2016b)
Figure 14 – Bipedal model without attack angle of the feet (After Mulas <i>et al.</i> , 2018)56

Figure 15 – The SMD model (a) on a rigid surface and (b) on a flexible surface (After Pfeil <i>et al.</i> , 2014)
Figure 16 – Human walking model (a) as a Damped Bipedal Inverted Pendulum, and (b) respective phases of walk (DBIP Model after Qin <i>et al.</i> , 2013)
Figure 17 - Typical GRFs generated by BMs from two set of initial conditions: adopting estimated initial conditions, and adopting initial conditions obtained from step cycles after model convergence
Figure 18 – Next impact point x_p definition (a) as a function of d_s and θ , (b) predicting x_p by setting $d_s = d_{s0}$, and (c) predicting x_p by setting the attack angle at the TD as θ_0 71
Figure 19 – Moving surface scenario for a given instant t during DS phase73
Figure 20 - Representation of the DBIP model interacting with a flexible surface (after Qin et al., 2013)
Figure 21 - Computational procedure for the HSI formulation adopting DBIP models (BM1 or BM2) implementation
Figure 22 - Aberfeldy Cable Stayed Footbridge (Pimentel, 1997)
Figure 23 – Aberfeldy footbridge elevation and experimental 1 st mode shape (After Pimentel, 1997)
Figure 24 – Panoramic view of the footbridge (Image previous used in Hawryszków <i>et al.</i> , 2021)
Figure 25 – Technical drawing of the structure (side view, cross-section and top view), with relevant dimensions. Selected measurement point on the left span, 16.0 m from the support (Image previous used in Hawryszków <i>et al.</i> , 2021)
Figure 26 – Vertical mode shapes of the structure (Image previous used in Hawryszków <i>et al.</i> , 2021).
Figure 27 – Pedestrian tests: (a) Example of instrumented leading pedestrian; (b) single crossing; (Image previous used in Hawryszków <i>et al.</i> , 2021)
Figure 28 – (a) Walking test subject wearing mocap suit in VSimulators facility, and (b) test's scheme depicting designated path

Figure 29 – Example of GRF time-history of both feet for TS1, rigid surface and slow walking scenario
Figure 30 – 3D model constructed in QTM Software® (2025)
Figure 31 – Example of recovered force signal in vibrating scenarios for TS1, slow walk and resonance conditions
Figure 32 – Example of experimental accelerations for TS1, rigid surface scenarios for: (a) slow walk; and (b) fast walk
Figure 33 – Example of leg force-length curves and respective curve-fit and R ² values for TS1 walking in rigid surface scenarios at a step frequency of (a) 1.64Hz (slow walk), (b) 1.84Hz (normal walk), and (c) 2.03Hz (fast walk). In addition, (d) an example of data exclusion criteria from the free walking scenario. Leg force is normalized by body weight and leg length is normalized to the leg length values obtained at the TD
Figure 34 – Example of cross-referencing heel and toe's vertical movement and force data for each leg
Figure 35 – Example of recovered filtered GRFs from TS1 slow walking for rigid surface scenario in (a) the time domain and (b) the frequency domain (Red dots highlight the expected harmonics of vertical forces in human gait)
Figure 36 – Example of correlation of $k_{leg,exp}$ and $L_{p,exp}$, along with the respective curve fit for TS1 in the slow walking scenario on a rigid surface.
Figure 37 – Computational procedure to implement DBIP models in MATLAB® (2024) 102
Figure 38 – Computational procedure to calibrate the DBIP models adopting the Monte Carlo simulation method
Figure 39 - Acceleration at the mid span of the footbridge - (a) Experimental x MF model; (b) Experimental x Interaction Model using the set of parameters from Toso <i>et al.</i> (2016). (Previous used in Silva <i>et al.</i> , 2020)
Figure 40 - Acceleration at the mid span of the footbridge - Experimental versus Interaction Model using the set of parameters from (a) Silva & Pimentel (2011); (b) Jiménez-Alonso & Sáez (2014); (c) Gomez <i>et al.</i> (2016); (d) Shahabpoor <i>et al.</i> (2016). (Previous used in Silva <i>et al.</i> , 2020).

Figure 41 - Obtaining damping ratios from the tail-end signal of pedestrian tests (Previous
used in Hawryszków et al., 2021)
Figure 42 - Damping ratios for the first structural mode (Previously used in Hawryszków <i>et al.</i> , 2021)
Figure 43 - Second crossing of Test Subject 2: (a) time response; (b) spectrum. (Previously used in Hawryszków <i>et al.</i> , 2021)
Figure 44 - Third crossing of Test Subject 2: (a) time response; (b) spectrum. (Previously used in Hawryszków <i>et al.</i> , 2021)
Figure 45 – Peak and RMS accelerations for models analysed. (Previous used in Hawryszków <i>et al.</i> , 2021)
Figure 46 - (a) DLFs for the first four harmonics and (b) GRF obtained by adopting Set 1 of BM ₁ parameters including step losing effects ($f_s = 1.57$ Hz for $22s < t < 24s$)116
Figure 47 - Acceleration at the node of interest for the TS-P1 single crossing adopting BM ₁ (L_p = 1.30m, k_{leg} = 18kN.m, ξ_{leg} = 13%, θ_0 = 63.76° and \dot{z} = -0.307) and compared (a) against experimental filtered acceleration and SMD model, and (b) against SMD model adopting two different DLFs for the first harmonic (in red, the peak values obtained by the BM ₁)
Figure 48 - (a) Acceleration at the node of interest for TS-P2 single crossing adopting BM ₁ (L_p = 1.30m, k_{leg} = 18kN.m ⁻¹ , ξ_{leg} = 13%, θ_0 = 72.65° and \dot{z} = -0.307) compared against the experimental filtered acceleration, and the SMD model adopting DLF ₁ from the BM ₁ simulation; (b) GRF generated from the BM ₁ along with to the respective simulated peak accelerations' progression of the structure.
Figure 49 – Comparisons of experimental and simulated DLF ₁ s for each test subject126
Figure 50 – Correlation of longitudinal speed v and (a) step frequency f_s and (b) DLF ₁ errors for all three test subjects. (only the results for BM ₁ are depicted in this figure since similar results were obtained for BM ₂)
Figure 51 – Experimental measured DLFs and respective linear fits
Figure 52 – Comparisons of experimental and simulated CoM vertical displacements and step forces for TS1 in (a) and (b) slow walking (crossing 5), (c) and (d) normal waking (crossing

7), (e) and (f) free walking (crossing 4), and (g) and (h) fast walking (crossing 8)	
adopting parameters from Table A.1	129
Figure 53 – Comparisons of experimental and simulated CoM vertical displacement	ts and step
forces for TS2 in (a) and (b) slow walking (crossing 5), (c) and (d) normal waking	g (crossing
4), (e) and (f) free walking (crossing 4), and (g) and (h) fast walking (crossing 2)	
adopting parameters in Table A.2	130
Figure 54 – Comparisons of experimental and simulated CoM vertical displacement	ts and step
forces for TS3 in (a) and (b) slow walking (crossing 5), (c) and (d) normal waking	g (crossing
4), (e) and (f) free walking (crossing 4), and (g) and (h) fast walking (crossing 5)	scenarios,
adopting parameters in Table A.3	131
Figure 55 – Speed and step frequency correlation after parameters adjustments	133
Figure 56 - Comparisons of experimental and simulated CoM vertical displacement	ts and step
forces for TS1 in (a) and (b) slow walking (crossing 5), (c) and (d) normal waking	g (crossing
7), (e) and (f) free walking (crossing 4), and (g) and (h) fast walking (crossing 8)	scenarios,
adopting parameters in Table A.4	135
Figure 57 - Comparisons of experimental and simulated CoM vertical displacement	ts and step
forces for TS2 in (a) and (b) slow walking (crossing 5), (c) and (d) normal waking	g (crossing
4), (e) and (f) free walking (crossing 4), and (g) and (h) fast walking (crossing 2)	scenarios,
adopting parameters in Table A.5	136
Figure 58 - Comparisons of experimental and simulated CoM vertical displacement	ts and step
forces for TS3 in (a) and (b) slow walking (crossing 5), (c) and (d) normal waking	g (crossing
4), (e) and (f) free walking (crossing 4), and (g) and (h) fast walking (crossing 5)	scenarios
adopting parameters in Table A.6	137
Figure 59 – An example of cross-referencing touchdown (TD) instants with the vertic	al position
of the platform for TS1, the slow walking scenario (1.6Hz), and surface accelera	ıtion peaks
of 1.5 m/s ² (pink dashed lines mark the beginning of each crossing)	139
Figure 60 – Illustrating phases in a typical sinusoidal signal	140
Figure 61 - Test subjects rating results for moving surface scenarios ranging from 1 ((vibrations
did not interfere walking) to 5 (vibrations strongly interfere in walking)	142

Figure 62 – Correlation of DLF ₁ and step frequency f_s for moving surface scenarios compared to rigid surface scenarios for TS1
Figure 63 – Correlation of DLF ₁ and step frequency f_s for moving surface scenarios compared to rigid surface scenarios for TS2
Figure 64 – Correlation of DLF ₁ and step frequency f_s for moving surface scenarios compared to rigid surface scenarios for TS3
Figure 65 – Percentage differences between mean DLF ₁ from the moving surface scenarios and from the rigid surface scenarios by step frequency ranges for TS1
Figure 66 – Percentage differences between mean DLF ₁ from the moving surface scenarios and from the rigid surface scenarios by step frequency ranges for TS2
Figure 67 – Percentage differences between mean DLF ₁ from the moving surface scenarios and from the rigid surface scenarios by step frequency ranges for TS3
Figure 68 – Correlation of DLF ₁ and step frequency f_s for moving surface scenarios compared to rigid surface scenarios for TS1
Figure 69 – Correlation of DLF ₁ and step frequency f_s for moving surface scenarios compared to rigid surface scenarios for TS2
Figure 70 – Correlation of DLF ₁ and step frequency f_s for moving surface scenarios compared to rigid surface scenarios for TS3
Figure 71 – Speed and step frequency correlations for moving surface scenarios compared to measurements on rigid surface scenarios for TS1
Figure 72 – Speed and step frequency correlations for moving surface scenarios compared to measurements on rigid surface scenarios for TS2
Figure 73 – Speed and step frequency correlations for moving surface scenarios compared to measurements on rigid surface scenarios for TS3
Figure 74 – Example of mean footfall forces for a scenario where TS-platform synchronization was identified for every crossing (TS2, fast walking, surface acceleration of 1.0m/s²). 152

Figure 75 – Example of mean footfall forces for a scenario where TS-platform synchronization
was identified for every crossing (TS1, normal walking, surface acceleration of 1.0m/s ²
Figure 76 – TD vertical positions at the platform, GRFs and single footfall force for TS1, slow walking, moving surface scenario (frequency of 1.6Hz and 1.5m/s²): (a), (b) and (c) phase case 2; (d), (e) and (f) phase case 3; and (g), (h) and (i) phase case 4
Figure 77 - TD vertical positions at the platform, GRFs and single footfall force for TS3, fas walking, moving surface scenario (frequency of 2.2 Hz and 0.5m/s²): (a), (b) and (c) phase case 2; (d), (e) and (f) phase case 1; and (g), (h) and (i) phase case 4
Figure 78 – Example of correlation of TD vertical position and GRFs for two different non synchronous crossings – (a) and (b) for crossing 2 (descending TD vertical position), and (c) and (d) for crossing 7 (ascending TD vertical position) – (TS3, free walking and surface vertical acceleration peaks of 0.5m/s ²).
Figure 79 – TD vertical position for BM ₁ adopting set 1 of parameters in Table 40, (a), (c), (e and (g) for setting step length d_s , for initial phase angle of 0°, 90°, 180° and 270° respectively; and (b), (d), (f) and (h) for setting attack angle θ_0 for initial phase angle of 0° 90°, 180° and 270°, respectively.
Figure 80 – TD vertical position for BM ₂ adopting set 2 of parameters in Table 40, (a), (c), (e) and (g) for setting step length d_s , for initial phase angle of 0°, 90°, 180° and 270° respectively; and (b), (d), (f) and (h) for setting attack angle θ_0 for initial phase angle of 0° 90°, 180° and 270°, respectively.
Figure 81 – TD vertical position at the structure from HSI formulation for TS1(sets 3 and for from Table 40) and Aberfeldy Footbridge.
Figure 82 – Step frequency variation from the HSI for TS1 and the Aberfeldy Footbridge 164
Figure 83 – Variations in DLF ₁ for each TD-platform phase for TS1 and sets of calibrated mode parameters from rigid surface scenarios in Table A.4
Figure 84 – Variations in DLF ₁ for each TD-platform phase for TS2 and sets of calibrated mode parameters from rigid surface scenarios in Table A.5

Figure 85 – Variations in DLF ₁ for each TD-platform phase for TS3 and sets of calibrated modern parameters from rigid surface scenarios in Table A.6.	
Figure 86 – Variations in footfall force for each TD-platform phase for TS1 and sets calibrated model parameters from rigid surface scenarios in Table A.4: (a), (b) and (c) slowalking crossing 8; (d), (e) and (f) normal walking crossing 7; (g), (h) and (i) fast walking crossing 5;	ing
Figure 87 – Variations in footfall force for each TD-platform phase for TS2 and sets calibrated model parameters from rigid surface scenarios in Table A.5: (a), (b) and (c) slowalking crossing 6; (d), (e) and (f) normal walking crossing 5; (g), (h) and (i) fast walking crossing 2	ow
Figure 88 – Variations in footfall force for each TD-platform phase for TS3 and sets calibrated model parameters from rigid surface scenarios in Table A.6: (a), (b) and (c) slowalking crossing 5; (d), (e) and (f) normal walking crossing 4; (g), (h) and (i) fast walking crossing 5;	ow
Figure 89 – Results for BM ₂ adopting the set of parameters from the regression expression introduced by Lin <i>et al.</i> (2023). (a) Acceleration-time-history, and (b) step frequent variation.	ncy
Figure 90 – (a) Total GRFs, and (b) Numerical surface vertical displacement of Aberfel marking the TD vertical positions for BM ₂ adopting parameters proposed by Lin <i>et</i> (2023).	al.
Figure 91 – Results for BM ₁ adopting the Set 3 of parameters in Table 42. (a) Acceleration time-history, and (b) step frequency variation	
Figure 92 - (a) Total GRFs, and (b) Numerical surface vertical displacement of Aberfel marking the TD vertical positions for BM ₁ , setting <i>d_s</i> , and adopting the Set 3 of parameter in Table 42	ers
Figure 93 - (a) Total GRFs, and (b) Numerical surface vertical displacement of Aberfel marking the TD vertical positions for BM_1 , setting d_s , and adopting the Set 3 of parameter in Table 42	ers

LIST OF TABLES

Table 1 – Case studies of excessive vibrations of footbridges induced by walking	36
Table 2 – Guidelines and standards for assessment of footbridges	37
Table 3 – Traffic class according to Hivoss (2008)	39
Table 4 – Bridge classification and recommended crowd densities (walking) according NA to BS (2008)	
Table 5 – Footbridges' classification according to Sétra (2006)	40
Table 6 – Recommended acceleration limit ranges for footbridges under human loads Sétra, 2006; and Hivoss, 2008)	
Γable 7 – Recommended values for the site usage factor k_l (UK NA to BS, 2008)	41
Γable 8 – Recommended values for the route redundancy factor k_2 (UK NA to BS, 2008)	3)41
Γable 9 – Recommended values for the structure height factor k_3 (UK NA to BS, 2008).	41
Γable 10 – Some proposals to determine the Dynamic Load Factor (DLF)	43
Table 11 – Some values for pacing rate proposed in the literature in walking activity	49
Table 12 – Proposed expressions for the SMD parameters	62
Table 13 – Proposed values for the SMD parameters.	62
Table 14 – Expressions and Ranges for DBIP model parameters found in the literature Ruiz <i>et al.</i> (2021) and Ruiz <i>et al.</i> (2022)	
Table 15 - Expressions for DBIP model parameters found in the literature from Ruiz (2023).	
Table 16 – Regression Expressions proposed by Lin <i>et al.</i> (2023)	75
Table 17 – Steps of the methods for the research development	81
Table 18 – First mode dynamic parameters of the structure and pedestrian characteristics on experimental data except where indicated	
Γable 19 – First mode dynamic parameters of the structure and relevant dimensions	88

Table 20 – Test subjects physical characteristics and age
Table 21 – Scenarios investigated for each frequency of the test platform92
Table 22 – Signal duration for the scenarios (in seconds)
Table 23 – Rating scale for the TS's vibrations perception
Table 24 – Aberfeldy footbridge classification according to currently guidelines and limit peak accelerations
Table 25 - Results obtained employing different values for the pedestrian parameters 106
Table 26 – Złotnicka footbridge classification according to currently guidelines and limit peak accelerations
Table 27 – Reference values of pedestrian dynamic parameters
Table 28 – Details of the experimental results of interest for this study and SMD model parameters
Table 29 – Set of BM ₁ parameters and initial conditions for the TS-P2116
Table 30 - Gait and model parameters extracted from experimental data for each test subject for rigid surface scenarios
Table 31 - Ranges obtained with the optimal initial conditions for rigid surface scenarios (numerical results), and R ² values for the CoM's vertical displacement
Table 32 – Ranges defined for the Monte Carlo simulations
Table 33 – Adjustments to walking speed v and Energy input E ₀ , along with step length d_s comparisons
Table 34 – Number of crossings for which TS-platform synchronization was identified within each moving surface scenario (values in parentheses indicate the total number of crossings).
Table 35 – Description of TS-platform phase cases
Table 36 – Compilation of each TS-platform phase case for each moving surface scenario. (***)

Table 37 – Percentage differences between mean DLF ₁ from the moving surface scenarios and
from the rigid surface scenarios by step frequency ranges for TS1. (*)
Table 38 – Percentage differences between mean DLF ₁ from the moving surface scenarios and
from the rigid surface scenarios by step frequency ranges for TS2. (*)
Table 39 – Percentage differences between mean DLF ₁ from the moving surface scenarios and
from the rigid surface scenarios by step frequency ranges for TS3. (*)
Table 40 - Sets of DBIP model parameters for BM ₁ and BM ₂ and related DLF ₁ from rigid
surface scenario chosen for model's functioning investigation (TS1, slow walking and
surface vertical acceleration peaks of 1.5m/s ²) (*)
Table 41 – Trials for TS-P2 body parameters estimation from BM ₂ based on Lin <i>et al.</i> (2023)
Table $42 - \text{Sets of BM}_1$ parameters from (1) Ruiz et al. (2023), (2) Ruiz et al. (2022), and (3)
adjusted based on the findings in this study

NOMENCLATURE

Acronyms

2DOF – Two-degrees-of-freedom 3DOF – Three-degrees-of-freedom

BM – Bipedal model

BM₁ – Bipedal Model 1(SDOF DBIP model) BM₂ – Bipedal Model 2 (2DOF DBIP model)

CoM, COM - Centre-of-mass

DBIP – Damped bipedal inverted pendulum

DLF – Dynamic Load Factor

DLF₁ – Dynamic Load Factor of the First Harmonic

DS – Double support

FEM – Finite Element Method

FP – Foot point

FP_i – Force plate number (i = 1: 9)

GRF - Ground Reaction Force

H2SI – Human-to-structure-interaction HSI – Human-structure-interaction

IP - Inverted pendulum
 MF - Moving Force Model
 RMS - Root mean square

S2HI – Structure-to-human-interaction SDOF – Single-degree-of-freedom SMD – Spring-mass-damper

SMDA – Spring-mass-damper-actuator

SS - Single support
TD - Heel touch-down
TO - Toe touch-off
TS - Test subject

VLO – Vertical Leg Orientation

Symbols

 ΔE — Energy differential Δt — Time increment

 Δx – Longitudinal position increment for Δt

*a*_{limit} – Acceleration limit

a_{max} – Maximum surface vertical acceleration

a_{rms} – Root mean square acceleration

C – Damping Matrix

 c_i – Structure's damping of the i^{th} mode

 c_l, c_t — Damping of leading and trailing leg, respectively

cleg – Leg damping coefficient

c_p – Pedestrian damping

 d_{max} — Maximum surface vertical position

 d_s – Step length.

 d_{s0} — Step length for t = 0 E(t) — Pedestrian total energy E₀ — Initial energy input

f – Surface vertical frequency

F – Force vector

F(t) – Ground Reaction Force in function of time t
 f_{critic} – Critical value for a structure's natural frequency

F_{ctrl} – Control force

 $F_{d,l}$, $F_{d,t}$ — Axial dissipative forces of leading and trailing leg, respectively

 $F_{int}(t)$ – Interaction forces f_n – Natural Frequency

 f_{np} – Pedestrian body natural frequency

 f_s – Step frequency

 $F_{s,l}$, $F_{s,t}$ — Axial elastic forces of leading and trailing leg, respectively

*f*_v – Mode frequency of interest

g – Gravity acceleration.

 GRF_l , GRF_t – GRF of leading and trailing leg, respectively

h – Pedestrian height
 K – Stiffness Matrix

 k_i - Structure's stiffness of the i^{th} mode

 k_{leg} – Leg stiffness coefficient k_D – Pedestrian stiffness

l – Subscript for leading leg

 L_l, L_t - Length of leading and trailing leg, respectively

 L_p – Leg resting length

 L_{t0} – Trailing leg length at TD

 \mathbf{M} — Mass matrix M, m_h — Body mass

 m_i – Structure's modal mass of the i^{th} mode

m_p – Pedestrian modal mass

n	_	Number of modes
n_s	_	Step number
t	_	time
t	_	Subscript for trailing leg
U	_	Displacement vector
u_p	_	Interaction vertical displacement
v	_	Walking speed
v_l, v_t	_	Axial velocities of leading and trailing leg, respectively
W	_	Body weight
x_l, x_t	_	Longitudinal position of the leading and trailing foot, respectively
x_p	_	Longitudinal position of the next impact point
x, \dot{x}, \dot{x}	_	Longitudinal position, velocity and acceleration of the CoM
$y(t), \dot{y}(t)$	_	Surface vertical position and velocity, respectively
Y_i	_	Mode coordinate
y_i, Y_i	_	General coordinate of the <i>i</i> th mode
z, ż, ż	_	Vertical position, velocity and acceleration of the CoM
$\alpha(t)$	_	Damping transition coefficient
θ	_	Leg orientation
$ heta_0$	_	Attack angle
$ heta_i$	_	Phase angle
ξ	_	Leg damping ratio
$oldsymbol{\xi}_p$	_	Pedestrian damping ratio
ф	_	Phase angle
ϕ_i	_	Mode shape of the <i>i</i> th mode
ω_i	_	Structure's angular frequency of the i^{th} mode

1 INTRODUCTION

1.1 Context and questions

The advances in technology, contemporary trends in architecture, and material science have led to the conception of structures using high-strength lightweight materials, featuring long-span and slender structures. These modern structures have low frequencies and low damping, which makes them more susceptible to vibrate excessively (Shahabpoor *et al.*, 2016a). Consequently, loads that usually did not cause problems in the past have been a target of studies, even if their magnitude is not significant, for example, human loads (Gonçalves *et al.*, 2019).

As a consequence, the last decades gather the main problems regarding excessive vibrations in structures. Hence, studies of the dynamic behaviour of such structures and their excitation sources have been extensively developed aiming to understand the phenomenon and present solutions to improve their performance (Caprani & Ahmadi, 2016).

Walking, running, and jumping are examples of human-induced loads that can cause excessive vibrations in civil structures, such as building floors (Pavic & Reynolds, 2002a), footbridges (Živanović *et al.*, 2005a), stairs (Kerr & Bishop, 2001), and grandstands (Brito & Pimentel, 2009), and can disturb the users leading to psychological fear or panic (Zhou *et al.*, 2015).

Besides some reports in the literature regarding safety problems due to excessive vibrations induced by human loads (Živanović *et al.*, 2005a), unacceptable vibration levels are more a matter of serviceability issue (Racic *et al.*, 2009; Caprani & Ahmadi, 2016; Shahabpoor *et al.*, 2016a). In this context, vibration serviceability has become the governing design criteria of civil structures, in which annoyance to occupants and equipment dysfunction are examples of the non-attendance of this limit state (Muhammad *et al.*, 2018).

Among the induced loads from human activities, walking motion is the most common scenario in civil structures. Regarding this subject, applying a pulsating moving force over the structure to model this action has been shown to not be sufficient to represent the behaviour of the human-structure system in some cases (Caprani & Ahmadi, 2016; Caprani *et al.*, 2011), since this approach ignores the interaction between the human body and the supporting structure (Živanović, 2015).

Since the human body has its own dynamic properties, i.e., stiffness, mass and damping, do not consider it as a contribution to the coupled system can present inaccurate dynamic responses, and sometimes overestimate them, as shown by Caprani & Ahmadi (2016) and Caprani *et al.* (2011).

The coupled pedestrian-structure system, if well modelled, can express the dynamic interaction between the occupants and the structure (Shahabpoor *et al.*, 2016a; Ahmadi *et al.*, 2019). Such an interaction, called human-structure interaction (HSI), occurs because the presence of individuals on a structure can change its dynamic properties (Živanović *et al.*, 2005b; Živanović *et al.*, 2009) featuring what is called human-to-structure-interaction (H2SI). Additionally, the vibrations of the structure's surface can provoke variations of the gait parameters of pedestrians (i.e., step frequency, step length, walking speed, etc.), changing the response of the structure over time (Bachmann & Ammann, 1987; Živanović *et al.*, 2005b), as part of the structure-to-human-interaction (S2HI).

Numerical simulations and approaches to account for HSI by investigating the reciprocal effects of the coupled system is an important issue regarding excessive vibrations and it is generally accepted by researchers to be essential in the vibration assessment of structures under human loads (Sachse *et al.*, 2003; Živanović *et al.*, 2005a; Shahabpoor *et al.*, 2016a; Ahmadi *et al.*, 2019).

Nevertheless, most of the guidelines and standards (e.g.: Sétra, 2006; Hivoss, 2008; UK NA to BS, 2008; SCI P354, 2009; CCIP, 2006) adopt Moving Force (MF) models in an attempt to prevent excessive vibrations due to dynamic loads induced by humans walking (as a ground reaction force - GRF), represented through a Fourier Series (Bachmann & Ammann, 1987). Meanwhile, Sétra (2006) and Hivoss (2008) guidelines try to include the influence of pedestrians in the system by considering them not only as loads but adding a part of their mass to calculate the natural frequency of footbridges.

In this matter, human walking models, widely investigated in the biomechanical field (Živanović, 2015; Dang, 2014), have become an object of interest for civil engineering purposes (Shahabpoor, *et al.* 2016a), as human-induced loads can cause excessive vibrations in pedestrian structures (Pimentel, 1997). These so-called biodynamic models are capable of simulating the HSI phenomenon.

When focusing on vertical walking dynamics, biodynamic models have been developed to represent a pedestrian behaviour, featuring a variety of approaches that differ in their mathematical formulations and kinematic representations of the human body (Caprani & Ahmadi, 2016; Shahabpoor *et al.*, 2016a).

However, it is important to recognize that a comprehensive understanding of all the complexities involved in human walking is beyond the scope of civil engineering. The primary interest lies in understanding how these forces influence the dynamic response of civil structures, with the aim of developing reliable and practical tools for predicting structural behaviour (Barker, 2002). This highlights the importance of deepen the investigation of simple biodynamic models.

Among the most commonly used human walking models in HSI studies are two simplified approaches: the single-degree-of-freedom (SDOF) Spring-Mass-Damper (SMD) model (Caprani *et al.*, 2011; Pfeil *et al.*, 2014; Venuti *et al.*, 2016; Shahabpoor *et al.*, 2016b) and the Inverted Pendulum (IP) models family (Bocian *et al.*, 2011; Qin *et al.*, 2013; Lin *et al.*, 2020; Ruiz *et al.*, 2022; Živanović *et al.*, 2022), including the so-called Bipedal Models (BMs).

The primary distinction between these two modelling approaches lies in how they represent the ground reaction force (GRF): while the SMD model – considered as the simplest biodynamic model – simplifies the GRF as a moving coupled force applied at a single contact point, IP models – a more complex biodynamic model – computes GRFs based on the system's motion and predefined parameters.

While numerous studies have employed SMD models to represent the pedestrian body in HSI simulations (e.g., Caprani *et al.*, 2011; Pfeil *et al.*, 2014; Venuti *et al.*, 2016; Shahabpoor *et al.*, 2016b) – primarily to evaluate the interaction effects on structural response – this modelling approach neglects the bipedal nature of walking. As a result, it limits the ability to investigate, in depth, how vibrations affect the walking gait patterns and the corresponding induced forces – the S2HI effects.

Such effects can be incorporated in the simulations when the pedestrian is modelled as a bipedal model (Lin *et al.*, 2020; Živanović *et al.*, 2022). Although it is potentially a reliable tool for predicting structural behaviour, there are still few studies validating the use of bipedal models for applications in the field of Civil Engineering.

When investigating the two simplest models from the IP family (not considering body damping) based on experimental data, Živanović *et al.* (2022) concluded that further research on more complex bipedal models is necessary, as no realistic simulation of the kinematic and kinetic features of walking was achieved. According to Lin *et al.* (2023), within the IP model family, the Damped Bipedal Inverted Pendulum (DBIP) model stands out due to its ability to provide a more realistic simulation of human gait compared to the simplified versions of the IP model.

To the best of the authors' knowledge, the work of Ruiz *et al.* (2022) was the first to correlate experimental results with numerical simulations using the DBIP model. In their study, the authors adopted a simplified version of the DBIP model introduced by Qin *et al.* (2013), reducing it to a single-degree-of-freedom (SDOF), and used the characteristic 'M-shape' of the footfall force as a reference for parameter calibration.

In contrast, Lin *et al.* (2023) retained the model as a two-degree-of-freedom (2DOF) system; in addition, their goal was to achieve the experimental step frequency and the dynamic load factor of the first harmonic (DLF₁) of the GRFs.

In the studies of Ruiz *et al.* (2022) and Lin *et al.* (2023), despite adopting bipedal models differently adapted from Qin *et al.* (2013), the numerical simulations were unable to simultaneously and accurately predict the three gait parameters crucial for investigating the dynamic behaviour of civil structures: walking speed, step frequency, and DLFs.

It is important to note that, in both approaches (Ruiz *et al.*, 2022; Lin *et al.*, 2023), parameter calibration and performance evaluation were conducted solely based on measurements taken on rigid surfaces. Hence, aspects related to structure-to-human interaction (S2HI) were not investigated in these studies, as they only analysed rigid surfaces or scenarios with very low structural accelerations.

While proposing parameter sets for varying vibration levels is not practical, it remains essential to assess whether IP models can accurately perform under conditions involving high vibration levels. As mentioned by Živanović et al. (2022), "unfortunately, the verification of these models, especially on lively structures, lags behind the theoretical developments". This highlights the importance of evaluating the performance of such models in HSI studies.

Additionally, despite the theoretical analysis (Qin et al., 2013; Lin et al., 2020) and experimental validations (Ruiz et al., 2022; Lin et al., 2023) of DBIP models in the literature,

it is clear that significant gaps remain in this field. In particular, the accuracy of these models in predicting key gait parameters – walking speed, step frequency, and DLFs – remains uncertain, especially under excessive vibration conditions. Furthermore, the implications of simplifying DBIP model to an SDOF system require further investigation to determine its accuracy in capturing S2HI effects.

In general, despite several studies that have been developed to understand the phenomenon of excessive vibrations and improve the structures' design in terms of dynamic behaviour under human walking loads, there are various questions to be clarified, chiefly in terms of mathematical and experimental validation of such simple biodynamic models. Bearing in mind that this remains a challenge, it is crucial to further investigate this issue, offering detailed insights into the functioning and reliability of simple models when compared to experimental results on both rigid and lively surfaces.

1.2 Objective

Based on the context presented, this study aims to investigate the interaction between pedestrians and structures by evaluating simple biodynamic models to represent pedestrians, using experimental measurements obtained from two lively test structures and a controlled platform. This approach enables the assessment of how varying vibration levels influence pedestrian-induced actions during walking, with a focus on applications to low-frequency structures.

The specific objectives of this study are:

- To investigate some biodynamic models found in the literature by:
 - o Presenting a comparative review of chosen biodynamic models.
 - Applying these models in numerical simulations and comparing the outcomes with real experimental data obtained from previous works to assess their performance.
- To carry out a series of pedestrian walking experiments that consider gait characteristics and varying vibration levels, in order to account for:
 - o Different walking conditions: slow, normal, fast, and free walking.
 - Multiple vibration levels.

- Test logistics, such as the influence of metronome beats for monitoring purposes.
- o Synchronized collection of kinetic and kinematic data.
- Bringing together experimental data and simulations, to investigate:
 - The experimental-numerical correlation for a selected biodynamic model.
 - Mathematical assumptions regarding human–structure interaction (HSI) found in the literature.
 - The influence of structural vibration levels on the walking behaviour of pedestrians, by comparing walking on low-frequency structures versus rigid surfaces.
- To propose parameter adjustments for a selected biodynamic model and:
 - Evaluate its efficiency by comparing numerical simulation results with experimental findings.

1.3 Justificative and Significance

Predicting structural response becomes particularly challenging when considering the Human-Structure Interaction (HSI) phenomenon, as it involves a wide range of interdependent factors – including pedestrian biomechanics, walking (inter- and intra-subject) variability, structural dynamics, and the feedback mechanisms between humans and vibrating surfaces. Accurately capturing of such mechanisms requires advanced modelling approaches and detailed experimental data, which are often difficult to obtain or validate.

Despite essentially different structures, footbridges and floors are conceived and consequently projected for the conveyance and accommodation of pedestrians, respectively. As a common load case scenario regarding such structures, a simple walking activity can input high levels of vibration causing discomfort to the users, as well as influence structural failures (Racic *et al.*, 2009). For this reason, it is of great importance to understand and avoid these problems at the early stages of the design by improving methodologies and approaches to deal with the prediction of dynamic responses and mitigate unacceptable vibration levels.

Another aspect worthy of attention is the design criterion of vibration assessment of footbridges and floors induced by walking excitation. Although it is generally accepted that the

human body should be modelled as a dynamic system to simulate HSI precisely, most guidelines and standards still treat the pedestrian merely as an external force acting on the structure. Thus, one of the consequences of disregarding such interaction is an expensive overestimation of the dynamic response from numerical simulations when compared to experimental measurements (Muhammad *et al.*, 2018; Shahabpoor *et al.*, 2017).

Therefore, ignoring this phenomenon of interaction between pedestrians and structure may lead to a significant overestimation of the vibratory response and, consequently, the design can fail in the serviceability verification, when, in fact, it could be within the normative limits (Živanović *et al.*, 2005b; Caprani *et al.*, 2011).

The adoption of biodynamic models in Civil Engineering aims to address this gap by improving practical tools for everyday structural design applications. However, despite the existence of several proposals in the literature to model the human body, many of these approaches still lack comprehensive experimental validation, which is essential for their broader adoption in practical engineering contexts.

It is important to emphasize that even with the advancement of more accurate biodynamic models, their complexity hampers for guidelines and standards to accept it as a practical tool for designing such structures. Thus, the improvement of simple biodynamic models is a great contribution to the design of civil structures.

Special emphasis is made on the limitation of the biodynamic models developed so far. Conventionally, most walking biodynamic models' studies have been conducted with low-frequency structures aiming to reproduce resonance conditions in the experiments since it is applicable to structures with this dynamic characteristic, such as footbridges (Shahabpoor *et al.*, 2016a). However, even for such applications, it is interesting to present a biodynamic model able to represent the HSI covering a large range of frequencies. This redirects the attention for the performance of the model and not the applicability to a certain structure.

At this point, it is worthy of attention the fact that analytical formulations to account for HSI should be more deeply investigated, in terms of comparison against experimental results and against each other. For example, a potential experimental correlation between ground reaction forces on rigid (or flexible) surfaces and inertial forces due to body movement. In addition, there is evidence that pedestrians change their behaviour under different levels of vibration, causing a variation in the applied forces on the structure (Živanović *et al.*, 2005b).

Furthermore, it is well known that the dynamic properties of structures occupied by pedestrians differ from their behaviour when unoccupied. This effect, which is part of the HSI phenomenon, has been widely studied, as the development of various experimental and numerical methods has made it practical to measure structural dynamic behaviour, facilitating the investigation of behavioural changes in such structures under human loads (Shahabpoor *et al.*, 2016a; Živanović *et al.* 2005a).

However, when it comes to the excitation source, there is a lack of experimental results discussing the changes in the applied forces by humans submitted to vibrations, which in turn feeds the HSI loop (Caloni *et al.*, 2025).

While human-induced loads, particularly those resulting from common activities such as walking on rigid surfaces, have been extensively investigated in the biomechanical field (Shahabpoor *et al.*, 2016a), the focus of these studies differs from that of civil engineering applications. In the biomechanical field, the primary interest is often the human body itself, with limited emphasis on its interaction with civil structures. This distinction may contribute to the gap in biodynamic model studies (chiefly simple models), particularly regarding the investigation of structure-to-human interaction (S2HI) effects.

In fact, according to Caloni *et al.* (2025), there is a predominant focus on HSI in the existing literature, with insufficient attention to S2HI – even in biomechanical applications. These authors emphasize the need for more precise studies to better understand how structural vibrations impact pedestrians. Another aspect brought to attention by these authors is that insights into S2HI can inform strategies for structural control and health monitoring, aiming to enhance footbridge performance and pedestrian comfort.

Because of that, despite existing many biodynamic models (including their investigations), the study of HSI remains in the literature as a challenge in dealing with its mathematical modelling and chiefly validation with experimental evidence. Shahabpoor *et al.* (2016a) say that "there is still no conclusive evidence on the most realistic and computationally efficient form of the walking human model to simulate HSI". Indeed, even after nearly a decade, this observation remains valid. This is because, despite numerous advancements, no model has yet been conclusively proven to incorporate the full complexity of human walking – addressing the HSI as a whole – while also maintaining computational efficiency and practical applicability.

Lastly, it is important to highlight the relevance of improving the design of civil structures to enable reliable predictions of their performance during the analysis stage. Achieving this requires a deep understanding of the nature of the dynamic actions involved.

1.4 Thesis structure

Chapter 1 presents the context of this research, focusing on excessive vibrations and the modelling of pedestrians. It also outlines the objective of the thesis, as well as the justification and significance of the study.

Chapter 2 provides background information on excessive vibrations in footbridges and discusses the guideline-based approaches used to represent human actions on structures. Additionally, this chapter discusses the modelling of human walking. It begins with a brief overview of human-induced loads, focusing specifically on walking. A literature review of existing biodynamic models is then presented, followed by an in-depth discussion of two selected models, including their formulation, functioning, and key parameters.

Chapter 3 details the methodology employed in this research. It outlines the step-by-step approach adopted throughout the study, providing a comprehensive description of the experimental campaign. Additionally, it presents the procedures used for data acquisition and extraction, ensuring transparency and replicability of the research process.

Chapter 4 focuses on evaluating the performance of selected biodynamic models from both Human-Structure Interaction (HSI) and Structure-to-Human Interaction (S2HI) perspectives. First, the SMD and DBIP models' performance is evaluated based on comparisons against experimental data from two real footbridges. In the S2HI context, one- and two-DOF versions of the DBIP model are assessed under rigid and moving surface conditions. The chapter concludes with a reanalysis of the DBIP model for HSI applications using adjusted parameters.

Chapter 5 presents the conclusions drawn from the research. It summarizes the main findings, highlights the contributions to the field of human-structure interaction, and outlines potential directions for future studies.

2 THEORETICAL BACKGROUND

The aim of this chapter is two-fold: (1) to present a brief background survey on the issue of excessive vibrations and the design code approaches related to low-frequency structures, such as footbridges; and (2) to address human walking as a source of dynamic loading on such structures. Since the investigations presented in this study focus on low-frequency structures, which may exhibit vertical natural frequencies close to pedestrians' step frequencies, this chapter includes a concise description of the human walking gait (with an emphasis on the vertical direction), followed by a critical analysis of various proposals for modelling human-induced loads. Special attention is given to biodynamic models and their correlation with the human-structure interaction (HSI) phenomenon. Additionally, the formulation and parameters of two selected biodynamic models are presented, along with a discussion of their functioning and insights related to their application in HSI interaction scenarios.

2.1 Excessive vibrations due to human loads

Over the years, structural projects have undergone noticeable changes in their limit states criterion, driven by new studies which improved the understanding of the materials behaviour and their application. One of its consequences is the development of bolder projects usually featuring lighter and slender structures (Gonçalves *et al.*, 2019).

Such trend brought a new study target: human loads would no longer be treated as forces only; their dynamic interaction with the structure should be considered in the design stage since many structures have become more susceptible to vibrations when subjected to dynamic loads, even with low magnitudes (Pavic & Reynolds, 2002a; Silva, 2011). This is explained by the cyclical character common to human activities such as walking, running, jumping etc (Bachmann & Ammann, 1987).

Walking activity is a common load case scenario on floor and footbridge structures. Such human movement, among others, can produce resonant, near resonant or impulsive structural vibrations (Muhammad *et al.*, 2018). The features of walking are such that pedestrians can cause vibrations in the lateral (more specific to footbridges) or vertical direction.

According to Thomson (1973), if the frequency of the excitation into a system is equal to its natural frequency f_n , the phenomenon called resonance occurs. When this happens, the

vibration amplitude increases abruptly and strongly, which can lead to system collapse of structures, such as buildings and bridges. However, a common scenario related to excessive vibrations is the significant annoyance to occupants featuring a serviceability subject.

Zhou et al. (2015) cited the importance to consider vibration serviceability as a part of structural design once exorbitant vibrations can cause psychological fear and discomfort to the users. Pretlove & Rainer (1995) said that "Human sensitivity to vibration is very acute. The human body can sense vibration displacement amplitudes as low as 0.001 mm".

Muhammad *et al.* (2018) say that a simple walking activity can produce excessive structural vibrations (resonant or impulsive). With more details in the review presented by these authors, in many cases, such dynamic instabilities make the environment uncomfortable or even intolerable, which can generate fear or panic, as well as affect the performance of more sensitive equipment (for instance, in floors).

The effect of human loads became more expressive over the years leading to a growing problem of excessive vibrations. Hence, the last two decades has concentrated an increased number of studies that aim to investigate the dynamic behaviour of structures under these dynamic loads (Shahabpoor *et al.*, 2016a). However,

Since these important aspects of walking forces have not been adequately researched in the past, the corresponding lack of knowledge has reflected badly on the quality of their Mathematical models used in vibration assessments of pedestrian structures such as footbridges, staircases and floors. (Racic *et al.*, 2009)

Regarding footbridges, there are several reported cases of excessive vibrations. The literature presents two benchmarks of excessive vibration cases in footbridges that intensified the investigations of dynamic problems due to pedestrians: the case of Millennium Bridge in London (Dallard *et al.*, 2001) and the case of The Solferino Bridge in Paris (Danbon & Grillaud, 2005) (Figure 1). In both events, the lateral movement of the pedestrians while walking matched with the lateral natural frequency of the structures, leading to a resonance condition.

As Pimentel (1997) stated, a factor that contributes to explain vibrations with large amplitudes in the lateral direction of footbridges (valid for bridges), is the fact that these structures are designed to support dead and live loads in the vertical direction and, therefore, less stiffness is required to counteract lateral loads. As emphasized by Silva (2011), pedestrians and wind action are the major live loads to footbridges. Table 1 gather some case studies of excessive vibrations of footbridges under human loads.

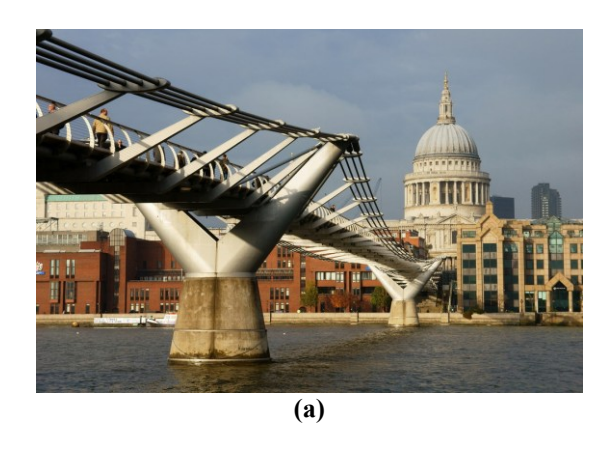




Figure 1 – (a) Millenium Bridge, London, UK (Geograph, 2025); and (b) Solferino Bridge, Paris, France (Wikipedia, 2025).

Table 1 – Case studies of excessive vibrations of footbridges induced by walking.

Study	Lateral	Vertical
Matsumoto (1978)		•
Eyre & Cullington (1985)		•
Bachmann & Ammann (1987)	•	•
Fujino et al. (1993)	•	
Brownjohn (1997)	•	
Pimentel (1997)		
Dallard et al. (2001)	•	
Danbon & Grillaud (2005)	•	
Pospíšil et al. (2013)	•	•
Hawryszków et al. (2017)		•

Currently, it is generally agreed among researchers that the excessive vibrations on structures are a matter of serviceability rather than safety problems. This line of reasoning is explained by the high human sensitivity to vibration levels, and then, this limit state tends to fail before any risk of structural damage (Racic *et al.*, 2009; Pavic & Reynolds, 2002a; Mohammed *et al.*, 2018; Muhammad *et al.*, 2018).

Consequently, most guidelines and standards treat this dynamic problem as a Serviceability Limit State (SLS), involving aspects such as structural dynamic properties and how to model human loads. Given this, excessive vibrations are now a critical design aspect of modern civil engineering structures. According to Mohammed *et al.* (2018), while modern structures usually meet the Ultimate Limit State (ULS) requirements, SLS criteria is increasingly govern the design aspect.

Next section brings a brief discussion regarding guidelines and standards approach to deal with vibration assessment of footbridges under walking excitation in the vertical direction.

2.2 Guideline's approach

Bearing in mind that excessive vibrations can entail structural reinforcements, it has been a target of design documents for footbridges on how to avoid this serviceability limit state problem due to human loads. In this context, the approach by standards and guidelines is twofold: (a) determine the dynamic properties of the structure and (b) how to apply pedestrian loads in the analysis.

Table 2 presents the guidelines and standards discussed herein. It is important to emphasize the need to refer to these normative documents for a comprehensive dynamic analysis involving human loads, as they address the problem in its entirety. However, this study focuses solely on the modelling of pedestrian walking in the vertical direction. Additionally, the focus of these documents is on the design stage, with no mention of structural reinforcements.

Table 2 – Guidelines and standards for assessment of footbridges.

Guideline	Description
Hivoss (2008)	Human Induced Vibration of Steel Structures: Background Document for Design of Footbridges
Sétra (2006)	 Assessment of vibrational behaviour of footbridges under pedestrian loading
UK NA to BS (2008)	 UK National Annex to Eurocode 1: Actions on structures - Part 2: Traffic loads on bridges
NBR 7188 (2024)	 Road and pedestrian live load on bridges, viaducts, footbridges and other structures
NBR 8800 (2024)	 Design of steel and composite structures for buildings
NBR 6118 (2023)	• Design of concrete structures — Procedure

One of the recommendations is to minimize the probability to present excessive vibrations by designing structures with natural frequencies out of critical ranges (related to human loads). This line of reasoning aims to prevent resonance conditions. These values can be calculated by several ways, as suggested by guidelines (Hivoss, 2008; Sétra, 2006; UK NA to BS, 2008). Ranging from Finite Element (FE) Method to hand formulas, such procedures are useful in a day-by-day design.

According to Hivoss (2008), the dominant contribution of the first harmonic of the pedestrian load leads to the following critical range for natural frequencies f_{critic} , as follows:

$$1.25 \text{ Hz} \le f_{critic} \le 2.3 \text{ Hz} \tag{1}$$

This range might be extended to 4.6 Hz if natural frequencies (f_n) lie in an interval susceptible of excitation by the 2nd harmonic of pedestrian excitation.

By gathering information from several studies and standards, Sétra (2006) presents, for vertical direction, four frequency ranges correlated with a decreasing risk of resonance, as shown in Figure 2. It should be highlighted that a previous critical range of natural frequencies defined by Hivoss (2008) is within the values defined by Sétra (2006).

Otherwise, in UK NA to BS (2008), critical ranges of natural frequency for bridges, in general, are defined based on span length of such structures. However, a range of 1.0 to 3.0 Hz is suggested by Eurocode 1 (2003) to evaluate resonance condition due to pedestrian walking loads for footbridges.

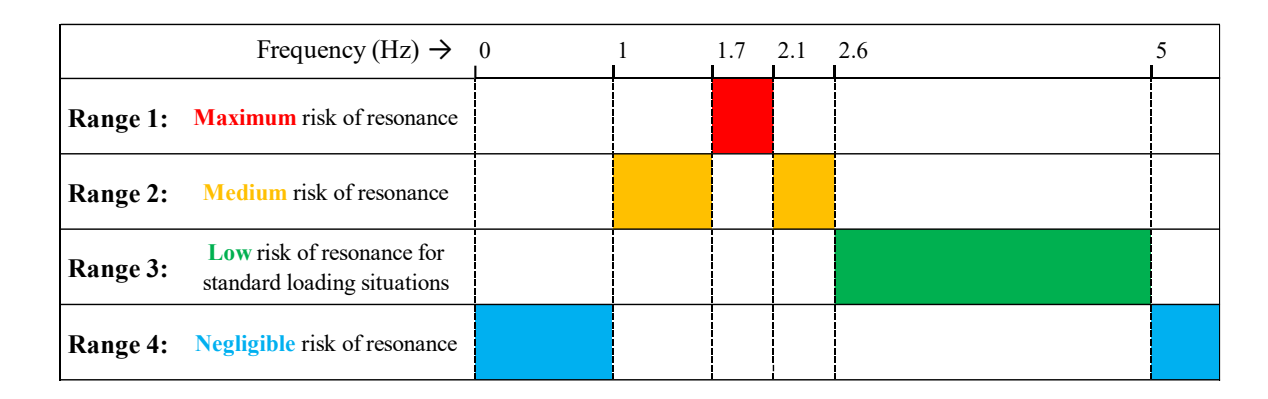


Figure 2 - Frequency ranges (Hz) of the vertical vibrations and associated risk of resonance level (After Sétra, 2006).

The NBR 6118 (2023) is highly conservative and deal with resonance risk by setting a minimum value for critical frequencies depending on the structure usage. For footbridges, the structure natural frequency cannot be lower than 1.2 times 4.5Hz. Conventionally, if this condition is not attended, some other standard must be used since there is no specific national standard to deal with vibration assessment for footbridges.

It is noteworthy that despite national standards for designing footbridges pay attention to serviceability failure due to human loads, such documents do not make clear how to include the pedestrian's action in the analysis or any deepen evaluation of structural dynamic behaviour (as in NBR 6118:2023). For example, NBR 7188 (2024) recommends a static distributed force of 5.0kN/m² to be applied on the unfavourable position of the structure. However, this standard document only mentions a need to further dynamic stability proof to special structures (light and slender, such as steel structures or suspension bridges) and no further recommendations or references are indicated.

Regarding steel structures, NBR 8800 (2024) takes into account excessive vibrations to floors but no reference to footbridges is given. In the point of view of Silva (2011), the absence of such national standards approaches to design footbridges can be explained by the low number of bolder projects when comparing to Asia, Europe, and North America.

At this point, concerning to footbridges' project, it is important to highlight factors that affect its design. According to Hivoss (2008) (Table 3), UK NA to BS (2008) (Table 4), and Sétra (2006) (Table 5), such structures might be categorized into bridge classes, in terms of usage and traffic density. This primary stage allows to determine group sizes or crowd densities to be considered in the analysis. It could be seen from Table 3, Table 4 and Table 5 that similar footbridges' classification by these guidelines lie in different values for crowd densities.

The serviceability limit state criterion is based on natural frequency limitation but also it should be proved that the peak vertical deck accelerations determined for these human actions are less than the limit values. Since excessive vibrations can lead to emotional reactions of pedestrians, the comfort level associated with this limitation is a matter of bridge usage but also is a criterion required by the owner.

Table 3 – Traffic class according to Hivoss (2008).

Traffic Class	Description	Characteristics	Crowd Density (persons/m²)
TC1	Very weak traffic	Groups of N pedestrians free to walk in an area A	N/A
TC2	Weak traffic	Comfortable and free walking. Overtaking is possible. Single pedestrians can freely choose pace	0.2
TC3	Dense traffic	Still unrestricted walking. Overtaking can intermittently be inhibited.	0.5
TC4	Very dense traffic	Freedom of movement is restricted. Obstructed walking. Overtaking is no longer possible	1.0
TC5	Exceptionally dense traffic	Unpleasant walking. Crowding begins. One can no longer freely choose pace	1.5

Table 4 – Bridge classification and recommended crowd densities (walking) according to UK NA to BS (2008).

Bridge Class	Bridge Usage	Group Size	Crowd density (persons/m²)
A	Rural locations seldom used and in sparsely populated areas.	N = 2	0
В	Suburban location likely to experience slight variations in pedestrian loading intensity on an occasional basis.	N = 4	0.4
C	Urban routes subject to significant variation in daily usage (e.g., structures serving access to offices or schools).	N = 8	0.8
D	Primary access to major public assembly facilities such as sports stadia or major public transportation facilities.	N = 16	1.5

Table 5 – Footbridges' classification according to Sétra (2006).

Class	Usage	Traffic characteristics	Crowd density (persons/m²)
I	Urban footbridge linking up high pedestrian density areas	Subjected to very heavy traffic.	1.0
II	Urban footbridge linking up populated areas	Subjected to heavy traffic and that may occasionally be loaded throughout its bearing area.	0.8
III	Footbridge for standard use	That may occasionally be crossed by large groups of people but that will never be loaded throughout its bearing area.	0.5
IV	Seldom used footbridge	Built to link sparsely populated areas or to ensure continuity of the pedestrian footpath in motorway or express lane areas.	Not mentioned

Whilst Hivoss (2008) and Sétra (2006) guidelines recommend serviceability range acceleration limits for use in design of footbridges based on the required comfort level (Table 6), UK NA to BS (2008) presents an expression (Eq.(2)) to determine the limit value as a function of bridge usage (factor k_1), route redundancy (factor k_2), and height of structure (factor k_3). In Eq.(2) k_4 "is an exposure factor which is to be taken as 1.0 unless determined otherwise for the individual project".¹

$$a_{limit} = 1.0 k_1 k_2 k_3 k_4 \quad (m/s^2)$$
 (2)

¹ More details in UK NA to BS (2008)

$$0.5 \le a_{limit} \le 2.0 \text{ (m/s}^2)$$

Table 6 – Recommended acceleration limit ranges for footbridges under human loads (After Sétra, 2006; and Hivoss, 2008).

Comfor	t level	Description	Vertical alimit	
Hivoss (2008)	Sétra (2006)	Description		
CL1 (Maximum)	Maximum	Accelerations undergone by the structure are practically imperceptible to the users.	$< 0.5 \text{ m/s}^2$	
CL2 (Medium)	Average	Accelerations undergone by the structure are merely perceptible to the users.	$0.5 - 1.0 \text{ m/s}^2$	
CL3 (Minimum)	Minimum	Accelerations undergone by the structure are perceived by the users, but do not become intolerable.	$1.0 - 2.5 \text{ m/s}^2$	
CL4 (Uncomfortable)	Uncomfortable	Acceleration levels that are not acceptable.	> 2.5 m/s ²	

Table 7 – Recommended values for the site usage factor k_I (UK NA to BS, 2008).

Bridge function	k 1
Primary route for hospitals or other high sensitivity routes	0.6
Primary route for school	0.8
Primary routes for sports stadia or other high usage routes	0.8
Major urban centres	1.0
Suburban crossings	1.3
Rural environments	1.6

Table 8 – Recommended values for the route redundancy factor k_2 (UK NA to BS, 2008).

Route redundancy	k_2
Sole means of access	0.7
Primary route	1.0
Alternative routes readily available	1.3

Table 9 – Recommended values for the structure height factor k_3 (UK NA to BS, 2008).

Bridge height	<i>k</i> ₃
Greater than 8 m	0.7
4 m to 8 m	1.0
Less than 4 m	1.1

It is worthy to note that UK NA to BS (2008) is more conservative since the maximum accepted acceleration a_{limit} do not exceed 2.0m/s² rather than a maximum value accepted by the others.

As previously mentioned, most of the guidelines adopt Moving Force (MF) models to reproduce the pedestrian walking across the structure, including or not a consideration of the number of pedestrians in the analysis. Due to the periodic nature of walking, the induced force by pedestrians can be approximated by a Fourier series (ISO 10137:2007; Sétra, 2006). Also called as ground reaction force (GRF), this time (t) varying force F(t), given in Eq.(3), is the sum of all single harmonic contribution and returns the total effect of the cyclical action.

$$F(t) = W + W_I \sin(2\pi f_s t) + \sum_{i=2}^{n} W_i \sin(2\pi i f_s t - \theta_i)$$
(3)

Where W is the weight of the pedestrian ($W = m_h g$, in which m_h is the pedestrian total mass, and g is the acceleration due to gravity), f_s is the step frequency, and θ_i is the phase angle of the i^{th} harmonic in relation to the first one (usually $\theta_2 = \theta_3 = \pi/2$). The harmonic amplitudes, given by W_i , are usually taken as a fraction of the static force W. To Sétra (2006), the mean value of 700 N may be taken for W, and:

$$W_1 = 0.4W$$

$$W_2 = W_3 \approx 0.1W$$
(4)

The Fourier's coefficient of the i^{th} harmonic, 0.4 and 0.1 in Eq.(4), called as Dynamic Load Factor (DLF), have been a target of researchers in an attempt to quantify such values. By measuring continuous single-person force from walking (and also running), Rainer *et al.* (1988) provided a greater work proving a strongly dependence of DLFs to step frequency (graphics are available in the reference). Other authors also proved this finding but suggesting expressions to determine such values. Table 10 gathers some proposals found on the literature to determine DLFs to 1^{st} and 2^{nd} harmonics.

Some authors, such as Rainer *et al.* (1988) and Pernica (1990), also provide values for DLFs depending on step frequency f_s , but no expressions are proposed by these authors.

Considering only the first harmonic, as this usually suffices for analyses of typical footbridges in resonance condition, and considering:

$$W_i = DLF \cdot W \tag{5}$$

Eq.(3) can be rewritten as follows:

$$F(t) = W(1 + DLF \cdot \sin(2\pi f_s t))$$
(6)

Defenere	Dynamic load factor (DLF)		
Reference	1 st harmonic	2 nd harmonic	
Sétra (2006)	0.4	0.1	
ISO 10137 (2007)	$0.37(f_s - 1.0)$	0.1	
Blanchard et al. (1977)	0.257	Not provided	
Kerr & Bishop (2001)	$-0.2649f_s^3 + 1.3206f_s^2 - 1.7597f_s + 0.7613$	0.07	
Bachmann & Ammann (1987)	$0.25f_s - 0.1$	0.1	
Young (2001)	$0.41(f_s - 0.95)$	$0.069 + 0.0056f_s$	
Brownjohn (2004)	$0.37f_s - 0.42$	0.053	
Butz et al. (2008)	$0.0115f_s^2 + 0.2803f_s - 0.2902$	$0.0669f_s^2 + 0.1067f_s - 0.0417$	
Dang & Živanović (2015)	$-0.0542f_{s}^{2}+0.6493f_{s}-0.7165$	Not provided	

Table 10 – Some proposals to determine the Dynamic Load Factor (DLF).

Depending on the Traffic Class (see Table 3), the load model proposed by Hivoss (2008) to consider the pedestrians action also consists in applying a pulsating force but distributed over the loaded area (in N/m^2), as given in Eq.(7) to vertical direction.

$$p(t) = W_1 \cdot \cos(2\pi f_s t) \cdot n' \cdot \Psi \tag{7}$$

Where n' is the equivalent number of pedestrians on the loaded surface, and Ψ is the reduction coefficient based on probability of the step frequency approaches the critical range of natural frequencies (1st and 2nd harmonics) under consideration (Figure 3).

With a different approach, UK NA to BS (2008) recommend calculating the maximum vertical acceleration of the structure analysed under human loads (single pedestrian or groups), by applying a pulsating force F(N) over time (function of N pedestrians) moving with a constant walking speed v (1.7m/s for walking) across the span, given in Eq.(8).

$$F(N) = F_0 \cdot k(f_v) \cdot \sqrt{1 + \gamma(N - 1)} \cdot \sin(2\pi f_v t)$$
(8)

For walking activity, reference load F_0 is assumed as 280N. The combined factor $k(f_v)$ considers the effects of a more realistic pedestrian population, harmonic responses, and human sensitivity to vibrations. This factor is determined depending on the human activity and the mode frequency f_v of interest (Figure 4).

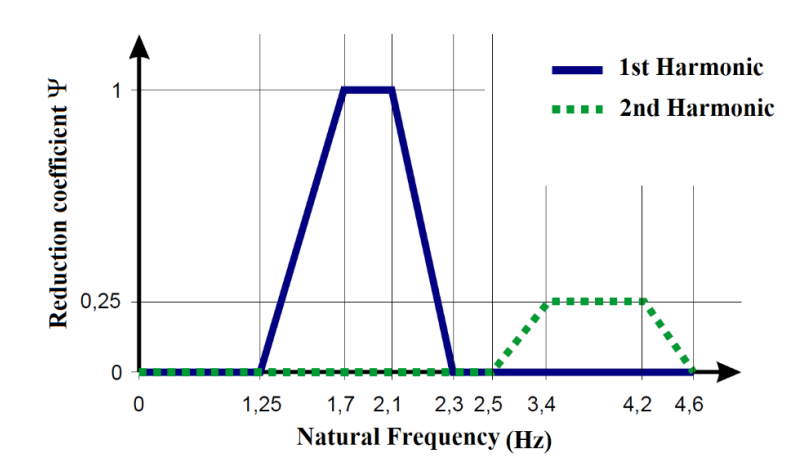


Figure 3 - Reduction coefficient Ψ (After Hivoss, 2008).

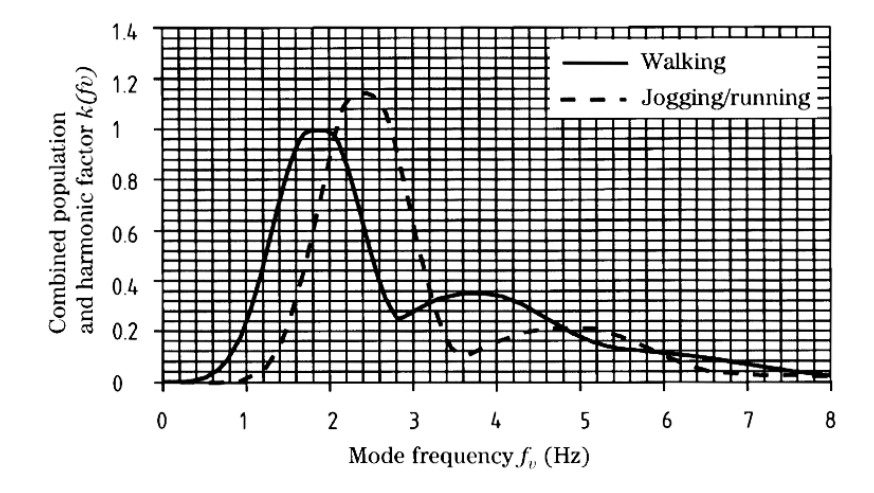


Figure 4 - Graphic to determine Combined Factor $k(f_v)$ (After UK NA to BS, 2008).

The desynchronization of pedestrians in a group is considered by the reduction factor γ , which is a function of structural damping δ and effective span S_{eff} (in all cases it is conservative to assume S_{eff} as the actual bridge span)², determined by Figure 5.

It is observed in Eq.(8) that the moving force applied over the structure does not consider the pacing rate of the pedestrians but the natural frequency of the structure, featuring a resonance condition. Hivoss (2008) also enrol the same approach by assuming the pacing rate equal to the footbridge natural frequency under consideration.

-

² More details in UK NA to BS (2008)

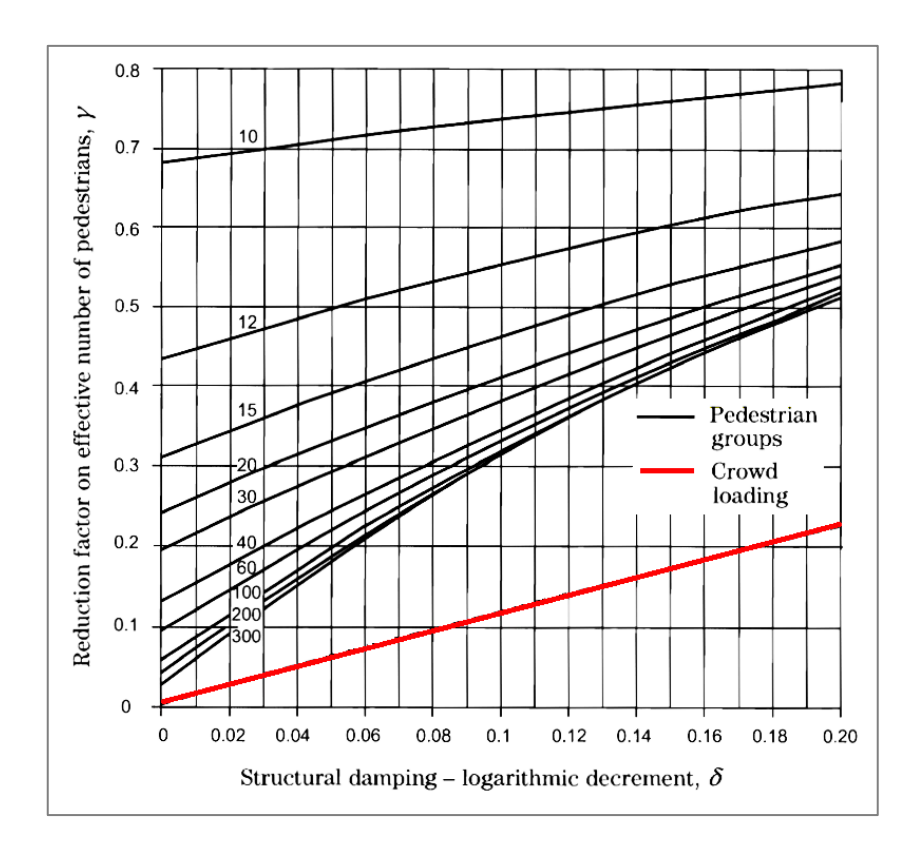


Figure 5 - Reduction factor, γ , to allow for the unsynchronized combination of pedestrian actions within groups and crowds (each curve represent effective span S_{eff}) (After UK NA to BS, 2008).

2.3 Human Induced Loads

Human-induced loads refer to the forces exerted by human activities – such as walking, running, or jumping – on structures like floors, footbridges, staircases, and grandstands. Understanding these loads is crucial in civil engineering to ensure structural integrity and occupant comfort, as meeting serviceability criteria has been more challenging due to the trend in modern buildings (Racic *et al.*, 2009).

Although this study does not aim to provide an extensive discussion on human-induced loads, it is important to highlight some aspects of walking gait, as it is the focus here.

From definitions in biomechanics (Pirker & Katzenschlager, 2017; Dong *et al.*, 2024; Carl *et al.*, 1994), walking is a cyclic movement that involves the alternating support and movement of the legs to propel the body forward while maintaining balance.

As mentioned by Racic *et al.* (2009), some authors refer to "gait" as the walking process itself. However, it is important to clarify that gait refers more to the manner of walking. It can

be characterized by parameters such as step frequency, walking speed, step length, and even the forces induced during movement.

A gait cycle can be defined as the interval between two successive events of the same foot. There is no strict definition in the literature for the beginning of the cycle, as any event can be considered as such. Within the gait cycle, there are two step cycles, defined as the interval between successive events of opposite feet. In turn, a stride corresponds to a full gait cycle.

For a better understanding of walking induced forces, Figure 6 depicts the gait cycle and respective phases aligned with the typical footfall forces from each foot.

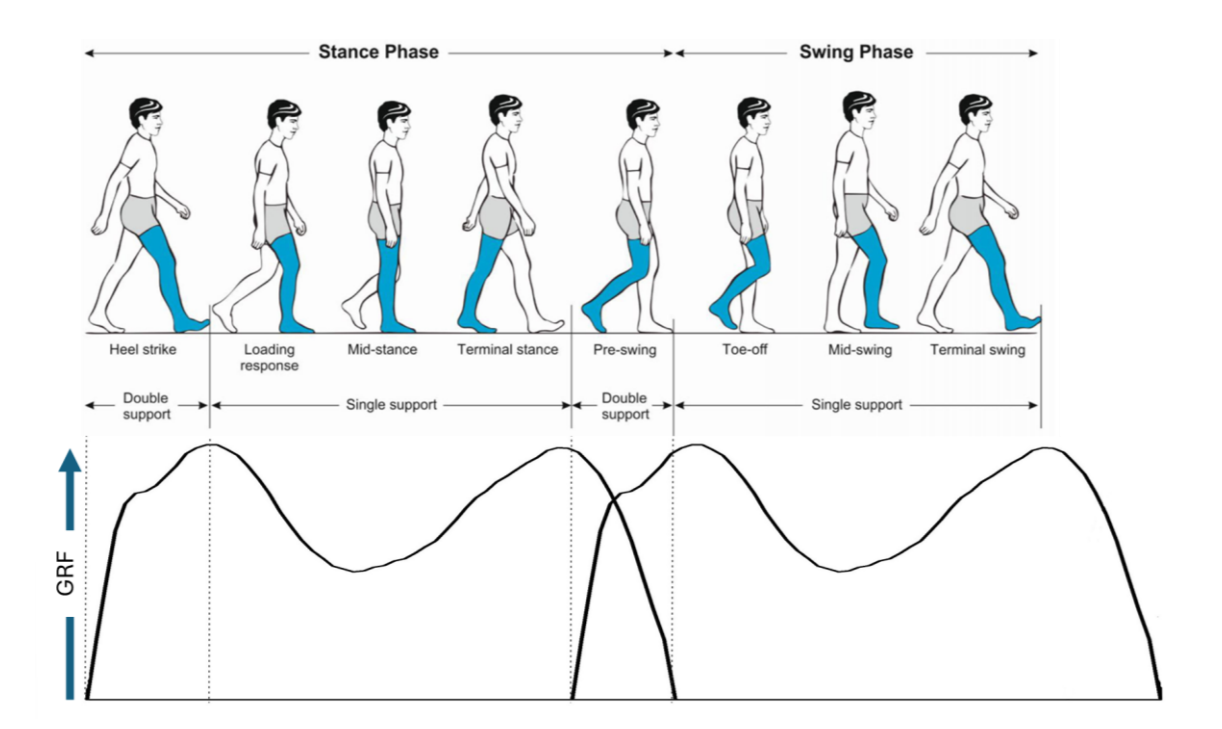


Figure 6 – Representation of a gait cycle with respective typical GRFs for each footfall (After Pirker & Katzenschlager, 2017; and Ruiz, 2021)

It is important to emphasize that within a gait cycle, there are two different phase categories. The first refers to the phases of a single foot within the cycle, which are the stance and swing phases. The former, accounting for around 60% of the gait cycle, occurs when the foot is in contact with the ground, while the latter, around 40% of the cycle, begins when the foot lifts off the ground and starts moving forward to reposition itself ahead of the body until the next ground contact.

As observed from Figure 6, the stance phase consists of four primary subphases:

- Loading response: also called initial support, this subphase begins at what is referred as heel-strike event, or (and from now on), as the touch-down (TD) event. In this phase the vertical GRF increases to the maximum first peak. Importantly, this phase occurs quickly after the TD.
- Mid-stance: the body 'oscillates' over the supporting foot and the other foot in swinging towards the next impact point. During mid-stance, the body's centre of mass (CoM) is at its highest vertical point, and the entire body weight is balanced over a single foot. At this moment, there is less vertical acceleration of the body compared to the initial contact (when the body is decelerating) and lift-off (when the body is accelerating upward and forward). As a result, the vertical GRF decreases, forming what is known as the mid-stance valley in the footfall force curve.
- Terminal stance: the heel lifts as the weight shifts to the front of the foot while the body begins to transfer its weight to the opposite foot. It is during this phase that the vertical GRF begins to rise again, reaching the second peak in the footfall force, just before losing contact with the ground thus forming the characteristic 'M-shape' footfall force pattern (Kerr & Bishop, 2001).
- Pre-swing: the toes lift off the ground, initiating the swing phase. At this exact moment there are zero contact forces between the foot and the ground. From now on this event will be called touch-off (TO).

The beginning of the swing phase is marked by the TO event, and this phase can be divided into three main parts:

- Initial Swing (Acceleration): the foot leaves the ground and starts moving forward.
- Mid-Swing: the foot reaches its highest position, clearing the ground.
- Terminal Swing (Deceleration): the foot prepares to land for the next step.

The second phase category refers to the type of support within a step cycle. If both feet support the body weight, it is called the double support phase (around 10 to 12% of the step cycle), meaning that the stance phases of both feet overlap. The single support phase, when only one foot supports the body weight, coincides with the swing phase of the opposite foot.

As will be seen in the next subsection, some mathematical models used to represent human walking may or may not account for the gait features explained here.

2.4 Human Structure Interaction and human walking models

It is known that induced loads by pedestrians over structures have become an important serviceability design criterion since a simple walking activity can cause vibrational disturbances (Živanović *et al.*, 2005a). Thus, as a part of the studies that aimed to understand the phenomena related to excessive vibrations in structures, it is required to understand how people would be inserted into the context of numerical modelling.

To deal with this, for design purposes, several ways of applying these loads to the structure have been presented (Caprani & Ahmadi, 2016). Focusing on the vertical direction and walking movement, the simplest model consists of applying a moving periodic force (MF) over the structure (Figure 7), mathematically expressed by a Fourier series (Bachmann & Ammann, 1987), as in Eq.(6).

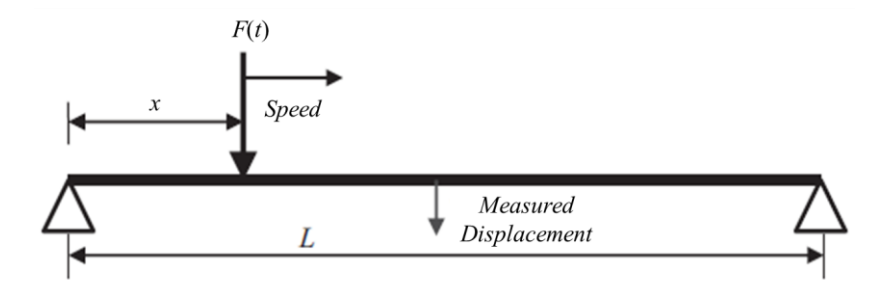


Figure 7 – Representation of MF model applied on a structure (After Caprani & Ahmadi, 2016).

There is in the literature an improved MF model with an inertial mass coupled to the moving pulsating force (Figure 8). O'Sullivan *et al.* (2012) present details about the formulation and particularities of this model.

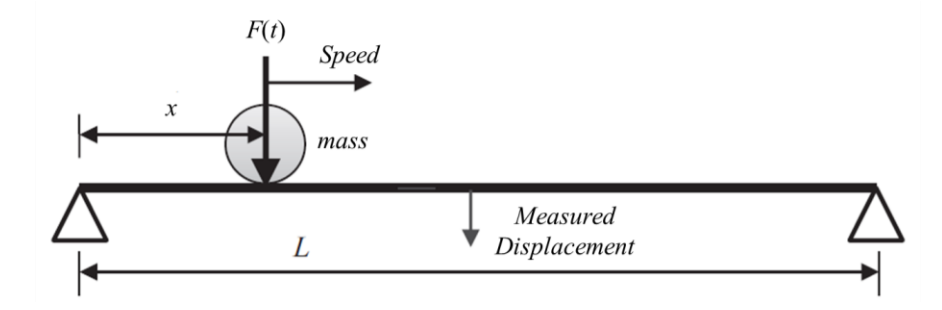


Figure 8 – Representation of MF model coupled with inertial mass applied on a structure (After Caprani & Ahmadi, 2016).

Several studies corroborate the differences in walking behaviour among different pedestrians, and even for the same pedestrian (Shahabpoor *et al.*, 2016a). In fact, inter and intrasubject variability of people arise from the complexity of the human body.

Inter-subject variability is expressive regarding step frequency, which stand among the dynamic parameters used to analyse structures under human loads, even in the simplest pedestrian model (it could be seen in Eq.(6)). Table 11 shows some values for step frequencies proposed in the literature. This variation observed for this parameter can be explained by etiological factors, such as environment, cultural behaviour, physical characteristics and even footwear type.

Step Frequency for walking Number of Study Test condition pedestrians activity Matsumoto et al. (1972) 505 Groups Mean 1.99 Hz (SD of 0.178 Hz) Bachmann et al. (1995) Range of 1.6 - 2.4 Hz* Kerr & Bishop (2001) Individual 40 Mean 1.9 Hz Živanović et al. (2005a) 1976 Groups Mean 1.87 Hz (SD of 0.186) Sahnaci & Kasperski (2005) 251 Individual Mean 1.82 Hz

Table 11 – Some values for pacing rate proposed in the literature in walking activity.

Currently included in most standards and guidelines (e.g.: Sétra, 2006; Hivoss, 2008; UK NA to BS, 2008; SCI P354, 2009; CCIP, 2006), the MF model cannot precisely estimate the dynamic properties of the system under human action, chiefly due to the effects of the dynamics of the human body. Thus, pedestrians cannot be realistically represented as a deterministic load (Ahmadi *et al.*, 2019).

A compromise of the effect regarding the presence of pedestrians not only as loads is considered by the Sétra (2006) and Hivoss (2008) guidelines, in which a fraction of the mass of the pedestrians is added when calculating the natural frequency of the structure.

Bearing in mind that pedestrians' bodies have their own dynamic properties, including such parameters on the analysis can improve the reliability of numerical simulations, as it has been evidenced in various studies. Caprani & Ahmadi (2016) presents a brief survey of several studies involving the modelling of pedestrians walking, in crowd situations or alone, as well as the type of modelling adopted for the structure.

^{*} Also adopted by Sétra (2006).

Barker (2002) states that "pedestrians can effectively input energy into a vibrating bridge even if their walking frequencies are far from the frequency of the vibrating structure." Hence, not only resonance conditions can provoke accelerations out of the accepted limits since pedestrians can mobilize higher vibrating modes.

Regarding structural behaviour and its dynamic properties, one of the outcomes from the literature over the years is the change in the capacity to absorb the vibration energy when such structures are occupied by pedestrians (stationary or moving). Živanović *et al.* (2009), Zhang *et al.* (2015), Van Nimmen *et al.* (2015), and Salyards and Hua (2015) concluded that pedestrians added damping to the structures analysed as well as they modified its natural frequency a little. By analysing a timber floor, the same result was observed by Ohlsson (1982); however, the modal mass of the structure was also increased.³

Bishop *et al.* (1993) and Pimentel & Waldron (1996) investigated structures under human loads (staircases and footbridge, respectively) and showed that moving human occupants add damping to structures they occupy. Furthermore, Shahabpoor *et al.* (2015) and Shahabpoor *et al.* (2016b) evidenced that the greater is the number of pedestrians over the structure the more significant is the effective changes in the modal parameters.

Those effects relate to what is called in the literature of Human-Structure-Interaction (HSI). In this regard, according to Shahabpoor *et al.* (2016a), the core understanding of the HSI is based on the concept of mutual simultaneous effects between the dynamic systems involved in the interaction: the reciprocal processes of human-to-structure interaction (H2SI) and structure-to-human interaction (S2HI).

Once the structure enters a vibratory state due to excitation caused by periodic human activities, such as walking, its dynamic properties tend to change as a consequence of human-to-structure interaction (H2SI) (Živanović *et al.*, 2009). Simultaneously, when perceiving vibrations, pedestrians may adjust their walking gait and related ground reaction forces (GRFs), thereby influencing the structural response through structure-to-human interaction (S2HI), mitigating or amplifying vibrations (Živanović *et al.*, 2005b). For scenarios featuring high levels of vibration, the HSI effects become more pronounced (Hawryszków *et al.*, 2021), requiring mathematical frameworks capable of simulating this aforementioned feedback loop.

³ An extensive literature review can be found in Shahabpoor *et al.* (2016a).

It is now generally accepted that the HSI is one of the keys to understand the behaviour of structures under human loads (Shahabpoor *et al.*, 2016a; Ahmadi *et al.*, 2019). This condition has been corroborated through the development of various theoretical and experimental studies (more details in Caprani & Ahmadi, 2016).

Literature pays attention to the fact that the dynamic properties of the pedestrianstructure system are not the same if it does not consider the dynamic contribution of the individuals in the analysis, and generally it could not reproduce accurate system responses, resulting, sometimes, in overestimated ones (Caprani *et al.*, 2011).

The target in HSI investigation is the reciprocal dynamic effects between the subject (single or crowd) and structure, and its representation through an analytical model and numerical framework. Among the relevant issues within the HSI, there is the action of a pedestrian walking on structures. Hence, modelling a pedestrian as a part of the system, not only as loads, is highly crucial to obtain reliable results (Sachse *et al.*, 2003; Živanović *et al.*, 2005a; Shahabpoor *et al.*, 2016a; Ahmadi *et al.*, 2019).

Aiming to improve the results obtained by applying the MF model, Archbold (2004) introduced the dynamic body parameters by coupling a single degree-of-freedom (SDOF) oscillator with mass, stiffness and damping to the GRF. Also applied by other authors (Fanning *et al.*, 2005; Silva *et al.*, 2013), this procedure does not account for an analytical formulation. Subsequently, analytical frameworks were introduced, and what is referred to as the biodynamic models has appeared in the literature with various formulations, differing in both mathematical assumptions and body kinematics (Caprani & Ahmadi, 2016; Shahabpoor *et al.*, 2016a).

The simplest biodynamic model is a single degree of freedom spring-mass-damper (SMD model), as shown in Figure 9. However, even among the SMD models, there are significant differences in the formulations, ranging from the absence of an analytical formulation (Archbold, 2004; Fanning *et al.*, 2005; Silva *et al.*, 2013) to the adoption of additional energy input that generates the pedestrian up and down movement by different means (e.g., actuators [Zhang *et al.*, 2016; Toso & Gomes, 2018; Dang & Živanović, 2013], heel movement [Pfeil *et al.*, 2014], additional velocity term [Gomez *et al.*, 2018]), or else none of these additions [Caprani *et al.*, 2011; Venuti *et al.*, 2016; Shahabpoor *et al.*, 2016b]).

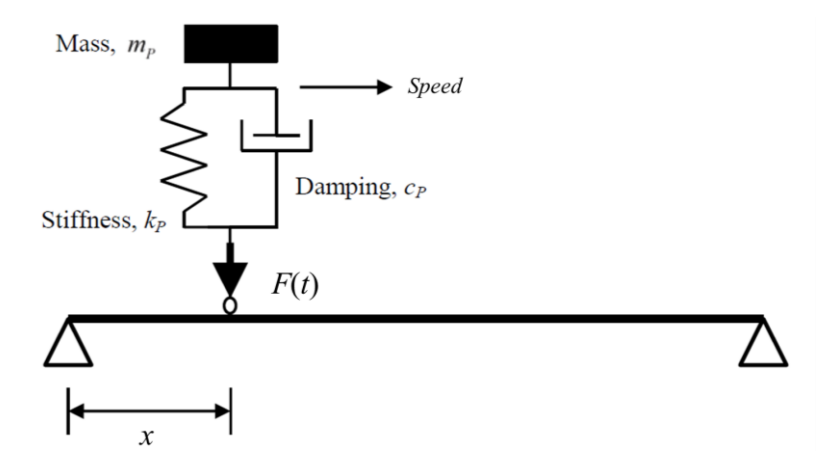


Figure 9 – SMD biodynamic model (After Caprani et al., 2011).

Besides the (aforementioned) variations of the biodynamic models, some of them also differ from each other in the number of degrees of freedom to model the pedestrians walking. According to research in academic databases, the first biodynamic model for walking pedestrians proposed was disclosed in the work of Miyamori *et al.* (2001), with three degrees of freedom (3DOF), as seen in Figure 10. Special emphasis is that there is still no evidence of experimental validation of the model, despite it being calibrated from real experimental test data, adopting an optimization algorithm based on genetics.

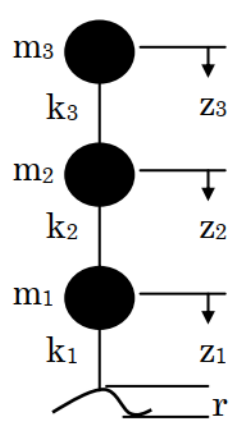


Figure 10 – 3DOF biodynamic model (Miyamori *et al.*, 2001).

Variations in the number of degrees of freedom are seen in several studies, such as in Kim *et al.* (2008). In that study, a two degree of freedom (2DOF) model provided by ISO 5982 (1981) to represent the dynamic behaviour of an individual walking was used (Figure 11a).

However, this study adopted the same normative document parameters that were established for stationary people, which proved to be inconsistent with people in walking motion (Shahabpoor *et al.*, 2016a). In addition, more complex models with 9 and 34 degrees of freedom were developed by Maca & Valasek (2011), shown in Figure 11b and c, respectively.

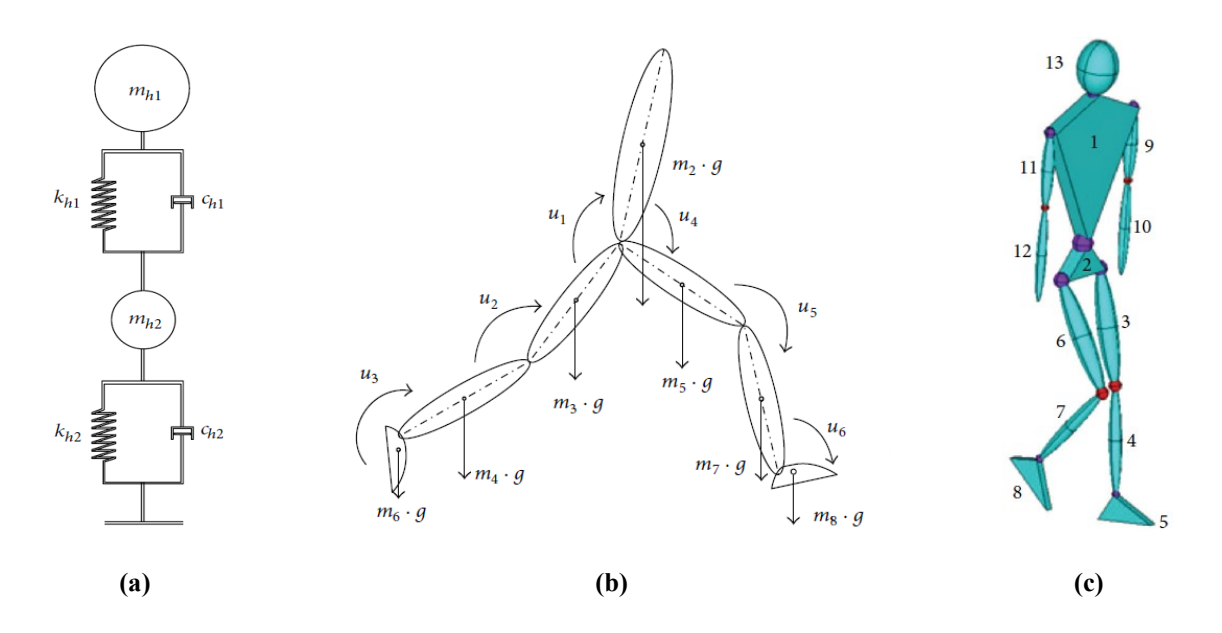


Figure 11 – Biodynamics models with (a) 2DOF (After ISO 5982, 1981), (b) 9DOF and (c) 34DOF (Maca & Valasek, 2011).

Afterwards, these models were studied with some variations, e.g., introducing actuators (Zhang *et al.*, 2016; Toso & Gomes, 2018; Dang & Živanović, 2013), or considering non-vibrating mass added in the model (Jiménez-Alonso & Sáez, 2014). The former is a matter of a more substantial conceptual modification of the SMD model: an actuator was introduced in parallel with the spring and damper, called here SMDA model (Figure 12).

One of the first works found in the literature that bring this concept was developed by Alexander (2006). The author introduced the actuator as the sole primary source of the pedestrian up and down movement. The interaction force between pedestrian and structure occurs through the actuator, spring, and damper forces. Crowd action is also investigated by the author.

Dang & Živanović (2013) adapted Alexander (2006) formulation for the case of a single pedestrian and brought back the use of GRF from walking on a rigid surface into the formulation. Zhang *et al.* (2016) and Toso & Gomes (2018) also employed SMDA models.

However, in Zhang *et al.* (2016) the aim was just to propose values for the SMDA parameters and walking on rigid surfaces was the only condition explored.

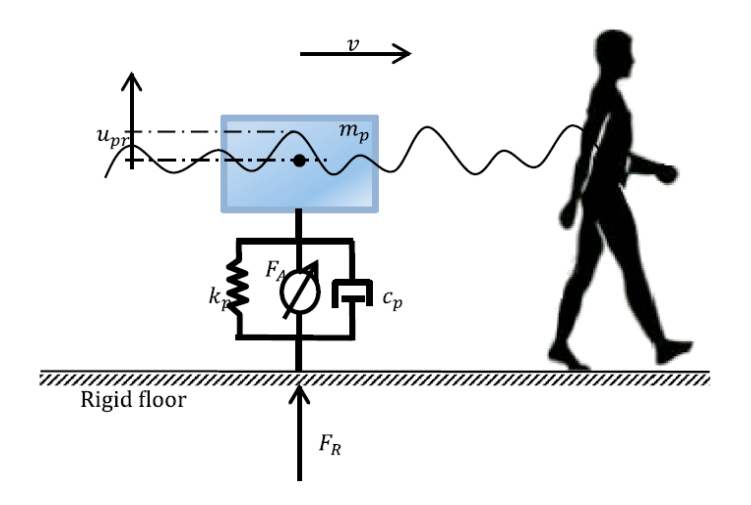


Figure 12 - SMDA biodynamic model (Toso & Gomes, 2018).

The key to understand the effect of the actuator is the condition of walking on a rigid surface, and it is important to explain that this is a conceptual strategy: the actuator can generate forces, whereas spring, damper and mass cannot (Toso & Gomes, 2018). Herein, the interaction forces are then named biomechanical forces.

Conceptually, the simplest biodynamic models, such as MF, SMD and SMDA models, disregard the features of walking by simplifying the kinematics of the body when suppressing the legs' movement from the model's concept and equations. Therefore, the reaction forces resulting from the two feet over time by these models are an approximation for the 'M' characteristic shape observed from experiments (Kerr & Bishop, 2001), and the HSI is assumed to occur through one contact point only at a time.

The development of studies related to the modelling of people walking was also due to considerations about the kinematics of the moving body. With a different treatment of the pedestrian gait, models considering the pedestrian legs were proposed to investigate the walking process more accurately.

Bocian *et al.* (2011) treated the pedestrian as a biomechanical model (without stiffness and damper) as an Inverted Pendulum (IP) in the analysis of the interaction between pedestrian and structure (Figure 13a). This is because studies of biodynamic models that could predict the bidirectional effects of the walking process (vertical and lateral) were deficient. Initially, the IP

model application aimed to analyse the details of the gait, being an interesting model to insert temporal and spatial walking parameters.

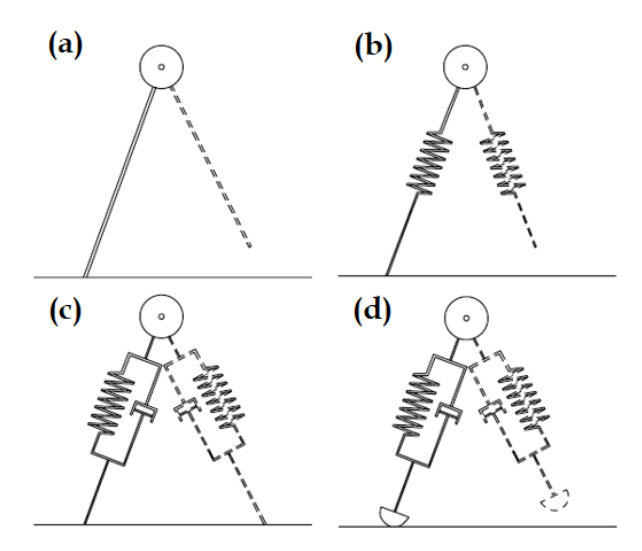


Figure 13 – Inverted pendulum biodynamic models with (a) mass concentrated on rigid legs; (b) mass and legs' stiffness; (c) mass, legs' stiffness, and damping; (d) mass, legs' stiffness, and damping with roller feet. (After Shahabpoor *et al.*, 2016b)

Besides, one of the targets of IP models is to reproduce the Ground Reaction Force (GRF) with more accuracy (Lin et al., 2023; Živanović et al., 2022). Among these models, as an improvement of the IP Model, Bipedal Models (BM) (as seen in Figure 13b, c and d) can simulate all phases of human walking and get a smoother trajectory of Centre of Mass (CoM) by considering each leg's movement and contact with the ground (Qin et al, 2013). The basic concept of a BM consists of a lumped mass concentrated at the body CoM (at the waist level) and attached to two symmetrical massless legs. Some of these models can even consider the leg's stiffness and damper, and additionally, more complex features such as roller feet and actuators (Shahabpoor et al, 2016a; Živanović et al., 2022).

The model seen in Figure 13b considering leg stiffness can be seen in Geyer (2005), while the consideration of leg damping (Figure 13c) is available in the work presented by Qin *et al.* (2013). Introduced by Whittington & Thelen (2009), the insertion of roller feet helps simulate realistically different phases of foot-ground contact during the gait (Figure 13d).

Bipedal models can evaluate the influence of force transferring from one foot to the other on walking (statistically measured in Racic & Brownjohn, 2011). It is worth mentioning that bipedal models can (Qin *et al.*, 2013; Qin *et al.*, 2014) or not (Mulas *et al.*, 2018) include

the attack angle of the leg. The latter considers the position of the centre of mass (CoM) in the body kinematics, as shown in Figure 14.

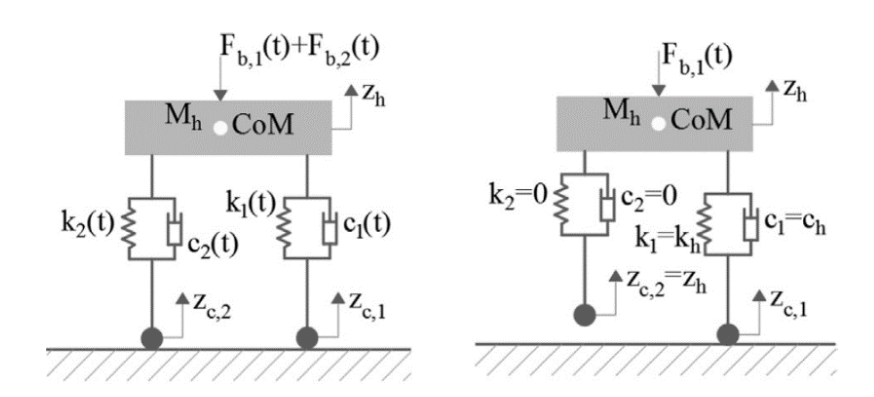


Figure 14 – Bipedal model without attack angle of the feet (After Mulas et al., 2018).

Although significant progress has been made in the field of structural dynamics, with continued efforts to improve biodynamic models through both analytical and experimental approaches, the statement by Shahabpoor *et al.* (2016a) remains highly relevant: "There is an urgent need for a detailed and extensive experimental and analytical research on the underlying mechanisms of the HSI during walking." This need persists, particularly in light of the complexity and variability still observed in experimental findings related to human-structure interaction.

All conceptual differences among human walking models presented in the literature, along with their respective advantages, are beyond the scope of the present study. However, two biodynamic models stand out among the proposals in the literature due to their practical applications in the field of Civil Engineering: the SMD models and Bipedal Models (from the IP family). These two biodynamic models were chosen for further investigation and correlation with experimental results. In the following, a discussion about their formulation and parameters is presented.

2.4.1 SMD models

2.4.1.1 Concepts and formulation

The first model known to the authors that proposed the modelling of a moving pedestrian as a dynamic system when calculating footbridge vibrations was proposed in Archbold (2004),

see also Fanning *et al.* (2005). Being called later on in the literature as a Moving Oscillator, this model consists of applying a ground reaction force F(t) (Eq. (6)) produced from walking on a rigid surface, simultaneously with an SMD model, the latter representing the dynamics of the pedestrian body.

It should be noted that there is no specific analytic formulation presented in Archbold (2004) and Fanning *et al.* (2005) to represent the interaction between pedestrian and footbridge. This proposal is, thus, just a procedure to include the dynamics of pedestrian. This same procedure was adopted by Silva *et al.* (2013).

A first analytical formulation to account explicitly for the interaction between pedestrian and footbridge can be found in the work of Caprani *et al.* (2011). It is considered that the ground reaction force produced by the pedestrian is the sum of elastic spring and dissipative forces, that is, the force is transmitted to the mass of the pedestrian through the spring and damper, while walking on a rigid or on a flexible surface.

The outcome of this formulation is that the ground reaction force is equal to the respective inertia force in each case, as will be shown later. Venuti *et al.* (2016) adopted the formulation of Caprani *et al.* (2011), but with a difference that the former opted to express the interaction force as the sum of the elastic spring and damping forces instead of the inertia force, which led to a different arrangement of terms in the formulation. Shahabpoor *et al.* (2016b) also adopted this formulation, for investigating the action of a pedestrian flow, which was assumed as continuous and stationary.

This formulation was employed with some modifications by Pfeil *et al.* (2014). First, a function was introduced to represent the up and down movement of the heels. One can think of this function as a conceptual cause of the up and down movement of the pedestrian. However, in the development of the formulation, it can be inferred that this function could be suppressed without affecting the equations of motion.

This way, by omitting this function for the sake of clarity, the model adopted by Pfeil *et al.* (2014) can be seen in Figure 15: a walking person represented as a SMD model, with respective modal mass (m_p) , damping (c_p) and stiffness (k_p) . By considering the equilibrium at the pedestrian's centre of mass (COM) and at contact point, the equation of motion of the pedestrian can be expressed in Eqs. (9) and (10), while walking on rigid and flexible surfaces, respectively.

$$F(t) = -c_p \, \dot{u}_{pr} - k_p \, u_{pr} = m_p \, \ddot{u}_{pr} \tag{9}$$

$$F_{int}(t) = -c_p (\dot{u}_{pr} + \dot{u}_p - \dot{u}_s) - k_p (u_{pr} + u_p - u_s) = m_p (\ddot{u}_{pr} + \ddot{u}_p)$$
(10)

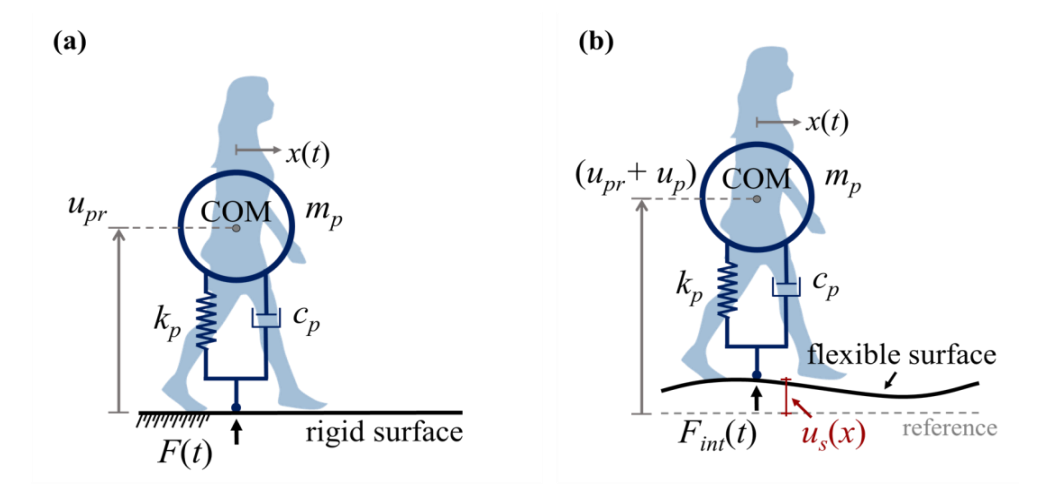


Figure 15 – The SMD model (a) on a rigid surface and (b) on a flexible surface (After Pfeil *et al.*, 2014).

In Eqs. (9) and (10), u_{pr} is the vertical displacement of the pedestrian's CoM while walking on a rigid surface; u_p is the vertical displacement while walking on flexible surface which takes into account the pedestrian-structure interaction; and u_s is the vertical displacement of the structure at the contact point. It should be noted, as indicated in Figure 15, that the forces F(t) and $F_{int}(t)$ represented in these equations act on the pedestrian. Equal and opposite forces are acting on the structure.

Considering all this, Pfeil *et al.* (2014) explicitly showed that the ground reaction force from the rigid surface F(t) could be introduced into the expression of the interaction force $F_{int}(t)$ while walking on a flexible surface. This is directly obtained by manipulating Eqs. (9) and (10). Then, by turning around F(t) and $F_{int}(t)$, in order to apply them at the structure, Eq. (11) is obtained:

$$F_{int}(t) = c_p \left(\dot{u}_p - \dot{u}_s \right) + k_p \left(u_p - u_s \right) + F(t)$$
(11)

The introduction into the formulation of the interaction displacement u_p as a part of the total displacement of the pedestrian's COM while walking on flexible surfaces, led to a difference in this formulation when compared to the ones adopted by the aforementioned

authors (Caprani et al., 2011; Venuti et al., 2016; Shahabpoor et al., 2016b). Adoption of u_p is necessary if the ground reaction force from walking on the rigid surface is to be employed into the formulation of walking on the flexible surface. The outcome is that the total displacement of the COM of the pedestrian while walking on a flexible surface $(u_p + u_{pr})$ differs from that adopted by Caprani et al. (2011).

The equation of motion of the pedestrian body, in terms of the interaction displacement u_p , can be obtained by combining Eqs. (9) and (10):

$$m_p \ddot{u}_p + c_p (\dot{u}_p - \dot{u}_s) + k_p (u_p - u_s) = 0$$
 (12)

Now, by using the concept of modal superposition, a coupled system (pedestrianstructure) with two degrees of freedom is formulated. For this purpose, the structure displacement (u_s) at the contact point, assuming a single mode structural response, can be expressed as:

$$u_s(x) = \phi_i(x) y_i \tag{13}$$

where y_i is the general coordinate corresponding to the i^{th} mode with the respective mode shape $\phi_i(x)$, and x stands for the pedestrian position at the structure.

Reminding that modal superposition equation is given by:

$$m_i \ddot{y}_i + c_i \dot{y}_i + k_i y_i = P_i$$
 (14)

where m_i , c_i and k_i are the modal mass, damping and stiffness of the i^{th} mode of the structure, and P_i is the generalized force, given by:

$$P_i = \phi_i(x) F_{int}(t) \tag{15}$$

The equation of motion of the joint pedestrian-structure system (unknowns y_i and u_p) can be expressed by Eq. (16), obtained by substituting Eq. (15) into (14), and considering Eqs. (11) and (13).

$$m_i \ddot{y}_i + (c_i + \phi_i^2 c_p) \dot{y}_i + (k_i + \phi_i^2 k_p) y_i - \phi_i c_p \dot{u}_p - \phi_i k_p u_p = \phi_i F(t)$$
 (16)

The coupled pedestrian-structure system can be also written in a matrix form, as stated by Pfeil *et al.* (2014):

$$\mathbf{M} \ddot{\mathbf{U}} + \mathbf{C} \dot{\mathbf{U}} + \mathbf{K} \mathbf{U} = \mathbf{F} \tag{17}$$

where,

$$\mathbf{M} = \begin{bmatrix} m_i & 0 \\ 0 & m_p \end{bmatrix}, \quad \mathbf{C} = \begin{bmatrix} c_i + \phi_i^2 c_p & -\phi_i c_p \\ -\phi_i c_p & c_p \end{bmatrix}, \quad \mathbf{K} = \begin{bmatrix} k_i + \phi_i^2 k_p & -\phi_i k_p \\ -\phi_i k_p & k_p \end{bmatrix},$$

$$\mathbf{F} = \begin{cases} \phi_i F(t) \\ 0 \end{cases} \quad \text{and} \quad \mathbf{U} = \begin{cases} y_i \\ u_p \end{cases}$$

Note that the equations are similar to the ones presented by Venuti *et al.* (2016). However, the variable representing the displacement of the pedestrian's COM herein consists only of the interaction displacement u_p of the COM while walking on a flexible surface. It is worth mentioning that the time varying force F(t) in this formulation consider the first harmonic only, as this usually suffices for analyses of typical footbridges in resonance condition. This study does not aim the investigation of crowd loads. For this end the reader is referred to the work of Venuti *et al.* (2016).

A slight modification of this formulation was introduced by Jiménez-Alonso & Sáez (2014) by placing a small part of the pedestrian mass at feet level and in permanent contact with the structure. By doing this, the interaction force $F_{int}(t)$ differs from the expression present in Eq. (10). Nonetheless, bearing in mind that the fraction of the total mass M of the pedestrian that is included in the SMD model (as a modal mass m_p) varies among proposals found in the literature (values will be discussed later), the modification introduced by Jiménez-Alonso & Sáez (2014) did not differ much from the previous formulations.

Finally, Gomez *et al.* (2016) conceived the source of external energy that caused the pedestrian up and down movement as an initial velocity condition applied to the SMD model when the heel hits the ground. By comparing their formulation with the one from Pfeil *et al.* (2014), this initial velocity condition replaced the use of the ground reaction force F(t) (applied on a rigid surface) when formulating the equations for walking on flexible surfaces.

However, this is more a matter of choice about using or not the ground reaction force from walking on a rigid surface into the formulation. It should be noted that using F(t) has advantages since expressions for it are very deeply studied in the literature (Caprani & Ahmadi, 2016; Shahabpoor *et al.*, 2016a).

The formulation from Pfeil *et al.* (2014) slightly modified by the suppression of the function representing the heel movement was, thus, considered as a basic one for SDOF SMD models in this study.

2.4.1.2 SMD parameters

Another aspect regarding the SMD models are the values adopted for the parameters mass, stiffness and damping, and several proposals can be found, in which such values were obtained in different ways. However, comparisons of performance of SMD models and associated parameters among each other and against the same experimental data are scarce or even non-existent.

There are studies that proposed values for the SMD parameters based on experimental tests with walking subjects. One of the first studies was conducted by Silva & Pimentel (2011). Values were determined based on tests with twenty subjects walking on a rigid surface, in which acceleration was measured at waist level only. Regression expressions were then proposed for the modal mass, stiffness, and damping, as a function of the total mass and pacing rate of the pedestrian. In a subsequent work, Silva *et al.* (2013) presented additional linear expressions to obtain stiffness and damping.

The study of Toso *et al.* (2016) also obtained SMD parameters from walking subjects. In this case, the ground reaction force from a rigid surface was measured simultaneously with the body acceleration for thirty-five subjects and used as an input to determine a set of regression expressions for the SMD parameters.

The main feature for obtaining the SMD parameters in these three studies was a formulation in which the equation of motion of the pedestrian assumed that all forces were applied at the pedestrian's COM, including the ground reaction force.

Gomez *et al.* (2016) applied the same test setup as Silva & Pimentel (2011) but enrolling only three subjects and employing a different formulation for the equation of motion (see Section 2.4.1), which led to values for stiffness and damping for each test subject. In addition, they also considered the modal mass as the respective total mass of the test subject.

In all these aforementioned works, the SMD parameters were determined directly from measurements on each individual, walking alone. However, a different approach is reported in other studies, where the values of the SMD parameters were obtained indirectly through measurements of the structural response. This line of reasoning was presented by Jiménez-Alonso & Sáez (2014), and they obtained values for the SMD parameters based on experimental

results carried out by Geogarkis & Jorgensen (2013), in which test subjects walked in group (in varied density scenarios) across a simply supported beam.

By using a genetic algorithm, average values for the SMD parameters for each scenario were obtained, and Jiménez-Alonso & Sáez (2014) concluded that there was no significant variability in the sprung mass, equivalent damping ratio and body natural frequency for different scenarios.

Shahabpoor *et al.* (2016b) also employed tests with group of pedestrians. They assumed that the modal mass was the total mass of the pedestrian and identified a range of values for the body natural frequency and damping.

A synthesis of all these findings is presented in Table 12 and Table 13 where ξ_p and f_{np} are respectively damping ratio and natural frequency of the pedestrian body.

	Silva & Pimentel (2011)	Silva <i>et al.</i> (2013)
$m_p(M, f_s)$	$97.082 + 0.275 M - 37.52 f_s$ (kg)	$97.082 + 0.275 M - 37.52 f_s$ (kg)
$c_p(m_p)$	29.041 $m_p^{0.883}$ (N.s/m)	$107.455 + 16.208 m_p \text{ (N.s/m)}$
$k_p(c_p)$	$30351.744 - 50.261 c_p + 0.035 c_p^2$ (N/m)	$5758.441 + 11.103 c_p \text{ (N/m)}$
	Toso et al.	(2016)
$m_p(M, f_s)$	$-231.34 + 3.69 M + 154.06 f_s - 1.97$	$Mf_s + 0.005 M^2 - 15.25 f_s^2$ (kg)
$c_p(M, m_p)$	$-1115.69 + 92.56 M - 108.94 m_p + 2.91$	$1 M m_p - 1.33 M^2 - 1.30 m_p^2$ (N.s/m)
$k_p(M, f_p)$	$75601.45 - 1295.32 M - 33786.75 f_s + 506$	$5.44 \mathrm{M} f_{\rm s} + 3.59 M^2 + 539.39 f_{\rm s}^2 $

Table 12 – Proposed expressions for the SMD parameters.

Table 13 – Proposed values for the SMD parameters.

	Jiménez Alonso & Sáez (2014)	Gomez et al. (2016)	Shahabpoor <i>et al.</i> (2016b)
m_p (kg)	83.97% of total mass	total mass	total mass
$\xi_{p}\left(\% ight)$	47.18	12 - 18	27.5 - 30
f_{np} (Hz)	2.76	2.29 - 2.52	2.75 - 3.00

2.4.2 Damped Bipedal Models

The interaction between pedestrians and civil structures using Inverted Pendulum (IP) models has been widely studied. However, the majority of these studies has primarily focused on lateral HSI (Macdonald, 2009). The use of an IP model to represent a pedestrian's body in vertical HSI investigations was explored by Bocian *et al.* (2011) and Bocian *et al.* (2013), as promising results had already been reported in the field of biomechanics (Hof *et al.* 2010). In

its simplest form, the pedestrian's body is represented as a single concentrated mass at the centre-of-mass (CoM), attached to a massless, rigid leg (Bocian *et al.*, 2011). In this basic version of the IP model, interaction forces are transmitted to the ground through a single point, around which the CoM oscillates. Additionally, body weight transfer from one leg to the other occurs instantaneously. Because of that, an impulse force must be applied to take into account the superposition of footfall forces at the double-support phase, during which both feet are in contact with the ground (Lin *et al.*, 2023).

An improvement to the IP model introduced by Qin *et al.* (2013) and shown in Figure 16a was chosen to represent a walking pedestrian in this study. Also referred to in the literature as a Bipedal Model (BM), this IP walking model with damped compliant legs is capable of simulating all phases of walking, including the simultaneous stance phase of both legs. This feature enables the simulation of the gradual transfer of force from one leg to the other during walking, making it possible to isolate the force of each footfall, resulting in the 'M-shape' pattern of the vertical GRF generated by each leg, as widely observed experimentally (Ruiz *et al*, 2022; Kerr & Bishop, 2001).

This study does not focus on the detailed discussion of the concepts and formulation of the adopted IP model. For this end, the reader can find an in-depth exploration of the nuances of this Damped Bipedal Inverted Pendulum (DBIP) model in Qin *et al.*, (2013), Lin *et al.*, (2020) and Ruiz *et al.* (2022). Thus, only key insights into the model's functioning and formulation are described below for further reference in this study.

Additionally, as later discussed in Chapter 3, the experimental data for vibrating scenarios were obtained from predefined periodic base movements, which do not accurately represent the actual behaviour of structures under human loads. Therefore, since this study also focuses solely on the S2HI effects, the formulation briefly outlined below is derived from rigid surface scenarios (Ruiz *et al.*, 2022). A procedure to add base movement to this formulation is then presented in Section 2.4.2.2. A model parameters' discussion is presented in Section 2.4.2.3, followed by the HSI formulation adopting DBIP models in Section 2.4.2.4 (from Qin *et al.*, 2013).

2.4.2.1 Concepts and formulation

In principle, the model features two-degrees-of-freedom (2DOF) at the sagittal plane (x and z, as shown in Figure 16a), with the mass (m_h) concentrated at the centre-of-mass (CoM) – usually at waist level. Each leg is modelled using a massless linear spring and a time-varying damper connected in parallel. The model overlooks potential locomotion impairments by assuming symmetrical legs, which leads to identical stiffness (k_{leg}) and damping coefficients (c_{leg}) for both legs. Moreover, the progression of the centre of pressure during stance phase – which can be simulated by adopting a roller foot (Whittington & Thelen, 2009) – is neglected in this model, for which each leg assumes a single point (henceforth referred to as the Foot Point, or FP – see Figure 16a) in contact with the ground.

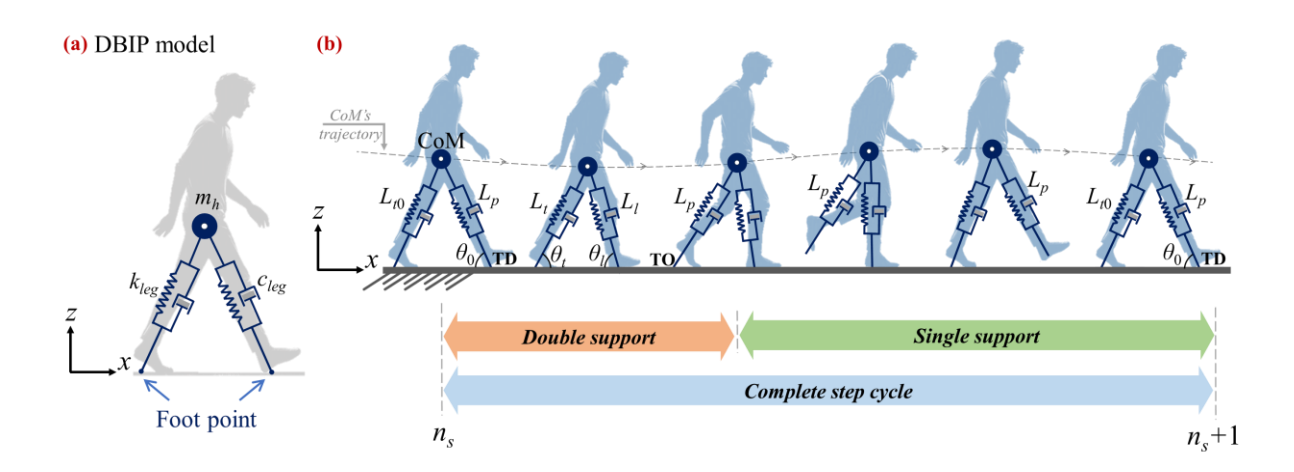


Figure 16 – Human walking model (a) as a Damped Bipedal Inverted Pendulum, and (b) respective phases of walk (DBIP Model after Qin *et al.*, 2013).

Despite the intra-variability of walking (Živanović *et al.*, 2005a) and its complexity, these models simplify the walking motion by considering a periodic movement and featuring the same initial conditions for every gait cycle, which is achieved every time the same gait event for opposite feet is achieved.

A step cycle, defined as the interval between successive heel-strikes, can be divided into two main stages (Figure 16b): the double support (DS) phase, when both feet are in contact with the ground (resulting in the superposition of each leg's GRFs), and the single support (SS) phase, when one leg – often referred to as *leading leg* – supports the body weight, while the other leg – *trailing leg* – swings moving toward the next point of impact positioned ahead the CoM.

The model can simulate the back-and-forth transition between the DS and SS phases (as illustrated in Figure 16b), based on the concept of the pendulum leg's length, L_p , also known as resting length, and the attack angle, θ_0 , which represents the leading leg orientation at the touch down (TD) event.

Once L_p mathematically represents the trailing leg's length during the swinging phase, the TD occurs when the virtual leg's length – or more precisely, the distance from the CoM to the next impact point (discussed later) – decreases to L_p after the vertical leg orientation (VLO) event (when the longitudinal position of the CoM equals that of the FP in the SS phase). This condition marks the beginning of the DS phase illustrated in Figure 1b, as expressed in Eq. (18).

$$z = L_p \sin \theta_0 \tag{18}$$

The transition from the DS to the SS phase occurs when the trailing leg's GRF decreases to zero, meaning the leg touches off (TO) the ground. Mathematically this happens when the trailing leg's length, L_t , reaches or exceeds the maximum leg extension, L_p .

As reported by Lin *et al.* (2023) and Qin *et al.* (2013), by incorporating leg damping into the model, a periodic human walking behaviour can be generated, exhibiting typical step frequencies and DLFs. In this matter, Qin *et al.* (2013) made it clear that a time-variant damper should be considered to ensure zero forces at the time the foot touches the ground. These authors presented a hypothesis that the sum of both legs damping (c_l and c_t , for leading and trailing leg, respectively) should be c_{leg} at any time, even at the DS phase. To ensure that, c_l and c_t in Eqs. (19) are expressed in terms of the damping transition coefficient $\alpha(t)$ given in Eq. (21) at any time instant (t).

$$c_{l} = \alpha(t)c_{leg}$$

$$c_{t} = (1 - \alpha(t))c_{leg}$$
(19)

$$\alpha(t) = \frac{L_t(t) - L_{t0}}{L_p - L_{t0}}$$
 (20)

$$c_{leg} = 2\xi \sqrt{k_{leg} m_h} \tag{21}$$

Where L_{t0} is the trailing leg's length at the beginning of the DS phase, ξ is the damping ratio, and subscriptions t and l refer to trailing and leading leg, respectively. A different approach can be seen in Lin et al. (2023) (adopted in Lin et al., 2020), where these authors adopt a time-varying damper as a function of elastic forces. For the present study, the damping transition from one leg to the other at the DS phase is computed through Eqs. (18) and (19).

The pedestrian's equation of motion can be derived from the force balance at the CoM (with adjustments from Ruiz *et al.*, 2022) and is expressed in its matrix form in Eq. (22).

$$\begin{bmatrix} m_h & 0 \\ 0 & m_h \end{bmatrix} \begin{pmatrix} \ddot{z} \\ \ddot{x} \end{pmatrix} + \begin{bmatrix} c_1 + c_2 & c_4 - c_3 \\ c_4 - c_3 & c_{leg} - c_1 - c_2 \end{bmatrix} \begin{pmatrix} \dot{z} \\ \dot{x} \end{pmatrix} + \begin{bmatrix} k_{l,z} + k_{l,z} & 0 \\ 0 & k_{l,x} - k_{t,x} \end{bmatrix} \begin{pmatrix} z \\ \chi \end{pmatrix} = \begin{pmatrix} -m_h g \\ 0 \end{pmatrix}$$
(22)

Where $m_h g$ is the pedestrian total weight. The damping and stiffness terms of the respective matrices are given by Eqs. (23) and (24).

$$c_{1} = c_{l} \sin^{2} \theta_{l}$$

$$c_{2} = c_{t} \sin^{2} \theta_{t}$$

$$c_{3} = c_{l} \sin \theta_{l} \cos \theta_{l}$$

$$c_{4} = c_{t} \sin \theta_{t} \cos \theta_{t}$$
(23)

$$k_{l,z} = k_{leg} \left(1 - \frac{L_p}{L_l(t)} \right)$$

$$k_{t,z} = k_{leg} \left(1 - \frac{L_p}{L_t(t)} \right)$$

$$k_{l,x} = k_{leg} \left(1 - \frac{L_p}{L_l(t)} \right) \left(\frac{x_l}{x(t)} - 1 \right)$$

$$k_{t,x} = k_{leg} \left(1 - \frac{L_p}{L_l(t)} \right) \left(1 - \frac{x_t}{x(t)} \right)$$

$$(24)$$

Where θ is the leg orientation. The legs' length $L_l(t)$ and $L_l(t)$ are computed through Eq. (25) as a function of the CoM's position (x(t) and z(t)) and the feet positions, x_l and x_t (discussed later).

$$L_{l}(t) = \sqrt{(x_{l} - x(t))^{2} + z(t)^{2}}$$

$$L_{t}(t) = \sqrt{(x(t) - x_{t})^{2} + z(t)^{2}}$$
(25)

Eq. (22) describes the pedestrian's vertical and longitudinal motion based on the balance of inertial, elastic, and dissipative forces at the CoM. In turn, the GRFs are transmitted to the ground through the spring and damper of each leg. Considering the legs' orientation θ during the DS phase, the GRF vertical component of each leg is given by Eq. (26) (Ruiz *et al.*, 2022).

$$GRF_{l} = (F_{s,l} + F_{d,l}) \sin \theta_{l}$$

$$GRF_{t} = (F_{s,t} + F_{d,t}) \sin \theta_{t}$$
(26)

Where the elastic forces, $F_{s,l}$ and $F_{s,t}$, and the dissipative forces, $F_{d,l}$ and $F_{d,t}$, are given by:

$$F_{s,l} = k_{leg} (L_l(t) - L_p)$$

$$F_{s,t} = k_{leg} (L_t(t) - L_p)$$

$$F_{d,l} = \alpha(t) c_{leg} v_l$$

$$F_{d,t} = (1 - \alpha(t)) c_{leg} v_t$$
(27)

The axial velocities v_l and v_t in Eq. (28) are obtained by deriving Eq. (25) with respect to time, and given by:

$$v_l = -\dot{x}(t)\cos\theta_l + \dot{z}(t)\sin\theta_l$$

$$v_t = \dot{x}(t)\cos\theta_t + \dot{z}(t)\sin\theta_t$$
(28)

It is important to note that all equations from Eq. (22) to Eq. (28) were assembled considering the DS phase. For the SS phase, these equations can still be applied by setting all variables related to the trailing leg to zero, except for $\alpha(t)$, which remains equal to 1.

The 2DOF mathematical model described above is capable of reproducing a gait cycle. However, after a few cycles, the model begins to dissipate energy due to the damping system, hindering the simulation of a periodic gait. Hence, a feedback mechanism to compensate such energy loss, and prevent the model to fall or move backwards, must be applied to maintain a stable gait (Qin *et al.*, 2013; Lin *et al.*, 2020).

In the literature (Qin *et al.*, 2013; Lin *et al.*, 2020), the compensation for energy loss in 2DOF DBIP models is based on the energy differential ΔE given by Eq. (29).

$$\Delta E = E(t) - E_0 \tag{29}$$

At any given time instant (t), the total energy E(t) in Eq. (29) is composed of the kinetic energy and gravitational potential energy of the CoM, along with the elastic potential energy stored in the leg springs, as can be seen in Eq. (30). E₀ is the initial energy input.

$$E(t) = \frac{1}{2} \left(m_h \dot{z}(t)^2 + m_h \dot{x}(t)^2 + k_{leg} \Delta L_l^2 + k_{leg} \Delta L_t^2 \right) + m_h g z(t)$$
(30)

Provided a reasonably small-time increment Δt is considered, it can be assumed that the quantity E(t) remains constant within the integration step. However, at the start of each time step, it is necessary to reassess the system's energy and implement a feedback mechanism to compensate for energy loss when ΔE is negative. To ensure that the total energy remains constant and preventing the system from slowing down or collapsing due to energy dissipation, one possible approach (Qin *et al.*, 2013) is to apply one hypothetical longitudinal impulse force acting on the CoM. This so-called control force, F_{ctrl} , can be calculated through Eq. (31), based on the assumption that the external work applied in the horizontal direction is equal to the energy lost in the system over time.

$$F_{ctrl} = \frac{\Delta E}{\Delta x(t)} \tag{31}$$

In Eq. (31), Δx is the horizontal displacement increment of CoM at the time t. When F_{ctrl} is included in the pedestrian's equation of motion, the force vector on the right-hand side of Eq. (22) is rewritten to incorporate the feedback mechanism in the longitudinal degree of freedom. It is important to emphasize that F_{ctrl} is not a force constantly acting on the model's CoM, nor does it govern the pedestrian's motion resulting from the balance of forces expressed in Eq. (22). Rather, it is a maneuver designed to reproduce a stable gait and should be reassessed at the end of every time step in simulations.

It should be noted that, in addition to the aforementioned parameters – body mass m_h , leg stiffness k_{leg} , damping coefficient c_{leg} , resting length L_p , and attack angle θ_0 – the energy input E₀ also plays a crucial role in determining the walking gait of the DBIP model (Qin *et al.*, 2013; Lin *et al.*, 2020). Unlike biodynamic models that incorporate an approximation of GRFs through a Fourier series (Pfeil *et al.*, 2014; Pfeil *et al.*, 2022), bipedal models generate a stable

gait by properly combining these parameters. The pedestrian's longitudinal speed v, step frequency f_s and GRFs are inherently determined by the interplay of these parameters that shape the dynamics of the pedestrian gait. Parametric approaches to investigating how the combination of these parameters affects those gait characteristics, such as step frequency and GRFs (Qin *et al.*, 2013; Ruiz *et al.*, 2017), or even to identifying parameter ranges that result in a stable gait (Lin *et al.*, 2020), can be found in the literature.

A simplified approach of the DBIP model can also be found in the literature (Gao *et al.*, 2017; Ruiz *et al.*, 2022), where, by assuming a constant longitudinal speed \dot{x} during walking, there is no need for a feedback mechanism to compensate for energy loss due to the dissipative nature of the formulation. This simplification results in a single-degree-of-freedom (SDOF) DBIP model, self-excited in the vertical direction. As a result, the pedestrian's equation of motion from Eq. (22) can be reduced to Eq. (32), thereby eliminating the need to set the E₀ input parameter.

$$m_h \ddot{z} + (c_1 + c_2)\dot{z} + (k_{l,z} + k_{t,z})z = -m_h g + (c_3 - c_4)\dot{x}$$
 (32)

For the sake of conciseness and further reference in this study, the SDOF DBIP model will be referred to as Bipedal Model 1 (BM₁), and the 2DOF DBIP model will be referred to as Bipedal Model 2 (BM₂).

Furthermore, and equally important, two aspects related to the functioning of these bipedal models still need to be addressed. They are: (1) how to initiate the model's motion, and (2) how to determine the position of the next point of impact. To trigger the models' movement demands setting the so-called initial conditions, which refer to the position (x(0)) and z(0) and velocity $(\dot{x}(0))$ and $\dot{z}(0)$ of the CoM at the beginning of the first step cycle (t = 0). Therefore, it is necessary to define which gait event is considered as the start of the step cycle.

As seen in Eq. (18), the vertical position of the CoM at the TD is directly related to two input parameters of BMs: L_p and θ_0 . This relationship may justify the choice of some approaches in the literature that consider the beginning of the DS phase as the starting point of the step cycle (Qin *et al.*, 2013; Gao *et al.*, 2017; Ruiz *et al.*, 2022). However, in the study by Lin *et al.* (2020) (also used in Lin *et al.*, 2023)), a different approach is adopted, where the step cycle begins at the VLO event, making it unnecessary to define the first step length. It is important to emphasize that the choice of the gait event that defines the beginning of the walking cycle is a methodological decision, and this does not affect the conceptual assumptions

of the model. This definition influences only the mathematical – and possibly experimental – approach used to determine the initial conditions of the step cycle. In this present study, the TD event was chosen as the start point of the step cycle.

Still regarding the selection of initial conditions, another aspect should be briefly mentioned. As previously emphasized, the gait features and induced forces generated by bipedal models result from the choice of the model's parameters. For each combination of parameters in a bipedal model (five for BM₁ or six for BM₂) that leads to a stable gait, there is only one specific set of initial conditions that defines the beginning of each step after the model converges. If such a set is not adopted, a few unstable steps will occur before stabilization, as can be seen in Figure 17. This highlights the importance of properly setting the initial conditions so that model convergence is achieved after just a few cycles, bearing in mind that not any values of initial conditions lead to a stable gait.

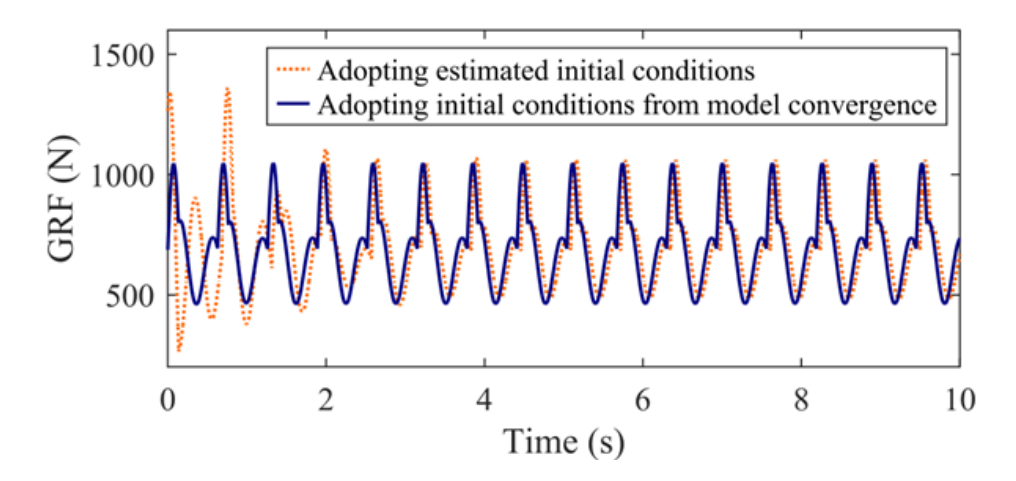


Figure 17 - Typical GRFs generated by BMs from two set of initial conditions: adopting estimated initial conditions, and adopting initial conditions obtained from step cycles after model convergence

Unlike the selection of initial conditions to set bipedal models into motion, which mainly affects the model convergence, the mathematical definition of the next impact point (x_p) , which directly affects the transition to the next step n_s , can have implications both on model convergence and on gait parameters.

In this regard, as observed in Figure 18a, defining x_p requires setting one of the gait parameters: step length d_s or attack angle θ_0 . In the case of setting d_s as equal to the first step length d_{s0} (Figure 18b), – meaning the distance from x_p to leading leg's foot point (x_l) position is d_{s0} – the attack angle after model convergence tends to differ from the initial input θ_0 . This

approach may not be suitable for moving surface scenarios, as x_p is determined solely by d_{s0} , disregarding the CoM trajectory during the SS phase. In this scenario, the positions of both feet, x_l and x_t , in every step number n_s can be computed by:

$$x_l = n_s d_{s0} x_t = (n_s - 1)d_{s0}$$
 (33)

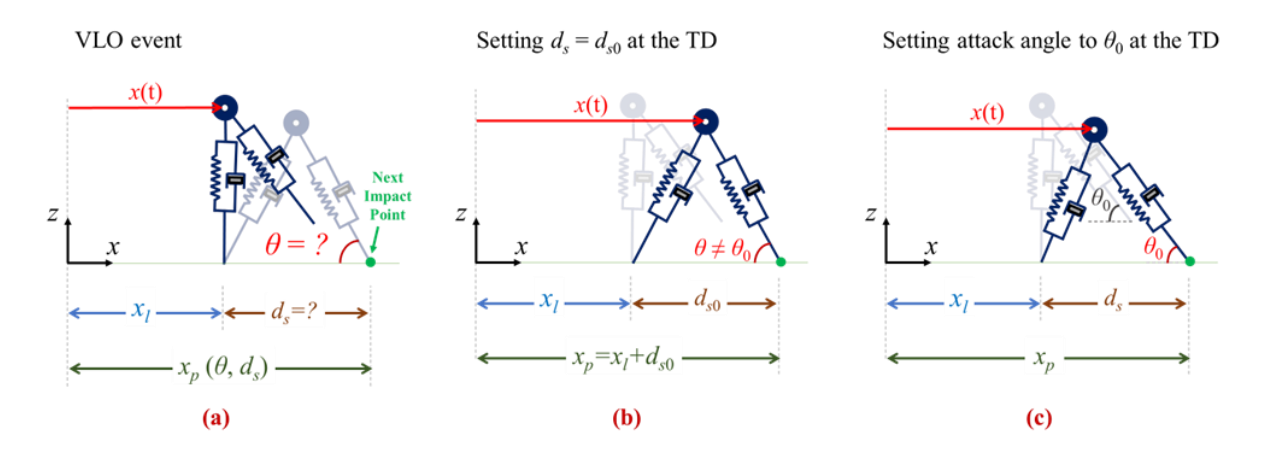


Figure 18 – Next impact point x_p definition (a) as a function of d_s and θ , (b) predicting x_p by setting d_s = d_{s0} , and (c) predicting x_p by setting the attack angle at the TD as θ_0 .

The opposite occurs when the attack angle θ_0 is chosen to remain constant for every step cycle. In this case, x_p is continuously updated from the VLO event until the TD. It is computed as the *x-intercept* of the linear projection of the trailing leg with a fixed angle (θ_0) and the surface (rigid or moving surface), as illustrated in Figure 18c. In this case, the feet positions should be updated when the next step begins (at the TD). Conversely, the step length d_s , initially set as d_{s0} in the initial conditions – including x_l and x_t for the first step – tends to converge to a (different) stable value.

In both cases, convergence occurs because the model adapts its gait to repeat the same initial conditions in every step cycle, thereby achieving a stable gait. The extent to which the choice of the parameter (either the attack angle or the step length) governing the definition of the next impact point affects the model, as well as its implications, will be discussed in Chapter 4.

2.4.2.2 Procedure to simulate moving surface scenarios

HSI formulations presented in the literature can incorporate the reciprocal effects of the coupled system through the mutual influence between the occupant (or crowds as in Venuti *et al.*, 2016) and the structure. This is achieved by coupling these two (or more, in the case of crowds) dynamic systems involved and investigating the effects that such an interaction loop has on the human-structure system behaviour. While the presence of the pedestrian on the structure can alter its dynamic properties (H2SI), conversely, the surface vibrations affect the kinetics and kinematics of the pedestrian's body (S2HI).

The procedure described here does not result in a formulation for a HSI system adopting DBIP models. For this purpose, the reader is referred to the Section 2.4.2.4. The approach presented in this subsection focuses on incorporating periodic base displacements into the pedestrian mathematical model to investigate the effects of vibrations on gait features and induced forces, thereby investigating only the S2HI effects.

While the kinetics resulting from the pedestrian model's movement depend solely on the CoM motion for analyses on rigid surface (Lin *et al.*, 2020; Ruiz *et al.*, 2022), in cases where surface vibrations are present, the combined kinematics of the CoM and, in the context of this study, the vertical displacement of the surface must be taken into account. Therefore, in the analysis of S2HI effects, both the relative vertical position of the feet during the stance phase must be incorporated into the formulation, and the vertical base displacement must be considered to compute the next impact point.

The moving surface scenario depicted in Figure 19 is simulated by incorporating a sinusoidal periodic signal for the vertical displacement y(t) of the surface described in Eq. (34).

$$y(t) = d_{max} \cdot \sin(2\pi f t + \phi)$$
(34)

Where d_{max} is the maximum amplitude surface displacement, calculated from a predefined pair of acceleration a_{max} and surface frequency f, as described in Eq. (35). ϕ is the phase angle.

$$d_{max} = \frac{a_{max}}{(2\pi f)^2} \tag{35}$$

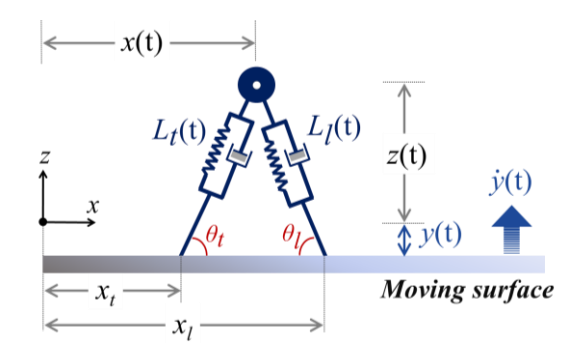


Figure 19 – Moving surface scenario for a given instant t during DS phase

Importantly, differing from HSI formulations adopting DBIP models (discussed in the Section 2.4.2.4), the vertical displacement *y* is constant for every point of the moving surface in any given instant. This means that both feet have the same vertical position during the DS phase. As observed from Figure 19, to incorporate such base motion into the pedestrian's model formulation, the calculation of the legs' length must be rewritten as given by Eq. (36).

$$L_{l}(t) = \sqrt{(x_{l} - x(t))^{2} + (z(t) - y(t))^{2}}$$

$$L_{t}(t) = \sqrt{(x(t) - x_{t})^{2} + (z(t) - y(t))^{2}}$$
(36)

Therefore, the axial velocities in Eq. (28) and the coefficients for the vertical degree of freedom in the stiffness matrices in Eq.(22) for BM₂, and in Eq. (32) for BM₁, should be rewritten as:

$$v_l = -\dot{x}(t)\cos\theta_l + (\dot{z}(t) - \dot{y}(t))\sin\theta_l$$

$$v_t = \dot{x}(t)\cos\theta_t + (\dot{z}(t) - \dot{y}(t))\sin\theta_t$$
(37)

$$k_{l,z} = k_{leg} \left(1 - \frac{L_p}{L_l(t)} \right) \left(1 - \frac{y(t)}{z(t)} \right)$$

$$k_{t,z} = k_{leg} \left(1 - \frac{L_p}{L_t(t)} \right) \left(1 - \frac{y(t)}{z(t)} \right)$$
(38)

Where $\dot{y}(t)$ is the vertical surface velocity, obtained by differentiating y(t) with respect to time. Moreover, the computation of sines and cosines for the legs' orientation over time should align with the configuration shown in Figure 19.

It should be noted that Eqs. (36) to (38) account for the surface movement and its effects on the pedestrian model motion, thus simulating S2HI effects. While similar expressions appear in HSI formulations adopting DBIP models, as explained further in the Section 2.4.2.4, the ones presented here differ slightly, as they do not take into account the deflection and velocity of the structure at each foot's position based on the mode shape of the respective investigated structural modes (Qin *et al.*, 2013; Gao *et al.*, 2017; Ruiz *et al.*, 2017).

2.4.2.3 <u>DBIP models' parameters</u>

Ruiz *et al.* (2022) appears to be the first work to experimentally validate a DBIP model, to the best of the authors' knowledge. Their work proposed regression expressions for the model parameters based on the correlation between kinematic and kinetic data extracted from controlled test experiments conducted on a purpose-built platform. Ruiz *et al.* (2017) had previously concluded that, for the investigated acceleration levels (around 0.16 m/s²), there were no significant differences between the results obtained on a rigid surface and those on flexible surfaces when applying a HSI formulation adopting bipedal models.

Bearing this in mind, the experimental calibration of the adopted bipedal model was based on measurements taken on a rigid surface (with very low acceleration levels). It is worth mentioning that in their work kinematic data were limited to acceleration measurements at the test subjects' waist level. The lack of additional pedestrian body measurements and low vibration levels hindered a more profound investigation of the S2HI.

Ruiz *et al.* (2021) had previously proposed different parameters expressions, and a better statistical approach provided better regression expressions in Ruiz *et al.* (2023). Table 14 and Table 15 gathers those expressions for the DBIP model parameters and initial conditions introduced by these authors. Additionally, some ranges for bipedal models compiled by the same authors and also considered in the present study are presented in Table 14. It is worth noting that the independent parameters are pedestrian's body mass m_h , height h, and walking speed v (as \dot{x} is constant once those authors adopted the BM₁).

The ranges of parameters for bipedal models presented in Table 14 were proposed or from identification from experimental tests (Whittington & Thellen, 2009; Kim & Park, 2011; Li *et al.*, 2019) or from a parametric study approach (Qin *et al.* (2013), and Lin *et al.*, 2020).

Table 14 – Expressions and Ranges for DBIP model parameters found in the literature from Ruiz et al. (2021) and Ruiz et al. (2022).

Parameters	Expressions (*) (**)	Ranges for bipedal models		
	Ruiz et al. (2022)	Ruiz et al. (2021)		
$f_s(Hz)$	-	-	1.42 - 2.42	
\dot{x} (m/s)	-	-	0.80 - 2.20	
$L_p(\mathbf{m})$	$= 0.24 + 0.37h + 0.21\dot{x}$	$= 0.52 + 0.11h + 0.34\dot{x}$	0.98 - 1.26	
$d_s(m)$	$= 0.13 + 0.28h + 0.22\dot{x}$	$= -0.16 + 0.28h + 0.27\dot{x}$	Depends on f_s and \dot{x}	
k_{leg} (N.m ⁻¹)	$=222.7m_h+5531$	$=233m_h+2989$	13000 - 34000	
ξ_{leg} (%)	$=2.98+0.05m_h+0.01\dot{x}$	$= -0.27 + 0.02m_h + 4.98x$	3 - 13	
\dot{z}_0 (m/s)	$=-0.13\dot{x}-0.05$	$=-0.16\dot{x}-0.06$	No range informed	
θ_0 (°)	$=71.3+2.66L_p-2.74\dot{x}$	$=63.1+9.67L_p-3.19\dot{x}$	68 - 74	

^(*) h stands for the pedestrian height.

Table 15 - Expressions for DBIP model parameters found in the literature from Ruiz et al. (2023).

Parameters	Expressions (*)(**)
	Ruiz et al. (2023)
$L_p(\mathbf{m})$	$=48.69-51.8h-51.79\dot{x}+14.16h^2+51.39h\dot{x}+7.85\dot{x}^2-12.99h^2\dot{x}-3.40h\dot{x}^2-0.59\dot{x}^3$
$d_s(m)^{(***)}$	$=0.64+0.03\overline{h}+0.07\overline{x}-0.001\overline{h}^2-0.007\overline{h}\overline{x}-0.005\overline{x}^2-0.001\overline{h}^2\overline{x}-0.008\overline{h}\overline{x}^2-0.014\overline{x}^3$
k_{leg} (kN.m ⁻¹)	$= -384.1 + 2.051 m_h + 938.6 \dot{x} - 0.017 m_h^2 - 2.024 m_h \dot{x} - 756.8 \dot{x}^2 + 0.017 m_h^2 \dot{x} + 0.114 m_h \dot{x}^2 + 211.6 \dot{x}^3$
$\xi_{leg}(\%)$	$= -512.6 + 15.13m_h + 464.2\dot{x} - 0.121m_h^2 - 11.58m_h\dot{x} - 71.08\dot{x}^2 + 0.06m_h^2\dot{x} + 1.3m_h\dot{x}^2 + 0.0002m_h^3$
\dot{z}_0 (m/s)	$=0.4486\dot{x}-0.1457$
θ_0 (°)	= $114.7 - 49.53L_p - 34.86\dot{x} - 14.94L_p^2 + 78.03L_p\dot{x} - 23.27\dot{x}^2$

^(*) h stands for the pedestrian height.

$$(***) \overline{h} = \frac{h-1.671}{0.078}, \overline{\dot{x}} = \frac{\dot{x}-1.195}{0.178}$$

Lin et al. (2023) also proposed regression expressions based on the experimental calibration of the bipedal model adapted in Lin et al. (2020). Although only rigid surface scenarios were investigated with pedestrians walking on a treadmill, a more complex experimental setup enabled a richer collection of synchronized kinematic and kinetic data providing promising results for rigid surface scenarios. These authors focus on a different approach from that of Ruiz et al. (2022) when, in addition to m_h , v, and h, the step frequency f_s and DLF₁ are the independent parameters. These expressions are presented in Table 16.

Table 16 – Regression Expressions proposed by Lin et al. (2023)

Parameter	Expression (*)
k_{leg} (N/m)	$= 14073.014 + 213.814m_h + 21414.521f_s - 20183.358v$
L_p (m)	=0.394+0.507h
$E_0(J)$	$=a_Ef_s+b_E$
$ heta_0$ (°)	$=a_{ heta}f_{s}+b_{ heta}$
a_E (J/Hz)	$=7.339-74.799DLF_1+0.290m_h+21.064v-9.869f_s$
$b_E(\mathrm{J})$	$=-87.926+13.579m_h$
$a_{\theta}(\text{deg/Hz})$	$= 11.624 + 24.274 DLF_1 - 4.932 f_s - 2.971 v$
b_{θ} (deg)	$=47.147-58.499DLF_1+16.091f_s$

^(*) For $52 \text{kg} < m_h < 87 \text{kg}$, 1.60 m < h < 1.83 m, and 1.04 m/s < v < 1.33 m/s

^(**) For $55 \text{kg} < m_h < 95 \text{kg}$, 1.60 m < h < 1.75 m, and $0.90 \text{m/s} < \dot{x} < 1.40 \text{m/s}$

^(**) For 55kg < m_h < 95kg, 1.60m < h< 1.75m, and 0.90m/s < \dot{x} < 1.40m/s (***) $\bar{h} = \frac{h-1.671}{0.078}$, $\dot{\bar{x}} = \frac{\dot{x}-1.195}{0.178}$

2.4.2.4 HSI formulation

The formulation presented in Sections 2.4.2.1 and 2.4.2.2 focus solely on the pedestrian modelling, including or not periodic surface movement. In this subsection the coupled human-structure system formulation is presented, considering both DBIP model versions (BM₁ and BM₂).

The equation of motion governing the interaction between pedestrian and structure can be obtained through the Lagrangian Equation at the double support (DS) phase depicted in Figure 20 (Qin *et al.*, 2013). Based on the modal superposition, for the 2DOF DBIP model (BM₂), the system's equation of motion can be expressed by Eq. (39).

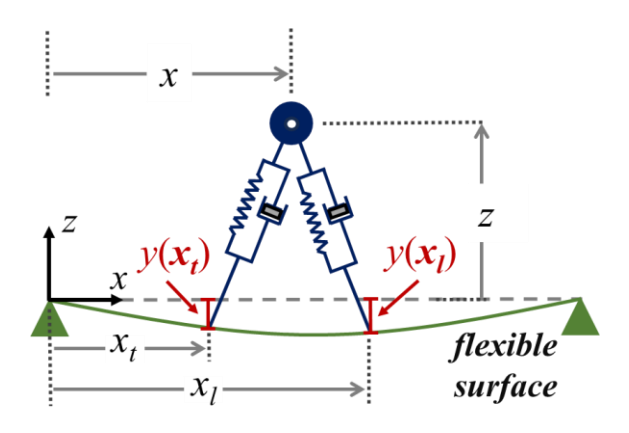


Figure 20 - Representation of the DBIP model interacting with a flexible surface (after Qin *et al.*, 2013)

$$\mathbf{M} \ddot{\mathbf{U}} + \mathbf{C} \dot{\mathbf{U}} + \mathbf{K} \mathbf{U} = \mathbf{F} \tag{39}$$

Where the mass, stiffness and damping matrices, and displacement and force vector, considering 'n' modes of the structure are given by:

$$\mathbf{M} = \begin{bmatrix} m_1 & 0 & \cdots & 0 & 0 \\ 0 & m_2 & \cdots & 0 & 0 \\ \cdots & \cdots & \cdots & \cdots & \cdots \\ 0 & 0 & \cdots & m_h & 0 \\ 0 & 0 & \cdots & 0 & m_h \end{bmatrix}_{(n+2)\times(n+2)}$$

$$\mathbf{C} = \begin{bmatrix} c_{1,1} & c_{1,2} & \cdots & c_{1,n+1} & c_{1,n+2} \\ c_{2,1} & c_{2,2} & \cdots & c_{2,n+1} & c_{2,n+2} \\ \cdots & \cdots & \cdots & \cdots \\ c_{n+1,1} & c_{n+1,2} & \cdots & c_1 + c_2 & c_4 - c_3 \\ c_{n+2,1} & c_{n+2,2} & \cdots & c_4 - c_3 & c_{leg} - c_1 - c_2 \end{bmatrix}_{(n+2)\times(n+2)}$$

$$\mathbf{K} = \begin{bmatrix} k_1 & 0 & \cdots & -k_{l,z}\phi_1(x_l) & -k_{l,z}\phi_1(x_l) & 0 \\ 0 & k_2 & \cdots & -k_{l,z}\phi_2(x_l) & -k_{l,z}\phi_2(x_l) & 0 \\ \cdots & \cdots & \cdots & \cdots & \cdots \\ 0 & 0 & \cdots & k_{l,z} + k_{l,z} & 0 \\ 0 & 0 & \cdots & 0 & k_{l,x} - k_{l,x} \end{bmatrix}_{(n+2)\times(n+2)}$$

$$\mathbf{F} = [0,0,\cdots,-m_hg,0]_{n+2}^{\mathsf{T}}, \mathbf{U} = [Y_1,Y_2,\cdots,Y_n,z,x]_{n+2}^{\mathsf{T}}$$

And the additional variables expressed above are:

$$\begin{split} c_{i,i} &= c_i + c_1 \phi_{i,i}(x_l) + c_2 \phi_{i,i}(x_t) & (i = 1, 2,, n), \\ c_{i,j} &= c_{j,i} + c_1 \phi_{i,j}(x_l) + c_2 \phi_{i,j}(x_t) & (i \neq j \leq n), \\ c_{i,n+1} &= c_{n+1,i} = -c_1 \phi_i(x_l) - c_2 \phi_i(x_t) & (i = 1, 2,, n), \\ c_{i,n+2} &= c_{n+2,i} = c_3 \phi_i(x_l) - c_4 \phi_i(x_t) & (i = 1, 2,, n), \\ k_{l,z} &= k_{leg} \left(1 - \frac{L_p}{L_l}\right) \left(1 - \frac{y(x_l)}{z(t)}\right), k_{l,z} = k_{leg} \left(1 - \frac{L_p}{L_t}\right) \left(1 - \frac{y(x_t)}{z}\right), \\ k_{l,z} &= k_{leg} \left(1 - \frac{L_p}{L_l(t)}\right) \left(\frac{x_l}{x(t)} - 1\right), k_{l,z} = k_{leg} \left(1 - \frac{L_p}{L_l(t)}\right) \left(1 - \frac{x_t}{x(t)}\right). \end{split}$$

Where: c_1 , c_2 , c_3 and c_4 are calculated through Eq. (23), $k_i = \omega_i^2 m_i$ and $\phi_{i,i} = \phi_i^2$. m_i , ξ_i , ω_i , ϕ_i and Y_i are the structure respective modal mass, damping coefficient, angular frequency, mode coordinate and mode shape of the i^{th} mode of the structure. $m_h g$ is the pedestrian total weight, $y(x_l)$ and $y(x_t)$ are the structure displacements at the contact point for leading and trailing leg's position x_l and x_t (see Figure 20), respectively.

The leg's length equations should be rewritten to consider that each foot will interact with the structure in different positions. Given that, $L_l(t)$ and $L_t(t)$ in Eq. (39) are:

$$L_{l}(t) = \sqrt{(x_{l} - x(t))^{2} + (z(t) - y(x_{l}))^{2}}$$

$$L_{t}(t) = \sqrt{(x(t) - x_{t})^{2} + (z(t) - y(x_{t}))^{2}}$$
(40)

As for the rigid surface formulation, the vertical GRF component of each foot can be calculated though Eq. (26). However, the axial velocities v_l and v_t should be obtained by deriving Eq. (40) with respect to time (which leads to a slight variation from Eq. (37)), as given by:

$$v_l = -\dot{x}(t)\cos\theta_l + (\dot{z}(t) - \dot{y}(x_l))\sin\theta_l$$

$$v_t = \dot{x}(t)\cos\theta_t + (\dot{z}(t) - \dot{y}(x_t))\sin\theta_t$$
(41)

For the human-structure coupled system, all discussions in terms of the DBIP models' functioning from Section 2.4.2.1 prevails. However, it is important to emphasize one aspect of the 2DOF formulation: the feedback mechanism for energy compensation. The pedestrian's body energy should be reassessed at the end of every integration step through Eqs. (29) to (31), so the force vector in Eq. (39) should be updated to Eq. (42) when ΔE is negative.

$$F = [0,0,\dots, -m_h g, F_{ctrl}]_{n+2}^{T}$$
(42)

Similarly to the rigid surface scenario, the DBIP model can be reduced to a single-degree-of-freedom by assuming a constant longitudinal velocity \dot{x} . Thus, in the equation of motion for the BM₁ model, it is sufficient to remove the 'n + 2' row and column from Eq. (39), which corresponds to the horizontal degree-of-freedom of the model (Ruiz *et al.*, 2017). The force vector should then be rewritten as:

$$F = [f_1, f_2, \dots, -(m_h g + \dot{x}(c_4 - c_3))]_{n+1}^{T}$$

$$f_i = -\dot{x}(c_3 \phi_i(x_l) - c_4 \phi_i(x_l)), \quad (i = 1, 2, ..., n)$$
(43)

2.5 Concluding remarks

In summary, excessive vibrations in footbridges remain a relevant concern in structural design, particularly for lightweight and slender systems with natural frequencies close to typical pedestrian step frequencies. While current guidelines provide valuable recommendations and

simplified criteria to assess serviceability and user comfort, they largely rely on predefined load models that do not explicitly account for the dynamics of the human body.

The absence of a more detailed representation of human-structure interaction (HSI) in these approaches highlights the need for further developments. Incorporating biodynamic aspects into design frameworks could contribute to more accurate predictions of structural responses under human loads and, ultimately, to safer and more efficient designs – particularly for structures prone to high vibration levels, as currently permitted by such normative documents.

There are many proposals for biodynamic models in the literature, particularly in the field of biomechanics, which aims to study the mechanisms of body function in daily activities. Although structural failures in service have driven the interest of the civil engineering field in adopting more complex human body models over the last decades – not merely a deterministic force model – the investigation and refinement of simplified models that incorporate the necessary elements for a realistic simulation of human-structure interaction remain a challenge for practical structural design applications.

Bearing in mind a practical application, two biodynamic models were chosen to represent a human walking for further investigation: a SDOF Spring-Mass-Damper (SMD) model (HSI formulation), and a Damped Bipedal Inverted Pendulum (DBIP) model (or Bipedal Model - BM). A major difference between DBIP and SMD models is that the later assumes a coupled moving force as an approximation of the GRF.

Additionally, BMs do not explicitly incorporate dynamic load factors (DLFs) usually present in GRF analytical expressions, nor the step frequency in their formulation; rather, the GRFs emerge as a result of the model's motion and the chosen model parameters and initial conditions (Silva, *et al.*, 2024). As a consequence, while interacting with the structure, the intrinsic forces of the BM may be altered due to the surface movement, potentially reflecting actual changes in walking patterns, such as variations in speed and step frequency (Živanović *et al.*, 2005b).

SMD models may be able to simulate changes in interaction forces (Pfeil *et al.*, 2014; Pfeil *et al.*, 2022). However, since this model explicitly define the pedestrian's step frequency and simplify the contact with the structure to a single point, they cannot naturally capture potential changes in walking patterns caused by the movement of flexible surfaces.

In fact, Cai *et al.* (2019) highlight the importance of human walking models capable of simulating what they refer to as a footfall overlap of forces – in other words, accounting for the double support phase – even for floors, which are typically affected by higher harmonics (Gonçalves *et al.*, 2019).

The next chapter will focus on the methodology adopted in this study for deepen investigations of the chosen biodynamic models, followed by the results and discussions from those analyses in Chapter 4.

3 MATERIAL AND METHODS

As mentioned before, even with the development and introduction of several biodynamic models, the literature lacks mathematical validation with experimental results about this subject. Bearing this in mind, after a literature review, experimental results with pedestrians walking (from previous works and carried out during and for this study) have the purpose to evaluate two biodynamic models. Table 17 presents a summary of the stages herein proposed and the following sections present a detailed description.

Table 17 – Steps of the methods for the research development

Steps	Activity	Description			
1	Literature review	 An initial narrative literature review was conducted to provide the theoretical foundation for the development of this study. This review followed a continuous and iterative process, being updated throughout the research to incorporate the most recent and relevant publications in the field: A brief discussion on excessive structural vibrations and the current guideline approaches for footbridges was presented. Furthermore, the literature on biodynamic models was reviewed, along with a discussion on the dynamic body parameters of pedestrians, as presented in recent studies. In addition, a critical discussion was carried out regarding the formulation and functioning of two chosen biodynamic models, highlighting their assumptions, limitations, and applicability within the context of the HSI. 			
2	Biodynamic model's application from the HSI perspective	 Numerical simulations with two biodynamic models found in the literature against experimental results obtained in previous works (Pimentel, 1997; Hawryszków et al., 2017) aiming to analyse their performance. This stage is twofold: simulations with simplest biodynamic models and their respective dynamic parameters (SMD model); simulations with more complex biodynamic models and their respective parameters from the literature (DBIP models). 			
3	Set of experimental tests	 An experimental campaign with walking tests aimed to collect new and extensive results to evaluate and validate the DBIP models previous investigated, chiefly from the S2HI perspective. This stage provided experimental results from different levels of vibration and walking speeds, which made it possible to analyse the performance of the DBIP models in the vertical direction and their applicability over structures, such as footbridges. 			
4	Evaluation of DBIP models from walking tests	 applicability over structures, such as footbridges. This stage concerns the applicability of the DBIP models in comparison to the experimental results obtained in the previous stage, with a particular focus on the S2HI. This analysis allowed for the assessment of response accuracy, the validation of these models, and the proposal of parameter adjustments where necessary. Subsequently, the performance of the DBIP models was re-evaluated from the HSI perspective, based on the findings from the earlier analysis. 			

3.1 Investigation of the human walking models

With the previous investigation of SMD models, it was possible to compare the differences and similarities between the simplest biodynamic model disposed on the literature. The formulation from Pfeil *et al.* (2014), slightly modified by the suppression of the function representing the heel movement, was, thus, selected as a basic one in this study, and was initially adopted for the analysis for some purposes:

- Analysis of the SMD parameters values proposed in the literature.
- Analysis of the SMD model performance against MF model and experimental results in scenario of single crossings.

It is worth mentioning that Eq.(17) was adapted to analyse the modelling of the pedestrians as force-only (MF model) by setting the pedestrian body parameters to null values. Another aspect worthy to pay attention to is that this modelling approach was preferred in comparison with a full finite element analysis because it takes into account the interaction between pedestrians and the structure, also considers vibrations in a single mode without loss of accuracy, but with a much quicker execution time.

Moreover, the discussions surrounding the DBIP model raised a few questions regarding its functioning and the simplified approaches presented in the literature. Aspects such as the reduction of the model to a single-degree-of-freedom system, as well as the choice of the parameter governing the prediction of the next impact point, are gaps yet to be addressed and were explored in this study.

3.2 Biodynamic models application from a HSI perspective

This stage of the research has the focus on investigating the application of existent biodynamic models and their parameters. In a previous investigation (Section 2.4.1), SMD models of the literature were critically analysed, and a basic analytical formulation was identified and adopted for further comparison against experimental data. When it comes to bipedal models, in the literature (Shahabpoor *et al.*, 2016a; Lin *et al.*, 2023), it is clear that the Damped Bipedal Inverted Pendulum (DBIP) model stands out among the Inverted Pendulum (IP) models, as it can reproduce more realistic walking parameters and induced forces.

As aforementioned, it was possible to select a basic formulation for the SMD model to account for HSI and carry out numerical simulations against experimental results from previous works. For this purpose, the formulation was implemented through an algorithm developed in the Math Tool MATLAB Platform® (2024).

Moreover, as discussed in the previous section, the SDOF DBIP model (BM₁) does not require an energy compensation mechanism due to the dissipative nature of the 2DOF formulation. Additionally, as discussed in the Chapter 4, although not explicitly included in the formulation, the step frequency can be imposed by considering a fixed step length for BM₁. Due to this practicality of BM₁, its performance was initially evaluated from the HSI perspective and compared to the SMD model. The computational procedure to solve the nonlinear equations is presented in Figure 21.

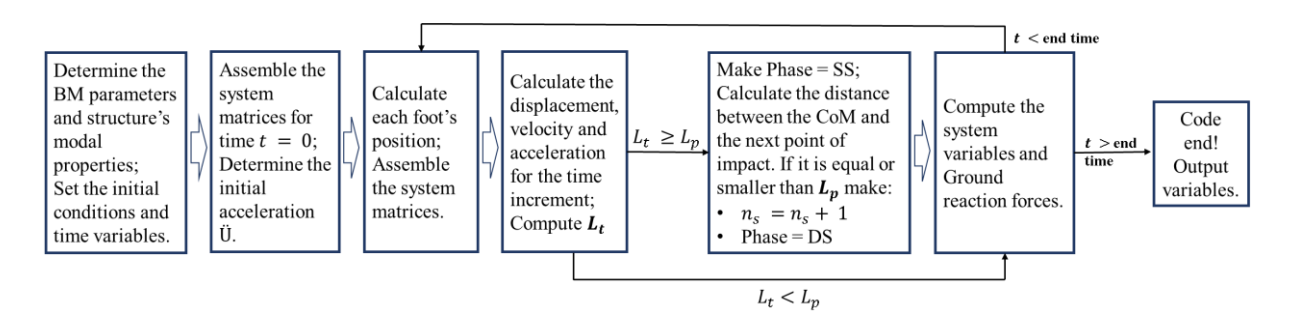


Figure 21 - Computational procedure for the HSI formulation adopting DBIP models (BM1 or BM2) implementation.

For the simulation of the HSI system, the selected test structures comply with some requirements to investigate both biodynamic models. First of all, since resonance conditions enhance the differences between models and feature the worst serviceability situation of structures under human loads, one of their vertical modes of vibration presents natural frequencies within the normal range of pedestrians walking. In addition, it is worth mentioning that the structures are in a quiet environment, which enabled the experimental campaigns.

With more details in the following subsections, two structures were chosen: Aberfeldy Footbridge (Pimentel, 1997) and Złotnicka Footbridge (Hawryszków *et al.*, 2017). The experimental results carried out in both structures were used to investigate a single pedestrian crossing the structure. However, the differences between their levels of vibration made it possible to compare the models' reliability in terms of HSI effects.

3.2.1 Aberfeldy Footbridge

The first structure analysed in this study to investigate the HSI is the Aberfeldy glass-reinforced plastic cable-stayed footbridge, in Scotland (Figure 22). The same structure was also investigated by Pimentel (1997)⁴, Cadei & Stratford (2002), Dang & Živanović & (2013) and Pfeil *et al.* (2014). Relevant characteristics of the footbridge constructed in 1990 (Harvey, 1993) are:

- It is a three-span structure, having a main span of 63m and two side spans of approximately 25m each.
- The height of the structure is not constant but vary to no more than 8m.
- Present a design of the towers in A-shaped frames.
- The cables are divided into two groups of 20 that connect the 2.12m wide deck to each tower.



Figure 22 - Aberfeldy Cable Stayed Footbridge (Pimentel, 1997).

A set of experimental tests was carried out by Pimentel (1997) aiming to analyse the vibrational performance of footbridges due to human-induced loads. Herein, the test result of interest is the filtered vertical acceleration response at mid-span due to the crossing of a single pedestrian walking in resonance with the first vertical mode of the structure, in which the maximum acceleration (a_{max}) and root mean square acceleration (a_{rms}) was respectively 2.14

-

⁴ More details about this test structure can be found elsewhere.

m/s² and 0.89 m/s². The whole measured time response signal was available for comparison with the numerical predictions.

Also investigated by Pfeil *et al.* (2014), it was observed by the authors that even with the control of the pedestrian gait with a help of a metronome, the strong deck vibrations led to a pace losing, causing disturbances in the response signal. This was also taken into account in this study.

On the other hand, by analysing the experimental mode shape in Figure 22, it is clear that the relevant response occurs while walking between the towers, then in order to be used in Eq.(17), a mathematical expression for unity scaled $\phi_i(i = 1)$ given in Eq.(44) was fit to the experimental mode shape.

$$\phi_I(x) = 0.11867 - \frac{1845.64}{4\pi(x - 31.881)^2 + 513.413\pi}$$
 (44)

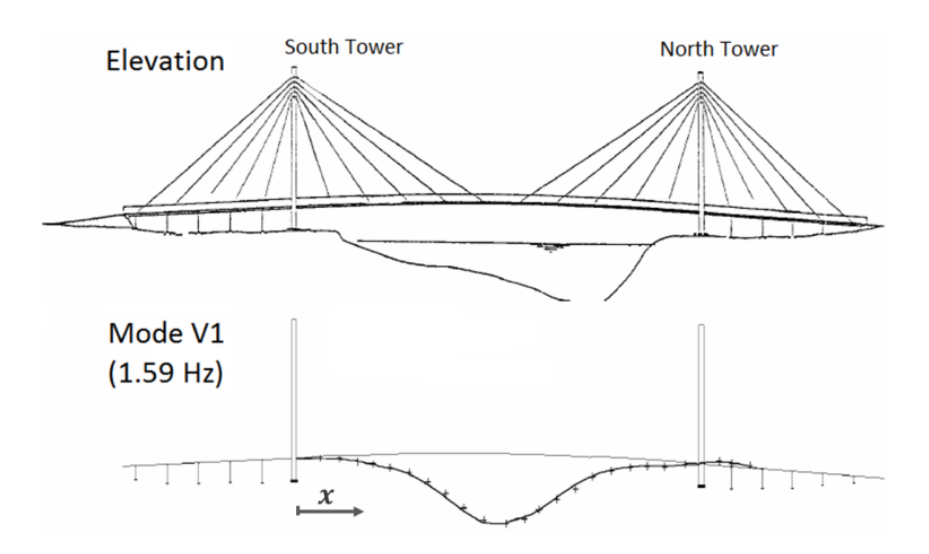


Figure 23 – Aberfeldy footbridge elevation and experimental 1st mode shape (After Pimentel, 1997)

Finally, the absence of some information from the experimental side led to a need of adopting values from the literature. The step length of the pedestrian was assumed as 0.90 m (Dang & Živanović, 2013). The DLFs of the pedestrian were not experimentally determined; and an initial value of 0.25 for DLF₁ was defined based on Young (2001) and adjusted in the analysis, as will be shown later on (Section 4.1.1.1). All information gathered for the analysis is presented in Table 18.

Table 18 – First mode dynamic parameters of the structure and pedestrian characteristics, based on experimental data except where indicated.

Test structure (1st mo	de)	Test Pedestrian		
Modal mass (m) (calculated)	2547 kg	Total mass (M)	80 kg	
Damping ratio (ξ)	0.84 %	Pacing rate (f_s)	Average of 1.56 Hz	
Natural frequency (f_n)	1.59 Hz	Step length (assumed)	0.90 m	

3.2.2 Złotnicka Footbridge

The second structure selected was a 68.0m long two-span cable-stayed footbridge named Złotnicka after its location in Złotnicki Park in Wrocław, Poland. It has central pylons to support the deck and to which the stays are attached (Figure 24 and Figure 25)⁵. As mentioned before, the selection of the structure adhered to both technical and logistical requirements. From the technical point of view, the structure had a natural frequency in the vertical direction within the range of the pacing rates of pedestrians and presented perceptible vibrations when crossed by them. In terms of logistics, it was in a quiet environment with sparse use, enabling a controlled test program to be carried out.

The structure was the subject of previous investigations, and detailed information regarding its geometry and finite element (FE) modelling can be found elsewhere (Hawryszków *et al.*, 2017). Herein, the focus is on the properties of interest for the purposes of this study (Table 19):

- A measured natural frequency of 2.07 Hz was identified, corresponding to the first vertical antisymmetric mode of vibration, with a node at the central support. Relevant mode shapes are shown in Figure 26 from the calibrated FE model.
- The modal mass related to this mode was also calculated from the calibrated FE model and had a value of 22,205.8 kg.
- By employing the natural frequency and the modal mass, the modal stiffness was
 calculated using the expression of the natural frequency of a single-degree-of-freedom
 system. This modal mass was scaled by considering a unity value for the maximum
 ordinate of the modal shape of the first mode.

⁵ More details about the structure can be found elsewhere (Hawryszków *et al.*, 2017).

• Regarding damping, the value was obtained from the tail end of the pedestrian tests and is discussed in Section 4.1.1.2.



Figure 24 – Panoramic view of the footbridge (Image previous used in Hawryszków et al., 2021).

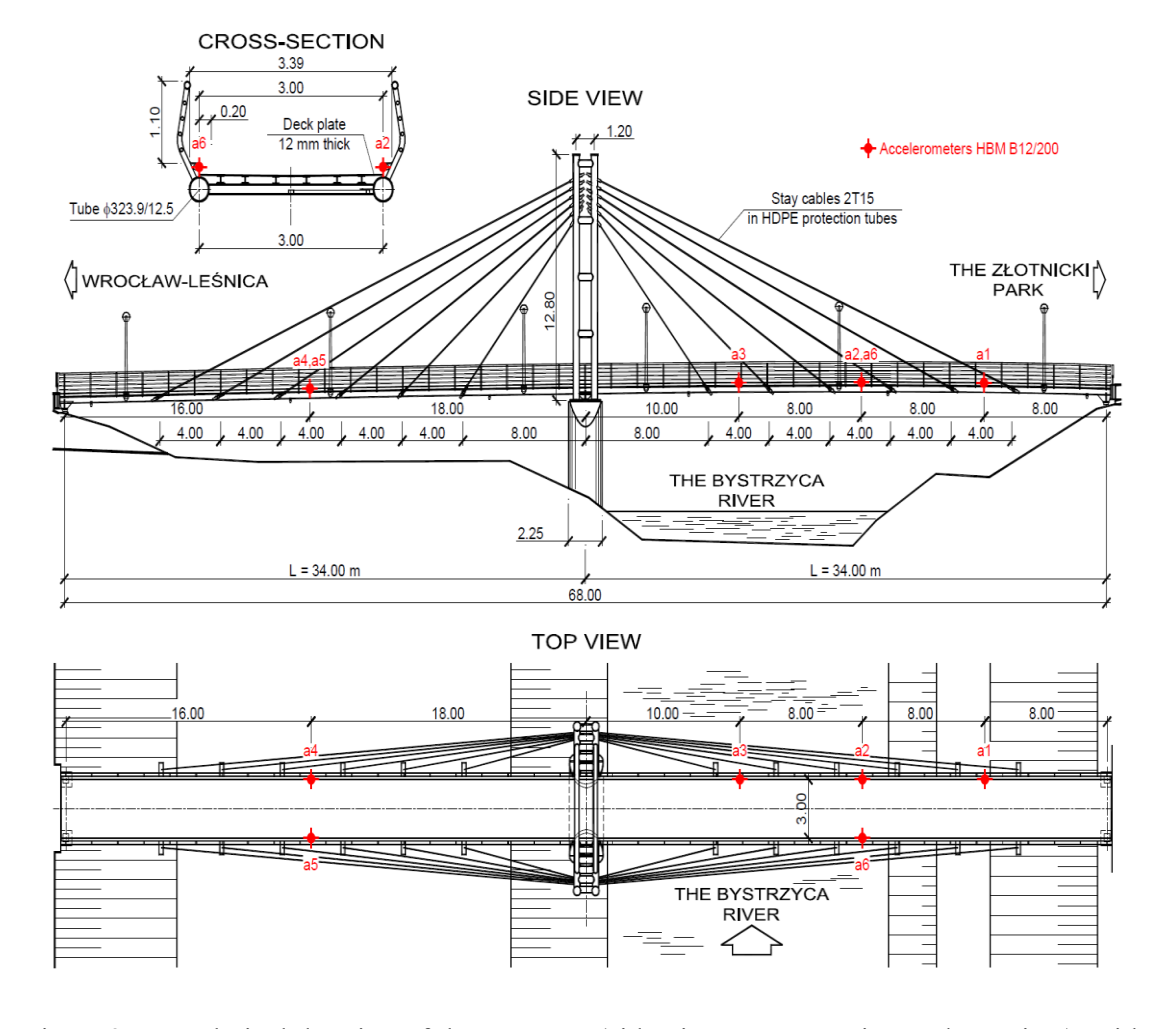


Figure 25 – Technical drawing of the structure (side view, cross-section and top view), with relevant dimensions. Selected measurement point on the left span, 16.0 m from the support (Image previous used in Hawryszków *et al.*, 2021).

	Test struct	ture (1st mode)				
	Modal mass (<i>m</i>) 22,205.8 kg					
	Damping ratio (ξ)	Variable*				
Natural frequency (f_n)		2.07 Hz				
•	Test structu	re (Dimensions)				
•	Span	68m (two 34m spans)				
	Height	Variable (No more than 8m)				

Table 19 – First mode dynamic parameters of the structure and relevant dimensions.

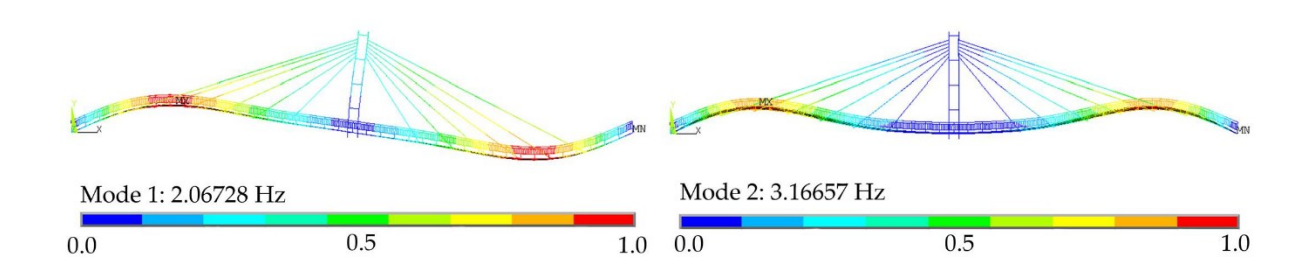


Figure 26 – Vertical mode shapes of the structure (Image previous used in Hawryszków et al., 2021).

Also, for Złotnicka footbridge, a mathematical expression for unity scaled $\phi_i(i=1)$ given in Eq. (45) was fit to the experimental mode shape in order to be used in Eq.(17) for single crossing since this is the mode of interest (see Figure 26).

$$\phi_I(x) = 2.96e^{-3} + 1.32e^{-1}x + 3.79e^{-3}x^2 - 1.24e^{-3}x^3 +$$

$$\dots + 6.41e^{-5}x^4 - 1.48e^{-6}x^5 + 1.60e^{-8}x^6 - 6.54e^{-11}x^7 - 1.37e^{-14}x^8$$
(45)

One test subject volunteered to take part in the experimental campaign (Figure 27). A metronome was employed during the crossings, and the reason for this was twofold: excitation in the resonance condition is the target of the codes of practice for designing footbridges against vibration serviceability, and the level of excitation should be as high as possible for the interest of this investigation. Therefore, the beating of the metronome was set to help the test subject to walk with a constant step frequency in order to excite the first mode of vibration in the resonance condition. It is worth mentioning that the experimental campaign also included group loading (Hawryszków *et al.*, 2021), which is not addressed in this study as it was not the focus here.

The test subject was carrying the metronome and instrumented with an HBM GmbH (type B12/200) accelerometer attached to their waist (Figure 27a), whereas the other accelerometers remained near the antinode of the first mode shape (see Figure 24 and Figure 25). The mass of the test subject is 48kg and was employed in the numerical simulations. A total of 10 tests were conducted for the crossings of this individual (Figure 27b), to account for the expected variability among the crossings, even in controlled situations.



Figure 27 – Pedestrian tests: (a) Example of instrumented leading pedestrian; (b) single crossing; (Image previous used in Hawryszków *et al.*, 2021).

3.3 Experimental Campaign – VSimulator

This section presents the details of the experimental campaign designed and conducted at the VSimulator facilities at the University of Exeter, UK, as part of the development of the present study. It presents a detailed description of the test program (equipment and test logistics), and data processing. In addition, it describes the methodology adopted for data extraction, which was used either as input for the DBIP model parameters or as a reference for experimental-numerical correlations.

3.3.1 Test program

A series of experimental tests was conducted at the VSimulators facility (2025) at the Engineering Research Centre of the University of Exeter. This facility comprises a 4 m x 4 m platform driven by electric actuators, capable of providing motion along all six degrees of freedom: three translational and three rotational axes (Figure 28a). VSimulator is optimized for

motion in the frequency range of 0.5-35 Hz. Additionally, it features nine multi-axis AMTI force plates for measuring ground reaction forces, as well as a human motion capture system employing both optical and inertial technologies (Optitrack Motion Capture System®, 2025).

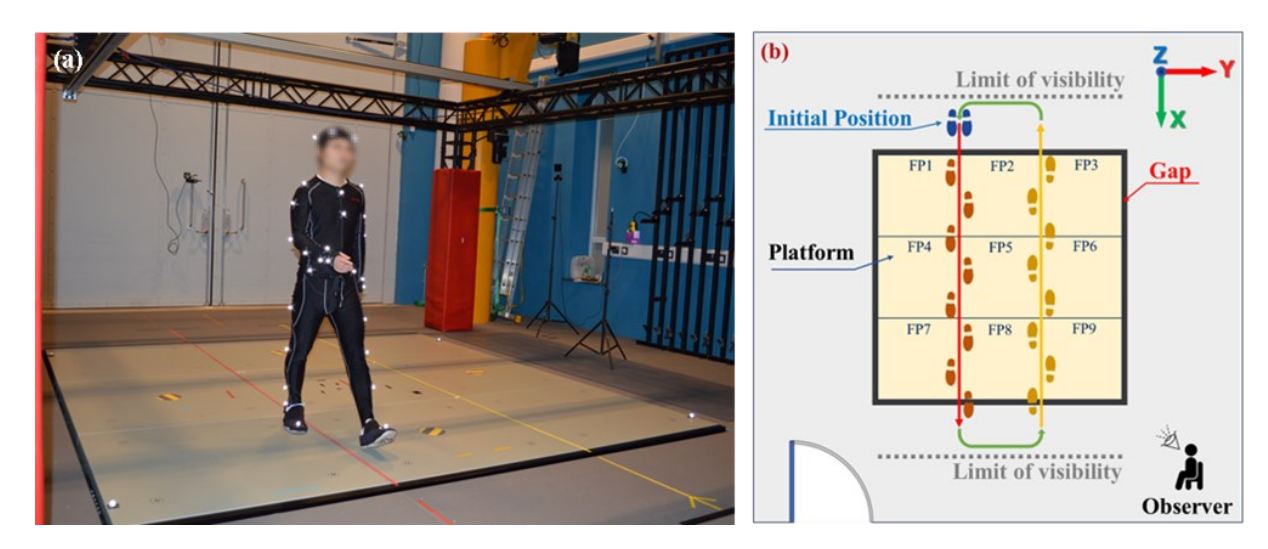


Figure 28 – (a) Walking test subject wearing mocap suit in VSimulators facility, and (b) test's scheme depicting designated path.

Additionally, to track the motion of the human body, the optical system equipped with strategically positioned cameras within the VSimulator room required participants to stay within the defined limits of visibility depicted in Figure 28b. For a deeper understanding of VSimulator's facilities and features, the reader is referred to (Brownjohn & Darby, 2018; Brownjohn *et al.*, 2019). This facility allows for the generation of vibration conditions across a relevant range of parameters, including vibration frequency, amplitude, and duration, and is capable of simulating visual scenes pertinent to the study of pedestrian structures.

To meet the University of Exeter Ethics Committee requirements, all test subjects (TSs) were chosen from volunteers at the university (staff or students). To ensure the integrity of the study and data reliability, all volunteers were asked to sign consent forms and answer questions regarding their health conditions, to be accepted as participants. Questions addressing their age (adults only), gender, weight (under 100 kg), history of mobility disability (such as walking impairments), and motion sickness were included. For the experimental campaign reported here, three healthy test subjects were selected to participate in the experiments. To ensure confidentiality in the participation of the experiments, each participant was assigned a number, and their physical characteristics, such as age, weight, height, and leg length, were registered, as presented in Table 20.

Table 20 – Test subjects physical characteristics and age

Test subject	Gender	Age (years)	Weight (kg)	Height (cm)	Leg's length (cm)
TS1	Female	36	71.7	176	105
TS2	Female	28	76.3	182	108
TS3	Male	30	69.2	180	99

The experimental campaign consisted of a single visit to ensure the complete collection of data for a given test subject. During this visit, each participant was asked to wear a mocap suit, with 39 reflective markers carefully attached to their body (see Figure 28a for reference). Proper marker placement at anatomical landmarks is crucial for accurately tracking body trajectory (Optitrack, 2025). Participants were strongly encouraged to wear comfortable shoes and tight-fitting clothing under the special suit. Additionally, four extra markers were placed on the moving platform to track the vibration scenarios (seen as white spots in Figure 28a).

The experimental campaign entailed recording 3D body motion trajectories and footfall forces over time while crossing the platform under various vibration scenarios. The study focused on structure-to-human interaction (S2HI) in the vertical direction, considering both resonance (as explained later) and rigid surface conditions. Base movements were defined by pairs of acceleration and frequency values, which were used to generate a drive file as input for the platform. Notably, although recorded at different sampling rates (100 Hz for marker trajectories and 1000 Hz for ground reaction forces), all raw data streams were synchronized to ensure accuracy.

In addition to free walking, the test subjects were asked to walk at three specific step frequencies: slow (1.6 Hz), normal (1.85 Hz), and fast walking (2.2 Hz). For all four walking gait cases, four surface vibration cases were investigated, resulting in 16 scenarios for each test subject (see Table 21). Complementary to rigid surface scenarios, sinusoidal excitation was employed with a frequency equal to the predefined walking rate, for three distinct acceleration peak levels (0.5, 1.0, and 1.5 m/s²). These vibrating scenarios (henceforth designated as resonance conditions) represent actual conditions for structure-to-human interaction (S2HI) effects, as civil structures are typically subjected to human-forced vibrations and tend to oscillate at pedestrian walking frequencies. To maintain test integrity, all scenarios were separated into sets of experiments, allowing for rest periods between them so as to avoid tiredness of the test subjects.

Table 21 – Scenarios investigated for each frequency of the test platform

Walking Scenario	Surface Scenario	Frequency (Hz)	Acceleration peaks (m/s²)	Displacement Amplitudes (cm)
Slow	Rigid			
	Resonance	1.60	0.5	0.49
	Resonance	1.60	1.0	0.99
	Resonance	1.60	1.5	1.48
Normal	Rigid			
	Resonance	1.85	0.5	0.37
	Resonance	1.85	1.0	0.74
	Resonance	1.85	1.5	1.11
Free	Rigid			
	Resonance	1.85	0.5	0.37
	Resonance	1.85	1.0	0.74
	Resonance	1.85	1.5	1.11
Fast	Rigid			
	Resonance	2.20	0.5	0.26
	Resonance	2.20	1.0	0.52
	Resonance	2.20	1.5	0.79

When necessary, a metronome sound synchronized with the drive file of the moving platform was used to ensure the desired walking rate (Hz). The 'pulstran' MATLAB® (2024) function was used to generate a metronome audio file for each set of scenarios. Each audio file included an extended beep to alert signal scenario changes within each set of experiments, aiding in test monitoring. Before each set, test subjects could listen to the metronome beats to familiarize themselves with the predefined step frequency (except for free walking gaits).

The test subjects were initially provided with instructions on how to walk over the platform guided by metronome beats, as needed. To ensure that the force-time history for each foot was recorded separately during the experiments, and to gather the maximum number of footfall forces for each scenario, each test subject was instructed to follow a designated path. Figure 28b illustrates the testing layout and the path itself, starting from the marked position on the diagram. The path was marked with both red and yellow tapes in the X-direction, as shown in Figure 28b. Each tape (red for the outbound journey and yellow for the return journey to the initial position) was placed along the border between the force plates, aligned with the desired walking path. A cycle was completed each time the test subject returned to the initial position.

In order to collect a good sample of footfall forces for each specified vibration scenario, each test subject was asked to complete at least 3 cycles for rigid surface conditions and at least 5 cycles for resonance conditions. To ensure that the required number of cycles would be

completed for each scenario, preliminary tests were conducted to determine the required signal duration. Table 22 presents the signal duration for each respective type of scenario.

Table 22 – Signal duration for the scenarios (in seconds)

Walking case	Resonance	Rigid surface	
Slow	90	60	
Normal and free walk	85	55	
Fast	80	50	

Participants were also instructed to avoid stepping directly on the tapes to ensure precise data collection. This precaution was necessary because when a foot contacts two side-by-side force plates (such as FP1 and FP2 in Figure 28b), it can interfere with the accurate tracking of the foot force history for each step, making it more difficult to identify the force contribution of each foot during the DS phase. Therefore, it was necessary to verify these possible interferences and exclude such measurements from future analyses, as seen in step 13 in Figure 29. Standing over two force plates aligned in the walking direction (such as FP1 and FP4 in Figure 28b) does not affect the determination of footfall forces.

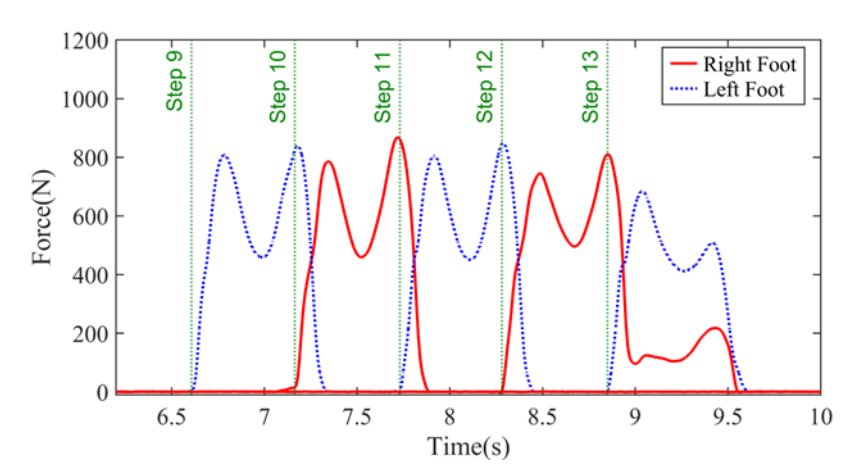


Figure 29 – Example of GRF time-history of both feet for TS1, rigid surface and slow walking scenario

At the end of each scenario, the test subjects were asked to respond to qualitative questions regarding their perception of vibrations. They were required to indicate whether they could perceive the vibrations and rate, on a scale of 1 to 5, the extent to which the vibrations interfered with their walking patterns, as described in Table 23.

Table 23 – Rating scale for the TS's vibrations perception

Rating Scale	Description
1	Vibrations did not interfere with walking
2	Vibrations caused minimal interference
3	Vibrations caused a moderate impact on walking
4	Vibrations significantly affected walking
5	Vibrations strongly interfered with walking

There were more limitations in conducting the test experiments, primarily due to the features of the platform and the logistics involved. The test subjects were asked to maintain a continuous walking flow, meaning no pauses between crossing cycles. The goal of this approach was to achieve a walking pattern that closely resembled a continuous flow in straight-line walking, despite the limitation imposed by the size of the platform and room. However, some measurements for each foot – particularly the first and last steps on the platform can exhibited erratic behaviour. Therefore, some steps were excluded, as discussed in the next subsection.

3.3.2 Data Processing

This subsection describes the procedures for extracting the experimental parameters of the TS's body and walking gait features, which are later used either as BM's input parameters or as a reference for the experimental-numerical comparisons. Figures showing examples of the data extraction process are included here for illustrative purposes only, as the methodology section describes solely the procedures adopted, not the extracted data itself.

3.3.2.1 Pre-processing

For each walking scenario, the raw marker data were initially analysed using the Qualisys Track Manager (QTM) Software[®] (2025) – in C3D format – to verify that the markers were correctly assigned to the body points of interest (Figure 30). Any gaps in the markers' trajectory tracking were filled using a polynomial method. This process ensured data consistency before generating the final file, which contained the unprocessed 3D trajectories of both the platform and the pedestrian's body.

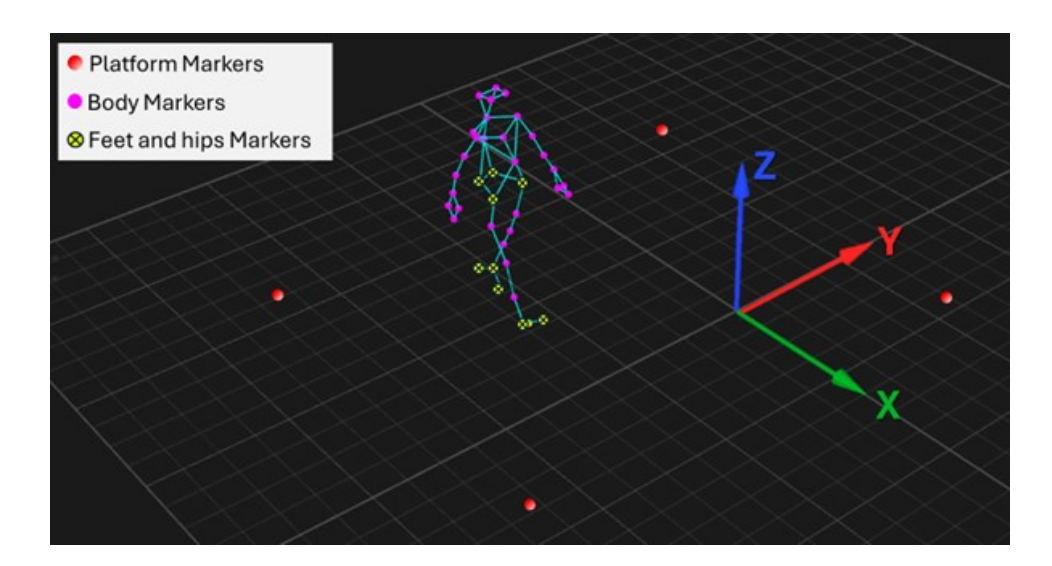


Figure 30 – 3D model constructed in QTM Software® (2025).

Both unprocessed kinetic (recovered force data from forceplates) and kinematic (3D body trajectories) data were analysed using MATLAB® (2024). The kinetic data of interest included the forces within the sagittal plane of the human body, specifically in the vertical (Z) and longitudinal (X) directions. To remove noise from data acquisition without altering the well-known 'M-shape' of footfall forces (Kerr & Bishop, 2001), these ground reaction forces (GRFs) were filtered using a MATLAB® low-pass, fourth-order Butterworth filter with a cut-off frequency of 24 Hz, which cover the harmonic components of interest (Shahabpoor *et al.*, 2018). The filtered data were subsequently downsampled to 100 Hz to align with the markers' data sampling rate.

According to the path scheme depicted in Figure 28b, force data from all nine force plates were analysed. GRFs from sequential force plates in the walking direction (e.g., FP1, FP4, and FP7) were summed to consider when a TS's foot partially overlapped the border between any pair of these force plates. This approach ensured a complete time-force history for each foot. Additionally, force data from specific forceplates were adjusted in the following way: for measurements on rigid floor scenarios, the forces were shifted to start from zero; in vibrating scenarios, the force data were centred to oscillate around zero values, and forces due to platform vertical movement were then subtracted from the total force signal to isolate the GRF component, as illustrated in Figure 31.

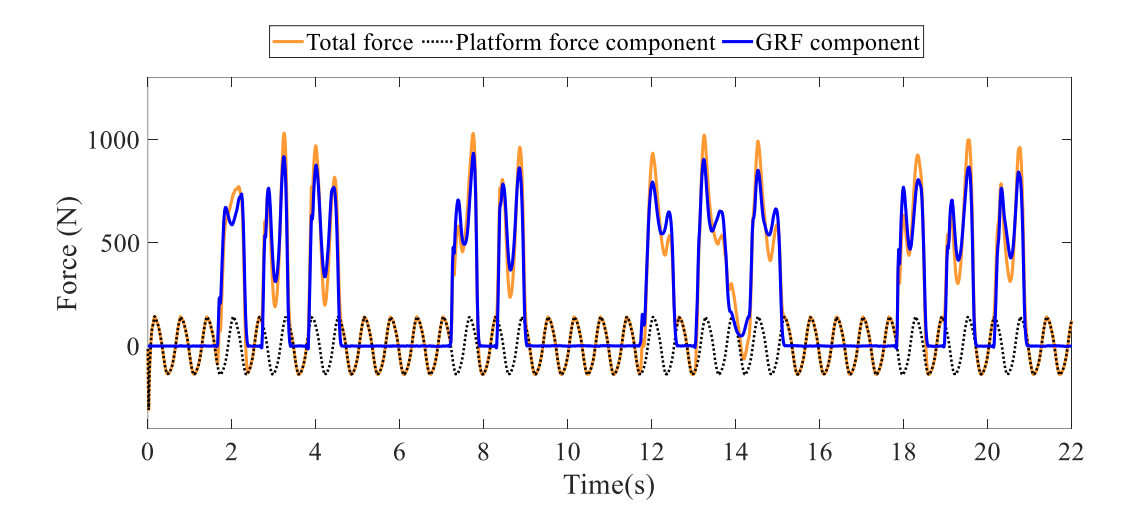


Figure 31 – Example of recovered force signal in vibrating scenarios for TS1, slow walk and resonance conditions

From the total of 39 markers, only the kinematic data for the feet and hips were used in this investigation (see yellow markers in Figure 30). Although the process of recording the 3D body trajectory by attaching markers to a special suit facilitated the execution of the tests, it still comes with some limitations (Smith *et al.*, 2024). During walking, as the suit's fabric deformed with movement, the markers could slightly shift from their original attachment points, with this effect becoming more pronounced at higher speeds. However, even if the markers were attached directly to the skin, achieving a perfect match between the marker position and the underlying bone structure is not guaranteed. This is due to the softness and movement of the tissues, which can introduce slight errors in the measurement and produce signal noise (Winter *et al.*, 1974).

These disturbances were mitigated by applying a second-order Butterworth filter in MATLAB® (2024) with a cut-off frequency of 6 Hz (Winter *et al.*, 1974). The centre of mass (CoM) trajectory over time was estimated by assuming that the body mass was concentrated 10 cm above the mean position of the four hip-level markers (anterior and posterior superior iliac spines, as shown in Figure 30) (Winter *et al.*, 1974; Geyer, 2005).

The CoM acceleration time-history was computed by differentiating its trajectory twice and subsequently compared to accelerations derived from force data. The latter was calculated by subtracting the body weight of the respective test subject from the total GRFs so as to isolate the dynamic force components, which were then divided by the body mass. As shown in Figure 32a, the synchronization of the data acquisition process was validated, and its quality

confirmed. However, notable discrepancies were observed during the DS phase in some fast-walking cases (see Figure 32b). These differences can be attributed to the fact that the markers were not directly attached to the TS's body.

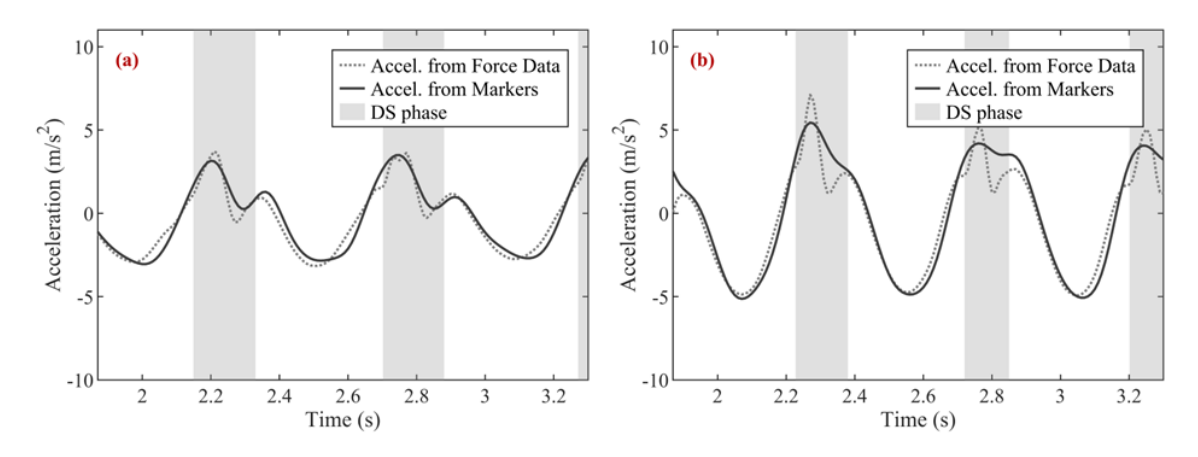


Figure 32 – Example of experimental accelerations for TS1, rigid surface scenarios for: (a) slow walk; and (b) fast walk

Moreover, an approach presented in Lipfert *et al.* (2012) (also seen in Lin *et al.*, 2023) was adopted in this study to verify the reliability of measured kinetic *versus* kinematic data, despite those authors adopted treadmills for data collection. This approach consists of plotting the actual leg force (in the sagittal plane and along the leg axis) as a function of leg length (Figure 33), the latter being considered as the distance from the CoM to the foot point. It is expected a near linear relationship between both variables for slow to normal speeds (Lipfert *et al.*, 2012), as elastic forces can prevail during walking. In the present study, a minimum acceptable R² (r-square) value of 0.77 for the linear adjusted leg force-length curve was adopted as an exclusion criterion for slow to normal step frequencies only, based on Lipfert *et al.* (2012). It should be noted that a linear curve fit is calculated to determine some model parameters, as discussed in the next section.

When it comes to fast walking scenarios, it was evident for most steps that the leg force-length curve fitting was greatly influenced by the segment between the peaks of the leg's axial force, which did not show a linear behaviour, as observed in Figure 33c. A similar pattern in the leg force-length curve at higher speeds was reported by Lipfert *et al.* (2012). This can be explained by the discrepancies in the DS phase between the kinetic and kinematic data illustrated in Figure 32b. In this matter, the exclusion criteria for fast walking scenarios differed, adopting a lower minimum acceptable R² values of 0.55. Additionally, a different approach for

parameter extraction from leg force-length curve for fast walking scenarios is presented in the next subsection.

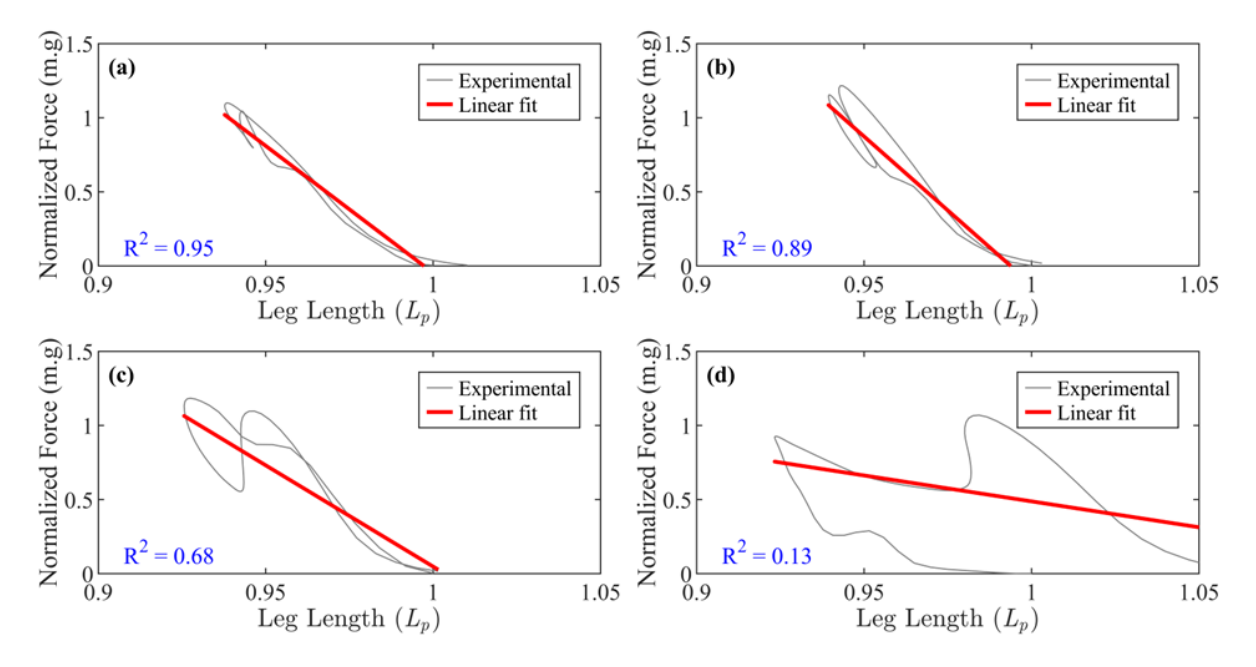


Figure 33 – Example of leg force-length curves and respective curve-fit and R² values for TS1 walking in rigid surface scenarios at a step frequency of (a) 1.64Hz (slow walk), (b) 1.84Hz (normal walk), and (c) 2.03Hz (fast walk). In addition, (d) an example of data exclusion criteria from the free walking scenario. Leg force is normalized by body weight and leg length is normalized to the leg length values obtained at the TD.

3.3.2.2 Model experimental parameters

Henceforth, for the sake of clarity, in order to differentiate the parameters extracted from the experiments from those set as input in the simulations, the subscript 'exp' will be included in the respective variables related to the former. Experimental gait events (TDs and TOs), gait parameters (walking speed v_{exp} , step frequency $f_{s,exp}$, step length $d_{s,exp}$, and DLFs), and model parameters (leg stiffness $k_{leg,exp}$, leg resting length $L_{p,exp}$, attack angle $\theta_{0,exp}$ and Energy input $E_{0,exp}$), that characterize the pedestrian gait were identified or calculated based on the observation and correlation of kinetic and kinematic data.

Gait events, such as touch-downs (TDs) and touch-offs (TOs), were identified by tracking the trajectories of the heels and toes and then cross-referencing these events with the force data for any adjustments (Figure 10). Footfall forces at the sagittal plane for each foot

were then isolated and interpolated to determine the corresponding zero-value time for each step.

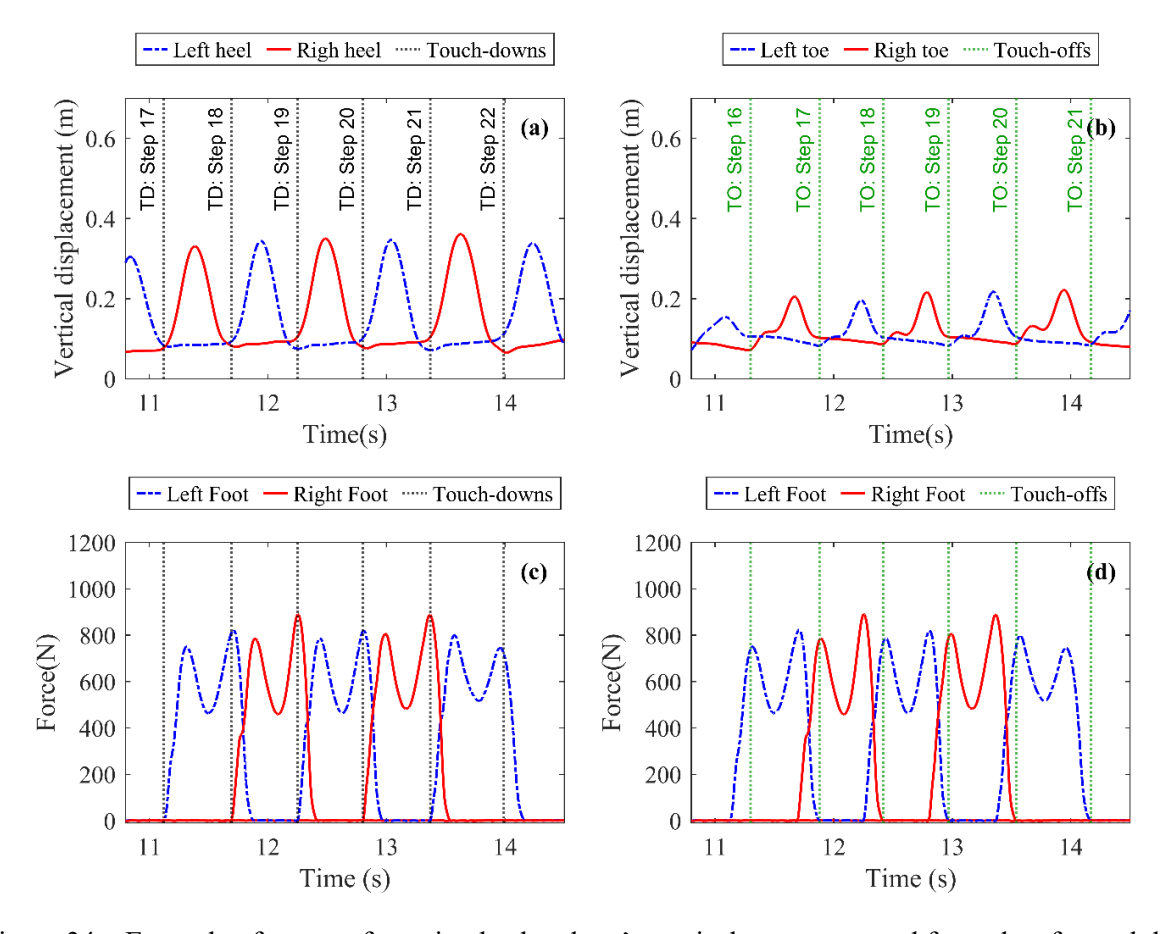


Figure 34 – Example of cross-referencing heel and toe's vertical movement and force data for each leg

Gait parameters for each crossing (when a test subject entered and left the platform) were calculated based on those TD instants. The respective walking speed v_{exp} per crossing was determined by the time and distance between the first and last TD over the platform, while the step lengths $d_{s,exp}$ were calculated as the longitudinal distance between successive TDs (X-direction in Figure 30). The dynamic load factors (DLFs) were derived from the frequency spectrum of total GRFs using the Fast Fourier Transform (FFT). For each crossing, the corresponding DLFs were computed as the ratio of the respective harmonic amplitude to the static component (TS's body weight). To determine the actual DLFs from the force time history, the force signal was repeated at least 100 times to eliminate any leakage when applying the FFT (Figure 35). Only the first harmonic of the FFT is of interest for this study, from which the two remaining gait parameters were derived: step frequency $f_{s,exp}$ and the associated DLF, referred to from now on as DLF₁.

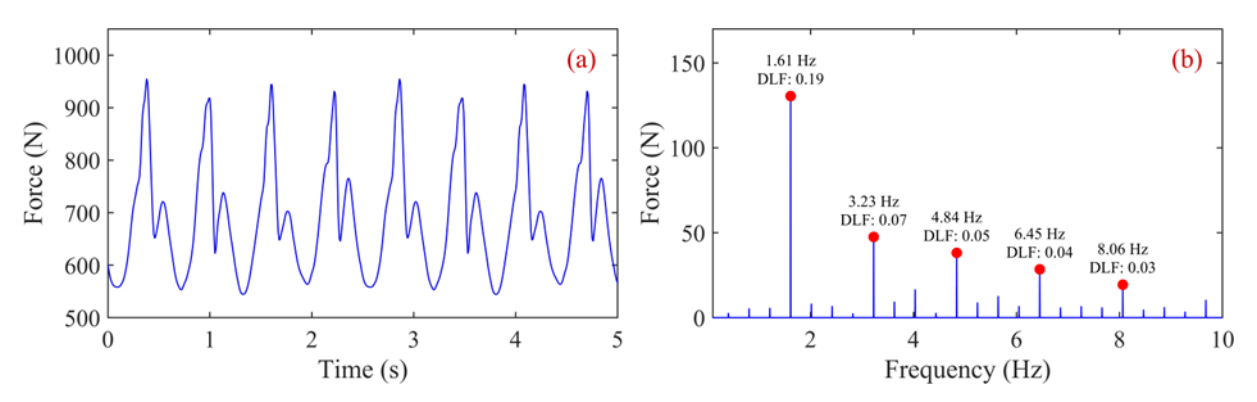


Figure 35 – Example of recovered filtered GRFs from TS1 slow walking for rigid surface scenario in (a) the time domain and (b) the frequency domain (Red dots highlight the expected harmonics of vertical forces in human gait)

Considering the exclusion criteria previously mentioned, for each valid footfall force in slow to normal walking speeds cases, the associated leg force-length curve (for example Figure 9a and b) was used to determine two model parameters (Lipfert *et al.*, 2012; Lin *et al.*, 2023): the experimental leg stiffness ($k_{leg,exp}$), which was determined as the modulus of the slope of the best linear fit to the curve, and the experimental leg resting length ($L_{p,exp}$), which was defined as the x-axis intercept of the linear fit. As shown in Figure 36, for each scenario, these pairs of variables ($k_{leg,exp}$ and $L_{p,exp}$) were plotted, revealing a linear relationship. A linear fit curve modelled $k_{leg,exp}$ as a function of $L_{p,exp}$, which was then used to determine the model leg stiffness k_{leg} for each crossing, based on the mean respective leg resting length value in the crossing, in turn used as the model resting length L_p .

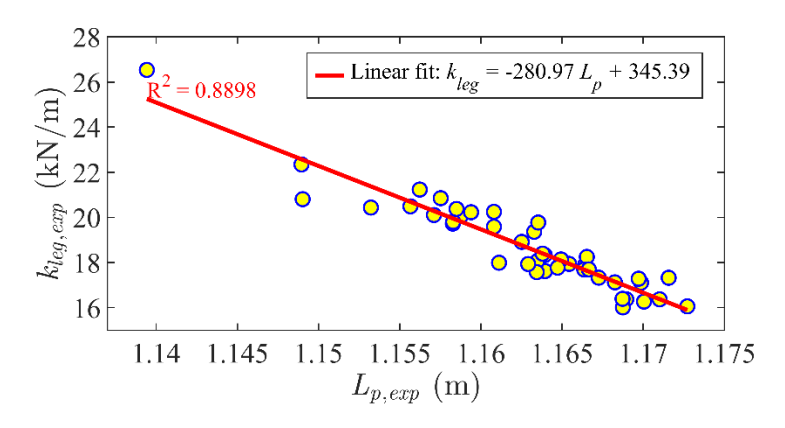


Figure 36 – Example of correlation of $k_{leg,exp}$ and $L_{p,exp}$, along with the respective curve fit for TS1 in the slow walking scenario on a rigid surface.

The approach adopted in this study to estimate the experimental value of leg stiffness in fast walking scenarios consisted of determining $k_{leg,exp}$ and $L_{p,exp}$ from curve fitting of the leg

force-length relationship while excluding the segments between the peaks of the leg's axial force.

The two remaining BM input parameters, $\theta_{0,exp}$ and $E_{0,exp}$, were calculated at the TD event for each step, with average values for each crossing adopted as reference for subsequent numerical simulations. The model's leg orientation $\theta_{0,exp}$ at the TD event was calculated from the kinematic data, and $E_{0,exp}$ was computed through Eq. (30) and the initial conditions identified at the beginning of every step cycle.

Following the methodology outlined in this section, sets of parameters that either characterize the walking gait (v, f_s) and DLF₁ or are reference for BM's input parameters (k_{leg}, L_p, θ_0) , and E₀) were extracted from the experimental data for each crossing within a given scenario, since the tests logistics hindered a continuous kinetic *versus* kinematic data collection.

It is important to note that, among the BM's input parameters, the damping coefficient c_{leg} is challenging to determine experimentally. However, parametric studies (Ruiz *et al.*, 2017) have assessed its influence on walking characteristics and GRFs, revealing that the numerical response shows little variation for a specific range of c_{leg} , chiefly when compared to leg stiffness k_{leg} and walking speed v. Therefore, considering the limitations in the experimental determination of this parameter, this study adopted c_{leg} values within the numerical ranges reported in the literature (see Section 2.4.2.3) for the simulations discussed in the following chapter.

3.4 Evaluation of DBIP models

The data extracted from the experiments described in the previous section were used to evaluate the DBIP models in terms of gait parameter predictions for both rigid surface and (what will be referred to as) moving surface scenarios.

The focus is on three gait parameters that characterize walking for applications involving low-frequency structures, such as footbridges: step frequency (f_s), walking speed (v), and the dynamic load factor for the first harmonic of the ground reaction forces (DLF₁).

For this end, the pedestrian's equation of motion was implemented in MATLAB® software (2025), and the Runge-Kutta 4th order method was adopted to solve the nonlinear

equations. The computational procedure depicted in Figure 37 is valid for both models, BM₁ and BM₂.

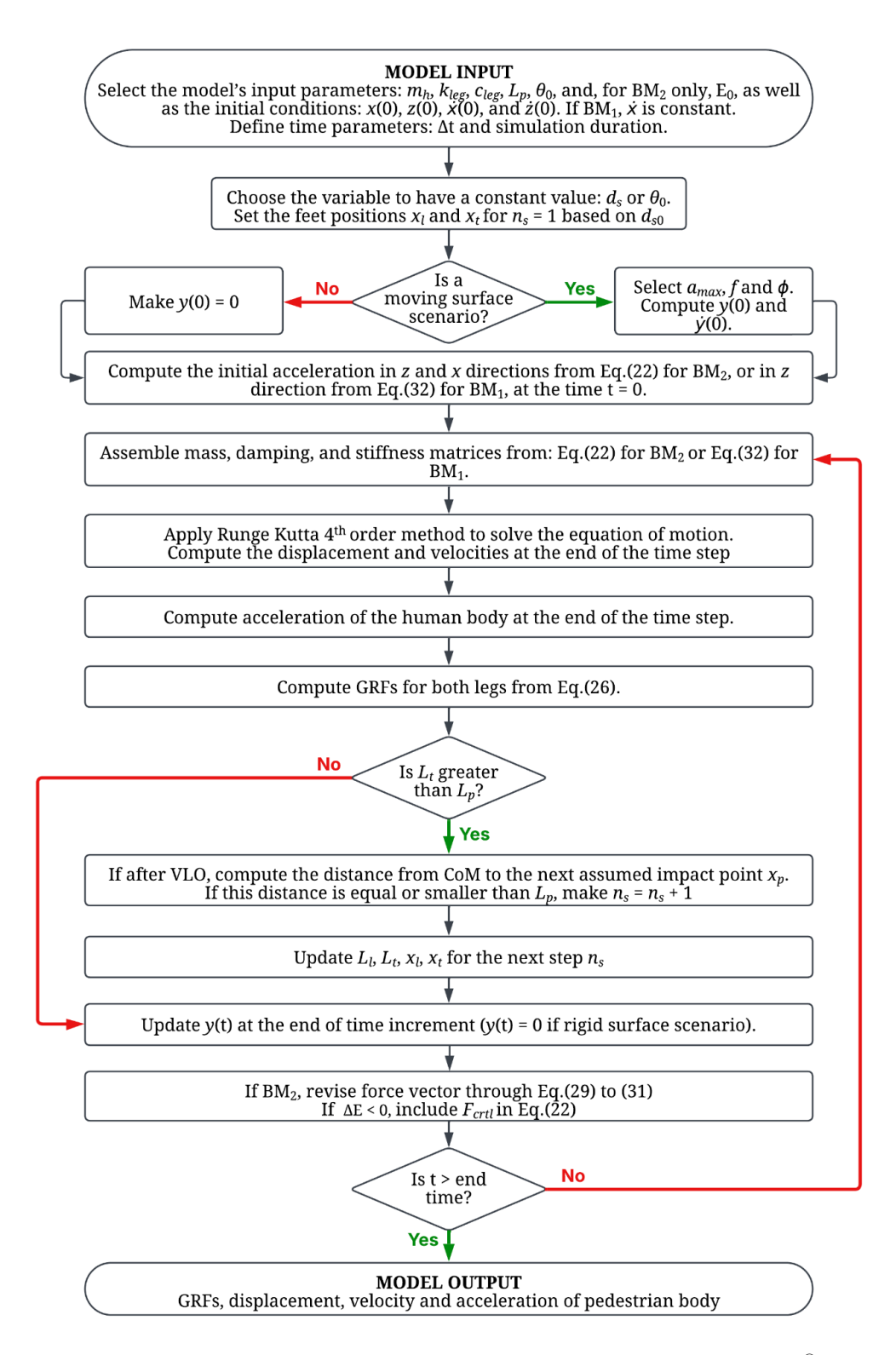


Figure 37 – Computational procedure to implement DBIP models in MATLAB® (2024)

It is worth mentioning that the main objective regarding HSI is to investigate the structural dynamic behaviour. However, since the sensitivity to vibration response is a matter of the pedestrian, comparisons will also be made of the vibration observed in the pedestrian body (that is, the pedestrian DOF).

3.4.1 Procedure for parameters calibration

After analysing the results from rigid surface scenarios, there was a need to proceed with a parameter adjustment to conduct the analyses considering the moving surface scenarios. For this purpose, Monte Carlo simulations were carried out following the calibration process depicted in Figure 38. Results in which the DLF for the second harmonic (or higher) was greater than DLF₁, or where the mid-stance footfall force peak was negative, were not considered to be a valid gait (referred as stable in Figure 38).

The strategy adopted in this study was to analyse the simulations results to select the set of parameters that best matched the gait parameters target (considering two decimal cases). After an initial analysis, it was concluded that five to ten thousand interactions, respectively for BM₁ and BM₂, were sufficient to achieve the target values for each crossing.

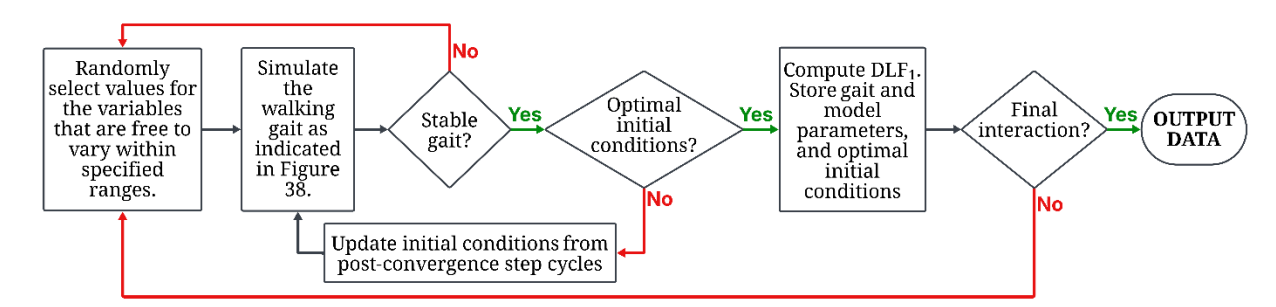


Figure 38 – Computational procedure to calibrate the DBIP models adopting the Monte Carlo simulation method

4 RESULTS AND DISCUSSIONS

The aim of this section is twofold: (1) evaluate the performance of the two previously selected biodynamic models from the Human-Structure-Interaction (HSI) perspective; and (2) evaluate the performance of DBIP models in predicting gait parameters and induced forces for rigid and moving surface scenarios from a Structure-to-Human-Interaction (S2HI) perspective.

First, the selected SMD model is analysed by comparing the numerical results against experimental data from tests carried out on the Aberfeldy Footbridge (Section 3.2.1) and Złotnicka Footbridge (Section 3.2.2). Subsequently, still within the context of applying biodynamic models for HSI simulation, both the SMD and BM₁ models were used to investigate the influence of the HSI contribution on structural response prediction when analysing both test structures.

To deepen the investigation into the functioning and performance of bipedal models, two versions of the DBIP model (single- and two-degrees-of-freedom) were evaluated based on results from an experimental campaign conducted on a controlled platform – initially on rigid surfaces, and subsequently under moving surface scenarios simulated in a vibrating platform environment to examine the effects of Structure-to-Human Interaction (S2HI).

Finally, based on the experimental-numerical correlation between the experimental results and numerical simulations adopting bipedal models, as well as the findings and insights obtained from this analysis, the DBIP models (BM₁ and BM₂) are reassessed from the perspective of human-structure interaction (HSI), incorporating adjusted parameters from the literature and the observations made in this study.

4.1 Performance of biodynamic models from a HSI perspective

Bearing in mind practical applications, this subsection focuses on the performance of both the SMD model and the SDOF DBIP model (BM₁), using as reference the experimental results obtained from the two test structures adopted in this study.

4.1.1 SMD models

The SMD basic formulation is adopted in this section to account for HSI and investigate the performance of the model against the MF model widely used by standards and guidelines nowadays. Experimental results obtained from previous works serve as a reference for comparisons. First, the formulation and parameters are analysed using the Aberfeldy Footbridge as a test structure, by investigating a single pedestrian crossing the footbridge in resonance. Then, the formulation and reliable parameters are adopted to analyse scenarios with Złotnicka Footbridge testing featuring lower acceleration levels.

4.1.1.1 <u>Aberfeldy Footbridge</u>

When it comes to the classification of this test structure according to the criteria defined in the normative documents, it is important to mention that the structure serves as the sole means route, but the access for the footbridge is very restricted since it is a private structure localised at the Aberfeldy Golf Club (Pimentel, 1997). According to the current design situations disposed on the normative documents (Section 2.2), the footbridge is classified as follows: with very weak traffic, the Hivoss (2008) classify the footbridge as a Traffic Class TC1, which complies to a minimum degree of comfort (Class CL3); Besides Sétra (2006) appoints the structure as a seldom usage (private structure), which corresponds to a Traffic Class IV, the minimum degree of comfort is still required; In the UK NA to BS (2008), considering the structure is in a rural environment (weaker traffic according to the guideline) and its respective height above ground, it was possible to determine the limit acceleration. Table 24 present the limit peak accelerations related to the guidelines' classification.

Table 24 – Aberfeldy footbridge classification according to currently guidelines and limit peak accelerations.

Guideline	Traffic	Comfort Class	Limit of vertical peak accelerations	
Hivoss (2008)	TC1 (very weak traffic)	CL3 (minimum degree of comfort)	Between 1.0 and 2.50 m/s ²	
Sétra (2006)	Traffic Class IV	Minimum Comfort	Between 1.0 and 2.50 m/s^2	
UK NA to BS (2008)	Rural Crossing	Not mentioned*	1.12m/s ² *	

^{*}This vibration limit is compatible with the aforementioned range proposed for the other guidelines.

It is worth mentioning that the measured peak acceleration of 2.14 m/s² was far above the limit recommended by the UK NA to BS (2008) of 1.12 m/s² resulting from the application of Eq. (2). However, the value is below the limit stated by Hivoss (2008) and Sétra (2006) Guidelines.

The performance of the SMD parameters was investigated by comparing numerical results obtained adopting the interaction model of Pfeil *et al.* (2014) against the experimental result (see Table 25). The results were compared in terms of the maximum (a_{max}) and root mean square (a_{rms}) acceleration, as well as the fit to the experimentally measured acceleration response time history (see Figure 39 and Figure 40).

For conciseness, only the best results obtained for each of the formulations are shown in Figure 39 and Figure 40. However, Table 25 contains the whole range of results obtained for all formulations. It can be noted that a range of values was proposed in some formulations for the pedestrian parameters in Gomez *et al.* (2016) and Shahabpoor *et al.* (2016b), and this is the reason why some combinations of these values (in particular, damping and natural frequency of the pedestrian body) were performed (see sets (1) to (4) in Table 25). On the other hand, for the formulations in which regression expressions or average values were proposed (Silva & Pimentel, 2011; Silva *et al.*, 2013; Toso *et al.*, 2016), the body parameters were obtained by employing the body parameters of the test subject.

Table 25 - Results obtained employing different values for the pedestrian parameters.

Set	Gomez et al. (2016)				Shahabpoor et al. (2016)			
	(1)	(2)	(3)	(4)*	(1)	(2)	(3)	(4)*
m_p (kg)	80	80	80	80	80	80	80	80
ξ_p (%)	12	18	12	18	27.5	30	27.5	30
f_{np} (Hz)	2.29	2.29	2.52	2.52	2.75	2.75	3.00	3.00
DLF	0.27	0.27	0.26	0.26	0.26	0.26	0.25	0.25
a_{max} (m/s ²)	2.19	2.08	2.25	2.17	2.18	2.17	2.16	2.15
a_{rms} (m/s ²)	0.93	0.90	0.95	0.93	0.94	0.93	0.93	0.92

	MF model	Jiménez Alonso & Sáez (2014)	Silva & Pimentel (2011)	Silva <i>et al.</i> (2013)**	Toso et al. (2016)
m_p (kg)	-	67.18	60.18 - 61.68	60.18 - 61.68	52.71 - 54.75
$\xi_{p}\left(\% ight)$	-	47.18	53.11 - 53.58	52.34 - 52.46	55.42 - 57.76
f_{np} (Hz)	-	2.76	2.67 - 2.69	2.72 - 2.74	1.74 - 1.81
DLF	0.26	0.26	0.27	0.27	0.29
a_{max} (m/s ²)	2.40	2.16	2.15	2.17	1.88
a_{rms} (m/s ²)	1.03	0.94	0.94	0.95	0.86

^{*} Best result obtained for the range of the proposed values.

Obs.: The variation in the SMD parameters from Silva *et al.* (2013), Silva & Pimentel (2011) and Toso *et al.* (2016) was due to the dependence of such parameters with the varied pacing rate throughout the crossing.

^{**} Values from Silva *et al.* (2013) were close to the ones from Silva & Pimentel (2011) and were not shown in Figure 40.

For each case, the unknown DLF₁ of the test subject was adjusted to produce a best fit, based on a trial-and-error process. However, it can be seen from Table 25 that this is not a significant issue since the best value of the DLF₁ obtained for each formulation varied slightly, around the value 0.27 stated in Pfeil *et al.* (2014).

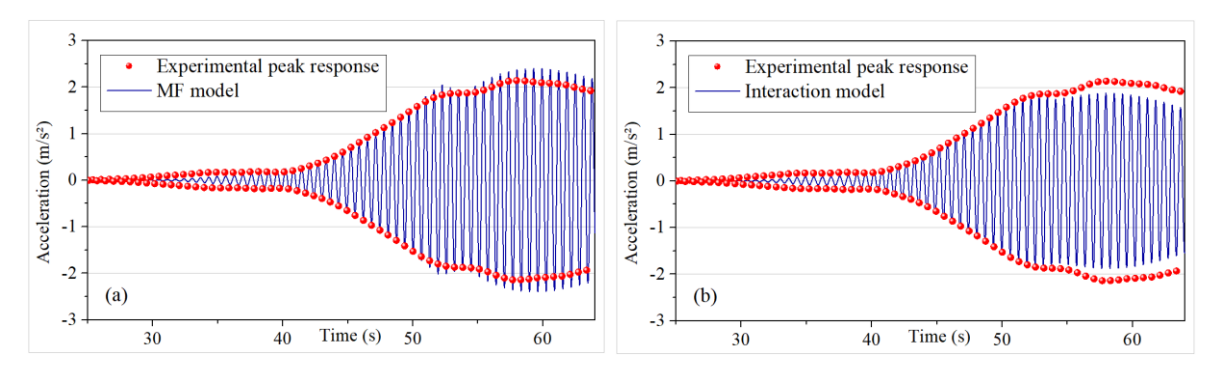


Figure 39 - Acceleration at the mid span of the footbridge - (a) Experimental x MF model; (b) Experimental x Interaction Model using the set of parameters from Toso *et al.* (2016). (Previous used in Silva *et al.*, 2020)

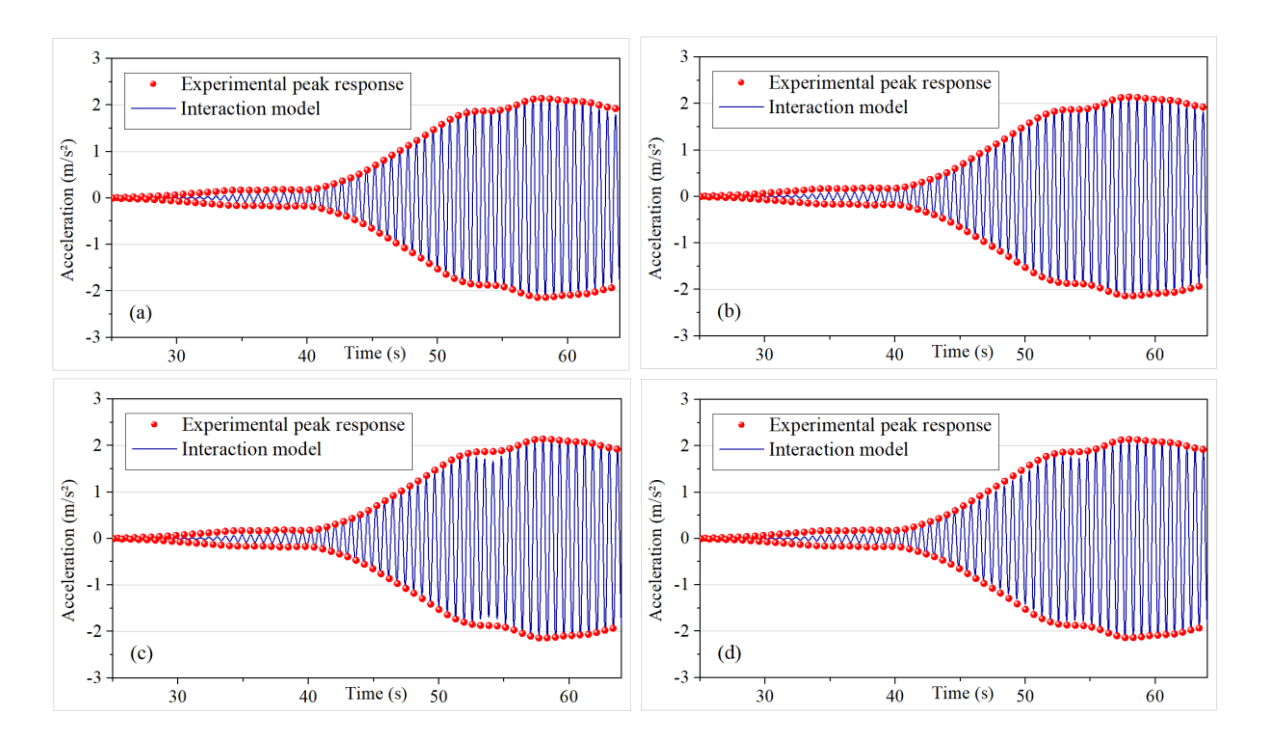


Figure 40 - Acceleration at the mid span of the footbridge - Experimental versus Interaction Model using the set of parameters from (a) Silva & Pimentel (2011); (b) Jiménez-Alonso & Sáez (2014); (c) Gomez *et al.* (2016); (d) Shahabpoor *et al.* (2016). (Previous used in Silva *et al.*, 2020)

Regarding the values of the SMD parameters, it is noted that despite the wide range of values of the parameters, no great difference was identified among the results (Figure 40).

However, some discrepancies were noted about the proposed values of the natural frequency f_{np} of the pedestrian body (see Table 27). Toso *et al.* (2016) values for this parameter are below all the other works and the results with their parameters were the least accurate among the whole set of SMD parameters investigated (Figure 39b). This requires further studies, with a larger sample of experimental data, to confirm or not the relevance of this parameter, since the natural frequency f_{np} may not be the sole cause of the discrepancy.

In general, despite the different ways of obtaining the SMD parameters, the results were in agreement with the experimental one and presented a much better performance against MF model (Figure 39a), which overestimated the bridge response. The difference in peak and RMS values between MF and biodynamic models might be small (see values in Table 25), but this was for a single pedestrian crossing. Actual design cases consider group or streams of pedestrians crossing the structure, which is analysed in the next section.

4.1.1.2 Złotnicka footbridge

According to currently design situations disposed on the normative documents (section 2.2), the footbridge is classified as follows: From the Hivoss (2008), a traffic class TC1 (very weak traffic) was considered. On the other hand, an appointed comfort class CL3 (minimum degree of comfort) was targeted; This corresponds to Traffic Class III (footbridge for standard use) and minimum comfort, according to the Sétra (2006); In the UK NA to BS (2008), the accepted peak acceleration was obtained by considering the structure as a suburban crossing and its respective height above ground. Table 26 present the limit peak accelerations related to the guidelines' classification.

Table 26 – Złotnicka footbridge classification according to currently guidelines and limit peak accelerations.

Guideline	Traffic	Comfort Class	Limit of vertical peak
Hivoss (2008)	TC1 (very weak traffic)	CL3 (minimum degree of comfort)	Between 1.0 and 2.50 m/s ²
Sétra (2006)	Traffic Class III	Minimum Comfort	Between 1.0 and 2.50 m/s^2
UK NA to BS (2008)	Suburban Crossing	Not mentioned*	1.3m/s^{2*}

^{*}This acceleration limit is compatible with the aforementioned range proposed by the other guidelines.

Since it presented great results in the previous analysis, the parameters of the body (modal mass m_p , damping c_p and stiffness k_p) were obtained from regression expressions

(Silva & Pimentel, 2011) for the test subject as a function of the total subject mass M and pacing rate f_p . Reference values of these parameters for the pedestrian are shown in Table 27 for a pacing rate of 2.07 Hz.

Table 27 – Reference values of pedestrian dynamic parameters.

Modal Mass m _p	Modal Stiffness kp	Modal Damping c_p		
(kg)	(N/m)	(Ns/m)		
32.65	12,574.66	630.68		

The following investigations were carried out according to this sequence of steps: (a) obtaining the structural damping ratio (so as to use it in Eq. (17)); (b) obtaining the DLF of the pedestrian from single crossings; (c) comparing the results for single crossings between measurements and simulations; and (d) investigating the effect of the number of pedestrians on the two modelling approaches (force-only and dynamic systems).

As previously mentioned, the structural damping was obtained from the tail end of the pedestrian tests, after the test subjects (here referring to all test subjects from Hawryszków *et al.*, 2021) left the structure. This was carried out by adjusting straight lines to a plot of the logarithm of peak values of the decay versus number of cycles, as shown in Figure 41. The slope of the straight line is the damping, in terms of logarithmic decrement. However, it was soon realized that damping had a strong dependence on the vibration level, which can be seen from the variation in the slopes in Figure 41.

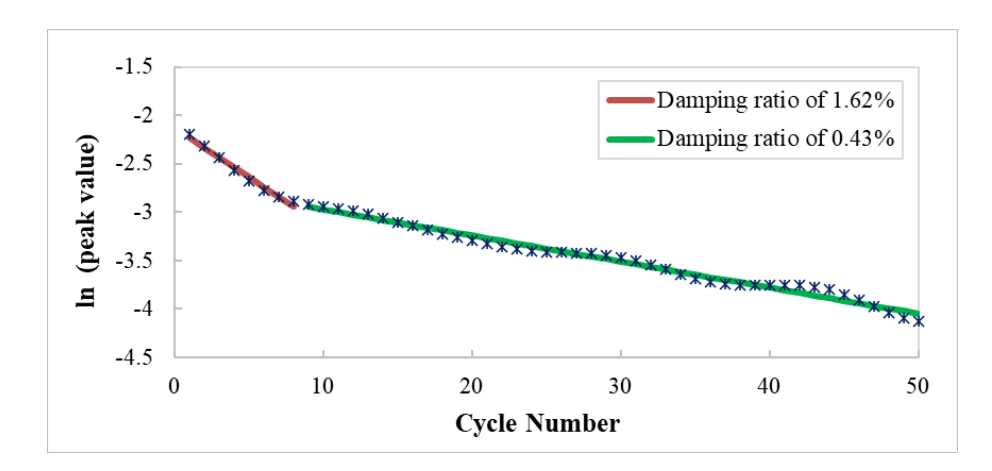


Figure 41 - Obtaining damping ratios from the tail-end signal of pedestrian tests (Previous used in Hawryszków *et al.*, 2021).

This was also noted by comparing the damping ratios obtained from single and group crossing signals, the latter presenting higher vibration levels than the former⁶. A collection of damping ratios obtained from several crossings are shown in Figure 42, taking as a reference the value of the acceleration amplitude at the beginning of the region of the decay signal that was employed for the respective calculation.

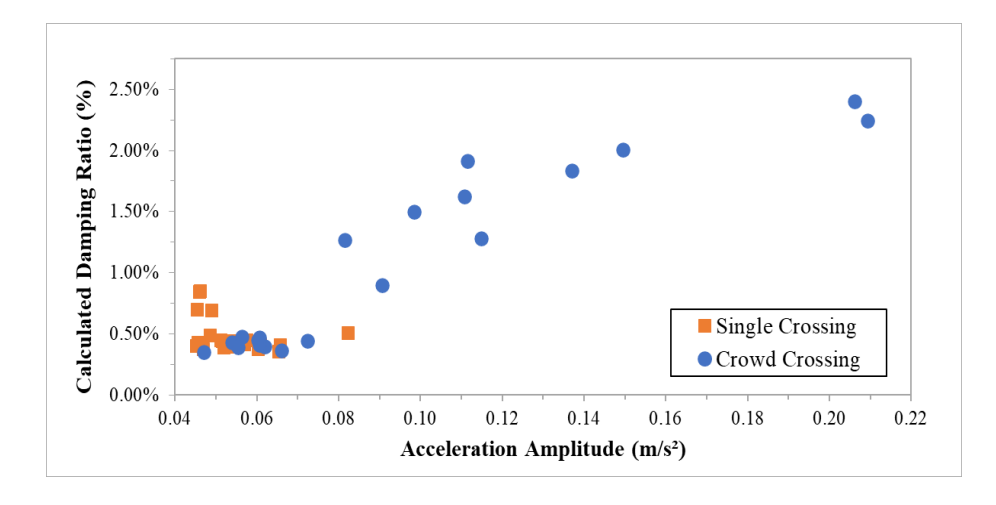


Figure 42 - Damping ratios for the first structural mode (Previously used in Hawryszków *et al.*, 2021).

This nonlinear behaviour adds a degree of uncertainty to the determination of the DLF₁ of the pedestrian since damping would in principle vary during the crossing. Another factor to consider is the small changes in walking rhythm, in spite of using a metronome. The effect of these changes is considered by employing the vibration signal measured at the pedestrian's waist to identify changes in the pedestrian pacing rate during the crossing. Such changes also imply the adjustment of the pedestrian body parameters during the crossing (see Table 27 for reference values), as they depend on the pacing rate.

The DLF₁ value were, thus, obtained by adjusting the numerical vibration signature to the respective measured one for several crossings of the test subject. A trial-and-error strategy was adopted according to the following rules of thumb: (a) changes in the value of the DLF₁ affect only the amplitude of the response signal; and (b) changes in damping affect both the

⁶ It is important to mention that, although the group loading is not the focus in this study, the damping ratio discussion also include the results for group crossings. More details can be seen in Hawryszków *et al.* (2021).

shape and the amplitude of the response signal. Damping ratios were adjusted to values of around 1.6% in most cases (for each crossing).

However, it is important to emphasize that the simulations conducted here account for step losings. Disregarding such gait changes during walking leads to different structural damping ratios in the simulation so as to match the acceleration time-history between experimental measurements and simulations (value discussed in the next section).

The selection of this value for damping was based on observed acceleration amplitudes during the crossing and the corresponding values for the damping ratios shown in the plot of Figure 42. A DLF₁ value of 0.26 was then obtained. It worth noting that such value is within the ranges from the literature (see Table 10).

Intra-subject variability was expected, as shown in Figure 43 and Figure 44, which show the results from two crossings of the same test subject. Another feature that can be observed from these figures is that for the single crossings and vibration levels with peak values of around 0.15 m/s², no substantial changes in the vibration response are noted in either the time response or spectrum between force-only and dynamic (interaction) models that represent the pedestrian action. It can also be noticed from both the time domain and spectral plots that a perfect match between measurements and simulations is not present. This is possibly related to the nonlinear behaviour of the structure, as it was previously seen that damping is strongly dependent on amplitude levels, which vary throughout the crossing.

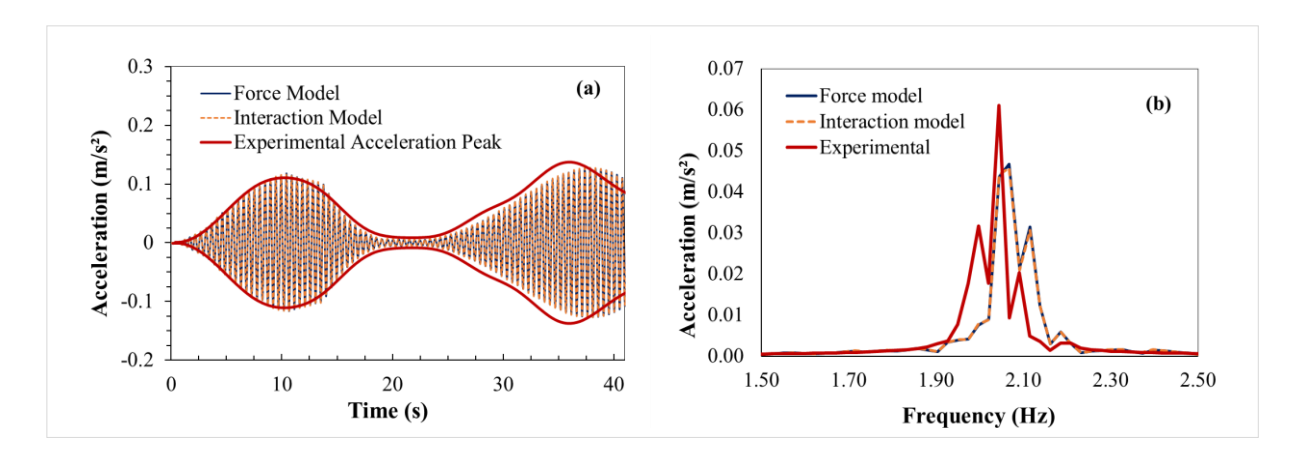


Figure 43 - Second crossing of Test Subject 2: (a) time response; (b) spectrum. (Previously used in Hawryszków *et al.*, 2021)

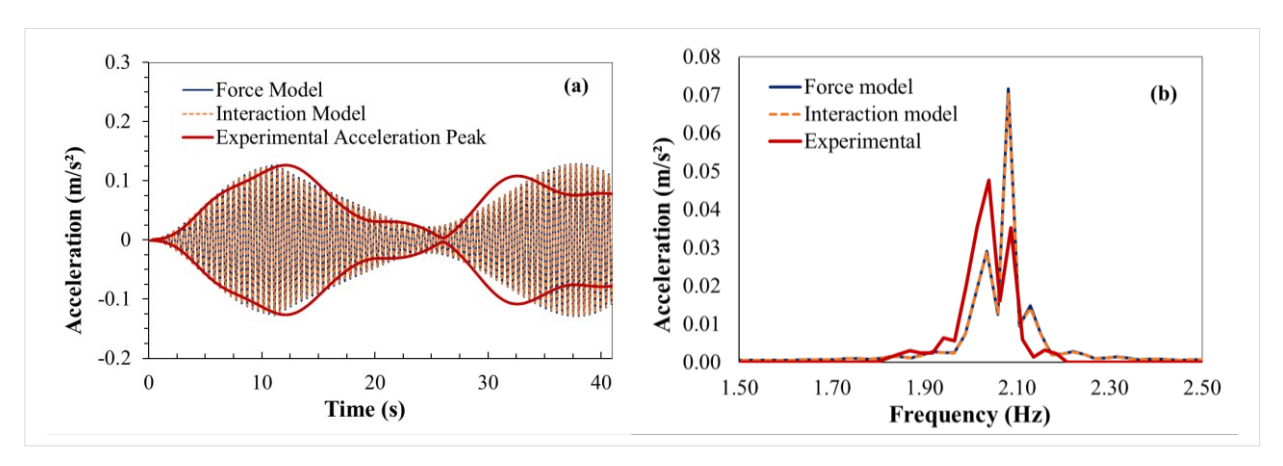


Figure 44 - Third crossing of Test Subject 2: (a) time response; (b) spectrum. (Previously used in Hawryszków *et al.*, 2021)

An additional analysis was carried out to investigate the correlation between the number of pedestrians (and intrinsic vibration levels) and the adoption of interaction models. By taking the UK NA to BS (2008) as a reference, the number of pedestrians to be considered in a group can vary from 2 (seldomly used, rurally located footbridges) to 16 (footbridges that serve as primary access to assembly facilities). Then, bearing in mind the differences previously observed in the modelling effect between force models and dynamic systems in terms of vibration response, it is worth investigating the effect that the number of pedestrians may present in terms of the difference between the (code) approach of modelling the action of pedestrians as force-only and as dynamic systems interacting with the structure.

For this end, a DLF₁ of 0.273 (from the group of test subjects in Hawryszków *et al.*, 2021), an individual total mass of 72.3 kg and a crossing speed of 1.51 m/s, were adopted for this investigation. The pedestrians were considered fully synchronized, as synchronization would affect both modelling strategies. Consider that the effect of pedestrians as dynamic systems is dependent on the level of vibration. In this analysis, peak accelerations changed from 0.29 m/s² for the case of a group of 2 pedestrians to 2.32 m/s² for the case of 16 pedestrians in the group. The results obtained are shown in Figure 45 in terms of the peak and RMS acceleration.

Many significant changes occurred between the modelling strategies for the case of 16 pedestrians in the group and for peak values, the latter metric being the one adopted in UK NA to BS (2008) to define comfort levels. In that case, a reduction of 25% occurred in the peak values (maximum acceleration) when pedestrians were modelled as dynamic systems. On

the other hand, for the small groups, the difference was not significant. It should be noted that all these values and comments are applicable to this case study only, since this depends on the footbridge geometry and the level of accelerations produced. However, modelling pedestrians as dynamic systems was shown to be more realistic from the previous analysis and led to reductions in the calculated values.

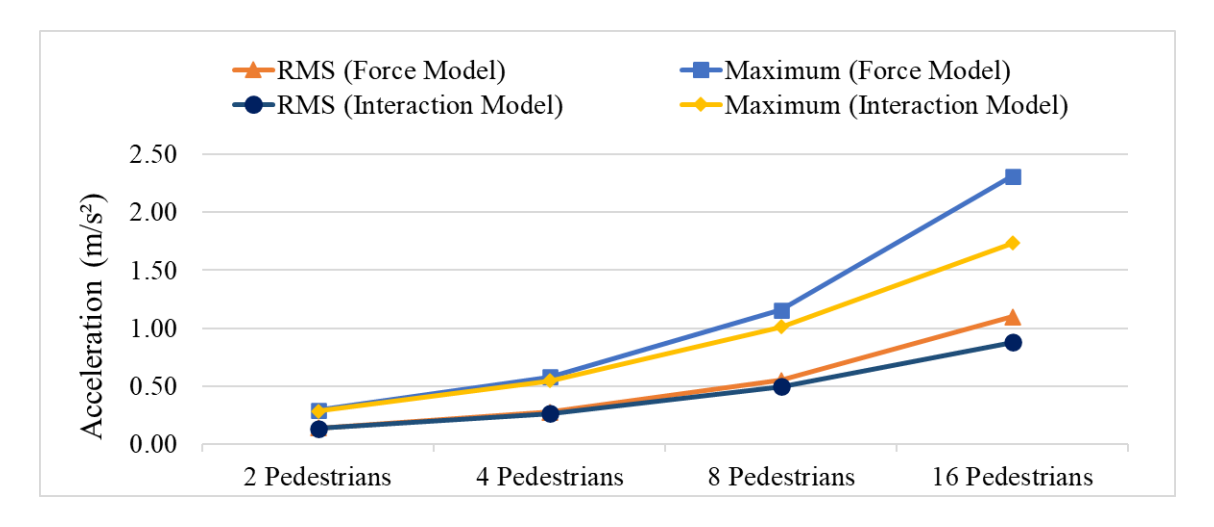


Figure 45 – Peak and RMS accelerations for models analysed. (Previous used in Hawryszków *et al.*, 2021)

4.1.2 SDOF DBIP model versus SMD model

In this section, the SDOF DBIP model (BM₁) performance is analysed for scenarios of low and high vibration levels, to investigate the model reliability regarding HSI predictions. For the sake of comparison, results using the selected SMD model (Section 2.4.1) adopting parameters introduced by Silva & Pimentel (2011) were adopted since promising results were previously obtained. An initial analysis discusses some of the model limitations concerning the selection of BM₁ parameters. For a better visualization of the test's details, Table 28 gather the important information from both test structures for the analysis.

	•	•	*
	Test Structure	Złotnicka Footbridge	Aberfeldy Footbridge
Structure	Modal mass (1st mode)	22205.8 kg	2547 kg
	Damping ratio (ξ_i)	Variable	0.84 %
	Natural frequency (f_n)	2.067 Hz	1.59 Hz
	Mode shape (ϕ)	From Finite Element Model	Experimentally obtained
	Accelerometer Position	16m from the bridge edge	Mid-span
	Maximum Acceleration*	0.14 m/s^2	2.14 m/s^2
Pedestrian	Pedestrian Identification**	TS-P1	TS-P2
	Pedestrian total mass	48 kg	80 kg
	Pacing rate (f_s)	Average of 2.07 Hz	Average of 1.56 Hz
	Longitudinal Speed (x)	1.588 m/s	1.404 m/s (assumed
SMD model	Modal Mass (m)	32.62 kg	60.55 kg
param. (Silva &	Stiffness (k)	12578 N.m ⁻¹	17100 N.m ⁻¹
Pimental, 2013)	Damping (c)	630.11N.s/m	1088 N.s/m

Table 28 – Details of the experimental results of interest for this study and SMD model parameters

4.1.2.1 <u>Initial analysis</u>

This study does not focus on discussing each BM₁ parameter's influence on the gait stability and GRFs. However, an initial analysis was carried out to select a set of parameters and initial conditions that reproduce a stable gait on a rigid ground for the upcoming HSI analysis. It is worth mentioning that no measurements were taken for the contact forces for both experimental campaigns. The absence of this information leads us to apply the following approaches to calibrate the GRFs for the simulations: (1) compare their DLFs to values presented in the literature, (2) verify whether the pedestrian body natural frequency is within the range appointed in the literature, and (3) reproduce a stable gait.

The analysis carried out in this section disregards the HSI term from the system's formulation by considering a null structural mode shape. Except for the step length that should be calculated based on the step frequency and walking speed to match the experimental results, BM₁ parameters were initially selected from the expressions from Ruiz *et al.* (2022) and taken as a reference despite the absence of the pedestrian height information.

Regarding the GRF simulation, the MF model is based on an approximation for the experimental GRFs, being calculated as a Fourier Series (Shahabpoor *et al.*, 2016a; Živanović *et al.*, 2005; Caprani *et al.*, 2011). It should be noted that this modelling strategy is also an explicit part of the formulation of SMD biodynamic models so as to reproduce the contact forces (see Section 2.4.1). In the MF model, Dynamic load factors (DLFs) were introduced to quantify the contribution of each harmonic component on the total force, and several studies

^{*} From filtered signal.

^{**} From now on each test subject will be referred as TS-P1 and TS-P2 for the sake of conciseness.

presented design values or expressions for such factors (Kerr & Bishop, 2001; Rainer *et al.*, 1988; Pernica, 1990; Young, 2001; Butz *et al.*, 2008).

However, it should be emphasized that for all proposed DLFs in Kerr & Bishop (2001), Rainer *et al.* (1988), Pernica (1990), Young (2001) and Butz *et al.* (2008), the step frequency appears as the only variable. Therefore, these proposals disregard the influence of pedestrian speed or step length on such parameters. Another noteworthy aspect is that the step length d_s can be independent of the step frequency f_s , as mentioned by Živanović *et al.* (2022). Hence, a pedestrian walking with a low step frequency can still have a considerably high speed, bearing in mind the correlation between speed, step length, and step frequency ($v = d_s f_s$). When it comes to the pedestrian speed influence on the DLFs, and consequently on the GRFs magnitude, some experimental results (Ruiz *et al.*, 2022) showed that higher speeds for the same step frequency resulted in a higher DLF for the first harmonic. In turn, BMs do not present any explicit DLFs on its formulation; instead, the GRFs are a consequence of the model's movement and the selection of the gait parameters.

Bearing this in mind, for the investigation of the actual related DLFs resulting from the BM₁, Figure 46a shows DLFs obtained from calculated GRFs due to a BM walking on rigid ground for TS-P2, adopting the parameters presented in Table 29, and compared them with the DLFs proposed by the aforementioned studies. It should be noted that a lower speed was assumed for the BM₁ (see Set 2), which falls within the range 0.98 – 1.03m/s, applicable to a step rate of 1.56Hz, according to some studies (Butz *et al.*, 2008; SCI, 2007; ASCE, 1982; Yoneda, 2002).

As evidenced in Figure 46a, the results achieved using Set 1 of parameters were significantly higher when compared to the 1st and 2nd DLFs from the literature (grey ranges in Figure 46a). In contrast, by adopting Set 2 of parameters resulted in values closer to the literature proposals except for Butz *et al.* (2008). When the correlation between speed and step frequency aligns with what is expected from the literature, the DLFs obtained from the BM₁ simulations can fall within the range of the literature's proposals. However, when walking at a higher speed for the same step frequency, pedestrians tend to naturally apply more force to the ground, implying higher DLFs. BMs might be able to capture this feature in such cases. Nevertheless, only additional investigations could confirm this line of reasoning as further explored in this study.

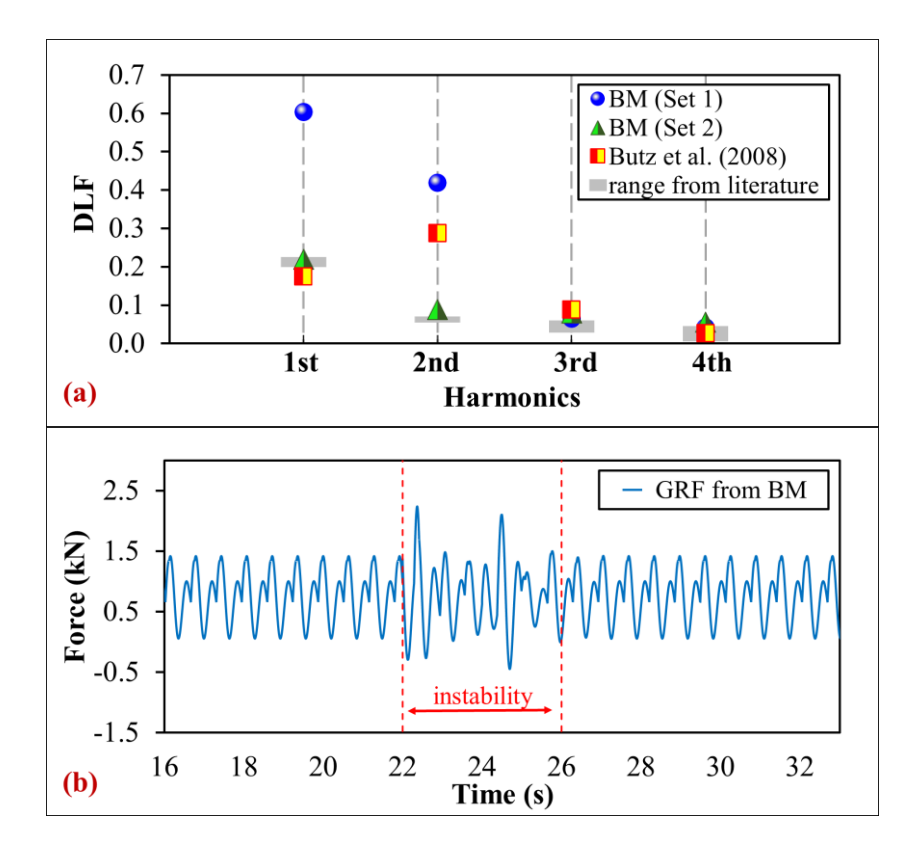


Figure 46 - (a) DLFs for the first four harmonics and (b) GRF obtained by adopting Set 1 of BM₁ parameters including step losing effects ($f_s = 1.57$ Hz for 22s < t < 24s)

Table 29 – Set of BM₁ parameters and initial conditions for the TS-P2.

Set	$\dot{x}(m/s)$	$f_s(Hz)$	$m_h(kg)$	$L_p(\mathbf{m})$	$k_{leg}(kN/m)$	$\xi_{leg}(\%)$	θ_0 (°)	\dot{z}_0 (m/s)
1	1.404	1.56	80	1.14	19.0	13	63.76	-0.307
2	1.000	1.56	80	1.14	19.0	13	70.04	-0.207

In addition, one BM₁ limitation could be observed, regarding the inclusion of step losing effects in the model, i.e., a slight variation in the step frequency. It should be noted that the BM₁ formulation does not present the step frequency as an input parameter. Any changes in step frequency (f_s) can be introduced by either a change on longitudinal speed (\dot{x}) or step length (d_s) . However, any d_s variation led to the model's instability for several step cycles (Figure 46b). Even more, any adjustments on longitudinal speed for achieving the aimed new f_s resulted in insignificant changes in the applied forces. Because of that, any step losing was disregarded in this section.

4.1.2.2 SDOF DBIP Model (BM₁) reliability

The interaction model (Section 2.4.2.4) intrinsically simulating the bipedal nature of the walk is adopted to investigate its reliability against experimental data from two lively footbridges and the influence of the DLFs produced by the BM_1 on the structural response. The BM_1 parameters were chosen based on the discussion presented in the previous section.

The analysis was initially conducted on the test structure with low vibration levels, the Złotnicka Footbridge, in order to first examine other aspects of BM₁'s performance. Some investigations were carried out for this test structure previously (more details in Hawryszków *et al.*, 2017; Hawryszków *et al.*, 2021). One important finding has a correlation with its possible high degree of non-linearity. This is because changes in its damping coefficient due to different vibration levels were identified. It could be observed that only a modal damping (ξ_i) adjustment for the numerical simulations could make the numerical results to follow the measured ones. With that in mind, for this analysis, a damping coefficient of 2.5% is assumed for the 1st vertical mode of vibration (disregarding step losings). Furthermore, since this test structure features low vibration levels (see peak acceleration in Table 28), the HSI has minor influence on the system response (see Section 4.1.1.2), which enabled other aspects of modelling to be investigated.

In Figure 47a, accelerations obtained from the BM₁ numerical simulation due to TS-P1 crossing are compared to the experimental filtered acceleration at the node of interest (see Table 28), and to results obtained by alternatively applying the SMD model. Initially, a DLF₁ value of 0.434 (mean value obtained from the literature proposals) was adopted for the SMD model. It is noteworthy that differences between both simulations (BM₁ and SMD model) and experimental data at the descending segment of the curves while TS-P1 crosses the first span are significant. Nonlinear effects or else a lack of accuracy on the identification of the actual mode shape could explain these differences, for which the FEM model (Hawryszków *et al.*, 2017) employed for the modal analysis could not predict.

Besides, the BM₁ overestimated the structure's response compared to the SMD model's performance, which provided more accurate results. In this matter, to investigate the influence of the intrinsic DLFs from BM₁ on the structural response, additional comparisons with the SMD model are depicted in Figure 46b. When a DLF₁ of 0.737, which was obtained from the GRFs of the BM₁, was adopted for the SMD model, no great differences were observed between the model's results. This finding reaffirms that an overestimation of DLFs by the BM₁ could be

an issue for a structure's behaviour analysis using such a model even for cases of minor HSI effects.

Moreover, despite the DLF₁ from BM is out of the normal range of the literature, only GRF measurements could confirm its reliability. The lack of this information leads us to believe that the BM₁ can overestimate the DLF for the first harmonic, as also concluded by Ruiz *et al.* (2022).

It should be noted that it is still necessary to evaluate whether the overestimation of DLFs is a consequence of assuming that the longitudinal speed \dot{x} is constant and equal to the walking speed v (investigated in Section 4.2).

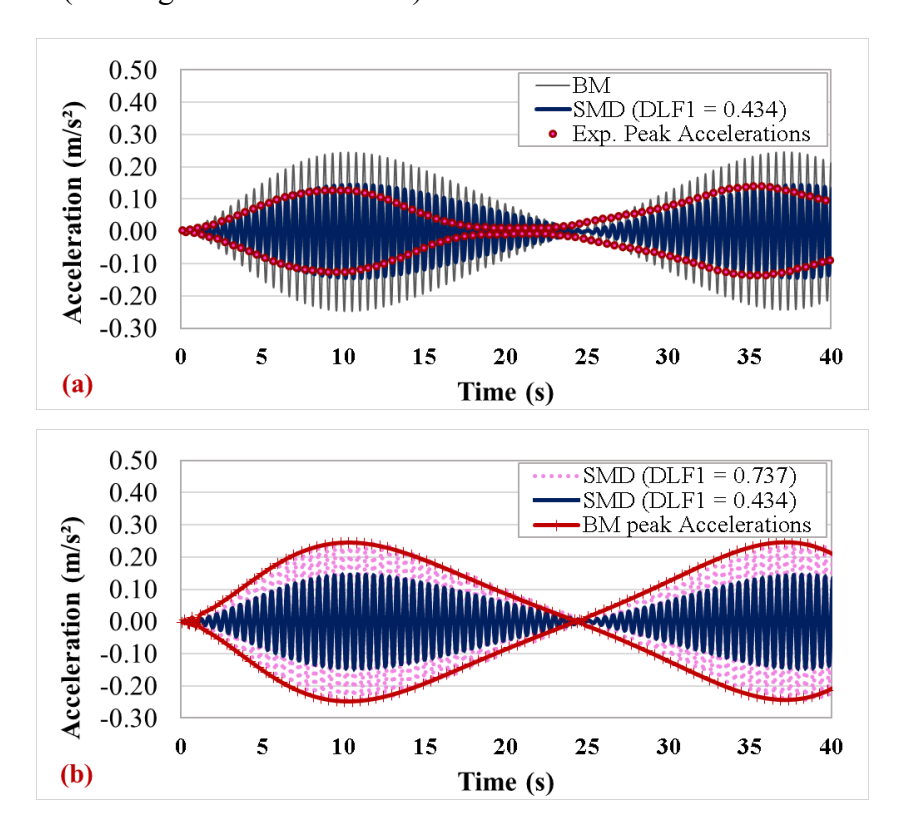


Figure 47 - Acceleration at the node of interest for the TS-P1 single crossing adopting BM₁ (L_p = 1.30m, k_{leg} = 18kN.m, ξ_{leg} = 13%, θ_0 = 63.76° and \dot{z} = -0.307) and compared (a) against experimental filtered acceleration and SMD model, and (b) against SMD model adopting two different DLFs for the first harmonic (in red, the peak values obtained by the BM₁)

The experimental results obtained from the Aberfeldy Footbridge allow the investigation of the BM₁'s performance in predicting the HSI effects due to high vibration levels observed at this structure. The BM₁ reliability is analysed by comparing its results to the SMD model simulations and measured accelerations. As for the previous structure, a similar approach

was considered: adopting a DLF₁ related to the BM₁ for the SMD model numerical simulation. Following this line of reasoning, it is possible to investigate the influence of the DLF₁ predictions, and consequently, the GRF predictions, on the pedestrian-structure's response. Figure 48 depicts the results.

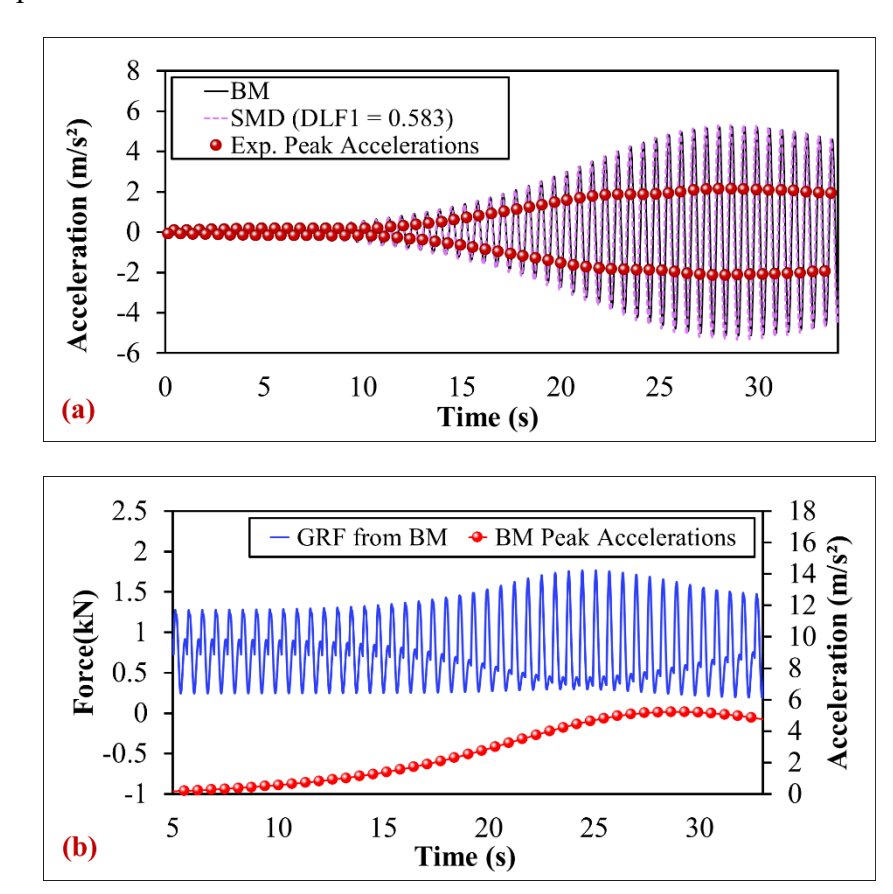


Figure 48 - (a) Acceleration at the node of interest for TS-P2 single crossing adopting BM₁ ($L_p = 1.30$ m, $k_{leg} = 18$ kN.m⁻¹, $\zeta_{leg} = 13\%$, $\theta_0 = 72.65^{\circ}$ and $\dot{z} = -0.307$) compared against the experimental filtered acceleration, and the SMD model adopting DLF₁ from the BM₁ simulation; (b) GRF generated from the BM₁ along with to the respective simulated peak accelerations' progression of the structure.

As seen in Figure 48a, significant differences between the BM₁ numerical simulations and the experimental data were obtained. It should be noted that the DLF₁ value of 0.583 related to the BM₁ is considerably higher than the literature proposals (see Figure 46a for the literature range). In an attempt to investigate whether the lack of accuracy when using the BM₁ is caused by an overestimation of DLFs solely, the BM₁ results were compared to the SMD model adopting such DLF₁, and no great differences were observed between these models' results. Therefore, the observed inaccuracy when using the BM₁ model can be attributed to the

overestimation of the DLF₁ value. It's worth mentioning that previously, the SMD model performed well when adopting a DLF₁ from the literature and accounting for step-losing effects.

Regarding the changes in the walking pattern due to the HSI, while walking on flexible surfaces, particularly in resonance conditions, individuals can perceive the vibrations and attempt to adjust their walking pattern to the structure's movement. However, how these changes occur depends on factors that require further investigation. The influence of acceleration levels is one such factor. This effect is illustrated in Figure 48b. It's worth noting that after a certain acceleration level (around 1.2m/s²), the growth of the GRF become more prominent.

4.1.3 Concluding Remarks

A discussion of SDOF SMD models proposed in the literature to model pedestrians in HSI studies was presented. It was shown that the formulations proposed to account for HSI were based on the same concept that the ground reaction force, either on a rigid or on a flexible surface, is equal to the inertia force of the pedestrian body. In general, this led to an analytical formulation to represent the coupled pedestrian-structure system.

The formulation presented by Pfeil *et al.* (2014) made it clear that the ground reaction force obtained from rigid surfaces (widely used in the literature) can be inserted into the equations that consider the deformability of the structure.

With a slight modification, this interaction model adopting an SDOF SMD model for the pedestrian (Pfeil *et al.*, 2014) was adopted to compare the performance of various SMD parameters proposed in the literature and obtained through experimental measurements with walking subjects, even though each set of parameters was obtained in different and independent ways.

Despite the different ways in obtaining the SMD parameters, the different proposals generally resulted in satisfactory agreement with the experimental result obtained from a pedestrian crossing a lively footbridge. However, a less accurate response was obtained from one of the formulations, when the proposed value for the natural frequency of the pedestrian body was lower.

An additional simulation investigated the effect of the number of pedestrians on a crossing group, and an expected increase in the differences between the two modelling approaches for the pedestrians (MF model and SMD interaction model), revealed that the latter led to reductions in the structural response, which is positive from the perspective of design. This highlights the importance of incorporating the dynamics of the body to HSI investigations.

A discussion on the functioning of the DBIP model was also presented, focusing on two key aspects: (a) the numerical consequences of reducing the model from a 2DOF model (BM₂) to a single-degree-of-freedom model (BM₁); and (b) the choice of the parameter that governs the prediction of the next impact point: setting the step length or the attack angle as constant in the simulations.

The decision to set a constant value to either the attack angle or the step length in successive step cycles, directly influences the ground reaction forces (GRFs) produced and the step frequency. It was concluded that, although step frequency is not an input parameter in DBIP models, setting a constant step length for each step cycle in BM₁ can indirectly impose the step frequency, since the longitudinal walking speed is constant in this version of the DBIP model.

Given this practical application, an interaction formulation adopting BM₁ was evaluated and compared to the SMD model performance. BM₁ was not successful in reproducing the experimental response, when the pairs of step frequency and walking speed obtained from the experiments were maintained. In both structures investigated, BM₁ overestimated the structural response, and it was concluded that this issue is related to the limitation of DBIP models in simultaneously simulating the gait parameters v, f_s and DLF related to the first harmonic of the GRFs (DLF₁), and not in the interaction contribution. The DLF₁ values were generally higher than those commonly reported in the literature.

This observation was further supported when the SMD model, using similar values for the DLF₁, produced similar results to the BM₁ simulations. Additionally, adaptations in walking gait in response to the structure's acceleration level significantly increased GRFs, consequently amplifying the structural response.

For the following analysis, it is important to emphasize that the investigation conducted in the previous subsection using BM₁ was performed without experimental ground reaction

forces (GRFs) for reference, as such data were not available at that stage. An overestimation of the structural response was observed, with evidence suggesting that it was caused by an overestimation of the DLF₁ values across both test structures analysed. To further investigate the behaviour of the DBIP models and verify whether this overestimation persists, a more comprehensive experimental dataset – including both kinetic and kinematic data – is now considered. This extended analysis aims to assess the suitability of the DBIP models for practical applications and to determine whether their predictive capacity is sufficient or inherently limited.

4.2 Performance of DBIP models from the S2HI perspective

This section addresses the performance of the DBIP models in their two versions (BM₁ and BM₂), focusing on gait parameter prediction and their ability to reproduce structure-to-human interaction (S2HI) effects. The assessment is based on results obtained from the experimental campaign conducted at the VSimulators facilities (2025). Initially, rigid surface scenarios are analysed to determine the model parameters used in the subsequent investigations involving moving surface scenarios (see Section 3.3 for the adopted methodology).

4.2.1 Rigid surface scenarios

For rigid surface scenarios, the simulations aim to investigate the implications of simplifying the DBIP model by assuming a constant longitudinal speed, as well as the influence of the choice of the parameter governing the definition of the next impact point in the model's gait – specifically, by setting d_s or θ_0 for every step cycle. Furthermore, the analyses presented in this section aim to evaluate the performance of the one- and two-degree-of-freedom bipedal models (BM₁ and BM₂) in simultaneously replicating the three walking parameters (v, f_s and DLF₁) relevant to civil engineering applications.

Importantly, this study does not focus on a statistical analysis for an application of the bipedal models, but rather on the performance and peculiarities of modelling the pedestrian's body with the simplifications previously presented.

4.2.1.1 <u>Experimental-numerical correlation</u>

First, it is worthwhile to evaluate the model's ability to replicate a walking gait that aligns with the experimental results. This preliminary investigation aims to determine whether DBIP models (BM₁ and BM₂), regardless of their simplifications, can simultaneously reproduce the three gait parameters (v, f_s and DLF₁) that characterize the walking gait.

As the objective is to assess the models' performance through experimental-numerical correlations, the simulations and analyses were conducted using experimental parameters extracted from each crossing within the ranges presented in Table 30 (see Tables A.1 to A.3 for the parameters corresponding to each crossing).

Table 30 - Gait and model parameters extracted from experimental data for each test subject for rigid surface scenarios

TS	Walking	Gait paramet	ters		DS phase	Model Parameters				
	scenario	$f_{s,exp}$ (Hz)	v_{exp} (m/s)	DLF_1	(seconds)	k_{leg} (kN/m)	$L_p(\mathbf{m})$	$E_{0,exp}(J)$	$\theta_{0,exp}$ (°)	
1	Slow	1.58 - 1.73	1.07 - 1.14	0.15 - 0.22	0.18 - 0.21	16.39 – 19.96	1.16 – 1.17	840.5 – 864.8	65.3 – 67.5	
	Normal	1.75 - 1.87	1.29 - 1.47	0.25 - 0.33	0.16 - 0.17	16.00 - 18.86	1.16 - 1.17	865.2 - 881.2	64.2 - 66.0	
	Free	1.71 - 1.79	1.22 - 1.36	0.24 - 0.31	0.17 - 0.19	16.14 - 18.32	1.16 - 1.17	860.9 - 874.8	64.2 - 66.3	
	Fast	1.98 - 2.13	1.50 - 1.71	0.35 - 0.42	0.12 - 0.17	20.75 - 24.20	1.15 - 1.16	869.7 - 905.6	64.9 - 68.1	
2	Slow	1.61 - 1.64	0.99 - 1.06	0.19 - 0.24	0.14 - 0.24	16.43 - 18.27	1.19 - 1.20	919.1 - 929.7	66.6 - 67.7	
	Normal	1.81 - 1.93	1.08 - 1.14	0.28 - 0.33	0.14 - 0.22	19.34 - 22.98	1.17 - 1.18	899.3 - 925.7	67.4 - 70.3	
	Free	1.71 - 1.79	1.05 - 1.16	0.22 - 0.28	0.14 - 0.23	16.47 - 20.88	1.18 - 1.20	914.9 - 924.5	66.5 - 68.7	
	Fast	2.10 - 2.16	1.27 - 1.40	0.35 - 0.39	0.14 - 0.19	23.33 - 26.18	1.18 - 1.18	933.7 - 950.6	69.1 - 71.8	
3	Slow	1.57 - 1.65	0.98 - 1.11	0.17 - 0.19	0.14 - 0.21	18.91 - 19.93	1.14 - 1.14	792.1 - 799.9	67.3 - 68.5	
	Normal	1.82 - 1.91	1.07 - 1.26	0.19 - 0.23	0.09 - 0.19	14.02 - 22.27	1.13 - 1.14	792.7 - 806.3	67.2 - 69.4	
	Free	1.63 - 1.74	1.07 - 1.16	0.17 - 0.19	0.14 - 0.23	16.37 - 18.96	1.14 - 1.15	789.5 - 797.6	67.4 - 68.2	
	Fast	2.16 - 2.22	1.26 - 1.39	0.24 - 0.28	0.14 - 0.16	28.87 - 33.66	1.12 - 1.12	795.2 - 811.7	70.5 - 72.4	

However, as expected, certain adjustments to the initial conditions were necessary to achieve a stable gait. The reasons for these adjustments, their consequences, and specific details about the simulations are described as follows:

• As previously mentioned, the model's ability to replicate a person's walking gait depends on predicting the next impact point x_p (for both BM₁ and BM₂), which, in turn, relies on the choice of a governing parameter: d_s or θ_0 . When one of these parameters is set – that is, defined as an input parameter – the other becomes a consequence of the model's functioning after convergence (usually by differing from the initial values for t = 0). From this limitation, DBIP models would be unlikely to be able to simultaneously predict both experimental values of parameters, d_s and θ_0 . Therefore, since the initial analyses aim to simulate the experimental gait and given the relationship $v = d_s f_s$, for

now, step length d_s was chosen to govern the definition of x_p . It worth mentioning that, if the attack angle θ_0 was set in the simulations using the mean experimental values as a reference (see Table 30), it was not possible to reproduce a stable gait with the typical 'M-shape' for the GRFs of each foot in most simulations. This can be explained by the fact that the attack angle is based on an assumption about the position of the CoM and the foot-point, suggesting that adjustments to this parameter would be indeed necessary.

- For each crossing, initial simulations aimed to determine the initial conditions for t = 0 from the models' post-convergence step cycles. This involved adjusting CoM's velocity $\dot{z}(0)$ and $\dot{x}(0)$ (the latter for BM₂ only, once \dot{x} is fixed for BM₁), and θ_0 (as a consequence of fixing d_s) to achieve a stable gait with minimal perturbations at the beginning of the simulation, that is, choosing optimal initial conditions.
- For BM₁, although the step frequency f_s is not a parameter input, when d_s governs the definition of x_p and is set as $d_s = v/f_s$, this simplified DBIP model can indirectly impose a step frequency value. On the other hand, if the attack angle is constant and equal to θ_0 , achieving the desired step frequency would depend on finding the appropriate θ_0 that results in the corresponding step length after convergence. It should be noted that this does not apply to BM₂. Since the longitudinal velocity \dot{x} changes in this model, even when d_s is fixed, reproducing v and f_s remains highly dependent on the energy input E₀. Therefore, for BM₂, adjusting the initial conditions of the simulations also required adjusting E₀, as it depends on the model's initial conditions (see Eq.(30)), and this is crucial for achieving the target values of v and f_s . These insights highlight a potential advantage of keeping the longitudinal velocity \dot{x} constant, as the step frequency is the most important gait parameter for civil engineering applications (Pedersen & Frier, 2010).
- Due to the lack of experimental reference values, c_{leg} was calculated using Eq.(21) based on ξ values within ranges found in the literature (Ruiz *et al.*, 2022) and was then adjusted in the simulations to achieve a stable gait and optimize the CoM's vertical trajectory (best R-square value). This adjustment was made specifically for the vertical CoM trajectory, as c_{leg} had little influence on the model's intrinsic DLFs.

The numerical simulations were conducted following the considerations outlined above. In these cases, since the pairs of gait parameters v and f_s were used as references in the simulations, the comparisons regarding the models' performance were based on the DLF₁

values of the GRFs produced by the BM₁ and BM₂. To optimize data visualization, only the numerical results obtained with the optimal initial conditions ($\dot{z}(0)$, $\dot{x}(0)$ and θ_0) are presented in the following. Table 31 presents the adjusted ranges for the attack angle θ_0 and Energy input E₀, as well as some other results for further discussions.

The post-convergence attack angle values of the model differed from the experimental reference values, mostly tending to be higher. In summary, the percentage differences for this parameter ranged from -3.04% to 6.06%. Similarly, to achieve the desired step frequency in the BM₂ simulations, adjustments to the Energy input E₀ were necessary, with percentage differences ranging from -2.63% to 4.06%. It is worth mentioning that slight variations in the E₀ (within the outcome percentage range) can lead to significant variations in the step frequency and DLFs (Lin *et al*, 2020).

Table 31 - Ranges obtained with the optimal initial conditions for rigid surface scenarios (numerical results), and R² values for the CoM's vertical displacement.

TS Walking		BM_1	BM_2	BM_2		terval (secs)	CoM - R ²		
	Scenario	θ_0 (°)	θ_0 (°)	$\mathbf{E_0}(\mathbf{J})$	BM_1	BM_2	BM_1	BM_2	
1	Slow	68.54 - 70.24	68.56 - 70.52	837.1 – 845.5	0.12 - 0.13	0.09 - 0.11	0.29 - 0.69	-0.26 - 0.68	
	Normal	65.65 - 68.58	66.13 - 68.95	853.5 - 880.0	0.11 - 0.12	0.10 - 0.11	-0.25 - 0.51	-0.28 - 0.44	
	Free	66.88 - 68.70	66.92 - 68.94	848.0 - 866.5	0.11 - 0.12	0.10 - 0.11	0.30 - 0.69	0.22 - 0.55	
	Fast	65.88 - 68.08	66.67 - 68.19	884.5 - 915.0	0.08 - 0.10	0.06 - 0.09	-1.35 - 0.15	-1.41 - 0.11	
2	Slow	70.22 - 71.30	70.23 - 71.23	907.5 - 916.3	0.14 - 0.17	0.13 - 0.15	0.92 - 0.97	0.91 - 0.96	
	Normal	71.30 - 72.66	71.09 - 72.51	904.0 - 914.5	0.12 - 0.13	0.11 - 0.13	0.91 - 0.97	0.92 - 0.97	
	Free	69.81 - 71.65	69.82 - 71.61	907.0 - 921.0	0.12 - 0.15	0.11 - 0.14	0.89 - 0.99	0.91 - 0.98	
	Fast	71.09 - 72.23	71.11 - 72.27	925.5 - 942.9	0.10 - 0.11	0.09 - 0.10	0.83 - 0.99	0.80 - 0.98	
3	Slow	69.63 - 71.07	70.07 - 71.77	790.8 - 800.5	0.12 - 0.13	0.10 - 0.11	0.64 - 0.90	0.25 - 0.80	
	Normal	68.00 - 72.31	68.03 - 72.37	791.6 - 809.5	0.10 - 0.14	0.09 - 0.13	-0.15 - 0.87	-0.35 - 0.81	
	Free	68.83 - 70.62	69.06 - 70.51	792.2 - 804.5	0.12 - 0.13	0.09 - 0.12	0.19 - 0.78	0.14 - 0.76	
	Fast	71.34 - 73.04	71.87 - 73.49	801.0 - 814.5	0.07 - 0.08	0.06 - 0.07	0.08 - 0.61	-0.08 - 0.63	

In general, as observed in Figure 49 and Figure 50 (see Table 30 for experimental reference ranges, and Figure 52 to Figure 54 for examples of experimental-numerical comparisons for each test subject), both models presented similar results and overestimated the DLF₁ for most of the simulations (96% of crossings investigated). However, for a few crossings in slow and normal walking scenarios for TS2, BM₁ and BM₂ either accurately predicted all three gait parameters simultaneously or underestimated DLF₁, with errors ranging from -15% to 59.5% for this test subject (see Figure 50b). The most significant errors were observed in fast walking scenarios, and this tendency was also observed for both TS1 and TS3. Even at lower speeds, the simulations for TS1 and TS3 significantly overestimated the DLF₁ values in the

respective crossings, with some cases showing values over 100% higher than the experimental measurements.

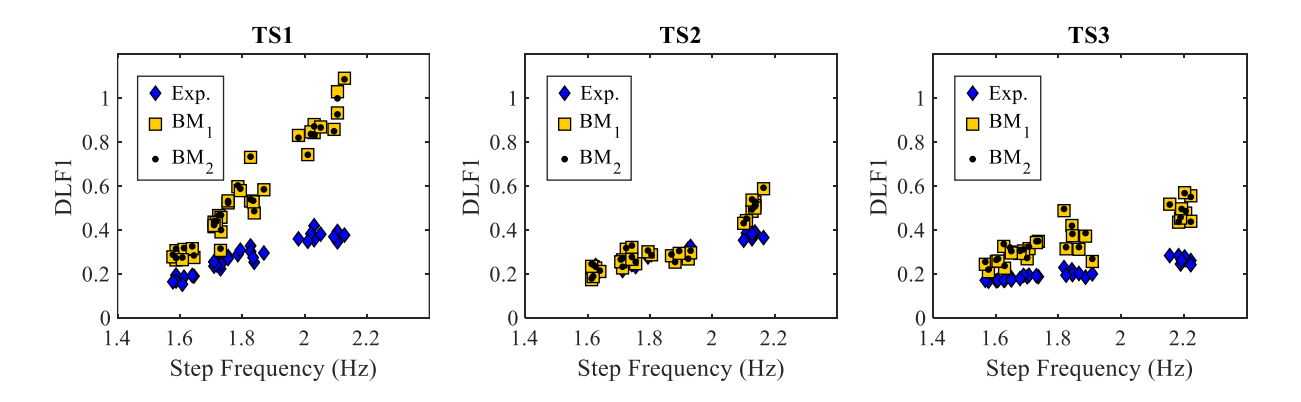


Figure 49 – Comparisons of experimental and simulated DLF₁s for each test subject.

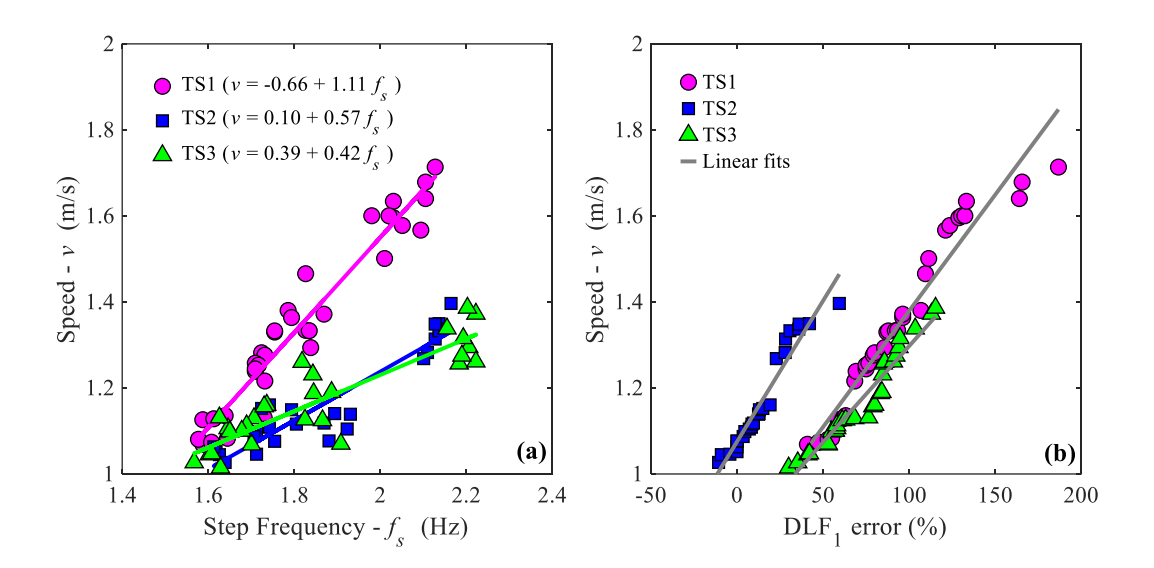


Figure 50 – Correlation of longitudinal speed v and (a) step frequency f_s and (b) DLF₁ errors for all three test subjects. (only the results for BM₁are depicted in this figure since similar results were obtained for BM₂)

An important outcome from this analysis lies on the correlation between walking speed and the errors in predicting the DLF₁. As it can be seen in Figure 50b, the DLF₁ errors (%) between the values extracted from experimental measurements and the simulated ones were proportional to the walking speed of the test subject. Bearing this in mind, a possible reason for the more significant percentage differences for TS1 (41 to 187%) is that, for the same step frequencies, TS1 exhibited higher walking speeds, as shown in Figure 50a, meaning a greater

step length. It worth mentioning that the speed-frequency correlation was close to the findings in the literature for TS1 only (Butz *et al.*, 2008; SCI, 2007).

Importantly, those differences cannot be related to the DLF₁ and step frequency correlation once, for example for TS1 and TS2, a similar linear fit for DLF₁ was identified, as seen in Figure 51. It is worth noting that the DLFs values for the test subjects fall within the range from the literature (Table 10).

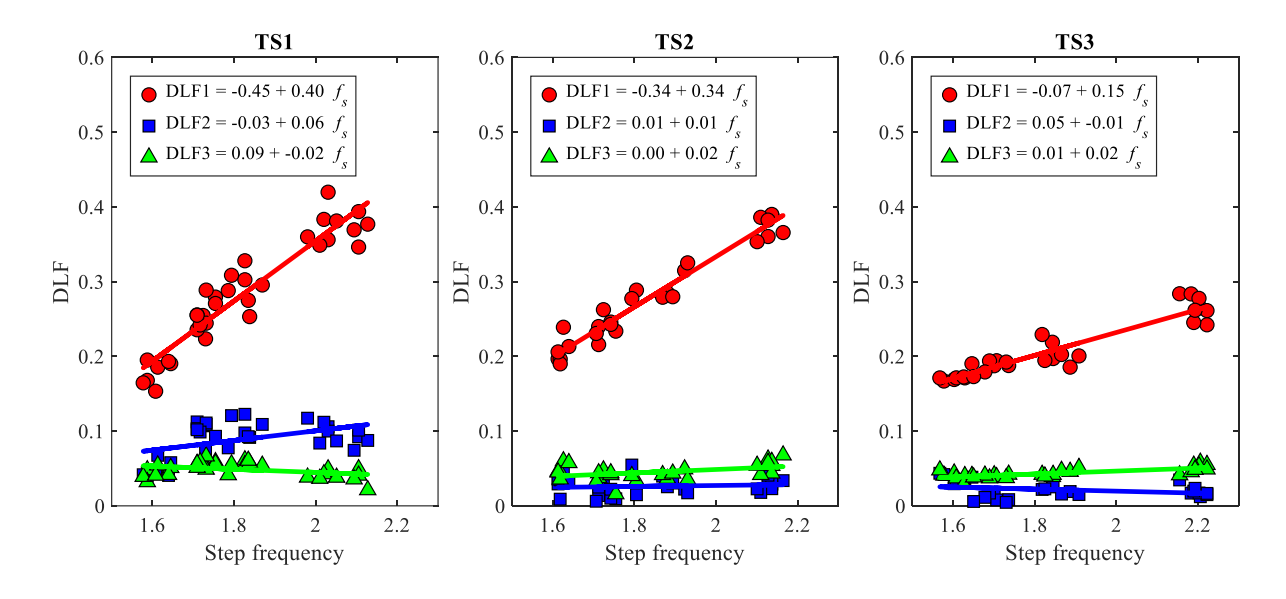


Figure 51 – Experimental measured DLFs and respective linear fits.

In this context, it was previously concluded that, when adopting the BM₁, the DLFs were smaller – and fell within the ranges found in the literature – when reducing the walking speed in the numerical simulations. This might represent a limitation for DBIP models in representing human walking for higher speeds. For instance, in the work of Ruiz *et al.* (2022), attempts to match the experimental and numerical footfall forces were difficult to achieve for speeds falling within the 1.54± 0.14 m/s range. Those authors brought to attention that disregarding the geometry of the foot in DBIP models by neglecting the centre of pressure progression, can increase the magnitude of the vertical peaks of footfall forces for higher speeds (Whittington & Thellen, 2009). Such differences can be observed in the fast walking scenarios shown in Figure 52 to Figure 54, where the experimental footfall forces were represented as the mean curve of all valid footfall forces for the specific crossing.

The absence of a roller feet (Whittington & Thellen, 2009) in DBIP models could also account for the discrepancies observed between experimental and numerical footfall force tail ends, as seen in Figure 52 to Figure 54. In these figures, it can be observed that while the transition from the DS to the SS phase is more gradual and smoother in the experimental measurements, the tail end of the footfall forces in the simulations exhibits a more linear behaviour, with the transition between walking phases being more abrupt. As a consequence, the foot contact time with the ground, and consequently the DS time intervals, are underestimated in the simulations (see DS phase interval values in Table 30 and Table 31 for comparisons), leading to an increase in the total GRFs and related DLFs (Lipfert *et al.*, 2012).

Although the focus of the analysis is on the gait parameters of interest for civil engineering applications, it is important to mention the experimental-numerical correlation of the CoM's vertical displacement. As presented in Table 31, a good agreement was achieved for most simulations for TS2 adopting both models, with R² values ranging from 0.80 to 0.99, calculated between the numerical and the mean measured CoM vertical displacement. In contrast, the prediction of the CoM's vertical movement for TS1 and TS3 did not have the same performance. It should be noted that these results align with the models' performance in terms of DLF₁ prediction, for which the smaller errors were found for TS2 (as seen in Figure 49 and Figure 50).

In summary, matching the three gait parameters (v, f_s and DLF₁) with the experimental reference values was not successful due to inherent limitations of the models. The following subsection presents the procedure used to calibrate the model parameters on a rigid surface, as a basis for further investigations under moving surface scenarios.

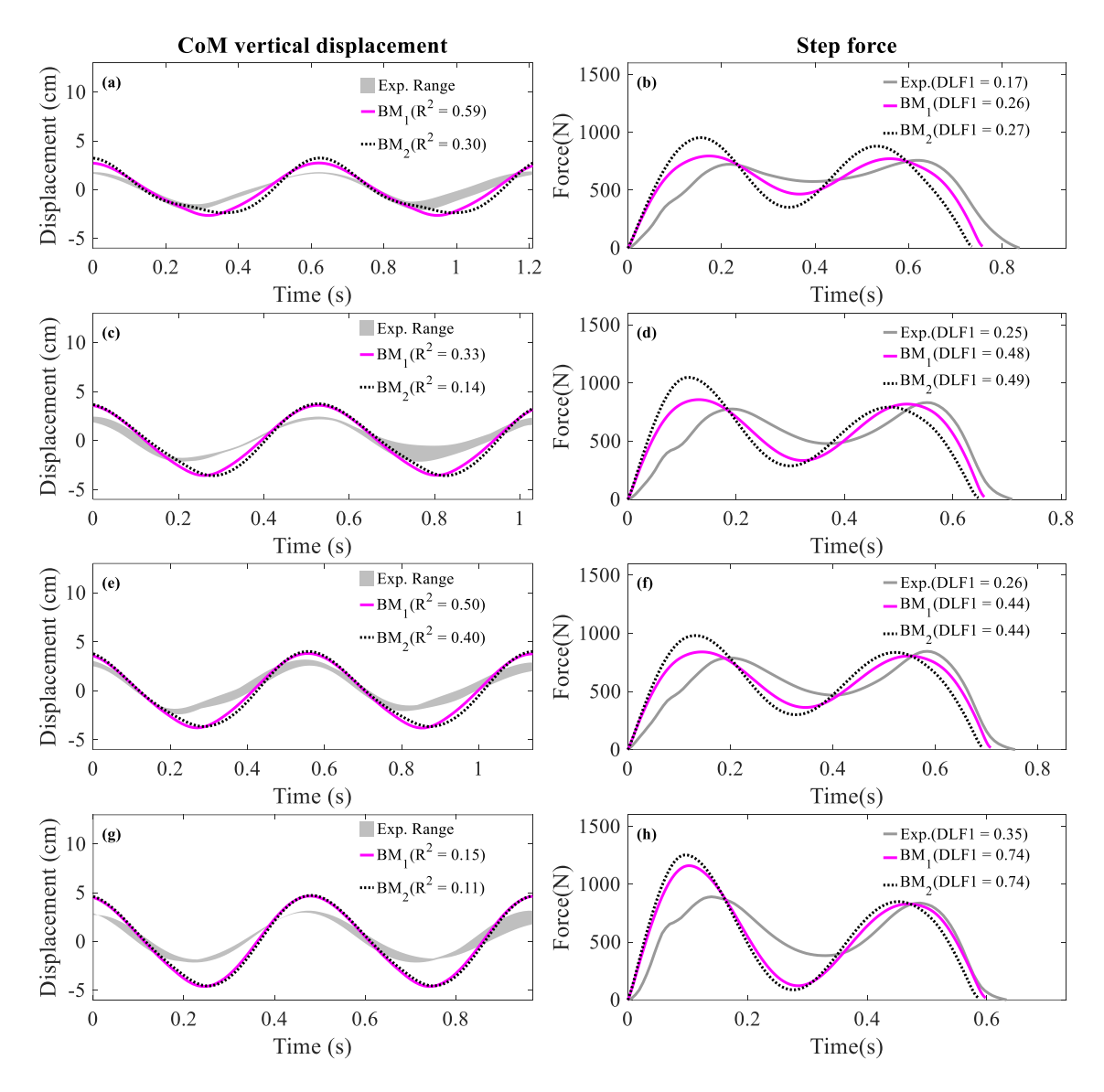


Figure 52 – Comparisons of experimental and simulated CoM vertical displacements and step forces for TS1 in (a) and (b) slow walking (crossing 5), (c) and (d) normal waking (crossing 7), (e) and (f) free walking (crossing 4), and (g) and (h) fast walking (crossing 8) scenarios, adopting parameters from Table A.1

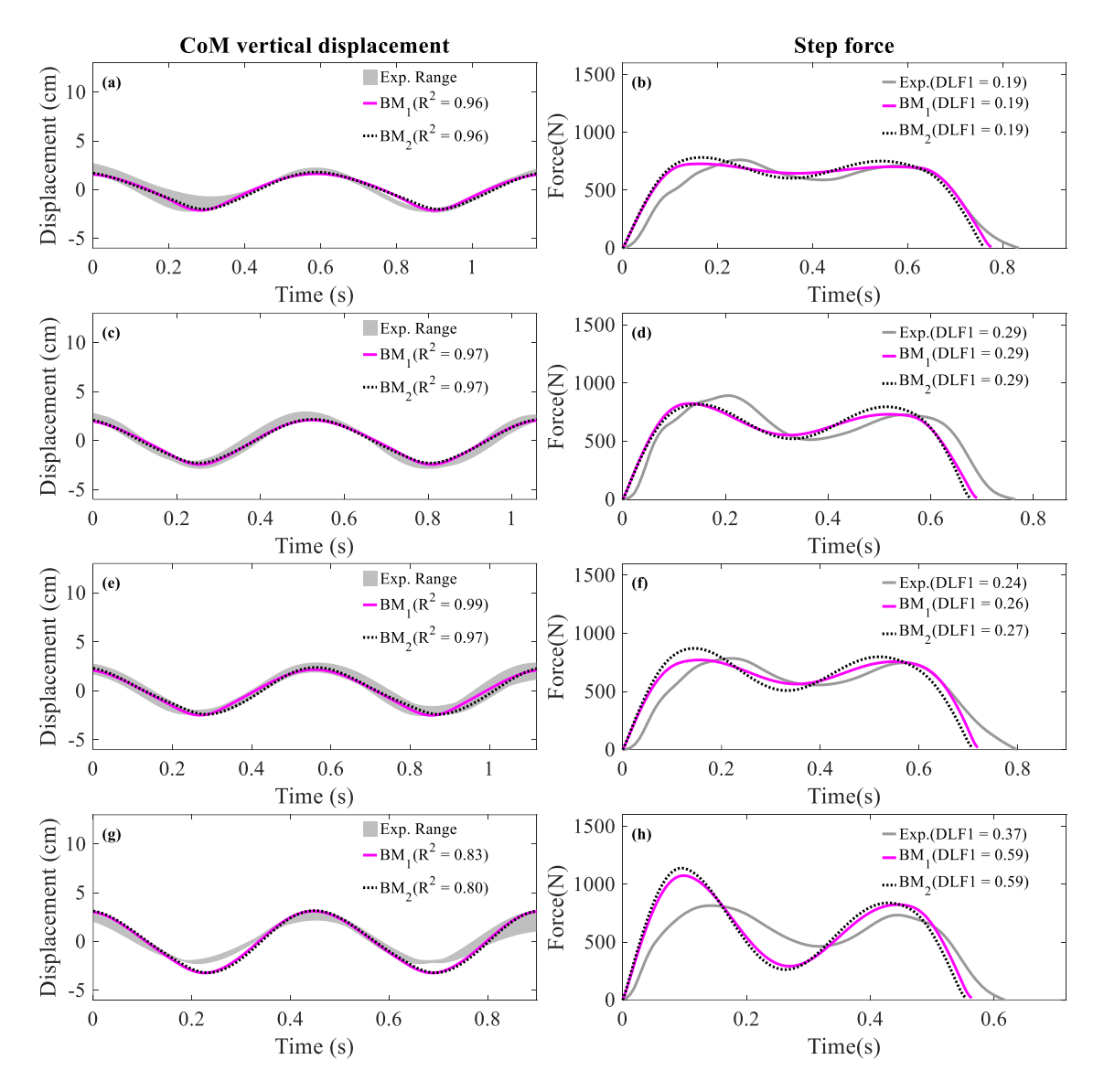


Figure 53 – Comparisons of experimental and simulated CoM vertical displacements and step forces for TS2 in (a) and (b) slow walking (crossing 5), (c) and (d) normal waking (crossing 4), (e) and (f) free walking (crossing 4), and (g) and (h) fast walking (crossing 2) scenarios, adopting parameters in Table A.2

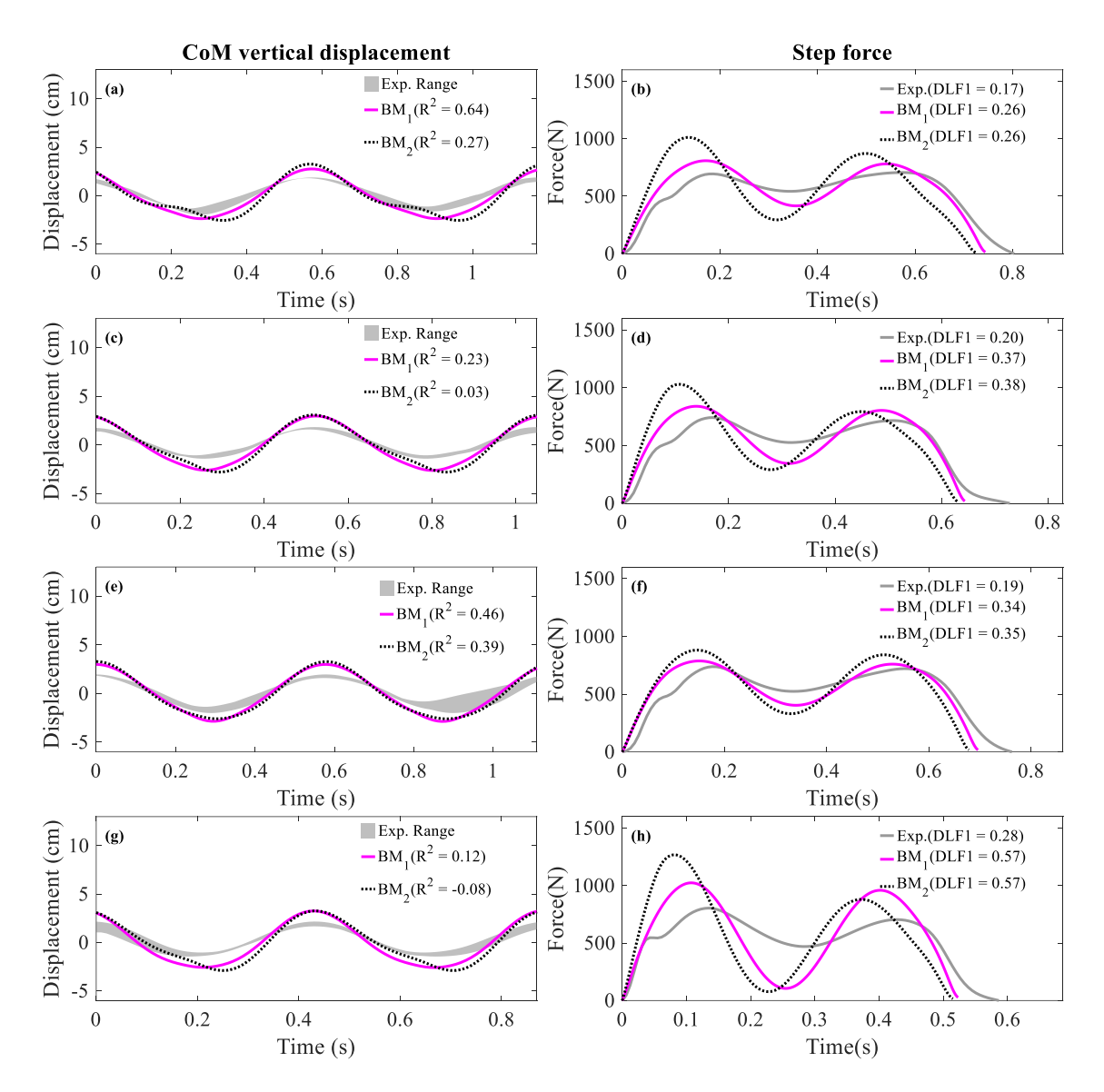


Figure 54 – Comparisons of experimental and simulated CoM vertical displacements and step forces for TS3 in (a) and (b) slow walking (crossing 5), (c) and (d) normal waking (crossing 4), (e) and (f) free walking (crossing 4), and (g) and (h) fast walking (crossing 5) scenarios, adopting parameters in Table A.3

4.2.1.2 Procedure for gait parameters adjustments

As highlighted by Živanović *et al.* (2022), while the step frequency f_s (or some integer multiple of it) being close to a natural frequency of the structure can lead to an unsatisfactory vibratory state in terms of serviceability performance, and DLFs influence the magnitude of such vibrations, the walking speed v is the gait parameter that determines the duration for which

the structure will be exposed to pedestrian-induced excitation. Therefore, walking speed has lower priority among these three gait parameters.

Bearing this in mind, Lin *et al.* (2023) chose to calibrate the DBIP model (Lin *et al.*, 2020) based on the step frequency f_s and DLF₁ only. Since walking speed was sacrificed in the process, the model's walking speeds were mostly lower than the experimental measurements for the sixteen test subjects investigated by these authors (errors ranging from -12.6% to 2%). However, those lower walking speeds indicate a longer exposure time to vibrations, which would be favourable from a safety design purpose. It should be noted that the investigated walking speeds by those authors fell within the range from slow to normal speeds (1.04 to 1.33m/s).

Indeed, prioritizing the DLF of the first harmonic over walking speed v is more important for structural design applications. Previously, when the performance of BM₁ was compared with a SMD model, it was observed that the overestimation of the structural response when using bipedal models was intrinsically related to DLF values exceeding the expected ranges found in the literature (Kerr & Bishop, 2001; Rainer *et al.*, 1988; Pernica, 1990; Young, 2001) and the ones identified in this study.

As discussed in the previous subsection, and considering the near linear relationship between walking speed and the error in predicting DLF₁, adjustments to walking speed v – as demonstrated by Lin *et al.* (2023) – are adopted in order to achieve the experimental DLF₁. As these authors considered the attack angle θ_0 to be the parameter governing the prediction of the next impact point x_p , searching to match f_s and DLF₁ led to adjustments to θ_0 and E₀. On the other hand, when considering d_s fixed (as in the analyses in this study), speed adjustments can be made by varying this parameter for the same step frequency. It is worth mentioning that fixing and adjusting the attack angle, θ_0 , or directly fixing and adjusting the step length for different speed levels so as to keep the same step frequency, is a matter of choice in the model's parameters calibration process for rigid surface scenarios.

Monte Carlo simulations following the calibration process depicted in Figure 38 were carried out bearing in mind to prioritize f_s and DLF₁. To this end, only adjustments to v (intrinsically related to d_s), ξ , and E₀ (when needed) were made for each crossing. The ranges for the simulation parameters are presented in Table 32.

Table 32 – Ranges defined for the Monte Carlo simulations

Walking Scenario	v (m/s)	ξ (%)	E ₀ (J)
Slow, normal and free	$0.80v_{exp} - 1.1v_{exp}$	3% - 13%	$0.95E_0 - 1.05E_0$
Fast	$0.70v_{exp} - 1.1 v_{exp}$	3% - 13%	$0.90E_0 - 1.1E_0$

As observed in Figure 50b, significant adjustments in the walking speed were expected so as to achieve the desired DLF₁ for higher speeds, which was confirmed by the simulations. Table 33 summarizes⁷ the walking speed values that resulted in the target DLF₁ for the same step frequency, along with ranges for Energy input E₀ and step length d_s . Figure 55 illustrates the experimental and adjusted walking speeds for all crossings of each test subject, suppressing the results from BM₁ once no great differences were observed. The walking speed adjustments for low and normal speeds aligned with the adjustment range reported in Lin *et al.* (2023). However, as expected, at higher speeds (above 1.4 m/s), the adjustments exceeded -20%.

Table 33 – Adjustments to walking speed v and Energy input E₀, along with step length d_s comparisons

Test	Walking spee	d v	Energy inpu	ıt E ₀	d_s (m)		
Subject	Range (m/s)	Variation (%)*	Range (J)	Variation	Experimental	Numerical	
				(%)*			
TS1	0.92 - 1.25	-30.0%9.9%	827 - 852	-6.3%1.5%	0.65 - 0.81	0.56 - 0.65	
TS2	0.99 - 1.24	-12.6% - +3.2%	828 - 924	-2.9% - +0.7%	0.57 - 0.67	0.56 - 0.64	
TS3	0.91 - 1.09	-22.7%7.1%	783 - 914	-2.8% - +0.7%	0.56 - 0.70	0.46 - 0.58	

^{*} Compared to the experimental measurements.

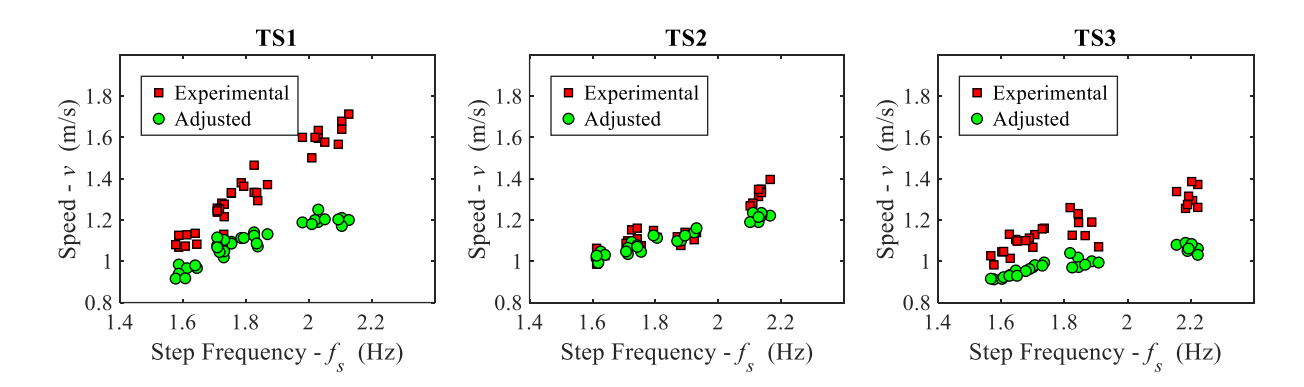


Figure 55 – Speed and step frequency correlation after parameters adjustments.

Figure 56 to Figure 58 present the footfall force and vertical CoM displacement after parameters calibration for the same selected crossing within each walking scenario under rigid

⁷ Appendix A presents tables (Tables A.4 to A.6) containing all calibrated parameters for each crossing within the walking scenarios under rigid surface conditions.

surface conditions, from the results shown in Figure 52 to Figure 54. Since the calibration of parameters focused on matching the target values of step frequency (f_s) and DLF₁, a good agreement between experimental and numerical footfall forces was not achieved. These results are consistent with those reported by Lin *et al.* (2023), in which the footfall force peaks were generally lower than the experimental measurements. It is important to note that those authors used treadmills, allowing for more representative footfall measurements due to a larger number of steps per test subject. Additionally, it was observed a better experimental-numerical correlation of the CoM's vertical displacement.

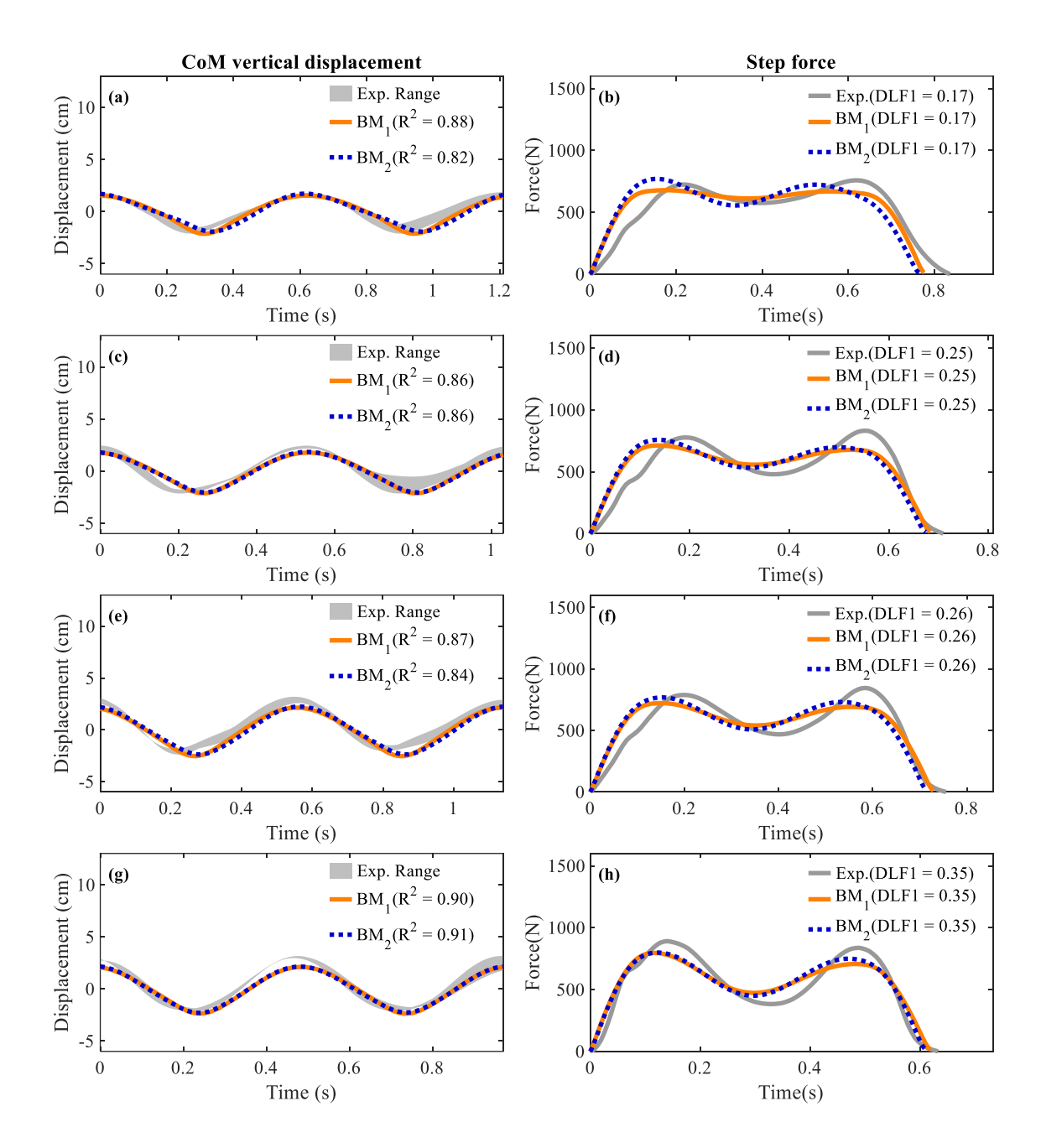


Figure 56 - Comparisons of experimental and simulated CoM vertical displacements and step forces for TS1 in (a) and (b) slow walking (crossing 5), (c) and (d) normal waking (crossing 7), (e) and (f) free walking (crossing 4), and (g) and (h) fast walking (crossing 8) scenarios, adopting parameters in Table A.4

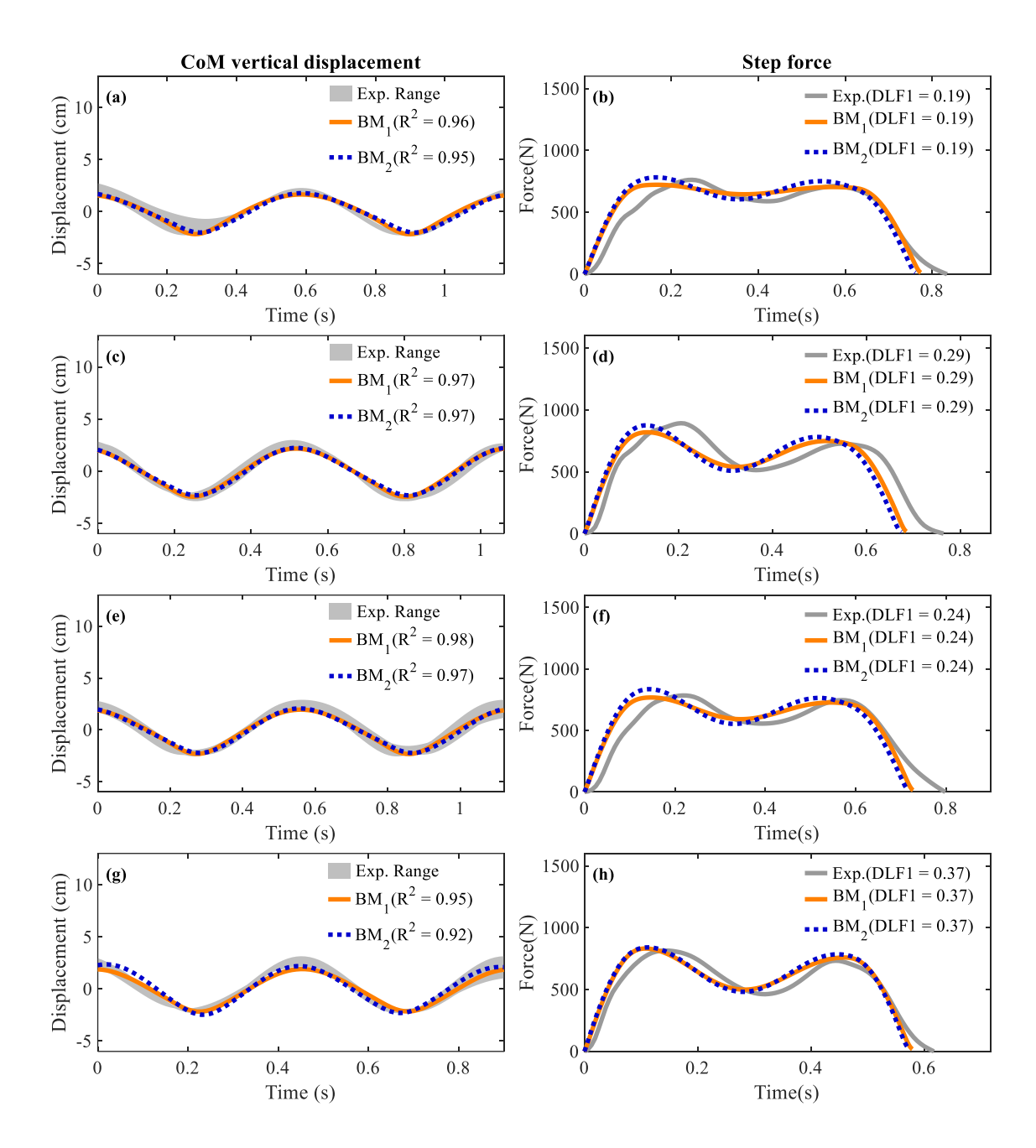


Figure 57 - Comparisons of experimental and simulated CoM vertical displacements and step forces for TS2 in (a) and (b) slow walking (crossing 5), (c) and (d) normal waking (crossing 4), (e) and (f) free walking (crossing 4), and (g) and (h) fast walking (crossing 2) scenarios, adopting parameters in Table A.5

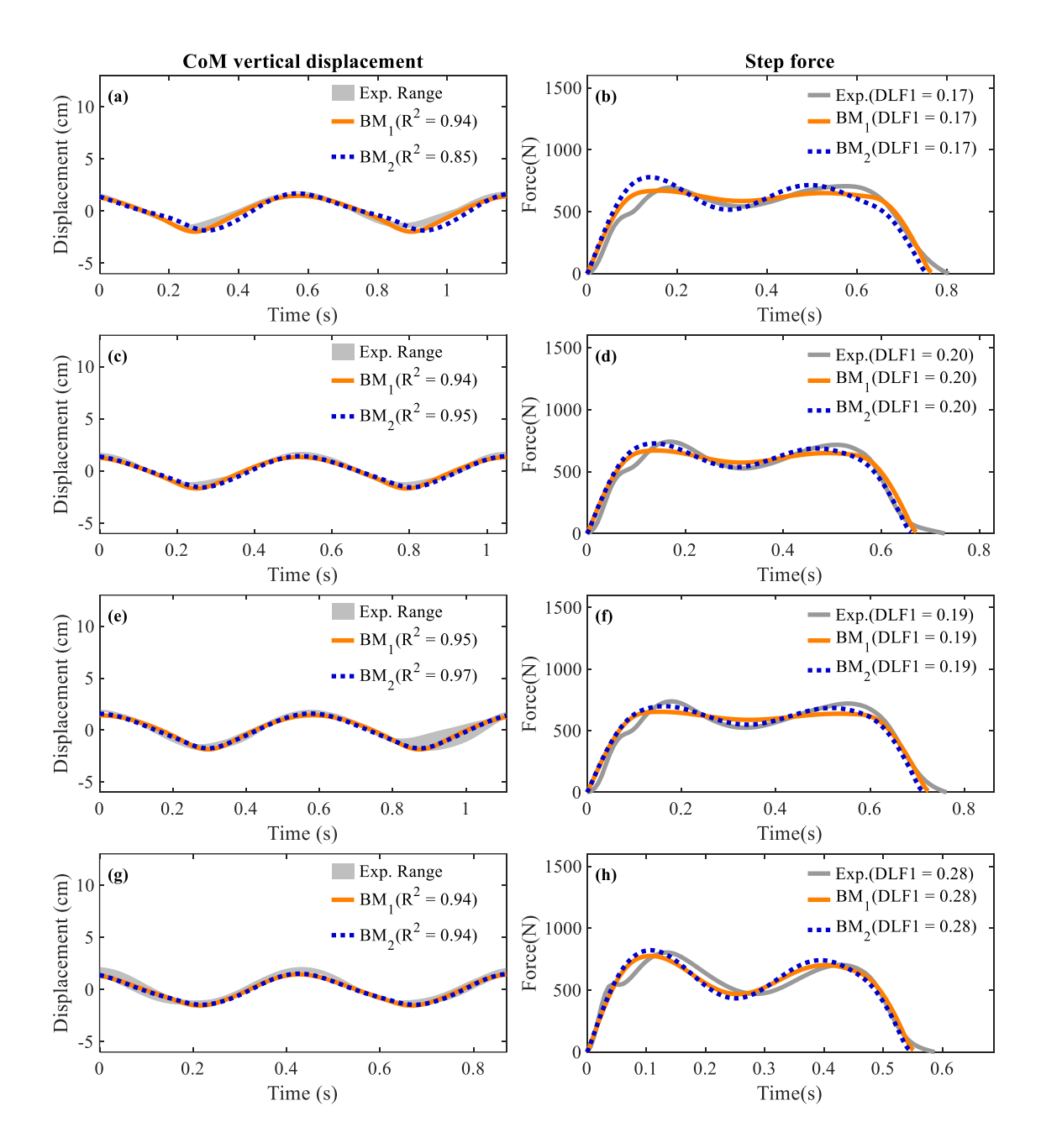


Figure 58 - Comparisons of experimental and simulated CoM vertical displacements and step forces for TS3 in (a) and (b) slow walking (crossing 5), (c) and (d) normal waking (crossing 4), (e) and (f) free walking (crossing 4), and (g) and (h) fast walking (crossing 5) scenarios, adopting parameters in Table A.6

4.2.2 Moving floor scenarios

This section presents a discussion aimed at addressing a gap related to S2HI effects: (1) how human-induced forces during walking are affected by surface vibrations; and (2) the

capability of DBIP models in predicting such effects. First, insights from experimental results are provided, followed by an analysis of how different vibration levels influence gait characteristics and the resulting forces. These discussions are grounded in the experimental data presented in Section 3.3. Given the limitations of SMD models in capturing gait behaviour, they are not assessed in this section. Instead, the focus is placed on evaluating the performance of both DBIP model versions (BM₁ and BM₂) in terms of their functionality and correlation with experimental results.

Importantly, the following analysis does not aim to investigate how the dynamic behaviour of structures is affected by the presence of people walking. Instead, the objective is to assess whether the proposed bipedal models, when coupled with structural systems, are capable of capturing changes in the pedestrian body's kinetics and kinematics in response to surface vibrations.

4.2.2.1 Experimental Results Insights

As previously mentioned, the experimental test setup allowed for the collection of synchronized kinetic and kinematic data for both the rigid surface scenarios and those referred to as resonance scenarios in Table 21. When it comes to the latter, it is important to discuss some insights regarding these scenarios in which surface vibrations were present.

The use of metronome beats in the tests guided the test subjects to walk at step frequencies close to the predefined surface movement of each scenario (see Table 21 for acceleration peaks and frequency values). From that perspective, the interaction between the test subject and the moving platform could be investigated based on two main aspects: (1) the synchronization between the test subject and the platform (their interaction will be referred as TS-platform from now on), and (2) the phases between them. It is worth noting that a TS-platform synchronization here refers to a close match between test subjects' step frequency and vertical surface frequency – frequency synchronization. Referring to a TS-platform phase synchronization will be made clear in a few comments.

The TS-platform synchronization relates to the simulation of resonance conditions and its effects on the S2HI. It is worth to mention that, since a constant walking flow was not possible due to the experiment's logistics, even when following metronome beats, the step frequency could differ from the predefined values (even for rigid surface scenarios – see Table

30 for reference). However, when the step frequency was close to the vertical surface frequency, it was possible to identify instances where the test subjects tended to synchronize with the platform's vertical movement, thus representing resonance conditions. Synchronization was identified by cross-referencing the touchdown (TD) instants with the vertical displacement of the surface, as shown in Figure 59.

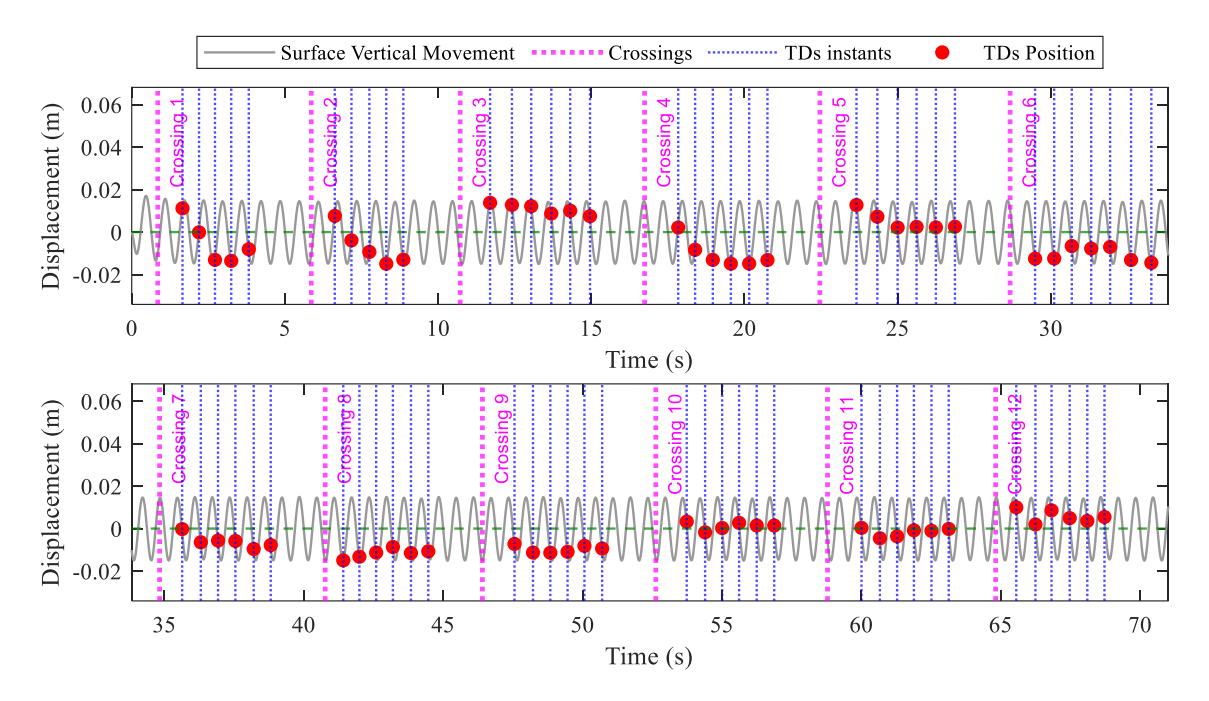


Figure 59 – An example of cross-referencing touchdown (TD) instants with the vertical position of the platform for TS1, the slow walking scenario (1.6Hz), and surface acceleration peaks of 1.5 m/s² (pink dashed lines mark the beginning of each crossing).

It is important to mention the criteria for determining TS-platform synchronization for each crossing within the specified scenario. As can be seen from Figure 59, for only a few consecutive steps within some crossings (e.g., last four steps in crossing 5) the interval between TD instants closely matched the oscillation period of the platform.

So as to extend the criteria for synchronization identification, it is important to highlight that even for the slow walking scenario and acceleration peaks of 1.5m/s², the vibrations amplitudes were around 1.48cm (as seen in Figure 59 and Table 21). Given the small vertical displacements observed, synchronization was also considered when the vertical position difference between TDs did not exceed 25% of the maximum displacement, e.g., crossings 3, 8, 9, 10 and 11 in Figure 59. A visual analysis was also adopted to confirm it.

Clearly, for some crossings, the step frequency differed considerably from the predefined walking rate within the scenario, for example crossings 1 and 2 (Figure 59). For the numerical analyses, only the TS-platform synchronous cases (47%, 40% and 57% for TS1, TS2 and TS3, respectively) were used as references for the S2HI investigations when applying DBIP models in Section 4.2.2.3.

It is worth mentioning that the calculated phase between the test subject and the platform was not used as an acceptance criterion, given that the vertical displacements are not linearly proportional to the phase angle, as illustrated in Figure 60.

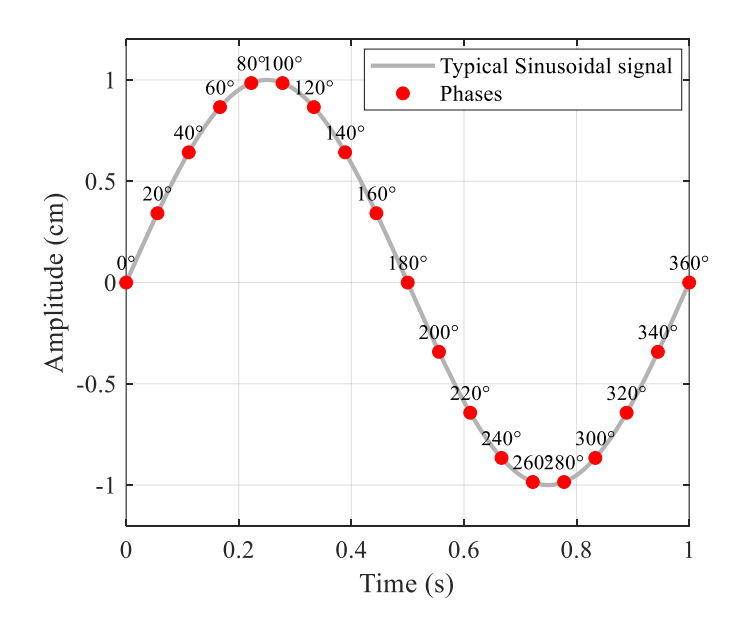


Figure 60 – Illustrating phases in a typical sinusoidal signal

Based on this criterion, Table 34 presents the number of crossings for which the TS-platform synchronization was identified.

As observed in Table 34, for most of the crossings in free walking scenarios, a TS-platform synchronization was not recognized (only 15% of free walking crossings). Since the test subjects walked freely in such cases (no metronome beats) and given that the crossing length was short (4m, maximum of 6 steps), there was not enough time for a pacing adaptation due to the perception of vibrations. Therefore, investigations on changes in walking patterns when pedestrians perceive vibrations could not be conducted. For this end, the reader is referred to Živanović *et al.* (2005b).

TS	Moving surface scenario											
	Slow Walk (1.6 Hz)			Normal Walk (1.85 Hz)		Free Walk (1.85 Hz)			Fast Walk (2.2 Hz)			
	0.5 m/s^2	1.0 m/s ²	1.5 m/s ²	0.5 m/s^2	1.0 m/s ²	1.5 m/s ²	0.5 m/s^2	1.0 m/s ²	1.5 m/s ²	0.5 m/s^2	1.0 m/s ²	1.5 m/s ²
1	9(12)	7(12)	6(12)	8(12)	12(12)	11(12)	2(16)	3(14)	4(14)	2(14)	2(14)	5(14)
2	2(12)	2(10)	5(12)	11(12)	12(12)	10(10)	0(12)	0(12)	3(12)	5(12)	0(12)	5(12)

12(12)

0(12)

3(10)

2(14)

10(12)

3(12)

10(12)

3

8(12)

9(12)

4(12)

10(10)

12(12)

Table 34 – Number of crossings for which TS-platform synchronization was identified within each moving surface scenario (values in parentheses indicate the total number of crossings).

Conversely, for 94% of crossings from normal walking scenarios (1.85Hz), a TS-platform synchronization was identified. A possible explanation is that this frequency is close to the natural frequency of the pedestrian's step (assuming a normal distribution – Živanović & Pavic, 2011). Consequently, when guided by metronome beats, test subjects could more easily adjust their gait to match the platform's motion, engaging the intrinsic mechanisms of biomechanical pace adaptation (Caloni *et al.*, 2025). In contrast, slow and fast walking required test subjects to adopt step frequencies that deviated significantly from their natural gait, achieving synchronization for just 49% and 38% of crossings within the specific walking scenario, respectively.

In an attempt to investigate whether the test subjects could perceive the vibrations and whether the platform dynamics could interfere with their walking pattern according to their perception, a qualitative approach was applied, as explained in Section 3.3.1. In terms of vibration perception, all three test subjects reported perceiving the platform's vibrations for all scenarios investigated. In fact, it was expected that this perception would occur at the investigated acceleration peak levels. As reported by Živanović *et al.* (2005b), based on investigations of pedestrians walking in three different footbridges, acceleration levels higher than 0.33 - 0.37 m/s² in the vertical direction constituted what is referred to as disturbing vibration levels for the walking pedestrians.

Additionally, Živanović *et al.* (2005b) brought to attention that a disturbing vibration level depends on the logistics of test's conduction. They concluded that when adopting metronome beats, the test subjects could maintain their pacing rate for higher structural acceleration levels when compared to tests conducted without metronome beats. Hence, this also highlights that even for acceleration levels of 0.5m/s², such vibrations can, in fact, disturb the pedestrian's free walk.

Although vibrations were perceived, all three test subjects reported that acceleration levels of 0.5 m/s² did not affect their walking pattern during free walking, as shown in Figure 61. Possibly given the short crossing. Furthermore, they indicated that higher vibration levels had a greater impact on their gait, with the exception of TS3 in the slow walking scenarios, who reported that the vibrations did not interfere with their walk.

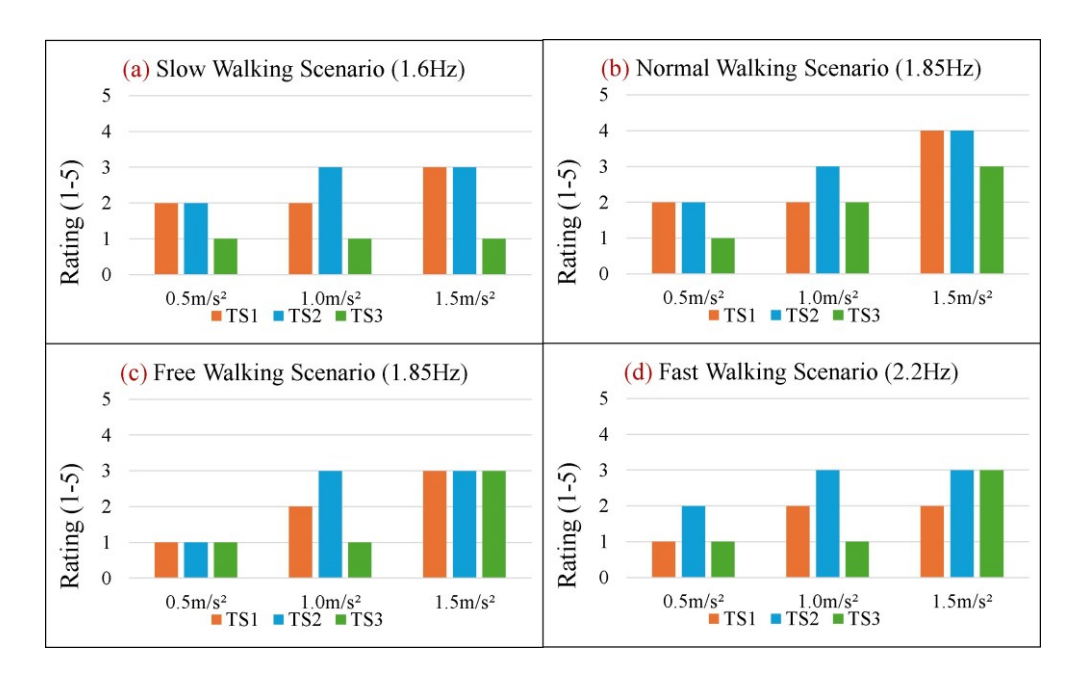


Figure 61 - Test subjects rating results for moving surface scenarios ranging from 1 (vibrations did not interfere walking) to 5 (vibrations strongly interfere in walking).

Once such TS-platform frequency synchronizations were identified, the second aspect of the S2HI investigations comes into focus: the touchdown (TD) vertical position at the platform.

Since the vertical positions of the touchdowns can vary between the minimum and maximum displacement peaks' values of the platform (see Table 21 for reference), and in order to simplify the analysis, the phase between the test subject and the platform (TS-platform phase) can be divided into four extreme situations, as described in Table 35.

Based on the phase cases in Table 35, Table 36 compiles the number of crossings for which frequency synchronization was identified specifying the related TS-platform phase. 'Inter' in Table 36 refers to intermediate cases in between the ones explained in Table 35.

Table 35 – Description of TS-platform phase cases

Case	Phase Range (°)	Description
1	350 – 10	• When the test subject stepped in the platform in small (around zero) vertical displacement levels, meaning the platform velocity was near the maximum absolute value, and the platform was "moving up"
2	60 – 130	• When the test subject stepped in the platform in high vertical displacement levels, around "maximum peaks", meaning the platform velocity was small or null
3	170 – 190	• When the test subject stepped in the platform in small (around zero) vertical displacement levels, meaning the platform velocity was near the maximum absolute value, and the platform was "moving down"
4	250 – 300	• When the test subject stepped in the platform in high vertical displacement levels, around "minimum peaks", meaning the platform velocity was small or null

Table 36 – Compilation of each TS-platform phase case for each moving surface scenario. (***)

T	TS-	Moving Surface Scenario												
\mathbf{S}	platform	platform Slow Walk			Norm	al Wall	ζ.	Free '	Free Walk Fast V (1.85Hz) (2.2 H			Fast Walk		
	phase	(1.6H)	z)		(1.851	(1.85Hz) $(1.85Hz)$						lz)		(%) *
		0.5	1.0	1.5	0.5	1.0	1.5	0.5	1.0	1.5	0.5	1.0	1.5	
		m/s^2	m/s^2	m/s^2	m/s^2	m/s^2	m/s^2	m/s^2	m/s^2	m/s^2	m/s^2	m/s^2	m/s^2	
1	350° - 10°	0	1	0	0	0	1	0	0	0	0	0	2	6%
	60° - 130°	0	0	1	2	0	1	0	0	0	2	2	2	14%
	170° - 190°	0	2	2	0	0	1	0	0	1	0	0	0	8%
	250° - 300°	7	2	2	5	12	7	2	3	2	0	0	0	59%
	Inter.**	2	2	1	1	0	1	0	0	1	0	0	1	13%
2	350° - 10°	0	0	0	0	0	0	0	0	0	4	0	5	16%
	60° - 130°	1	0	2	0	0	0	0	0	1	0	0	0	7%
	170° - 190°	0	1	2	0	0	0	0	0	0	0	0	0	5%
	250° - 300°	0	0	0	11	12	10	0	0	2	0	0	0	64%
	Inter.**	1	1	1	0	0	0	0	0	0	1	0	0	7%
3	350° - 10°	0	0	0	0	0	0	0	0	0	2	2	6	12%
	60° - 130°	0	0	0	0	0	0	0	0	0	5	0	1	7%
	170° - 190°	0	2	2	0	0	0	0	0	0	0	0	0	5%
	250° - 300°	5	2	1	9	12	12	0	2	3	1	1	0	58%
	Inter.**	3	5	1	1	0	0	0	0	0	2	0	3	18%

^{*} Percentage is calculated based on the values presented in Table 34

On one hand, 60% of the synchronous crossings (considering all test subjects) fit the fourth situation described in Table 35, where the feet stepped onto the platform at the lower vertical displacement peaks. In this case, the platform tended to move downward (in the same direction as the foot movement) with near-zero velocities, possibly representing the most comfortable situation while walking on vibrating surfaces, since the CoM trajectory phase matches the surface movement phase. On the other hand, for only 6% of the crossings where TS-platform frequency synchronization was identified, the test subject stepped onto the platform when its vertical position was at the highest peaks. A possible explanation for this is

^{**} Intermediate cases for which synchronization was also identified

^{***} In red the most common phase case for each TS

that, in these cases, the foot-platform 'encounter' occurred earlier than expected, which can represent a certain discomfort while walking, in addition to the fact that the surface vertical movement is opposed to the vertical CoM trajectory. Further discussion in this matter is presented in the next subsection.

Despite no reports of vertical phase synchronization are found in the literature (Caloni *et al.*, 2025; Shahabpoor *et al.*, 2016a), this discussion highlights that, for certain levels of vibration (i.e., vertical displacement amplitudes), a convergence of pedestrian-structure phase can indeed occur if a preferred (most comfortable) surface vertical position exists where pedestrians naturally tend to step. However, confirming this would require measurements with a larger sample of test subjects and longer crossing durations.

After recognition of the TS-platform's frequency synchronization and phases, it is possible to evaluate the changes in the applied forces and gait characteristics based on these two aspects, so the investigation of the S2HI effects can be addressed, as discussed in the next subsection. Before entering such discussions, an important insight should be mentioned.

Due to the platform's size limitation preventing a continuous straight-line walking flow, it was not possible to determine whether, even in the case of frequency synchronization, the test subject would tend to converge their movement to a specific phase with the structure. In other words, if phase synchronization would occur regardless of the phase at which the pedestrian begins interacting with the structure: the phenomenon known in the literature as the lock-in effect (Strogatz *et al.*, 2005; Fitzpatrick *et al.*, 2001; McRobie *et al.*, 2003).

To investigate such effects, tests conducted on longer walking segments or using treadmills (requiring mathematical methods to isolate each footfall force – Shahabpoor & Pavic, 2018; Lin *et al.*, 2023) could yield results that facilitate this analysis. However, there are one important factor to consider. It relates to the fact that, in real situations, a pedestrian would not be subjected to constant vibration levels while crossing an existing structure. Therefore, investigating this phase shift (adapting until achieve a lock-in effect) in the vertical direction using treadmills would only be realistic if the tests can simulate real vibrations while considering the structure's mode shapes. Thus, analysing resonance conditions in which the pedestrian is in different phases with the structure in the vertical direction is a representative approach.

4.2.2.2 Experimental gait parameters correlation

This subsection presents comparisons between gait parameters from moving surface and rigid surface experimental measurements, so as to discuss the S2HI effects. Additionally, it is discussed the influence of stepping in the structure in different phases in the gait parameters (walking speed v and DLF_1 – and related induced forces).

Initially, the discussion is based on all measurements from the moving surface scenarios, including those where TS-platform synchronization was not detected. The goal is to analyse, in general, whether pedestrians tend to adapt their speed and exhibit variations in DLFs for the same step frequency. Since DLFs influence vibration amplitudes, the initial discussions aim to assess whether surface vibrations can indeed induce variations in GRFs, which play a fundamental role in the HSI phenomenon. Figure 62 to Figure 64 present the correlation of step frequency and DLF₁ for each respective test subject.

The analysis of DLFs reveals that, in general, the DLF₁ values were higher compared to those obtained in scenarios involving a rigid surface. On average, the DLF₁ values exhibited the variations presented in Table 37 to Table 39 and Figure 65 to Figure 67 (for better visualization), respective for each test subject, comparing the mean DLF₁ values for the indicated step frequency range from the moving surface scenarios with the mean value of the curve fit obtained for the rigid surface scenario within the same step frequency range.

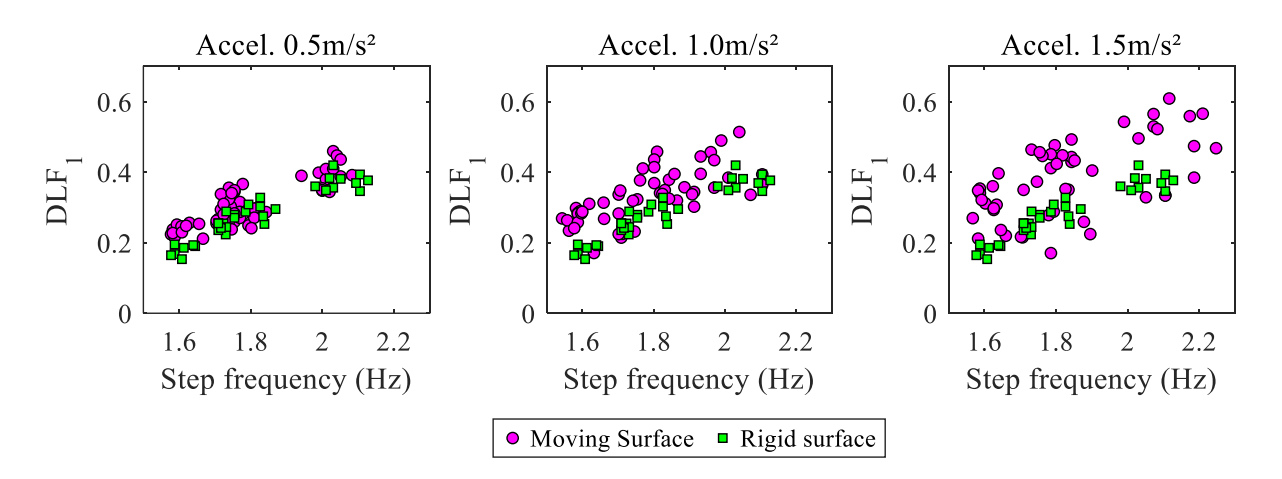


Figure 62 – Correlation of DLF₁ and step frequency f_s for moving surface scenarios compared to rigid surface scenarios for TS1.

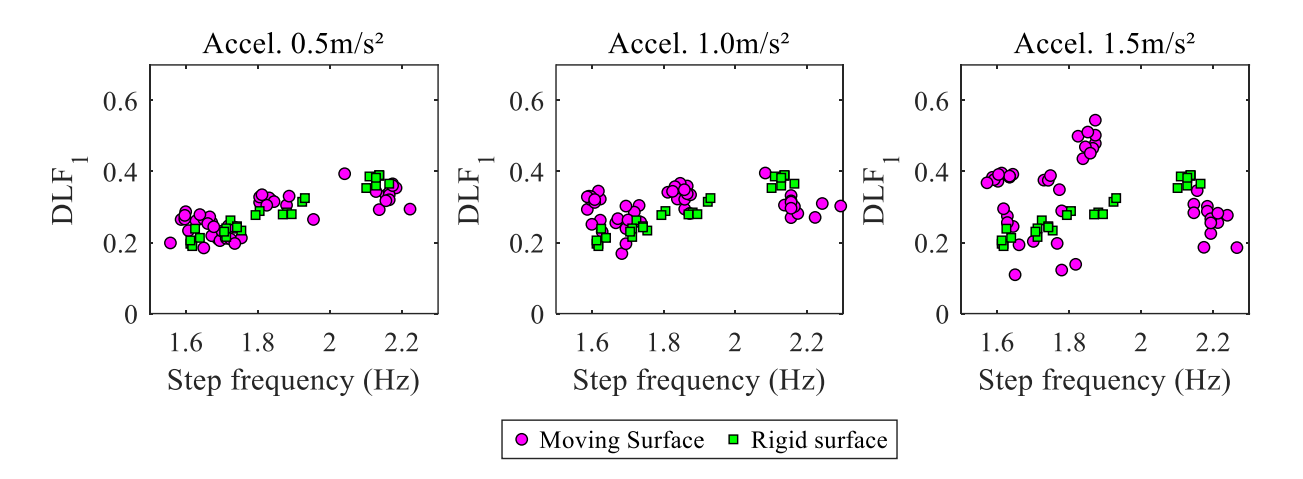


Figure 63 – Correlation of DLF₁ and step frequency f_s for moving surface scenarios compared to rigid surface scenarios for TS2.

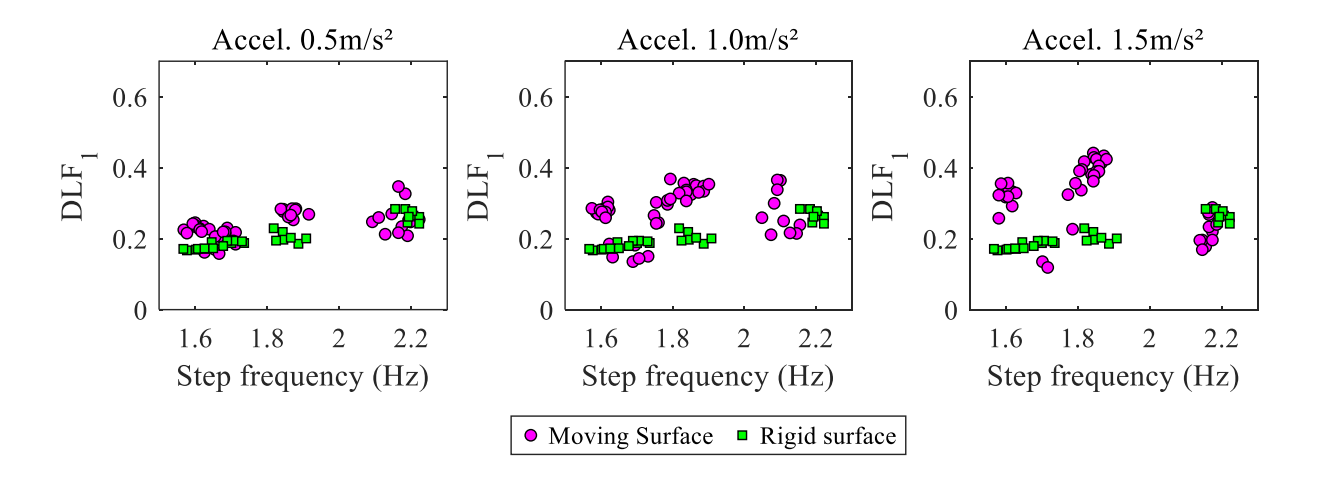


Figure 64 – Correlation of DLF₁ and step frequency f_s for moving surface scenarios compared to rigid surface scenarios for TS3.

Importantly, the non-synchronous cases (also presented in Figure 62 to Figure 64) do not differentiate whether the pedestrian stepped onto the platform while it was moving upward or downward, given the fact that an expressive variation on the phases was observed (e.g., crossings 1 and 2 in Figure 59).

Table 37 – Percentage differences between mean DLF₁ from the moving surface scenarios and from the rigid surface scenarios by step frequency ranges for TS1. (*)

Accel. Peaks (m/s²)	f _s (Hz) 1.5≤f _s < 1.6	1.6≤f _s <1.7	1.7≤ <i>f</i> s <1.8	1.8≤ f _s <1.9	1.9≤f _s <2.0	2.0≤f _s <2.1	2.1≤f _s <2.2	2.2≤f _s <2.3
0.5	+33.1%	+12.6%	+16.9	-5.2%	+17.9%	+4.9%	-	-
1.0	+55.6%	+26.3%	+17.8	+26.9%	+18.3%	+9.8%	-8.6%	-
1.5	+77.0%	+41.6%	+39.2	+31.1%	+41.7%	+30.4%	+8.3%	+13.7%

^(*) In red the ranges for which acceleration level/DLF₁ absolute differences were not directly proportional

Table 38 – Percentage differences between mean DLF₁ from the moving surface scenarios and from the rigid surface scenarios by step frequency ranges for TS2. (*)

Accel. Peaks (m/s²)	f _s (Hz) 1.5≤f _s < 1.6	1.6≤f _s <1.7	1.7≤f _s <1.8	1.8≤f _s <1.9	1.9≤ f _s <2.0	2.0≤f _s <2.1	$ \begin{array}{c} 2.1 \leq f_s \\ < 2.2 \end{array} $	$ \begin{array}{c} 2.2 \leq f_s \\ < 2.3 \end{array} $
0.5	+38%	+13.1%	-11%	+12.5%	-16.3%	+12.5%	-12.4%	-29.5%
1.0	+75.7%	+23.9%	+11.4%	+18.1%	-	+13%	-21.2%	-29.4%
1.5	+106.4%	+45.5%	+15.3%	+59.4%	-	-	-28.7%	-40%

^(*) In red the ranges for which acceleration level/DLF₁ absolute differences were not directly proportional

Table 39 – Percentage differences between mean DLF₁ from the moving surface scenarios and from the rigid surface scenarios by step frequency ranges for TS3. (*)

	f _s (Hz) 1.5≤f _s < 1.6	1.6≤ f _s <1.7	1.7≤ <i>f</i> s <1.8	1.8≤f _s <1.9	1.9≤ f _s <2.0	2.0≤ f _s <2.1	2.1≤f _s <2.2	2.2≤f _s <2.3
0.5	+39.7%	+19.8%	+2.5%	+31.5%	+19.8%	+3.3%	+0.9%	-6%
1.0	+70.2%	+34.8%	+36.1%	+60.9%	+57.6%	+22.9%	+0.7%	-
1.5	+91.3%	+83.3%	+19.9%	+91.3%	-	-	-13.7%	-

^(*) In red the ranges for which acceleration level/DLF₁ absolute differences were not directly proportional

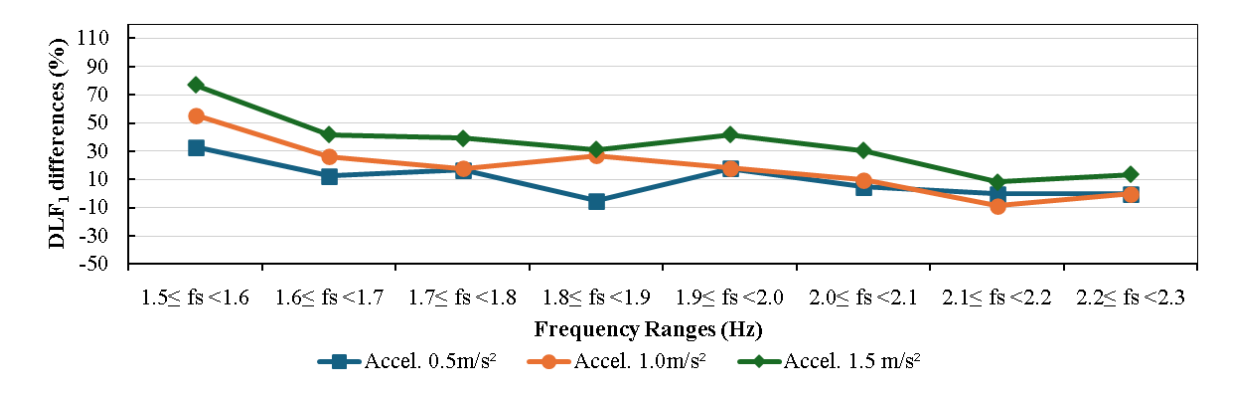


Figure 65 – Percentage differences between mean DLF₁ from the moving surface scenarios and from the rigid surface scenarios by step frequency ranges for TS1.

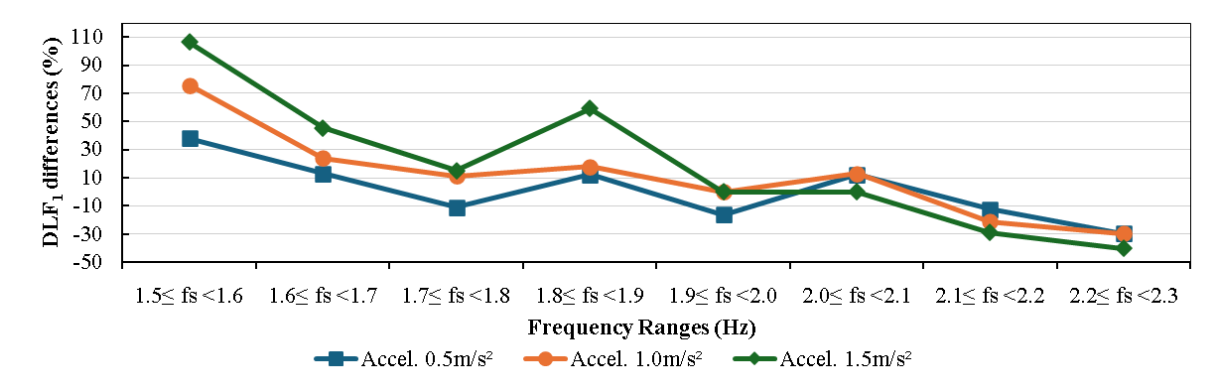


Figure 66 – Percentage differences between mean DLF₁ from the moving surface scenarios and from the rigid surface scenarios by step frequency ranges for TS2.

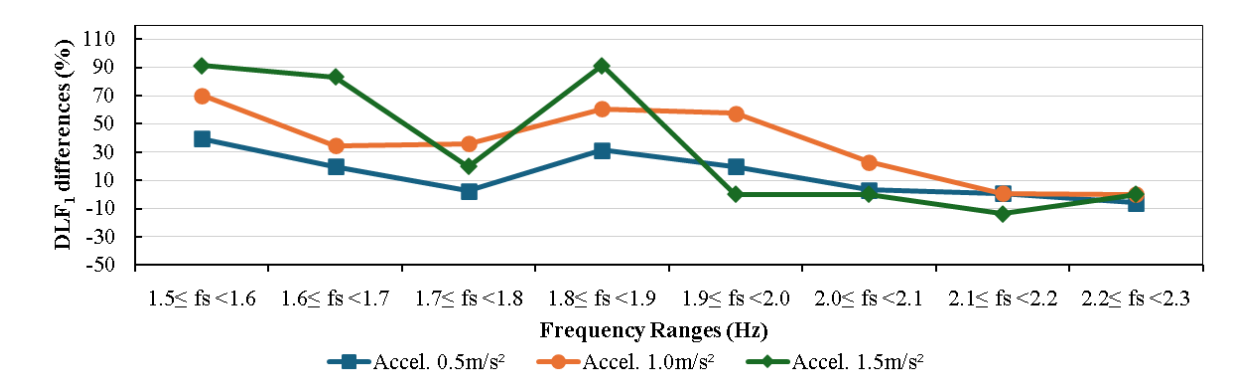


Figure 67 – Percentage differences between mean DLF₁ from the moving surface scenarios and from the rigid surface scenarios by step frequency ranges for TS3.

To evaluate the influence of the TD-platform phase for synchronous crossings exclusively, Figure 68 to Figure 70 presents the same results as before, but with non-synchronous crossings suppressed. Additionally, the figures differentiate between the phase conditions as defined in Table 35. For comparison purposes, a linear curve fit for DLF₁ derived from the rigid surface scenarios is also included.

As observed from Figure 68 to Figure 70, the increase in the DLF₁ trend was particularly evident in the most common phase case (fourth case in Table 35 – red star in Figure 68 to Figure 70), where the pedestrian's interaction with the platform resulted in amplified dynamic effects (discussed later).

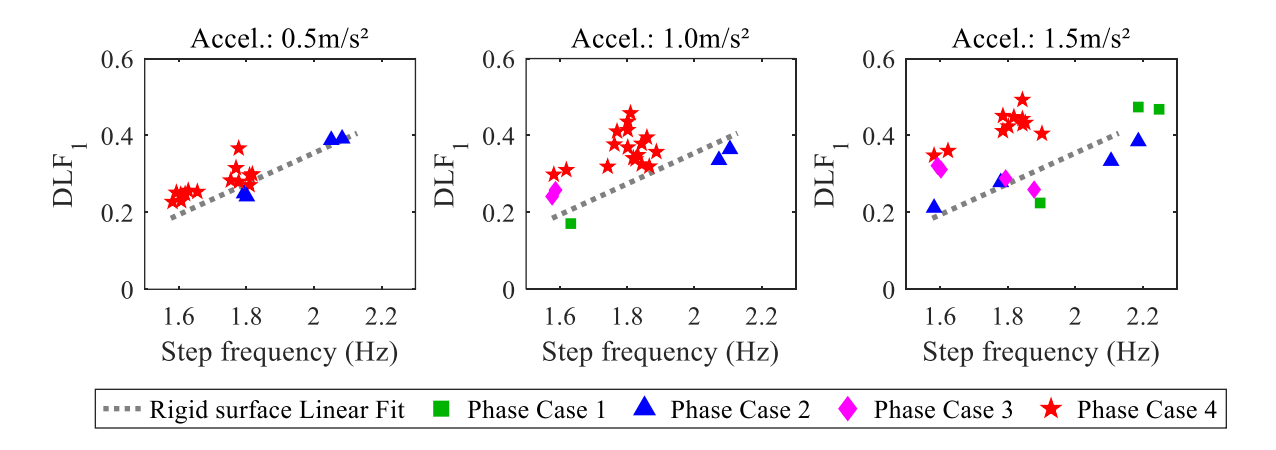


Figure 68 – Correlation of DLF₁ and step frequency f_s for moving surface scenarios compared to rigid surface scenarios for TS1

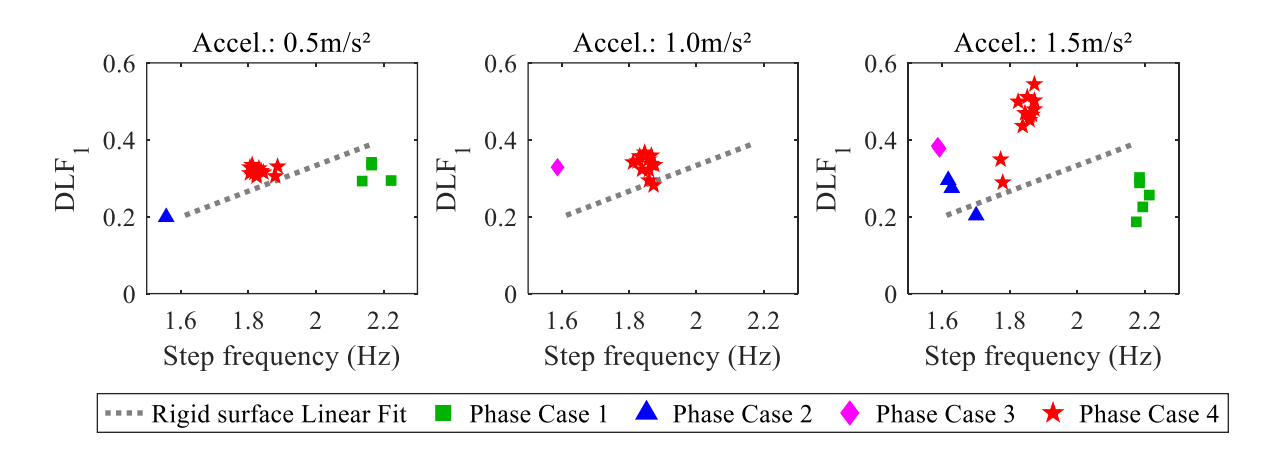


Figure 69 – Correlation of DLF₁ and step frequency f_s for moving surface scenarios compared to rigid surface scenarios for TS2

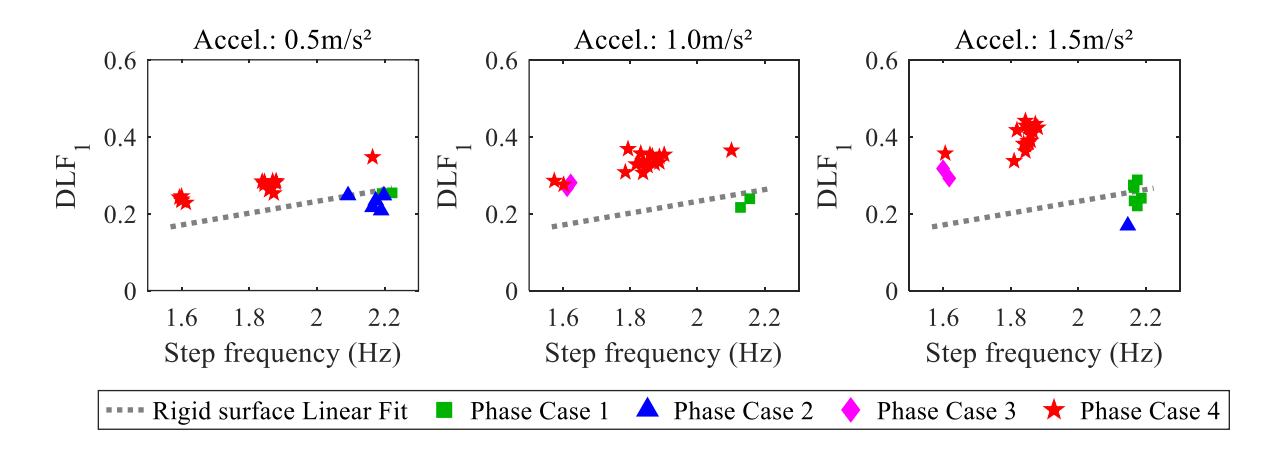


Figure 70 – Correlation of DLF₁ and step frequency f_s for moving surface scenarios compared to rigid surface scenarios for TS3

Importantly, the observed differences in DLF₁ values were not only greater (mostly) but also proportional to the acceleration levels. This suggests that as the platform's acceleration increased, the dynamic response of the pedestrian-induced loads became more pronounced, leading to elevated DLF values. This trend was not observed for only three comparisons for specific ranges for TS1 and TS3, given the sample within the range were not representative for all TS-platform phase cases investigated (see ranges in red in Table 37 and Table 39, and Figure 62 and Figure 64).

However, it is still necessary to assess whether these variations in the DLFs of the first harmonic of the GRFs result from significant changes in walking speed (intrinsically linked to step length), given the proportionality between these variables (Živanović *et al.*, 2022), rather

than solely from the vertical movement of the surface. Figure 71 to Figure 73 presents the correlations between step frequency and walking speed for the respective test subjects and all acceleration levels investigated.

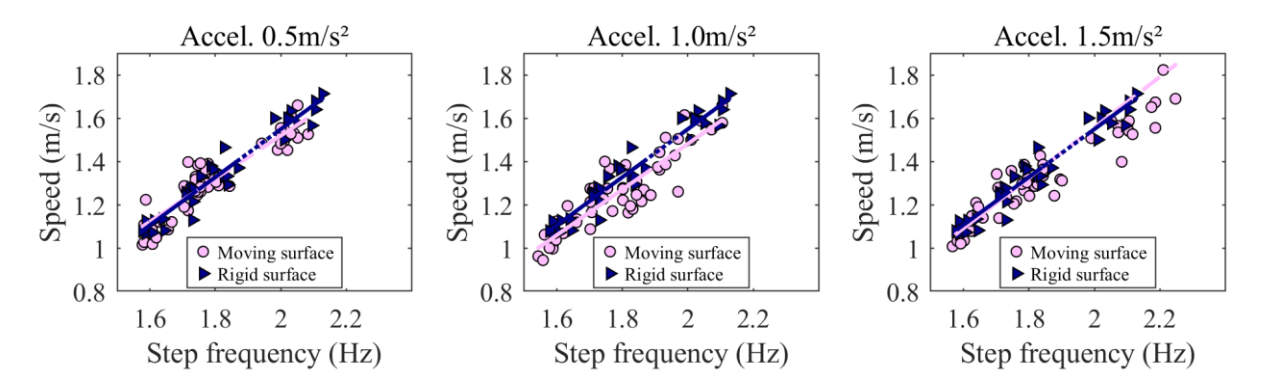


Figure 71 – Speed and step frequency correlations for moving surface scenarios compared to measurements on rigid surface scenarios for TS1

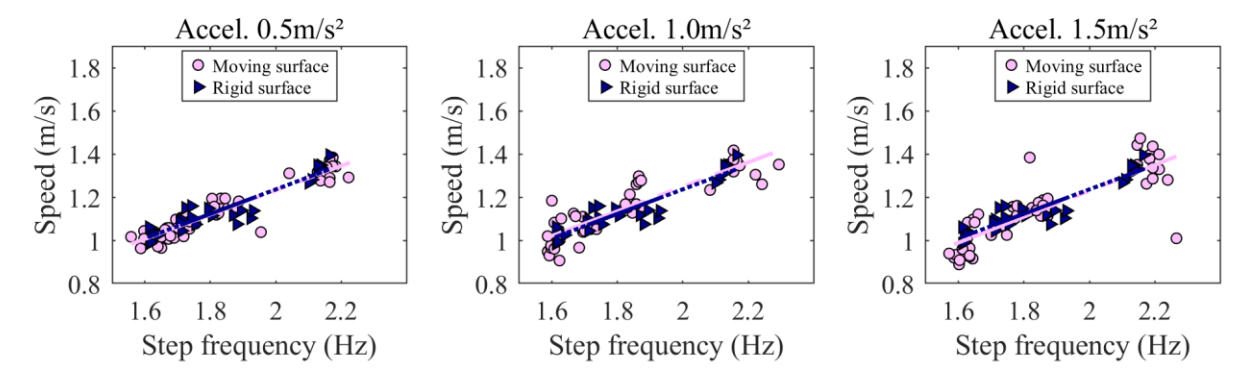


Figure 72 – Speed and step frequency correlations for moving surface scenarios compared to measurements on rigid surface scenarios for TS2

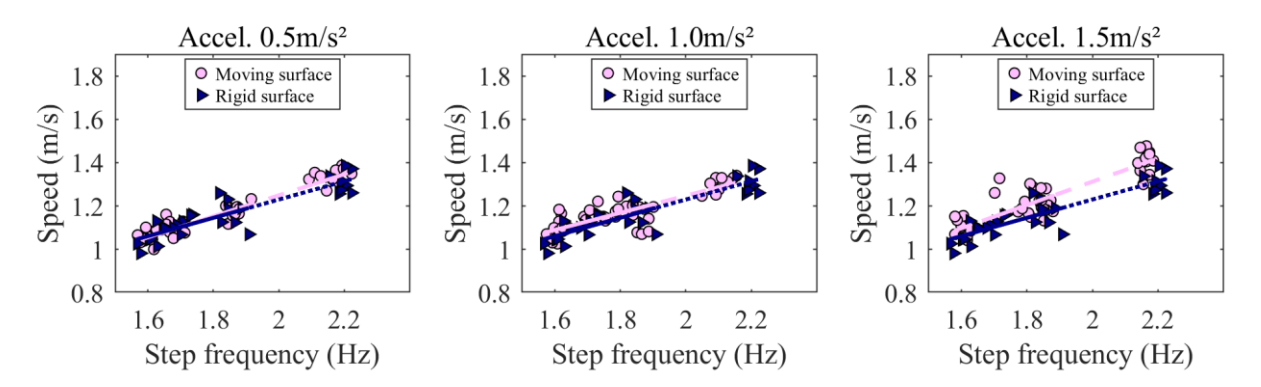


Figure 73 – Speed and step frequency correlations for moving surface scenarios compared to measurements on rigid surface scenarios for TS3

What could be observed from the experimental measurements is that there is no evident relationship between variations in walking speed v and the DLF₁ values, despite the walking speed values being sparser for surface accelerations of 1.5 m/s² for all three test subjects. This sparsity may be a consequence of different adaptation needs due to vibrations while walking, as well as the vertical position at which the TDs occurred. In fact, even when the test subject reduced their walking speed, DLF₁ values were higher in certain cases – for example for TS1 and fast walking scenario – suggesting that lower speed did not necessarily mitigate dynamic amplification in moving surface scenarios.

Furthermore, another aspect that supports this interpretation is that, despite the absence of significant changes in step length across all three test subjects at acceleration levels of 0.5 m/s², DLF₁ values increased by up to 40% (slow walking) on average compared to the rigid surface scenarios.

Therefore, the variations in DLF_1 values in the moving surface scenarios cannot be attributed to changes in walking speed (i.e., shorter, or longer, step length d_s due to the perception of vibrations). Instead, there is evidence that the significant variations in DLF_1 are chiefly due to the movement of the structure.

To better understand how surface movement and different phases influence GRFs and related DLFs, the following analyses are based only on the cases where TS-platform frequency synchronization was detected. The reason for this relies on the fact that the mean footfall force within crossings could not be representative in cases where the test subjects' step frequency significantly differed from the surface vertical frequency. For example, in the fast-walking scenario (2.2 Hz) with a surface vertical peak acceleration of 1.0 m/s² for TS2, none of the crossings were synchronous, as seen in Figure 74, where a great variation of footfall forces was observed. This contrasts with cases where TS-platform frequency synchronization was identified for all crossings within the scenario, such as the normal-walking scenario (1.85 Hz) with a surface vertical peak acceleration of 1.0 m/s² for TS1, as seen in Figure 75.

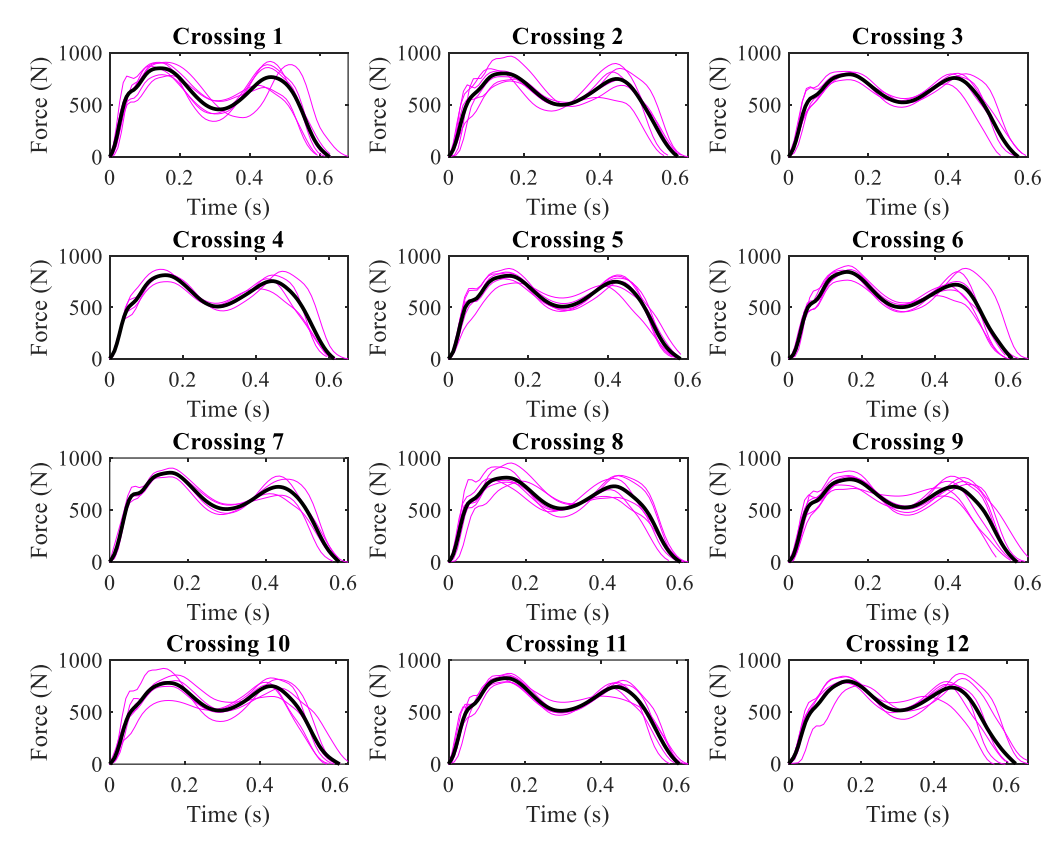


Figure 74 – Example of mean footfall forces for a scenario where TS-platform synchronization was identified for every crossing (TS2, fast walking, surface acceleration of 1.0m/s²)

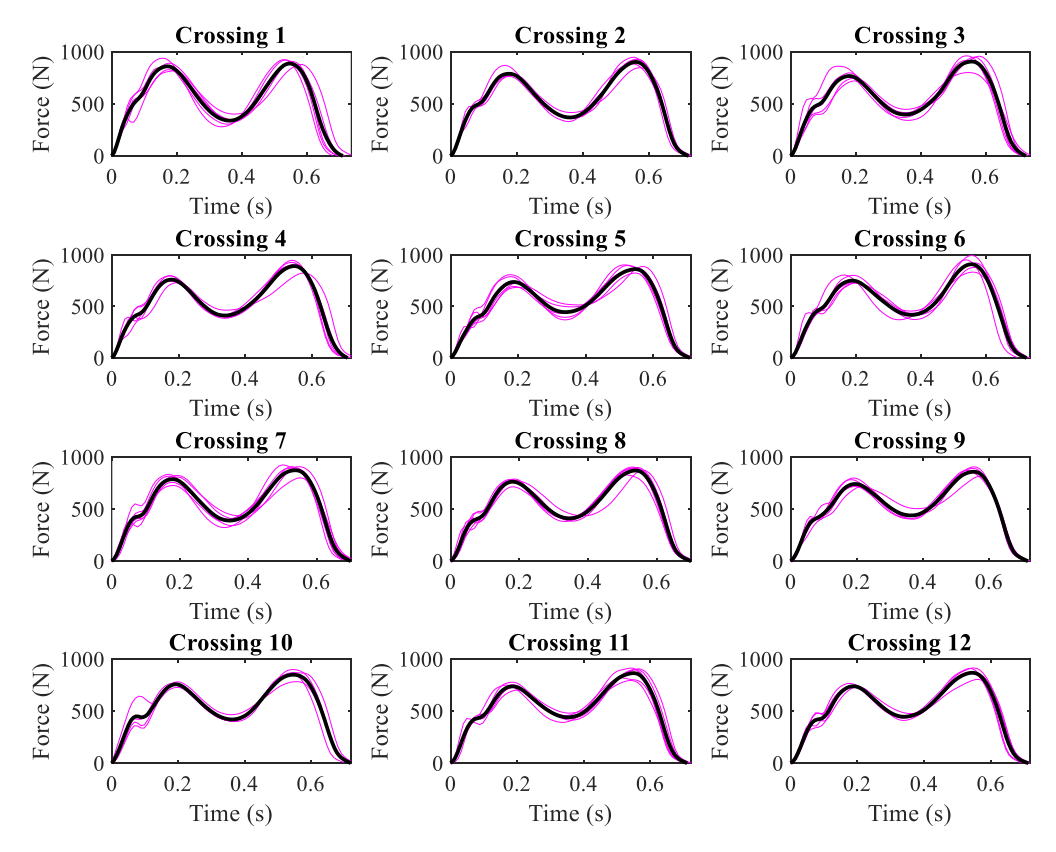


Figure 75 – Example of mean footfall forces for a scenario where TS-platform synchronization was identified for every crossing (TS1, normal walking, surface acceleration of 1.0m/s²)

At this point, it is important to mention that the exclusion criteria for footfall force measurements based on the R² value from the leg force-length curve fit (Lipfert *et al.*, 2012) – described in Section 3.3.2.1 – do not apply to measurements from moving surface scenarios, since the aim here is to evaluate changes in applied forces rather than to extract model parameters. However, footfall forces depicted in Figure 74 and Figure 75 (and from this point forward) do not include measurements in which side-by-side force plate readings overlapped during the double support (DS) phase.

In comparative terms regarding the TS-platform phase (depicted in Figure 76 and Figure 77 — more examples in Appendix B), observations from synchronous crossings provided insights into the influence of the foot's TD vertical position on the platform by analysing two extreme cases: phase cases 2 and 4 from Table 35. When the test subject, walking with a step frequency close to the platform's vertical frequency, stepped onto the platform while it was at its highest (or near-highest) vertical displacement level (phase case 2), the first footfall force peak (during the foot's initial support phase) tended to increase (as seen in Figure 76c).

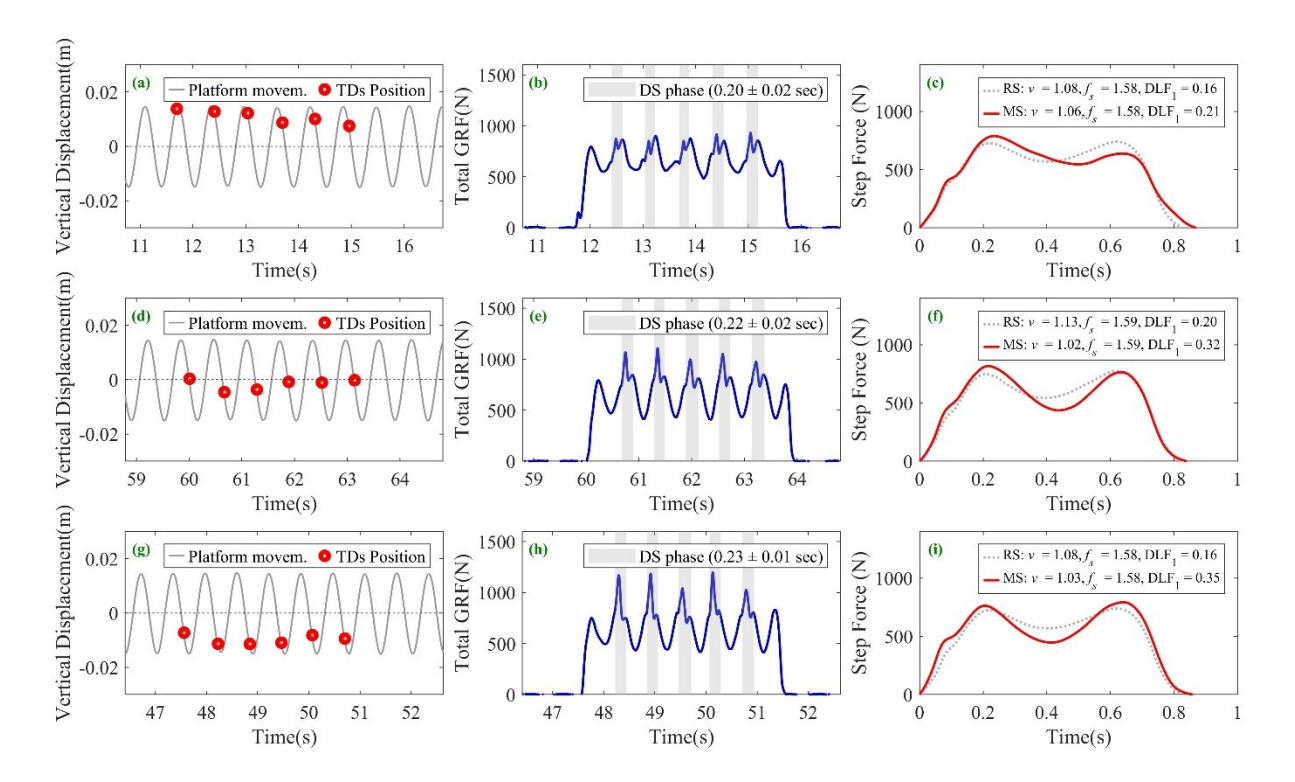


Figure 76 – TD vertical positions at the platform, GRFs and single footfall force for TS1, slow walking, moving surface scenario (frequency of 1.6Hz and 1.5m/s²): (a), (b) and (c) phase case 2; (d), (e) and (f) phase case 3; and (g), (h) and (i) phase case 4.

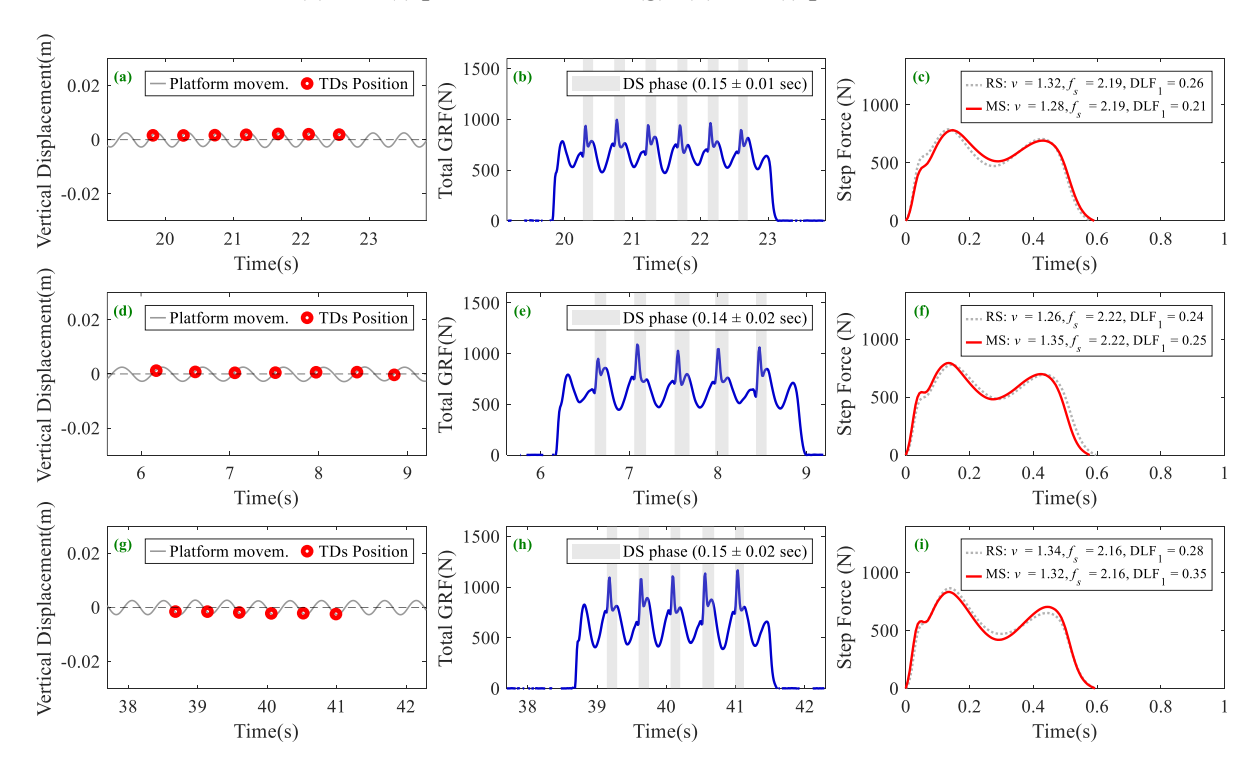


Figure 77 - TD vertical positions at the platform, GRFs and single footfall force for TS3, fast walking, moving surface scenario (frequency of 2.2 Hz and 0.5m/s²): (a), (b) and (c) phase case 2; (d), (e) and (f) phase case 1; and (g), (h) and (i) phase case 4.

A possible explanation is that, since the foot-platform 'encounter' occurred earlier than expected, the swinging (trailing) leg was not fully 'relaxed' at touchdown – in other words, it remained more rigid (Carl *et al.*, 1994). Furthermore, during the foot's final support phase, the platform was moving in the same direction that the foot was preparing to lift off, which could explain why the second footfall force peak was smaller, as seen in Figure 76c.

It is worth mentioning that there was no evidence that an increase or decrease in GRFs would occur for the same step frequency in such cases. Among the 20 crossings where this phase case was detected, the test subject could either walk faster or slower to maintain balance, influencing the DS phase interval and consequently the DLFs. Only a larger sample would confirm whether there is a tendency for changes in the DLFs in these cases. What was observed, however, is that for similar walking speeds (without significant differences), DLF₁ tended to be lower.

Conversely, for the opposite phase case, where the foot stepped on the platform when it was close or at its lowest vertical displacement levels (phase case 4), the DLF₁ was higher than the values obtained for a rigid surface, even at lower walking speeds (see Figure 68 to Figure 70 for reference). Based on the walking biomechanics (Carl *et al.*, 1994), a possible explanation for the observed increase in the second footfall force peak could be that, since the foot tends to be more rigid when preparing to lift off, acting as a rigid lever, when the platform is moving in the opposite direction as the foot – in other words, "escaping" from the foot – its rigidity should increase, thereby promoting the necessary propulsion to lift off the platform.

Additionally, a deeper mid-stance valley peak was observed for such phase case. It can be explained by the fact that at the mid-stance period, when the foot is in full contact with the ground, the platform is moving up, in opposite direction to the gravity, reducing the leg's rigidity. It is important to emphasize that this was the most common TD-platform phase case among the crossings where frequency synchronization was detected.

The same tendency was observed for lower surface vertical displacements, as seen in Figure 77. However, as expected, the changes in the applied forces were smaller, highlighting that vertical surface movement indeed plays a crucial role in the S2HI.

Although the focus here was on the synchronous crossings (TS-platform frequency synchronization) and the extreme phase cases described in Table 35, the same pattern for isolated footfall forces was detected from all kinetic *versus* kinematic data from moving surface

scenarios not mentioned in this analysis, as can be seen in Figure 78. This figure presents two examples of non-synchronous crossings: in Figure 78a and Figure 78b, an example of a descending TD vertical position within the crossing, and in Figure 78c and Figure 78d, an example of an ascending TD vertical position within the crossing.

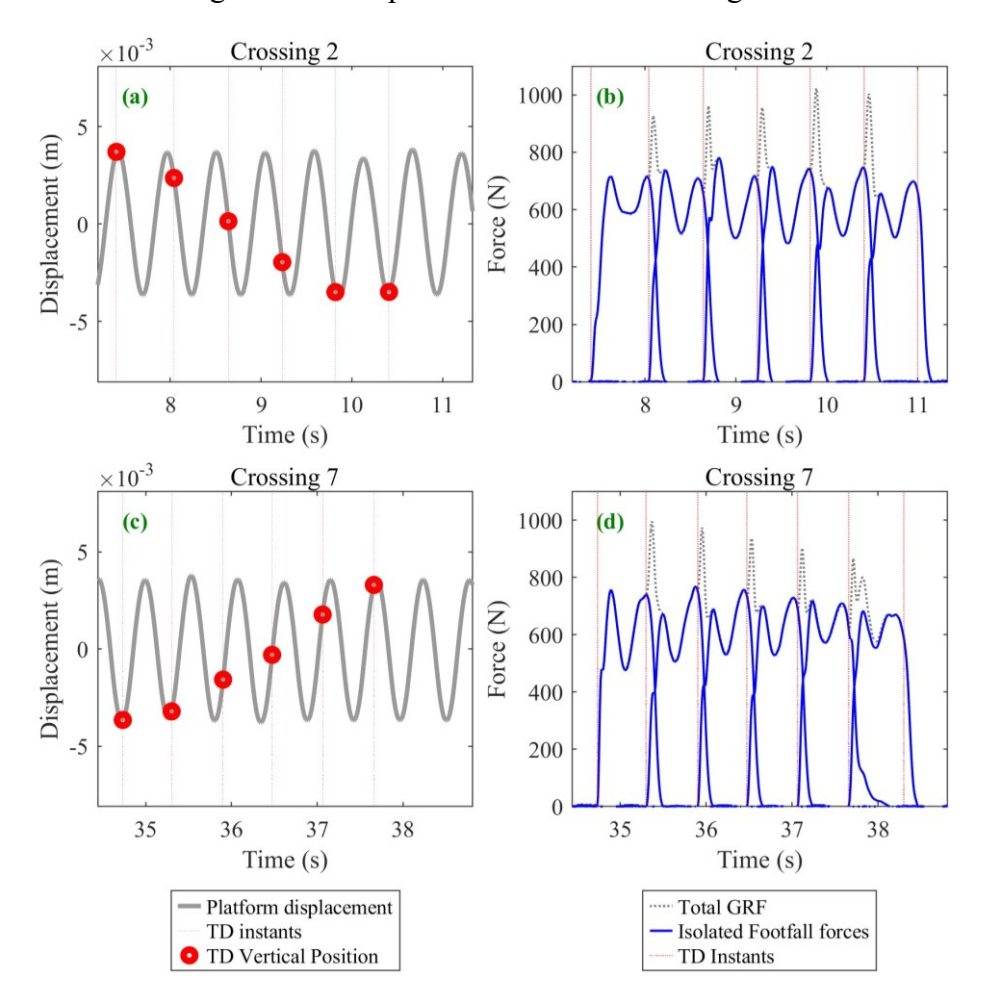


Figure 78 – Example of correlation of TD vertical position and GRFs for two different non-synchronous crossings – (a) and (b) for crossing 2 (descending TD vertical position), and (c) and (d) for crossing 7 (ascending TD vertical position) – (TS3, free walking and surface vertical acceleration peaks of 0.5m/s^2).

As observed in Figure 78, the TD vertical position is proportional to the peaks of the isolated footfall forces, resulting in sharper peaks, and to the total GRFs, implying an increase (in the case of a descending TD vertical position) or a decrease (in the case of an ascending TD vertical position) in the DLFs.

At this stage, it is important to emphasize that the guidelines and standard approaches (see Section 2.2) typically neglect the dynamic behaviour of the human body – despite its well-

documented influence on structural response (Shahabpoor et al., 2016a). Moreover, these approaches often fail to consider the overlapping of footfall forces during the double support (DS) phase, a factor considered to significantly affect human-induced loads (Cai *et al.*, 2019). As a result, the formulations for human walking models – such as the Moving Force model – are predominantly based on measurements carried out on rigid surfaces, limiting their accuracy for more realistic conditions where vibrations are present.

However, based on the findings regarding the moving surface experimental results discussed in this section, it can be concluded that, if indeed there is a preferred vertical phase when interacting with a structure, and it is when the pedestrian tends to step at the structure close or at its lowest displacement levels, the DLFs values in reality, tends to be higher when vibrations are present than those obtained for rigid surfaces (in some cases in this study 100% higher). This was detected even for slow walking speeds. In fact, only for some crossings where the phase case 2 was detected (the least common), the DLFs were smaller.

The dynamic load factor estimates adopted by these normative documents may therefore be underestimating the ground reaction forces in pedestrian modelling for applications where vibration levels are higher. It is also important to note that these standards and guidelines allow for acceleration levels even higher than those investigated in this study (see Section 2.2).

In the context discussed in this subsection, an evaluation of the DBIP models is presented in the following subsection. The aim is to verify if DBIP models have the ability to reproduce the S2HI effects herein discussed.

It is important to clarify that the goal of simulations using DBIP models to investigate S2HI effects is not to propose a set of parameters for different vibration levels to which pedestrians would be subjected. There is little practicality in proposing changes to these parameters based on vibration levels, as in real situations, vibration amplitudes are unpredictable due to the continuous update of vibrations resulting from HSI. However, it is important, based on measurements from rigid surface scenarios, to investigate whether DBIP models' functioning can reflect the changes in the applied forces under different vibration levels and also to discuss their degree of reliability from the S2HI perspective.

In terms of human-to-structure interaction (H2SI), since it has been established that the issue with bipedal models relies solely on the overestimation of DLFs when attempting to simultaneously reproduce the gait parameters of walking speed v and step frequency f_s pairs,

the subsequent analysis will be carried out using the calibrated parameters (adjusting the walking speed v, ξ – and E_0 for BM_2), as the focus is on step frequency f_s and DLF_1 (from Tables A.4 to A.6).

Additionally, the following analysis, investigating the DBIP model's capability of reproducing S2HI effects, relies on experimental data extracted from crossings where frequency synchronization was detected. It is worth noting that despite the numerical simulations will not address HSI as a whole but focus exclusively on its S2HI component, some discussions adopting the HSI formulation are presented.

The aim is to evaluate the influence of the DBIP model's simplifications (reducing it to a SDOF model) and functioning when vibrations are present. First, the numerical consequences of selecting the parameter that governs the prediction of the next impact point x_p are presented for both BM₁ and BM₂. Later, numerical results are provided so as to qualitatively assess the models' reliability.

4.2.2.3 Numerical simulations using DBIP models

As a first step, the analysis must focus on evaluating the functioning of the DBIP models under vibratory conditions. This is essential to understand how the models respond to structural excitation before investigating their ability to reproduce structure-to-human-interaction (S2HI) effects.

As mentioned in Section 4.2.1, setting the step length d_s as constant in the simulations can be advantageous when applying the SDOF DBIP model (BM₁) for rigid surface scenarios, as the step frequency can be imposed given the $v = f_s d_s$ relationship. However, it is still necessary to assess the implications of the choice of the parameter that governs the next impact point in the DBIP models' functioning when vibrations are present.

Importantly, the focus of the analysis in this subsection is not on experimental-numerical comparisons. Because of that, only two crossings and respective calibrated parameters for each DBIP model presented in Section 4.2.1 are used as a reference, as shown in Table 40.

Initially, once the focus is on S2HI investigations, the DBIP models' formulation incorporates the surface movement as described in Section 2.4.2.2. To investigate resonance conditions, the platform vertical frequency was slightly adjusted to match the experimental step

frequency of the sets investigated (sets 1 and 2) in Table 40. Sets 3 and 4 are reference for further investigations when applying the HSI formulation (Section 2.4.2.4).

Table 40 – Sets of DBIP model parameters for BM_1 and BM_2 and related DLF_1 from rigid surface scenario chosen for model's functioning investigation (TS1, slow walking and surface vertical acceleration peaks of 1.5m/s^2) (*)

SET	DBIP model	f _s (Hz)	v (m/s)	DFL ₁	<i>L_p</i> (m)	k _{leg} (kN.m)	ξ (%)	θ ₀ (°)	E ₀ (J)	<i>ż</i> (0) (m/s)	x(0) (m/s)
1	BM_1	1.61	0.93	0.15	1.16	18.66	12.7	72.1		-0.203	
2	BM_2	1.61	0.92	0.15	1.16	18.66	8.9	72.2	828.13	-0.162	1.02
3	BM_1	1.59	0.96	0.17	1.16	18.60	6.24	71.5		-0.199	
4	BM_2	1.59	0.94	0.17	1.16	18.60	10.65	71.6	829.57	-0.165	1.06

^(*) Sets 1 and 2, for crossing 8; Sets 3 and 4 for crossing 5.

For the simulations, four phase angles were established for the first TD at the moving surface: 0° , 90° , 180° , and 270° , representing the phase cases described in Table 35. It was analysed how the models behave given this phase conditioning in both situations: setting step length d_s or attack angle θ_0 as constant in the simulations. Figure 79 and Figure 80 present the results for BM₁ and BM₂, respectively. Although the discussions presented below are based on the highest vibration levels investigated in this study (surface frequency and acceleration peaks of 1.6Hz and 1.5m/s², respectively), the conclusions are relevant to the other moving surface scenarios.

It was observed that, for BM₁, considering constant vibration levels, the impact of setting either d_s or θ_0 as fixed in the simulations does not affect the walking gait (based on the relationship $v = f_s d_s$) but the induced forces only (see DLF₁ values in Figure 79).

When setting $d_s = d_{s0}$, the BM₁ model is forced to step on the structure at the same vertical position from the first TD in resonance cases, as seen in Figure 79a, c, e, and g. In those cases, the initial conditions tend to converge to different values than those reflecting a stable gait from rigid surface scenarios (vertical velocity \dot{z} and attack angle θ_0 at the TD). Additionally, the DLFs vary depending on the first TD phase angle at the platform. BM₂ did not perform well under those conditions, given the great variation in step frequency, as can be seen from Figure 80a, c, e, and g.

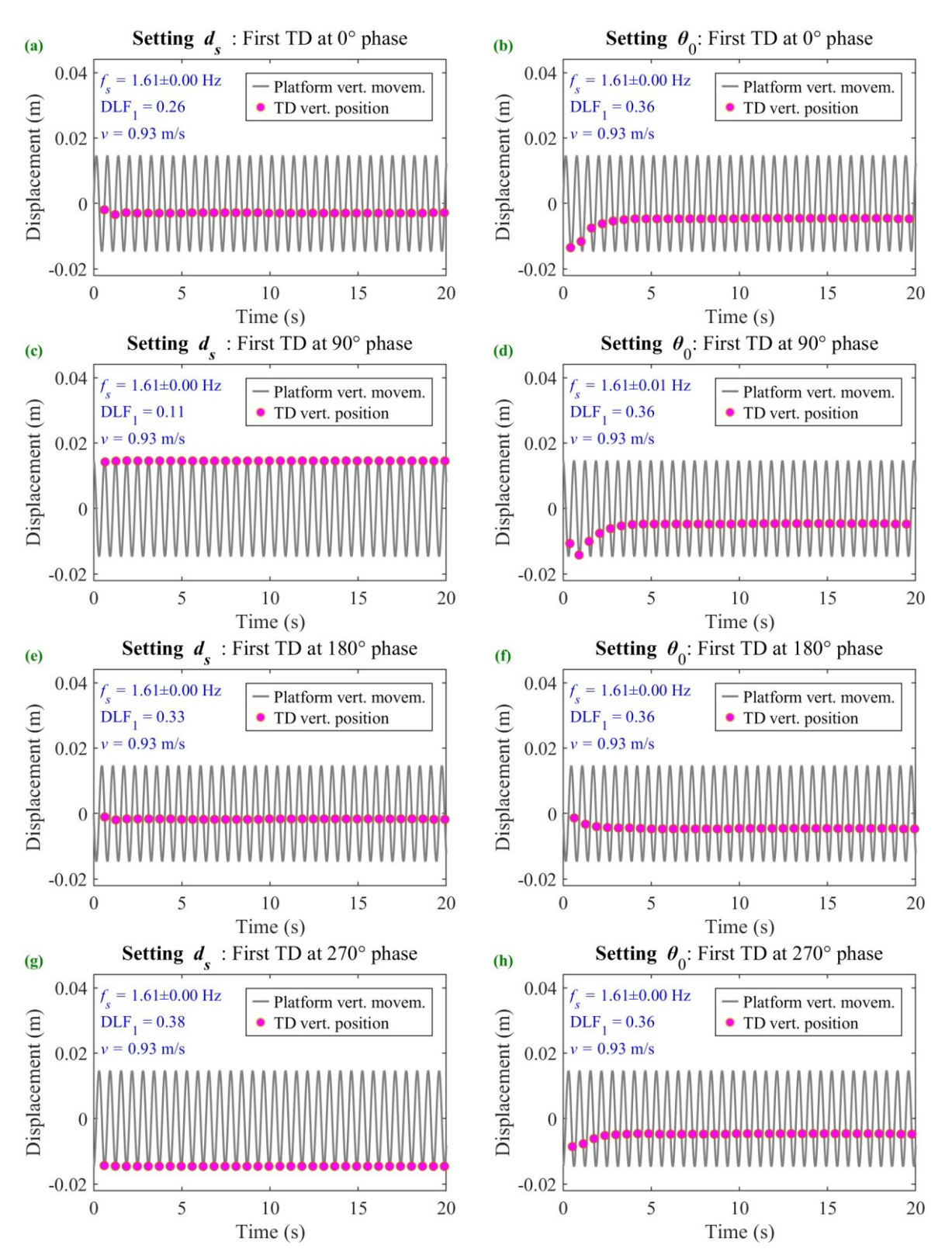


Figure 79 – TD vertical position for BM₁ adopting set 1 of parameters in Table 40, (a), (c), (e) and (g) for setting step length d_s , for initial phase angle of 0°, 90°, 180° and 270°, respectively; and (b), (d), (f) and (h) for setting attack angle θ_0 for initial phase angle of 0°, 90°, 180° and 270°, respectively.

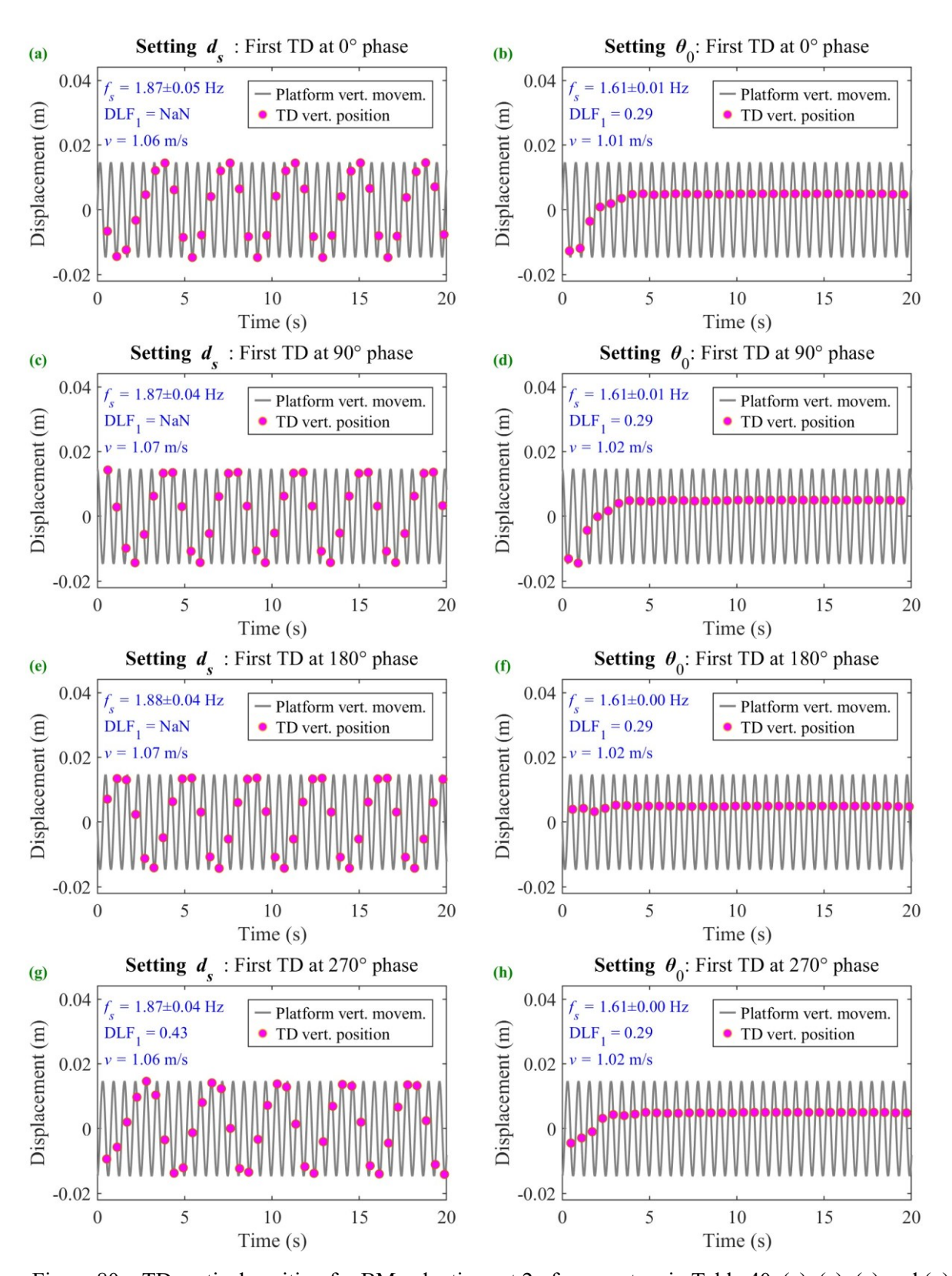


Figure 80 - TD vertical position for BM₂ adopting set 2 of parameters in Table 40, (a), (c), (e) and (g) for setting step length d_s , for initial phase angle of 0°, 90°, 180° and 270°, respectively; and (b), (d), (f) and (h) for setting attack angle θ_0 for initial phase angle of 0°, 90°, 180° and 270°, respectively.

When the step length d_s is free to converge, meaning the attack angle θ_0 is the constant walking gait parameter, the vertical position of the TDs tends to converge to a specific phase angle, regardless of the DBIP model version and the initial phase at the beginning of the interaction. For both models, despite converging to different phase angles (199° and 161°, for BM₁ and BM₂, respectively), the TDs vertical position converged to the descending movement of the surface.

It is worth noting that, since the experimental results did not confirm whether phase convergence occurs — or what it would be — it is not possible to conclude whether this convergence is realistic.

Furthermore, in the moving surface scenario investigated, the walking speed increased in 11% when adopting BM_2 while setting θ_0 as constant in the simulations. This was also detected for the remaining scenarios, with speed variations ranging from 1% to 11%, proportional to the vibration levels.

In addition to the analysis that adopts the DBIP model formulation while incorporating surface movement, this study also examines the model's behaviour when vibration levels increase proportionally to the interaction time with the structure. This is achieved by applying the HSI formulation from Section 2.4.2.4.

The chosen test structure was the Aberfeldy Footbridge (refer to Section 3.2.1 for details). To simulate resonance conditions, crossing 5 from the rigid surface and slow walking scenario for TS1 was selected – sets 3 and 4 in Table 40 for BM₁ and BM₂, respectively. This choice was based on the close match between the pedestrian step frequency and the structure's first-mode natural frequency, as shown in Table 18 and Table 40. Once the focus is on resonance conditions, only the first mode is considered.

As this is a numerical analysis of forced vibration caused by a single pedestrian, it is not possible to consider different phases between the pedestrian and the structure. Instead, only phase convergence is analysed, taking into account the gradual increase in vibrations and analysing possible variations in step frequency. Figure 81 presents the numerical TD vertical position at the test structure from BM₁ and BM₂ coupled with the structure, both considering setting d_s or θ_0 as constant in the simulations, and Figure 82 presents the step frequency variation from the respective HSI formulation (for BM₁ and BM₂).

As observed from Figure 81, the results confirm that for BM₁, while setting step length as constant, the pedestrian-structure phase tends to remain the same from the first TD (Figure 81a) keeping the same step frequency. Clearly, making step length free to converge leads to a phase convergency (Figure 81b) but presenting variations in the step frequency (slower) proportional to the vibration levels (Figure 82).

Different than the previous analysis under the same conditions, BM₂ performed better when considering a gradual increase in the vibration amplitudes and choosing step length as constant (Figure 81c), despite a clear step losing detected, as seen in Figure 82. For this DBIP model version, regardless of choosing d_s or θ_0 as constant, an increase of step frequency was observed.

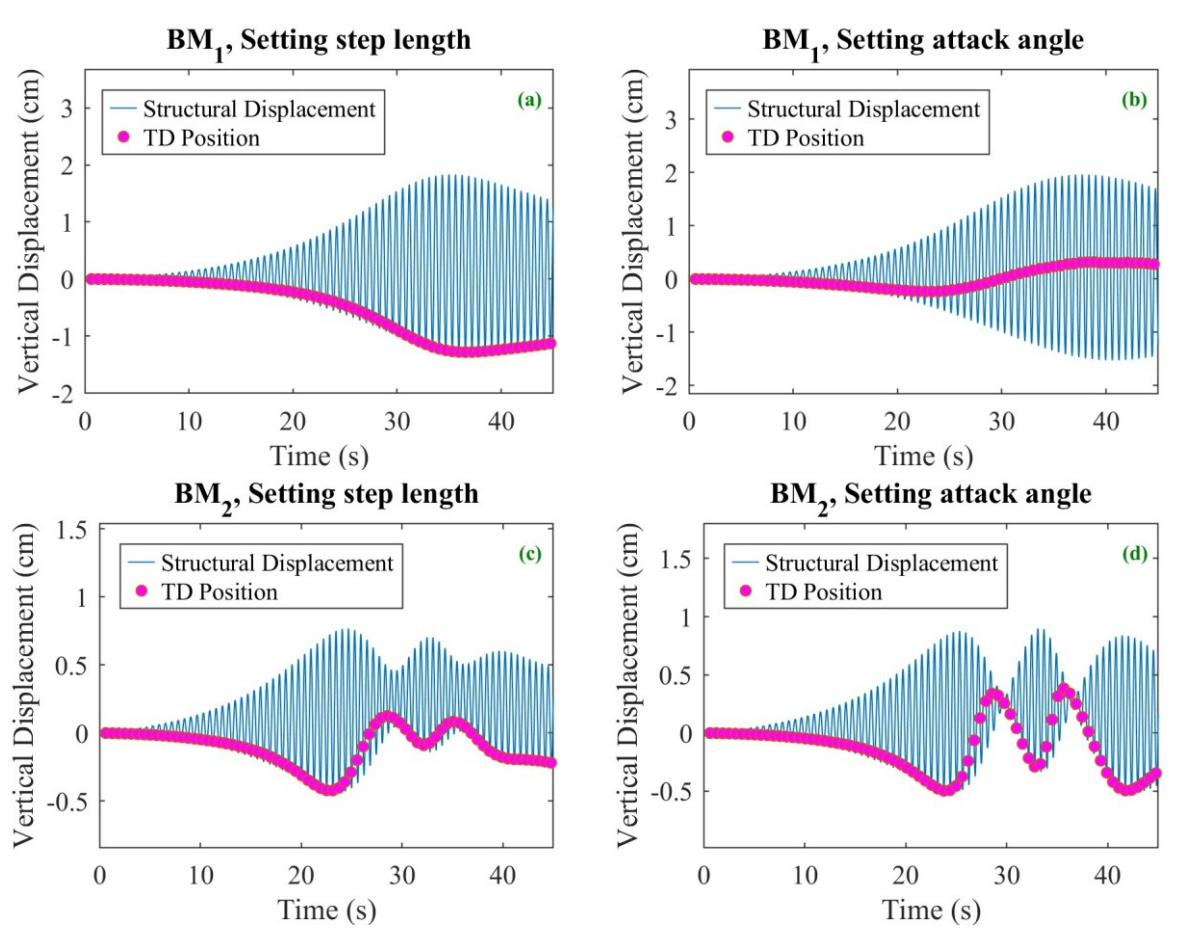


Figure 81 – TD vertical position at the structure from HSI formulation for TS1(sets 3 and for from Table 40) and Aberfeldy Footbridge.

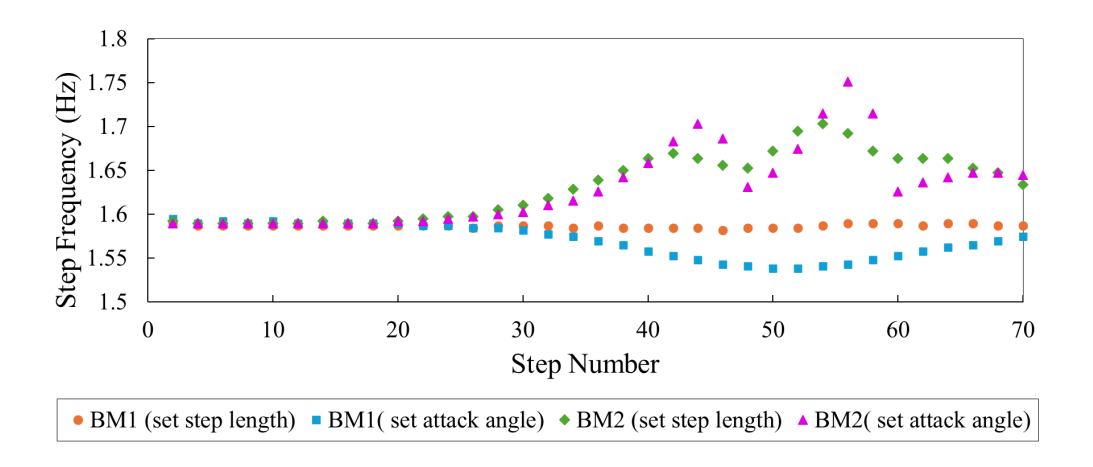


Figure 82 – Step frequency variation from the HSI for TS1 and the Aberfeldy Footbridge.

In general, it was clear that, unlike applications for rigid surface scenarios, the choice of the parameter that governs the prediction of the next impact point in moving surface scenarios – or from the HSI perspective – is not just a matter of a mathematical approach influencing the model's practicability, but also plays an important role in the simulation of vibrations inherent to changes in the applied forces and walking gait. It is still worth investigating whether considering the beginning of the step as the vertical leg orientation (VLO) would lead to different phase angles in the simulations.

The aim of the next subsection is to present numerical results for moving surface scenarios, considering all crossings where TS-platform frequency synchronization was identified – more specifically, the four phase cases presented in Table 35.

Before proceeding, it is important to emphasize two previously mentioned aspects: (1) the vibrations simulated in the VSimulator facilities are not representative of real structures, as the acceleration peak levels remained constant within each moving surface scenario; and (2) due to the short walking path, phase convergence could not be identified. For these reasons, and based on the results discussed in this subsection, BM_1 was selected as the DBIP model for the subsequent analysis, while d_s was set as a constant in the simulations.

Prior to discussing BM₁'s performance in simulating S2HI effects in terms of DLF₁ predictions, it is important to note that, based on the experimental results, the test subject maintained the same (or very similar) walking speed for a given step frequency in only a few measurements. Given this variability – and considering that BM₁ assumes a constant (unaltered)

walking speed – quantitative comparisons will not be conducted, as they could lead to inconsistent or misleading conclusions.

Bearing this in mind, the subsequent analysis aims to examine the trends in variations of numerical DLF₁values, as well as the changes in the characteristic 'M-shape' of footfall force profiles simulated, given different TS-platform phases and vibration levels. The objective is to qualitatively assess whether this DBIP model is capable of capturing these variations observed from the experimental measurements.

Initially, it is analysed the changes in the numerical DLF₁ values based on different phase angles (the same phase angles investigated in the previous subsection – 0°, 90°, 180° and 270°) for all crossings from rigid surface scenarios (see model's parameters in Table A.4 to A.6). As observed from Figure 83 to Figure 85 (supressing invalid values), similar to the experimental results, the DLF₁ values tend to increase when the TDs occurs in the lowest surface vertical position, that is, phase case 4 represented here by 270° phase.

The opposite trend is observed when the numerical TD occurs while the surface is at its highest vertical position (phase case $2-90^{\circ}$ phase), for which a decrease in DLF₁ values is detected across all analysed crossings. As previously mentioned, experimental observations for phase case 2 where the pedestrian maintained a consistent step length for a given step frequency also indicated a reduction in DLF₁. However, due to the limited number of valid synchronous crossing measurements available for this TS-platform phase, it is not possible to conclusively determine whether the DBIP models can predict such variations.

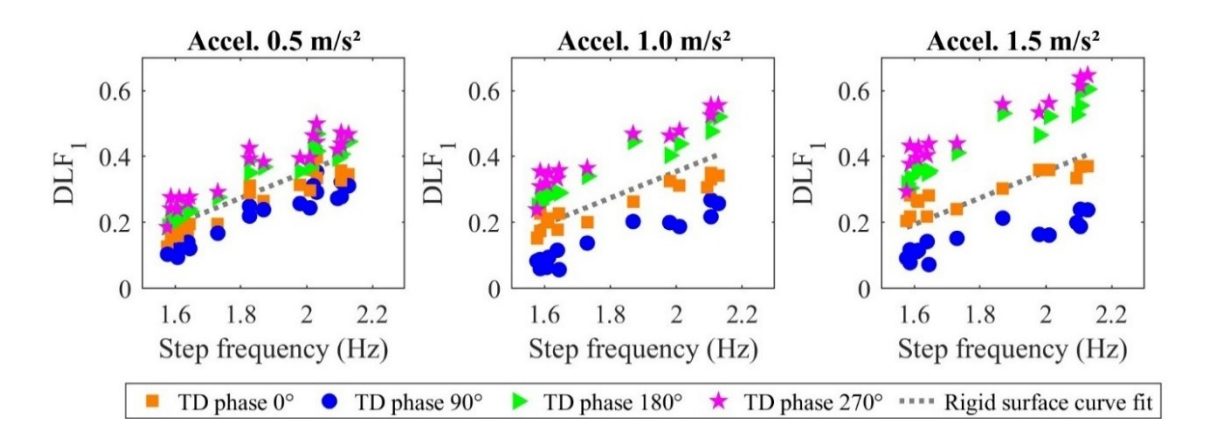


Figure 83 – Variations in DLF₁ for each TD-platform phase for TS1 and sets of calibrated model parameters from rigid surface scenarios in Table A.4.

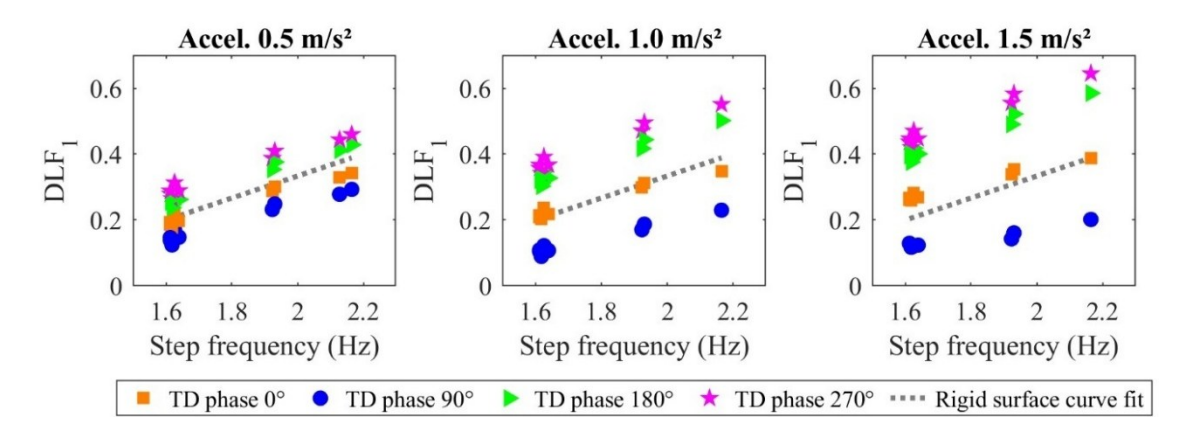


Figure 84 – Variations in DLF₁ for each TD-platform phase for TS2 and sets of calibrated model parameters from rigid surface scenarios in Table A.5.

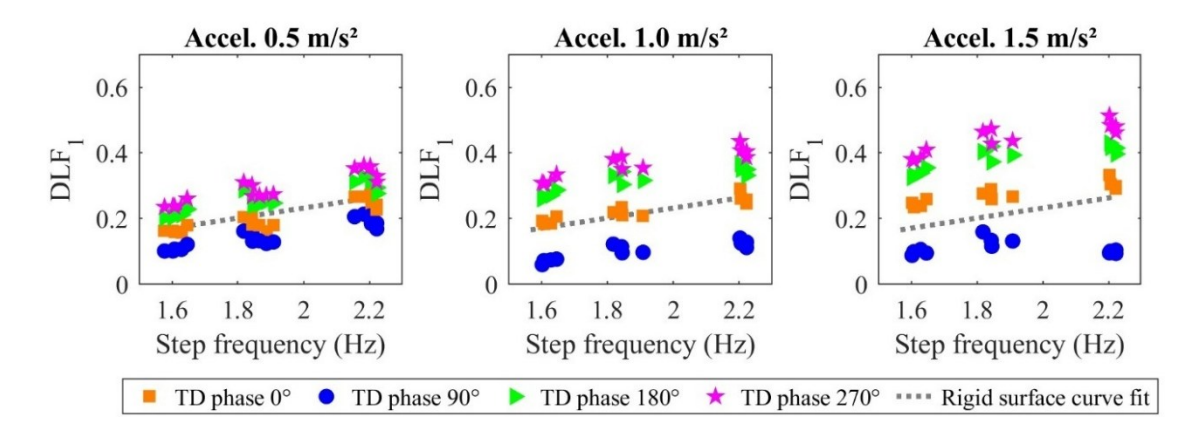


Figure 85 – Variations in DLF₁ for each TD-platform phase for TS3 and sets of calibrated model parameters from rigid surface scenarios in Table A.6.

Additionally, for all test subjects and acceleration peaks investigated, no significant differences were observed in the numerical DLF₁ values for phase case 1 (TD at 0° phase) when compared to the curve fit derived from the rigid surface scenarios. This trend was also observed in the experimental results, with the exception of TS2, for whom lower DLF₁ values were detected – possibly due to a walking speed adaptation (i.e., reduced speed), as correlating Figure 69 and Figure 72.

For most of the experimental measurements where phase case 3 (TD at 180° phase) was detected, an increase in the DLF₁ values was observed. This trend can be seen from the numerical DLF₁ under the same conditions.

Although a quantitative approach is not pursued in this subsection, it is worth highlighting that the trends in numerical variations of DLF₁ values are consistent with the experimental results, as seen by comparing Figure 68 to Figure 70 and Figure 83 to Figure 85.

At this point, it is important to evaluate whether the variations in the numerical DLF₁ values are a consequence of gait adaptations – such as a shorter stance phase duration – or if the model is capable of predicting the trends observed in the experimental results regarding changes in the characteristic 'M-shape' of the footfall force.

For the sake of conciseness, only one crossing from each walking scenario – slow, normal, and fast – was selected for presentation, as similar trends were observed across the remaining crossings (free walking also suppressed). Figure 86 to Figure 88 illustrate the numerical footfall forces obtained for these representative crossings under rigid surface conditions and moving surface conditions, considering all three acceleration peak levels investigated and the range of TS-platform phase angles (0°, 90°, 180° and 270°).

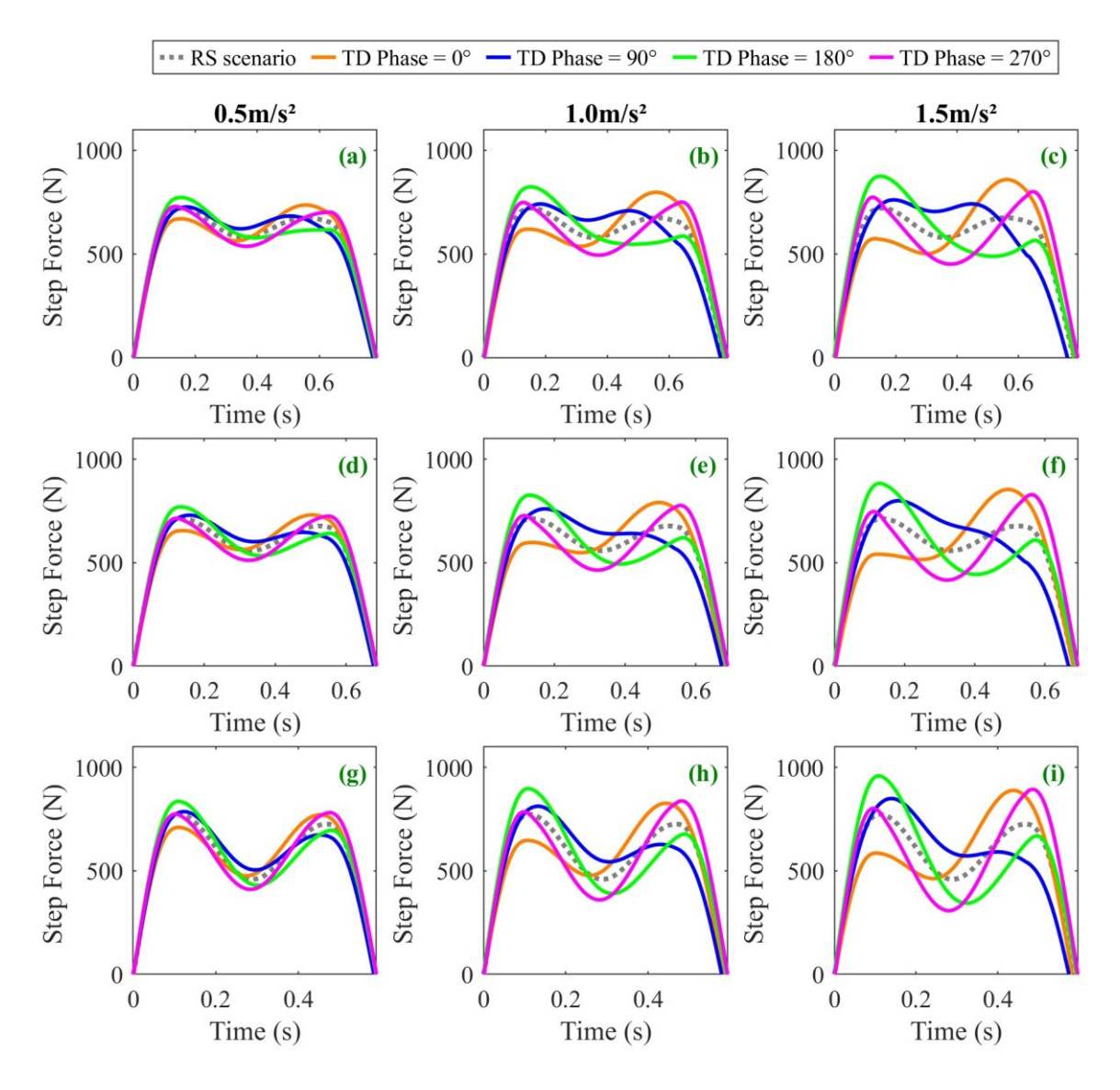


Figure 86 – Variations in footfall force for each TD-platform phase for TS1 and sets of calibrated model parameters from rigid surface scenarios in Table A.4: (a), (b) and (c) slow walking crossing 8; (d), (e) and (f) normal walking crossing 7; (g), (h) and (i) fast walking crossing 5;

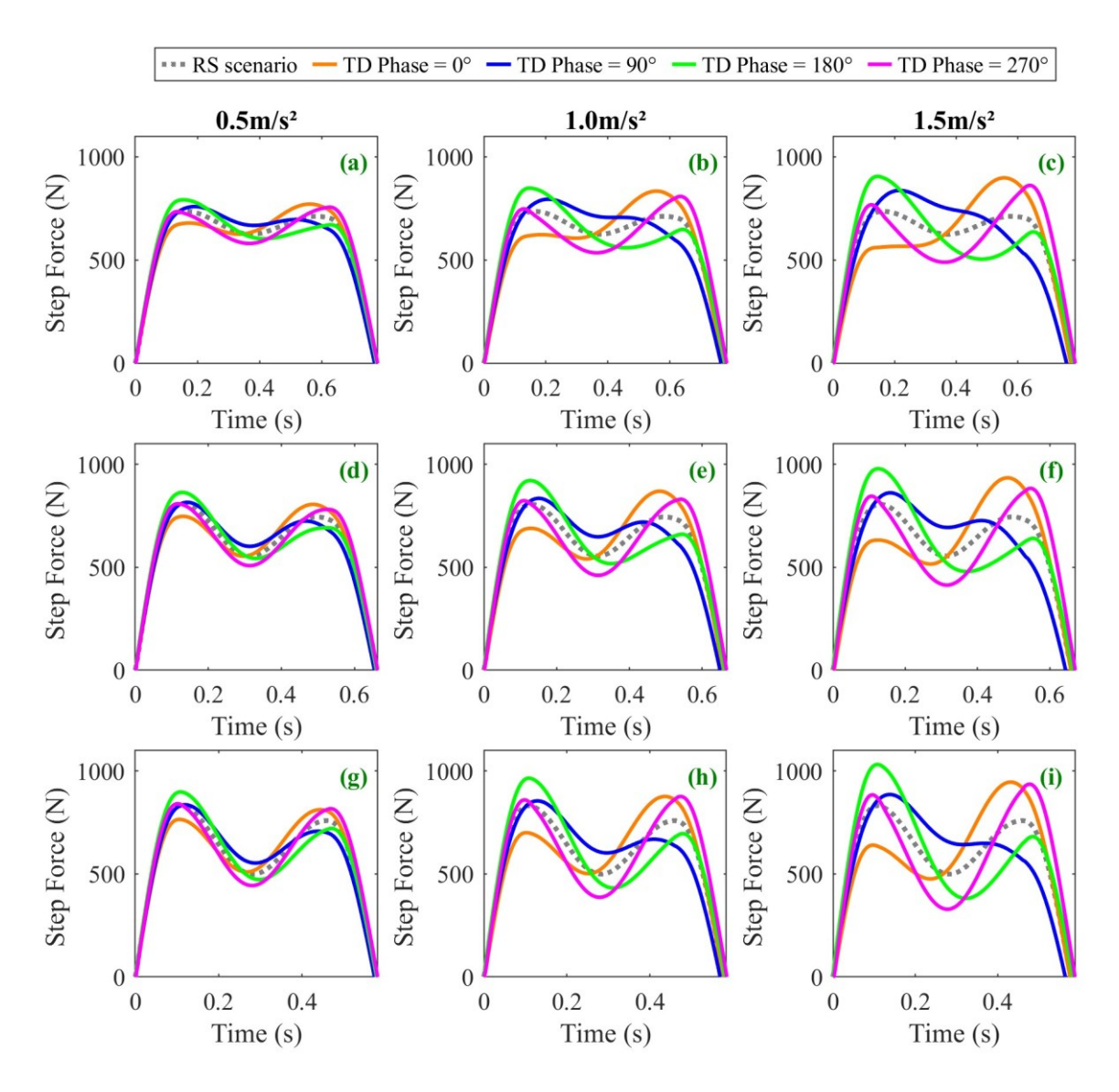


Figure 87 – Variations in footfall force for each TD-platform phase for TS2 and sets of calibrated model parameters from rigid surface scenarios in Table A.5: (a), (b) and (c) slow walking crossing 6; (d), (e) and (f) normal walking crossing 5; (g), (h) and (i) fast walking crossing 2.

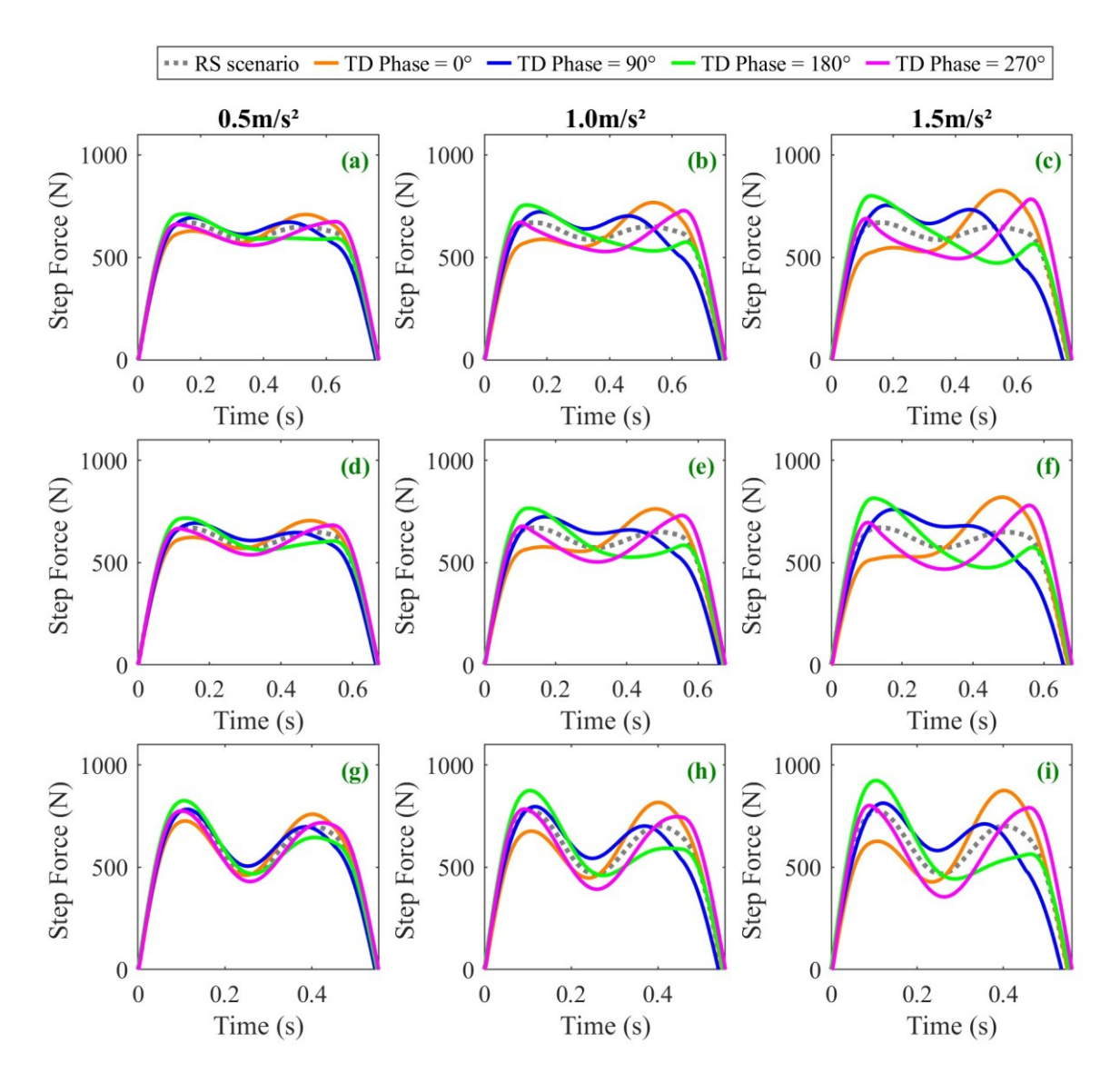


Figure 88 – Variations in footfall force for each TD-platform phase for TS3 and sets of calibrated model parameters from rigid surface scenarios in Table A.6: (a), (b) and (c) slow walking crossing 5; (d), (e) and (f) normal walking crossing 4; (g), (h) and (i) fast walking crossing 5;

For the sake of clarity, each phase angle case will be addressed individually, based on the observations from numerical results depicted in Figure 86 to Figure 88 (footfall forces from moving surface scenarios compared to the ones from rigid surface scenarios):

• 0° phase (orange curves): A reduction in the first peak was observed, proportional to the increase in the second peak, while maintaining similar stance phase periods. This results in total GRF peaks comparable to those from rigid surface scenarios, which helps explain why no great variations in DLF₁ were observed for this phase angle.

Experimentally, those tendencies can be seen on the second and third steps from Figure 78c and d.

- 90° phase (blue curves): There was an increase in the first peak and decrease for the second one for all numerical simulations, as for the experimental results. A slight reduction in the double support phase was observed (given the reduction in the stance phase period for the same step frequency). There was no clear correlation between the shift of the mid-stance valley and the DLF₁ values when analysing all three test subjects.
- 180° phase (green curves): As for 90° phase angle, there was an increase in the first peak and decrease in the second one for all crossings analysed, but more pronounced. In fact, it was observed that these tendencies occurred for the experimental results, as seen in the third step from Figure 78a and b. There was a clear shift of the mid-stance valley to the right while keeping the same stance phase duration, possibly explaining the increase in the numerical DLF₁ values detected.
- 270° phase (pink curves): There is a tendency for a more pronounced increase in the second peak of the footfall force, while the variation in the first peak is relatively small a behaviour also observed in the isolated GRFs of each foot from the experimental measurements. Similarly to the experimental curves, a deepening of the mid-stance valley was also identified. Since this was the most commonly detected phase case in the experiments (phase case 4), Appendix B presents additional examples illustrating the influence of platform vibrations on the footfall forces obtained from the experimental analyses in which this phase case was identified for comparison.

Although the discussion focuses on the changes in GRFs' 'M-shape' for each foot, it is important to mention that, as observed in the experimental measurements, variations in the numerical footfall forces increased proportionally with the vibration levels.

In general, the trends observed in the experiments could be reproduced by applying the BM₁ formulation with the incorporation of surface motion. BM₂ may also perform well under different phase cases in practical applications. However, as previously explained, numerical analyses using this DBIP model version could not be carried out in this study due to the phase convergence issues observed in the simulations, as discussed in the previous subsection.

4.2.3 Concluding Remarks

In this subsection, DBIP models were further investigated through experimental-numerical correlations using data obtained from the controlled platform. This was motivated by the poor performance of BM₁ in reproducing the experimental structural response, even when experimental values for walking speed (v) and step frequency (f_s) were maintained. The discrepancy pointed not to the interaction contribution itself, but to the model's limitation in simultaneously reproducing key gait parameters – v, f_s , and DLF₁ (the later overestimated when compared to values reported in the literature).

This limitation was confirmed through the analysis of both BM₁ and BM₂. For this purpose, model and gait parameters were extracted by cross-referencing kinetic and kinematic data obtained from the vibrating platform. The performance of both models was first evaluated based on measurements taken on a rigid surface under various walking conditions (i.e., slow, normal, fast, and free walking).

The numerical DLF₁ values related to the GRFs were generally higher (-15% to 187%) than the ones extracted from the experiments (in 96% of the crossings investigated), with no significant differences observed between the two DBIP model versions.

Although this effect was more pronounced at higher walking speeds, it was also evident at lower speeds. Importantly, a linear proportional correlation between DLF₁ errors and walking speed was observed for the three test subjects investigated.

Such findings might appear to be a limitation of DBIP models in performing well at high speeds. This might imply a step length limit value related to remaining model parameters. In this matter, DBIP models accounting the foot centre-of-pressure progression have the potential to soften the footfall force peaks and increase the double support phase interval, in turn decreasing the total GRFs peaks and related DLFs. Investigate the incorporation of roller-feet based on experimental-numerical correlation for such purpose can be an alternative to improve the DBIP models performance.

Investigations showed that more accurate DLF predictions were generally achieved by lowering the walking speed while keeping the same step frequency. In general, the adjustments were proportional to the walking speed, ranging from -30% to +3.2%.

For rigid surface scenarios, since the simplification of the DBIP model did not lead to significant differences in the numerical response, reducing the model to a single degree of freedom proved to be advantageous. This is because it eliminates the need to determine the energy input parameter and allows for the imposition of the desired step frequency, which is a key parameter in the study of vibrations of pedestrian structures.

The structure-to-human interaction (S2HI) effects were also addressed in this subsection, and experimental insights into changes in the applied forces and gait parameters under vibrating conditions were discussed. These discussions were based on measurements taken on the vibrating platform, considering different vibration levels and walking speeds.

In general, an average increase in the applied forces was observed through the DLF1 values associated with ground reaction forces (GRFs) across all three investigated vibration levels (surface acceleration peaks of 0.5, 1.0, and 1.5 m/s²), reaching up to +106.4%.

These variations in DLF₁ values were proportional to the vibration levels, although no clear correlation with pacing adaptation was identified when analysing the corresponding walking speed for the respective step frequencies. This corroborates the finding that vibrations alone can induce variations in human-induced loads.

To better understand the causes of such variations, the interaction between the test subject and the platform (TS-platform) was analysed from two perspectives: (1) the frequency synchronization between the step frequency and the platform's vertical frequency; and (2) the phase at which foot touchdowns occurred.

After identifying crossings where frequency synchronization occurred (48% of those investigated), the effect of different TS-platform phases on the induced forces was analysed. It was clear that changes in the applied forces depended on the TS-platform phase. Stepping on the vibrating surface at different vertical positions of the platform led to variations in the footfall force 'M-shape' compared to those obtained on rigid surfaces, providing an explanation for the observed variations in DLF₁ values.

It was also observed that, among the 209 crossings in which frequency synchronization was detected, approximately 60% of the test subjects' touchdowns occurred when the platform was near or at its lowest position. It is also the case for which the highest increases of DLF1 values were observed. A potential explanation is that the platform moved in the same direction

as the vertical centre-of-mass (CoM) trajectory, possibly representing the most comfortable phase of interaction.

In terms of numerically predicting S2HI effects, only the performance of the DBIP models could be assessed, as SMD models lack the capability to simulate variations in walking gait.

Initially, the DBIP model's functioning was analysed considering the presence of vibrations. To this end, a procedure to incorporate surface vertical motion was applied. Different phase relationships between the pedestrian and the vibrating surface could only be simulated using BM₁ with a constant step length (d_s). In this approach, the model could qualitatively predict the trends in variations of the footfall force 'M-shape' and the DLF₁ values. In contrast, for the other approaches – BM₁ and BM₂ with a constant attack angle θ_0 – the simulations consistently resulted in phase convergence.

4.3 Analysis of DBIP models after calibration: accounting for HSI

Since it was observed in Section 4.1.2 that the BM₁ overestimated the DLF₁ values when the experimental walking frequency (f_s) and speed (v) were maintained, the objective here is to investigate whether a reduction in walking speed (v) so as to achieve the DLF₁ values from the literature (also observed in this study) can reproduce the experimental peak accelerations.

As the Aberfeldy Footbridge features high vibration levels, the following analysis will be carried out considering it as the test structure. For this purpose, both DBIP model versions will be evaluated.

It is important to highlight that the current objective is not to reproduce the acceleration time-history, as this may not be achievable due to adjustments made to the walking speed. Moreover, the experimental campaign for this test structure lacks measurements at the pedestrian degree of freedom, requiring the estimation of unknown gait and body parameters.

As seen in Table 18, the test subject's height is not reported in Pimentel (1997), as it was considered irrelevant at the time. However, according to the aforementioned author (personal communication, September 2023), the test subject's height is estimated to be 1.75 m. This value will be adopted in the following simulations, as it is essential for calculating certain DBIP model parameters based on existing proposals in the literature.

Walking speed v and DLF₁ values are estimated based on proposals from the literature. For f_s equal to 1.56Hz, an average walking speed (v) value of 1.06m/s are adopted based on Živanović (2012), Butz *et al.* (2008), and Yoneda (2002). DLF₁ is estimated based on the proposals presented in Table 10 (except for Sétra, 2006), providing and average value of 0.22 related to this step frequency.

4.3.1 2DOF DBIP model (BM₂)

The regression expressions presented by Lin *et al.* (2023) are adopted as a reference to estimate the BM₂ parameters. It is important to highlight that, as with those authors, the step length will be considered free to converge when applying BM₂.

Lin *et al.* (2023)' regression expressions consider the pedestrian body mass (m_h) , height (h), step frequency (f_s) , walking speed (v), and DLF₁, as the independent variables to calculate the remaining model's parameters $(k_{leg}, L_p, E_0, \text{ and } \theta_0)$. For these authors, f_s , v and DLF₁ are the target but less priority is given to the walking speed v.

Their proposal for modelling pedestrians is based on adjustments to the energy input E_0 and attack angle θ_0 so as to achieve the target gait parameters values (herein f_s and DLF₁). Importantly, those authors do not provide explicit expressions for the initial conditions, due to the high variability observed. Instead, they adopted a strategy to determine the optimal initial conditions using a Poincare return map method (refer to these authors for more details). Here, the optimal initial conditions will be taken from the post-convergence gait.

Those authors indicate an initial estimate for E_0 , calculated based on the following expression:

$$E_0 = 1.028 m_h g L_p$$
 (46)

Table 41 presents the target parameters and calculated ones through the regression expressions presented in Table 16 for rigid surface scenarios. As indicated by Lin *et al.* (2023), it is necessary to adjust E_0 to achieve the DLF₁ target, and adjustments to θ_0 so as to achieve the step frequency target. This process should be repeated until the target pair of f_s and DLF₁ is achieved. In Table 41 only the first and last trial is presented.

Table 41 – Trials for TS-P2 body parameters estimation from BM₂ based on Lin et al. (2023)

Gait	Gait Target				Calculated				Output			
Trial	f_s	ν	DLF_1	k_{leg}	L_p	E_0	$ heta_0$ _	f_s	ν	DLF_1		
	(Hz)	(m/s)	value	(kN/m)	(m)	(J)	(°)	(Hz)	(m/s)	value		
1 st	1.56	1.06	0.22	15.04	1.28	1033.7	68.93	1.22	1.09	0.213	No	
last	1.56	1.06	0.22	15.04	1.28	1029	69.96	1.56	1.13	0.250	Yes	

As observed from the results, attempts to achieve the target pair were unsuccessful, as no stable gait was found for the test subject under those conditions. However, considering that the DLF₁ target is only an estimate and the obtained value falls within the range reported in the literature, the final gait trial presented in Table 41 is adopted to assess the model's HSI performance.

The numerical acceleration time-history is presented in Figure 89a compared to experimental filtered acceleration peaks. As observed from these results and previously discussed in Section 4.2.2.3, no matter if step length is or not free to converge, BM₂ tends to adjust the step frequency due to the increase of vibrations, as seen in Figure 89b. This step losing led to the disturbances seen in the numerical acceleration depicted in Figure 89a. Numerically, disturbances happened when the step frequency increased in 10.3% (to 1.72Hz).

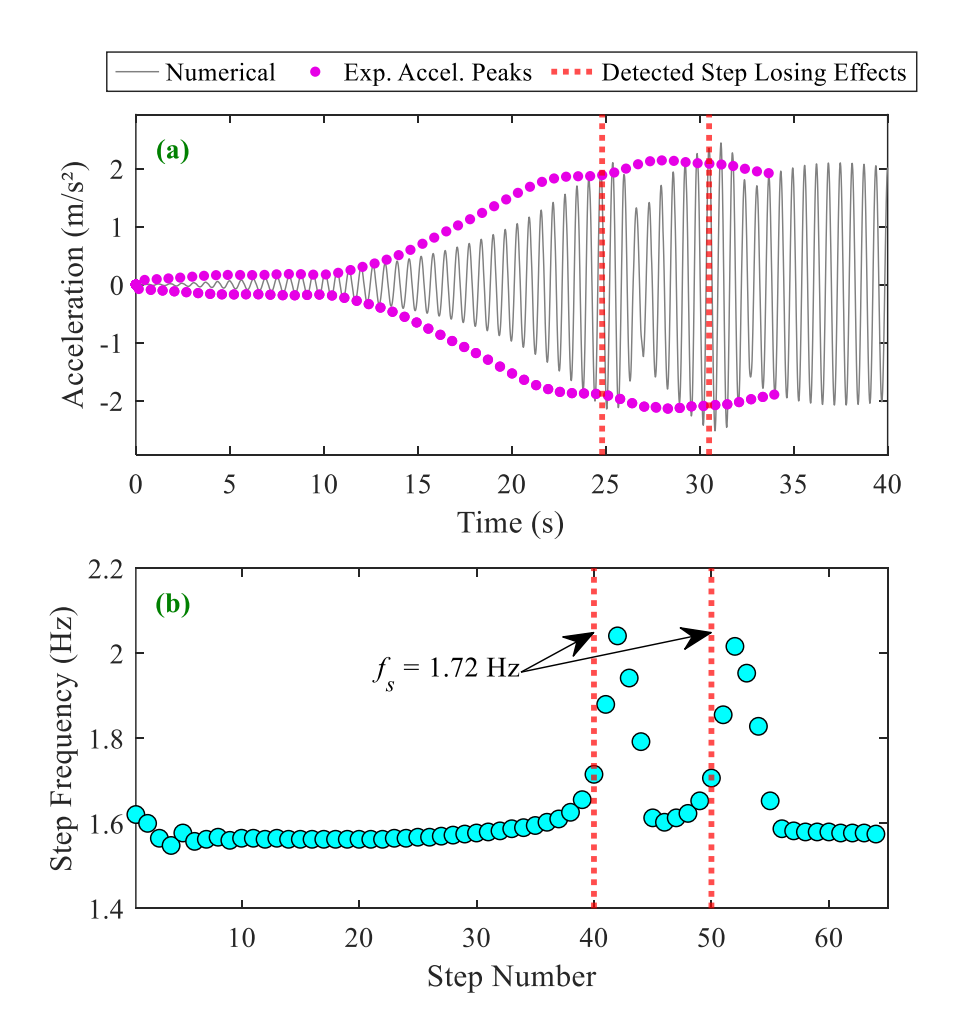


Figure 89 – Results for BM₂ adopting the set of parameters from the regression expressions introduced by Lin *et al.* (2023). (a) Acceleration-time-history, and (b) step frequency variation.

Additionally, the maximum numerical acceleration peak was 2.37m/s^2 , 11% higher than the experimental observations. It worth remembering that the DLF₁ value of 0.22 was not achieved even for the rigid surface.

A segment of the numerical vertical displacement signal of the structure, marking the respective TDs, is presented in Figure 90b, along with the GRFs in the same time interval in Figure 90a. It is possible to observe that during the interaction with the structure, the forces from each foot vary in accordance with the experimental trends also observed on the vibrating platform. This indicates that the BM₂ model is also capable of capturing the force variations resulting from the different phases of interaction between the pedestrian and the structure.

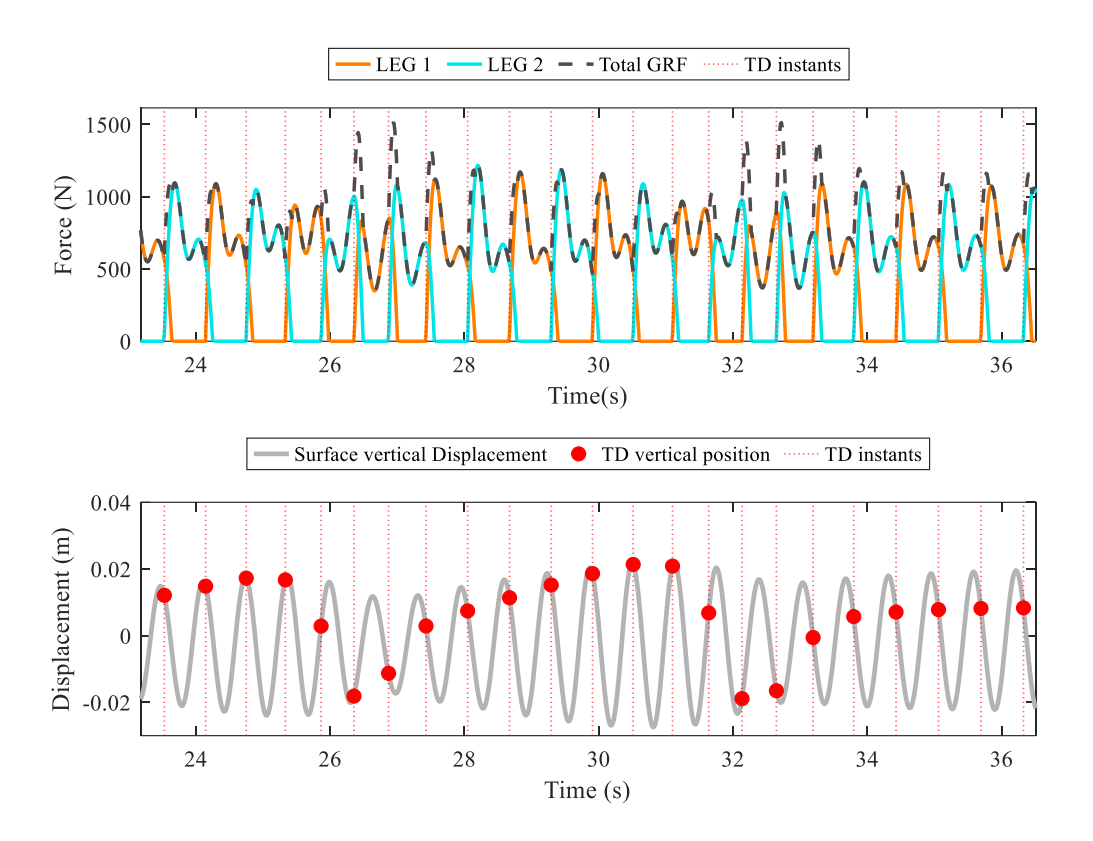


Figure 90 – (a) Total GRFs, and (b) Numerical surface vertical displacement of Aberfeldy marking the TD vertical positions for BM₂ adopting parameters proposed by Lin *et al.* (2023).

4.3.2 SDOF DBIP model (BM₁)

The simulations conducted with BM₁ are carried out using the body parameters estimated by the regression expressions presented by Ruiz *et al.* (2022) and Ruiz *et al.* (2023), for comparison. Both proposals in Ruiz *et al.* (2022) and Ruiz *et al.* (2023) adopted the BM₁ setting step length d_s as constant in the simulations. Because of that, regression expressions for this variable are also provided (see Table 15). However, once the aim is to simulate the intended pair of step frequency f_s and DLF₁, in this study d_s is calculated from the relationship $v = f_s d_s$.

The proposals presented by Ruiz *et al.* in both works consider only the pedestrian body mass m_h , height h, and walking speed v as the independent variables. For this study, it is analysed both scenarios: step length d_s is considered either constant or free to converge.

Initially, simulations for rigid surface scenarios, assuming a constant d_s , were conducted to find the set of parameters that could closely reproduce the target pair of f_s and DLF₁, since

this does not affect the final pair of parameters d_s e θ_0 after convergence. The set was then adopted to evaluate the BM₁ performance from the HSI perspective.

Table 42 presents the sets of parameters calculated based on the regression expressions provided by (1) Ruiz *et al.* (2023), (2) Ruiz *et al.* (2022), and (3) adjusted in this study, along with the resulting gait parameters.

Table 42 – Sets of BM₁ parameters from (1) Ruiz *et al.* (2023), (2) Ruiz *et al.* (2022), and (3) adjusted based on the findings in this study

Set	Input						Output	t		
	L_p	k_{leg}	ξ	d_s	$ heta_0$ *	$\dot{z}(0)^*$	f_s	ν	DLF_1	Stable?
	(m)	(kN/m)	(%)	(m)	(°)	(m/s)	(Hz)	(m/s)	value	
(1)	1.10	21.72	-20	0.68	-	-	-			No
(2)	1.11	23.35	7	0.68	69.84	-0.14	1.56	1.06	0.29	Yes
(3)	1.17	15.60	3	0.68	68.78	-0.24	1.56	1.06	0.24	Yes

^{*} Value after convergence

As shown in Table 42, despite the more robust statistical approach presented in Ruiz *et al.* (2023), the regression expressions proposed in that study resulted in a damping ratio (ξ) of -20% when applied to the physical characteristics of the test subject and an estimated walking speed of 1.06 m/s² (Set 1). Because of that, no stable gait was achieved.

When considering the previous proposal by the same authors (Ruiz *et al.*, 2022), – Set 2 in Table 42 – a stable gait was achieved. However, as the resulting DLF₁ was 31.8% higher than the target value, likely due to the high leg stiffness (k_{leg}), a third attempt was carried to reduce the DLF₁.

For this purpose, adjustments to the test subject's leg resting length (L_p) and stiffness (k_{leg}) were made. By adopting Set 3 of parameters from Table 42, a stable gait was achieved, and a DLF₁ value of 0.24 was obtained. This parameter set is subsequently used for the HSI investigation.

The functioning of BM₁ from the HSI perspective is evaluated based on which parameter is held constant in the simulations – either d_s or θ_0 – and how variations in step frequency affect the structural response. As shown in Figure 91, adopting BM₁ does not result in numerical instability. Even when θ_0 is kept constant, the step frequency gradually decreases, in contrast to BM₂, where abrupt changes in step frequency can lead to instability. This gradual step loss may explain the improved results when θ_0 governs the prediction of the next impact

point. The numerical acceleration peaks for BM₁ are 2.82m/s^2 (+ 31.8%) and 1.92m/s^2 (-10.4%) for setting d_s and θ_0 , respectively.

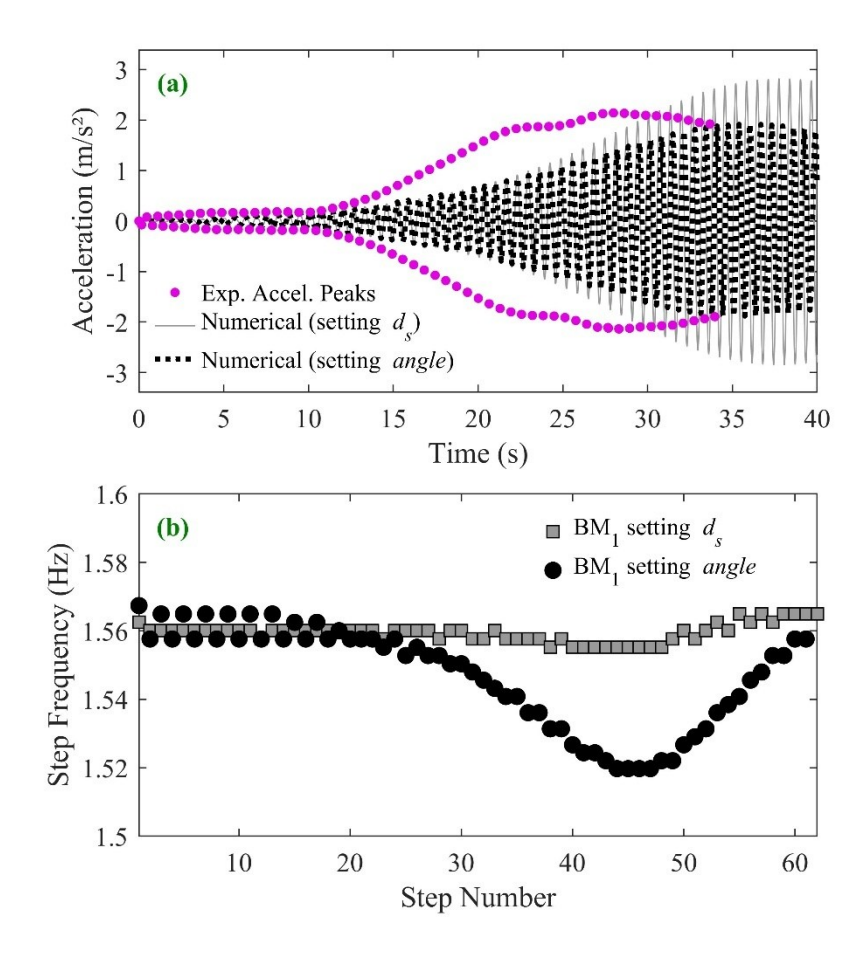


Figure 91 – Results for BM₁ adopting the Set 3 of parameters in Table 42. (a) Acceleration-time-history, and (b) step frequency variation.

As for BM₂, Figure 92 and Figure 93 present the numerical TD vertical position at the structure and related GRFs by applying BM₁ respectively for setting d_s or θ_0 , for comparison. As observed from both figures, the numerical TDs occurred between 90° and 200° phase with the structure, leading to a decrease in the second footfall force peak. Trend also observed experimentally.

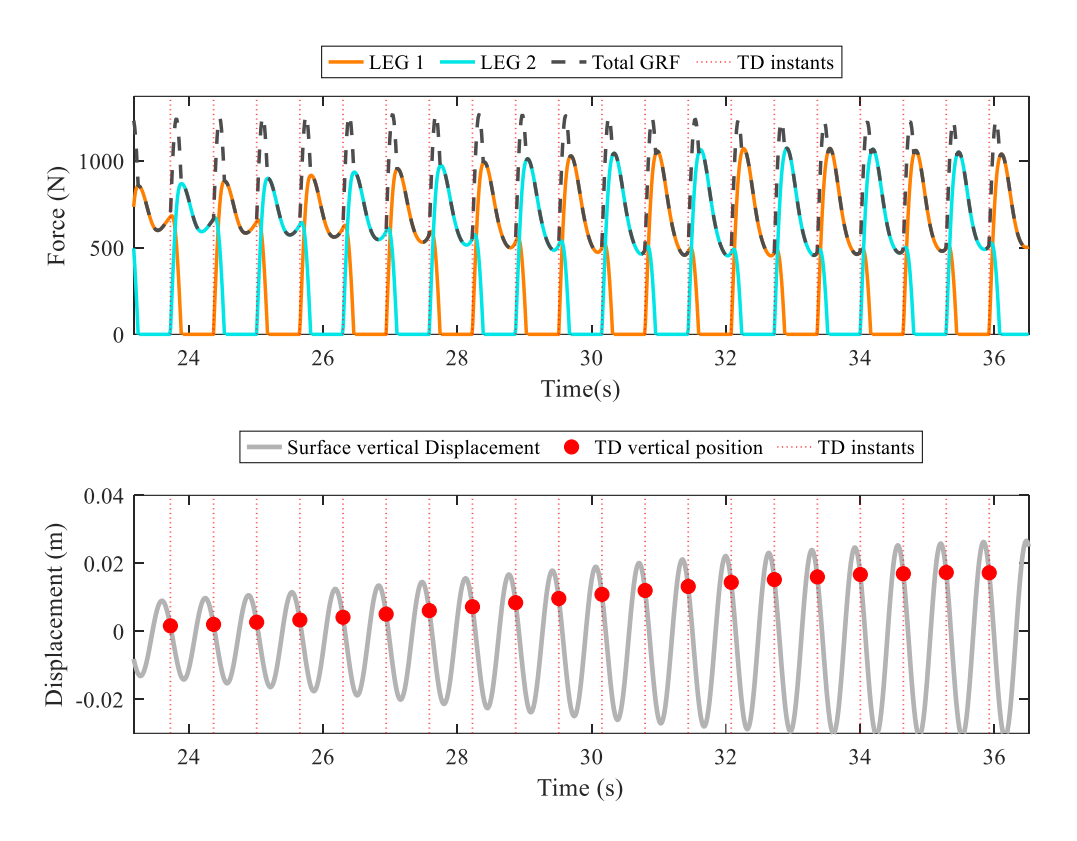


Figure 92 - (a) Total GRFs, and (b) Numerical surface vertical displacement of Aberfeldy marking the TD vertical positions for BM₁, setting d_s , and adopting the Set 3 of parameters in Table 42.

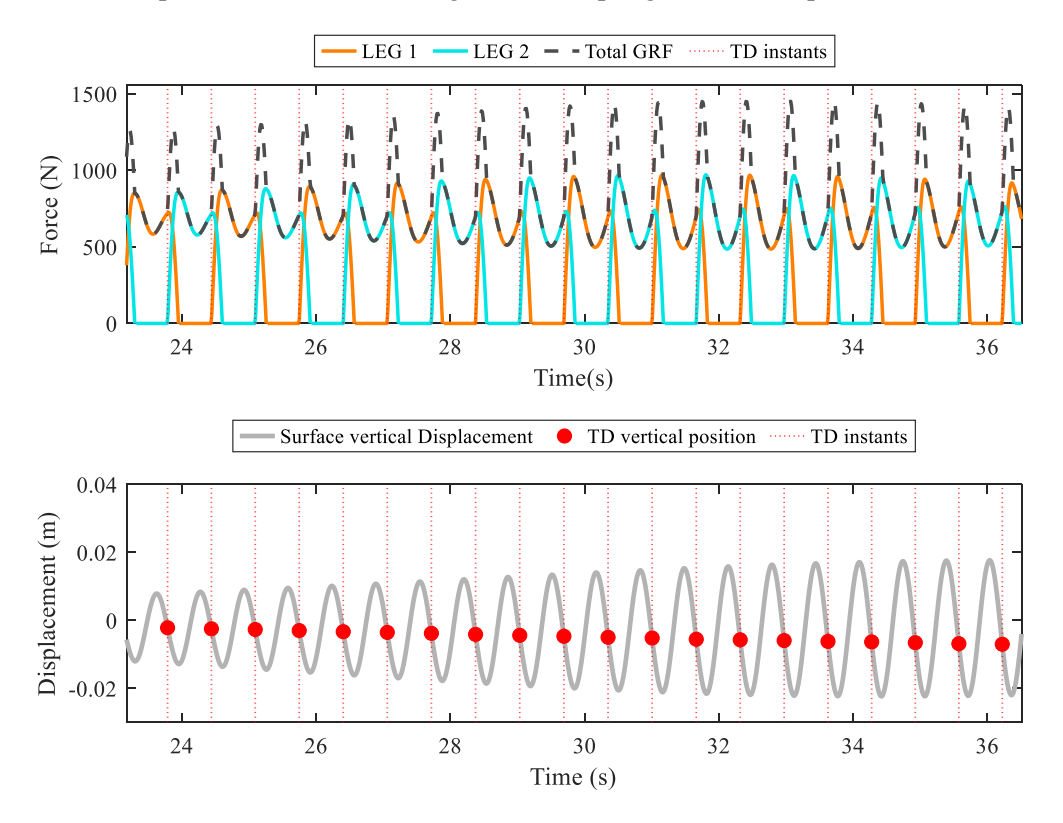


Figure 93 - (a) Total GRFs, and (b) Numerical surface vertical displacement of Aberfeldy marking the TD vertical positions for BM₁, setting d_s , and adopting the Set 3 of parameters in Table 42.

4.3.3 Concluding Remarks

The DBIP model (in its single- and two-degrees-of-freedom versions) was reassessed from the HSI perspective by adjusting the gait in an attempt to achieve the target combination of step frequency and DLF₁. The objective was to verify whether the experimental peak accelerations could be reproduced in the simulations by modifying the walking speed. The models' parameters were estimated either using regression expressions from the literature or selected based on the findings of this study, with each approach analysed separately.

It was concluded that BM₂ with a fixed attack angle and BM₁ with a fixed step length overestimated the peak acceleration values, whereas BM₁ with a fixed attack angle underestimated them. Furthermore, depending on the adopted approach, step frequency tended to adapt in response to the vibrations – except for the case of BM₁ with a fixed step length, where the frequency remained stable.

Only for BM₁ with a fixed attack angle, the step frequency was gradually decreasing with higher vibration levels.

5 CONCLUSIONS

5.1 General Conclusions

In this study, two simple biodynamic models representing pedestrians walking in the vertical direction were investigated: the single-degree-of-freedom (SDOF) Spring-Mass-Damper (SMD) model and the Damped Bipedal Inverted Pendulum (DBIP) model. In addition to a key discussion on the functioning, formulation, and conceptual differences of these models, their performance was evaluated by comparing numerical simulations with experimental results, as well as by comparing the models with each other. The goal was to deepen the understanding of human–structure interaction (HSI), with particular attention to structure-to-human interaction (S2HI), which remained underexplored in the literature.

The experimental results used as references in the analyses were obtained either from measurements on full-scale lively footbridges (from previous studies) or from a purpose-built platform capable of simulating vertical vibrations relevant to pedestrian walking, on which experiments with three test subjects were conducted as part of this study. While the Human-Structure-Interaction (HSI), as a whole, could be investigated in the former, only the Structure-to-Human-Interaction (S2HI) component could be addressed using the latter.

Although the primary focus in Civil Engineering is often on human-to-structure interaction (H2SI), the effects of vibrations on human-induced loads (the structure-to-human-interaction – S2HI) play an important role in the subject. This is because, in order to understand the HSI in its entirety, it is essential to fully understand how the feedback loop operates. In this context, one interesting outcome from this thesis relates to S2HI effects: it was experimentally demonstrated how structural vibrations influence human gait and induced forces – phenomena often simplified or ignored in most design approaches.

Overall, for the investigated vibration levels, it was observed that the induced forces depend not only on physical body characteristics and gait parameters (such as step frequency and walking speed), but also on the vertical relative position of the touchdowns (TDs) at the vibrating surface, indicating what is referred to as a phase-dependent foot-surface interaction on force magnitude and related dynamic load factors (DLFs).

With no clear evidence of a pacing adaptation when comparing the average walking speeds in scenarios with and without vibrations, it was found that, on average, DLF₁ values (related to the first harmonic of ground reaction forces – GRFs) tended to be higher than those measured on rigid surfaces for specific step frequency ranges. This trend supports the idea that DLFs increase with higher vibration levels, challenging the common assumption of constant DLF values typically adopted in structural design codes.

This can be explained by the fact that lower DLF₁ values (compared to rigid surfaces) were observed only in a few instances – specifically when test subjects stepped onto the moving platform at or near its highest vertical displacement. This was the least frequent phase case recorded, possibly because it represents the most uncomfortable form of test subject-surface interaction.

By comparing experimental and numerical results across multiple scenarios, this study revealed how each investigated biodynamic model represents those S2HI trends and where its limitations lie. These findings offer important insights into the suitability of simplified models in engineering practice and contribute to addressing the experimental validation gap identified in the literature.

Regarding model-specific contributions, the SMD model proved effective in simulating structural response from HSI applications when properly calibrated – mainly through adjustments in dynamic load factor (DLF) values – especially in scenarios where gait adaptation is not critical. Its simplicity and direct application make it a practical choice for design purposes, although it depends on GRFs obtained from rigid surfaces and cannot reproduce walking adaptations in response to structural vibrations – that is, it cannot simulate S2HI effects.

On the other hand, the DBIP model captured important aspects of S2HI, such as phase-dependent interactions and variability in GRFs due to vibration levels. While much sensitive and less stable, it enabled a more detailed representation of human response. Nonetheless, its performance is dependent on careful parameter selection and was less reliable at higher walking speeds, given the observed overestimation of DLF₁ values. This limitation led to inaccuracies in predicting the structural response.

For this model, a linear correlation was observed between walking speed and errors in predicting DLF₁ values (most overestimated), suggesting that DBIP models should be improved if the goal is to simultaneously reproduce the three relevant gait parameters for applications in

the design of low-frequency structures, such as footbridges: step frequency, walking speed, and DLF₁.

Bearing in mind the clear influence of the foot touchdown phase relative to the structural vertical movement on the applied forces, these results underscore the importance of incorporating synchronization and phase effects into biodynamic modelling efforts. While DBIP models have demonstrated value in capturing qualitative trends, the findings also highlight the need for further refinement to enhance their reliability and applicability in quantitative analyses.

The complexity of applying the DBIP model is also due to its sensitivity to the parameters defined to simulate gait characteristics during walking. The dissipative nature of the two-degree-of-freedom (2DOF) formulation requires a mechanism to compensate for energy loss, which can be disregarded if the model assumes a constant longitudinal speed – effectively reducing it to a single-degree-of-freedom (SDOF) model. This simplification, in addition to reducing the number of model parameters to be defined, makes the model more suitable for practical applications. This is because, beyond allowing the imposition of step frequency and walking speed in the simulation – which is also achievable when adopting SMD models – , no significant differences were observed in the numerical responses between the one- and two-degree-of-freedom DBIP model versions, even in scenarios featuring high vibration levels.

In summary, through numerical simulations and comparisons with experimental data, this study clarified the role of such biodynamic models – SMD and DBIP models – in capturing key aspects of human–structure interaction (HSI), particularly the often-overlooked structure-to-human interaction (S2HI). It compared the performance of both models, highlighting their respective advantages for different design scenarios, and provided experimental-numerical evidence to support model validation and future refinements. Rather than proposing a definitive model, this research demonstrates how each respond under varying conditions and vibration levels. The results reveal general trends that can guide engineering applications but should be interpreted considering the limitations of the experimental setup and sample size.

5.2 Recommendations for future research

Recognizing that the primary goal in Civil Engineering is not to model the full biomechanical complexity of walking, but to understand its effects on structural performance,

further experimental campaigns with larger samples and more varied vibration scenarios are necessary. These would help identify the minimum model complexity required for practical applications and clarify model limitations in more general terms.

Based on the limitations identified throughout the analyses and the opportunities for further exploration, the following future research directions are suggested to enhance the understanding and practical application of biodynamic models in the context of human-structure interaction:

- Expand the sample size and subject diversity to capture inter-subject biomechanical variability.
- Investigate the performance of DBIP models incorporating roller-foot mechanics to account for the centre-of-pressure progression to improve force shape accuracy and better simulate double support phases.
- Calibrate the SDOF version of the DBIP model to reproduce step frequency and DLF₁, aiming to enhance its practicality and relevance for civil engineering applications.
- Perform synchronized full-scale experiments on lively footbridges to validate and calibrate models under real walking and vibration conditions.
- Explore phase synchronization phenomena in real HSI scenarios to better understand the influence of timing on applied forces.
- Evaluate whether simplified SMD models, when coupled to structures, can reliably capture trends in interaction force variations for practical design applications, even without representing the bipedal nature of walking.
- Develop improved optimization algorithms for calibrating biodynamic model parameters, aiming at more robust and automatic fitting to experimental gait data.
- Examine the implications of DLF variability with vibration level on current design codes and propose adjustments where necessary.
- Define the minimum model complexity required to balance simulation accuracy and practical applicability in structural design process.

REFERENCES

Ahmadi, E., Caprani, C., Živanović, S., Heidarpour, A. (2019). Assessment of human-structure interaction on a lively lightweight GFRP footbridge. Engineering Structures, v 199, Article ID 109687.

Alexander, N.A. (2006). Theoretical treatment of crowd structure interaction dynamics. Structures and Buildings, v 159, p 329-338.

Archbold, P.J. (2004). Interactive load models for pedestrian footbridges [Ph.D. thesis], National University of Ireland, University College Dublin, Dublin.

Bachmann, H., Ammann, W. (1987). Vibration in structures induced by man and machines. Structural Engineering (document n.3), International Association for bridge and Structure Engineering, Zurich, Switzerland.

Bachmann, H., Pretlove, A.J., Rainer, H. (1995). Dynamic forces from rhythmical human body motions. In Vibration Problems in Structures: Practical Guidelines (Appendix G), Birkha user, Basel.

Barker, C. Some observations on the nature of the mechanism that drives the self-excited lateral response of footbridges, in: Proceedings of the International Conference on Design and Dynamic Behaviour of Footbridges, Paris, France, 2002.

Bishop, N.W.M., Willford, M., Pumphrey, R. (1993). Multi-Person Excitation of Modern Slender Staircases. Engineering for Crowd Safety, London, UK.

Blanchard, J., Davies, B., Smith, J. (1977). Design Criteria and Analysis for dynamic Loading of Footbridges. Symposium on Dynamic Behaviour of Bridges, TRRL Supplementary Report 275, p 90-106.

Bocian, M. J. Macdonald, J. Burn. (2013). Biomechanically inspired modelling of pedestrian-induced vertical self-excited forces, Journal of Bridge Engineering 18 1336–1346. https://doi.org/10.1061/(ASCE)BE.1943-5592.0000490.

Bocian, M. J. Macdonald, J. Burn, Modelling of self-excited vertical forces on structures due to walking pedestrians, in: Proceedings of the 8th International Conference on Structural Dynamics (EURODYN 2011), Leuven, Belgium, 2011.

Brito, V.L., Pimentel, R.L. (2009). Cases of Collapse of Demountable Grandstands, Journal of Performance of Constructed Facilities, v. 23 (3).

Brownjohn, J. A. Darby, A. Pavic, Vsimulators: Human factors simulation for motion and serviceability in the built environment, SECED conference, Greenwich London, September, 2019.

Brownjohn, J. A. Darby, Human factors simulation for motion and serviceability in the built environment, 13th UK Conference on Wind Engineering, Leeds, 2018. Available online:

https://ore.exeter.ac.uk/repository/bitstream/handle/10871/35513/EA56_VSIMULATORS_20180712.pdf?sequence=1

Brownjohn, J.M., Pavic, A., Omenzetter, P. (2004). A spectral density approach for modelling continuous vertical forces on pedestrian structures due to walking. Canadian Journal in Civil Engineering, v 3, p 65–77.

Brownjohn, J.M.W. (1997). Vibration characteristics of a suspension footbridge. Journal of Sound and Vibration, v 202, p 29–46.

Butz, C. M. Feldmann, C. Heinemeyer, Advanced load models for synchronous pedestrian excitation and optimized design guidelines for steel footbridges, Technical Report RFSRCT-2003-00019, European Commission, Brussels, Belgium, 2008.

Cadei, J., Stratford, T. (2002). The design, construction, and in-service performance of the all-composite Aberfeldy footbridge. Advanced Polymer Composites for Structural Applications in Construction, p 445-453, ICE Publishing.

Cai, Y., Gong, G., Xia, J., He, J. Hao, J. (2019) Simulations of human-induced floor vibrations considering walking overlap. SN Applied Sciences 2:19 https://doi.org/10.1007/s42452-019-1817-1.

Caloni, A., Morfino, M., Civera M., Surace C. (2025) Structure-to-Human Interaction (H2SI): Pedestrian Response to Oscillating Footbridges and Considerations on Their Structural Control and Health Monitoring. Infrastructures, 10, 9. https://doi.org/10.3390/infrastructures10010009.

Caprani, C.C., Ahmadi, E. (2016). Formulation of human-structure system models for vertical vibration. Journal of Sound and Vibration, v 377, p 346–367.

Caprani, C.C., Keogh, J., Archbold, P., Fanning, P. (2011). Characteristic vertical response of a footbridge due to crowd loading. Proceeding of the 8th International Conference on Structural Dynamics (Eurodyn'11), p 978–985, Leuven, Belgium.

Carl, W., Chan, M.D., Rudins, A (1994). Foot Biomechanics During Walking and Running. Mayo Clin Proc 1994;69:448-461.

CCIP (2006). Willford, M., Young, P. A Design Guide for Footfall Induced Vibration of Structures. Concrete Centre: Surry, UK.

Dallard, P., Fitzpatrick, T., Flint, A. (2001). London Millennium Bridge: Pedestrian-Induced Lateral Vibration. Journal of Bridge Engineering, v 6(6), p 412-417.

Danbon, F., Grillaud, G. (2005). Dynamic Behaviour of a Steel Footbridge: Characterization and modelling of the Dynamic Loading Induced by a Moving Crowd on the Solferino Footbridge. In Paris Footbridge 2005 – Second International Conference, Itália.

Dang, H. Experimental and numerical modelling of walking locomotion on vertically vibrating low-frequency structures, Ph.D. thesis, University of Warwick, England, UK, 2014.

Dang, H., Živanović, S. (2013). Modelling pedestrian interaction with perceptibly vibrating footbridges, FME Transactions, v 41, p 271–278.

Dang, H.V., Živanović, S (2015). Experimental characterisation of walking locomotion on rigid level surfaces using motion capture system. Eng. Struct. 91 (2015) 141–154.

Dong, Y., Noh, H. Y. (2024). Ubiquitous Gait Analysis through Footstep-Induced Floor Vibrations. Sensors, 24(8), 2496; https://doi.org/10.3390/s24082496

Eurocode 1 (2003). EN, Eurocode 1: Actions on structures. Part 2: Traffic loads on bridges, EN 1991-2:2003, European Committee of Standardization.

Eyre, R., Cullington, D.W. (1985). Experience with vibration absorbers on footbridges. TRRL Research Report N°18, Transport and Road Research Laboratory, UK.

Fanning, P.J., Archbold, P., Pavic, A. (2005). A novel interactive pedestrian load model for flexible footbridges. Proceedings of the SEM Annual Conference and Exposition on Experimental and Applied Mechanics, p 573–580, Portland, Ore, USA.

Fitzpatrick, A., P. Dallard, S. le Bourva, A. Low, R. Ridsill-Smith, M. Willford Linking London: the Millennium Bridge The Royal Academy of Engineering, London (2001)

Fujino, Y., Pacheo, B.M., Nakamura, S.I., and Warnitchai, P. (1993). Synchronisation of human walking observed during lateral vibration of a congested pedestrian bridge. Earthquake Engineering and Structural Dynamics, v 22, p 741–758.

Gao, Y., Yang, Q., Qin, J. Bipedal crowd–structure interaction including social force effects. International Journal of Structural Stability and Dynamics, vol 17(7), p31, 2017.

Geograph (2025). The Millennium Bridge, London. Available in https://www.geograph.org.uk/photo/2694345. Access in April 2025.

Georgakis, C.T., Jorgensen, N.G. (2013). Change in mass and damping on vertically vibrating footbridges due to pedestrians. Proceedings of the 31st Conference on Structural Dynamics (IMAC '13) 3, p 37–45.

Geyer, H. (2005). Simple models of legged locomotion based on compliant limb behaviour [Ph.D. thesis]. Friedrich-Schiller-Universität Jena, Jena, Germany.

Gomez, D., Dyke, S.J., Rietdyk, S. (2018). Experimental Verification of a Substructure-Based Model to Describe Pedestrian–Bridge Interaction. Journal of Bridge Engineering, v 23(4) Article ID 04018013.

Gonçalves, M.S., Pavic, A., Pimentel, R.L. (2019). Vibration serviceability assessment of office floors for realistic walking and floor layout scenarios: Literature review. Advances in Structural Engineering, v 23/6, p 1238-1255.

Harvey, W. (1993). A reinforced plastic footbridge, Aberfeldy, UK, Structural Engineering International, v 4, p 229-232.

- Hawryszków P., Pimentel R., Silva R., Silva F. (2021). Vertical vibrations of footbridges due to group loading: effect of pedestrian structure interaction. Applied Sciences, MDPI 2021, v11(4), p 1355.
- Hawryszków, P., Pimentel, R., Silva, F. (2017). Vibration effects of loads due to groups crossing a lively footbridge. Procedia Engineering, v 199, p 2808–2813.
- Hivoss (2008). Feldmann, M., Heinemeyer, Ch., Lukic M., et al., Human-Induced Vibration of Steel Structures, Research Fund for Coal and Steel, European Commission.
- Hof, A. S. Vermerris, W. Gjaltema, Balance responses to lateral perturbations in human treadmill walking, J. Exp. Biol. 213 (2010) 2655–2664. https://doi.org/10.1242/jeb.042572.
- ISO 10137 (2007). Bases for design of structures: serviceability of buildings and walkways against vibrations. International Organization for Standardization (ISO), Geneva, Switzerland.
- ISO 5982 (1981). Vibration and Shock-Mechanical driving point impedance of the human body. International Organization for Standardization (ISO): Bases for Design of Structures.
- Jiménez Alonso, J. F., Sáez, A. (2014). A direct pedestrian structure interaction model to characterize the human induced vibrations on slender footbridges. Informes de la Construcción, v 66, n.1, article m007.
- Kerr, S.C., Bishop, N.W.M. Human induced loading on flexible staircases. Engineering Structures, vol 2, p. 37–45, 2001.
- Kim, S., S. Park, Leg stiffness increases with speed to modulate gait frequency and propulsion energy, J. Biomech. 44 (7) (2011) 1253–1258, http://dx.doi.org/10.1016/j.jbiomech.2011.02.072.
- Kim, S.H., Cho, K.I., Choi, M.S., Lim, J.Y. (2008). Development of human body model for the dynamic analysis of footbridges under pedestrian induced excitation. International Journal of Steel Structures, v 8(4), p 333–345.
- Li, T., Q. Li, T. Liu, An actuated dissipative spring-mass walking model: Predicting human-like ground reaction forces and the effects of model parameters, J. Biomech. 90 (2019) 58–64, http://dx.doi.org/10.1016/j.jbiomech.2019.04.028.
- Lin, B. K. Zhang, F. Fan, S. Shen, A damped bipedal inverted pendulum for human–structure interaction analysis, Applied Mathematics and Modelling 87 (2020) 606–624. https://doi.org/10.1016/j.apm.2020.06.027.
- Lin, B., Živanović, S., Zhang, Q., Fan, F. Implementation of damped bipedal inverted pendulum model of pedestrian into FE environment for prediction of vertical structural vibration. Structures, vol 48, p. 523–532, 2023.
- Lipfert, S. M. Gunther, D. Renjewski, S. Grimmer, A. Seyfarth, A model-experiment comparison of system dynamics for human walking and running, J. Theor. Biol. 292 (2012) 11–17. https://doi.org/10.1016/j.jtbi.2011.09.021.

Maca, J. Valasek, M. (2011). Interaction of human gait and footbridges. In Proceedings of the 8th International Conference on Structural Dynamics (EURODYN '11), Leuven, Belgium.

Macdonald, J. Lateral excitation of bridges by balancing pedestrians, in: Proceedings of the Royal Society A 465 (2009) 1055–1073.

MATLAB Platform® (2024). Math. Graphics. Programming. Available in: https://www.mathworks.com/products/matlab.html. Accessed in July 2024.

Matsumoto, Y., Nishioka, T., Shiojiri, H., Matsuzaki, K. (1978). Dynamic design of footbridges. IABSE Proceedings, v 17/78, p 1–15.

Matsumoto, Y., Sato, S., Nishioka, T., et al. (1972). A Study on Dynamic Design of Pedestrian Over-Bridges, Transactions of JSCE, v 4, p 50–51.

McRobie, A., G. Morgenthal, J. Lasenby, M. Ringer Section model tests on human–structure lock-in. Bridge Engineering, 156 (2003), pp. 71-79

Miyamori, Y. Obata, T. Hayashikawa, T. Sato, K. (2001). Study on identification of human walking model based on dynamic response characteristics of pedestrian bridges. The Eighth East Asia-Pacific conference on structural engineering and construction. In: Proceedings CD-ROM, Paper No. 1066.

Mohammed, A.S., Pavic, A., Racic, V. (2018). Improved model for human induced vibrations of high-frequency floors. Engineering Structures, v 168, p 950–966.

Muhammad, Z., Reynolds, P., Avci, O., Hussein, M. (2018). Review of Pedestrian Load Models for Vibration Serviceability Assessment of Floor Structures. Vibration, v 2, p 1–24.

Mulas, M.G. Lai, E. Lastrico, G. (2018). Coupled analysis of footbridge-pedestrian dynamic interaction. Journal of Engineering Structures, v 176, p 127–142.

NBR 6118 (2023). Design of concrete structures: Procedure. Brazilian Association of Technical Standards - ABNT.

NBR 7188 (2024). Road and pedestrian live load on bridges, viaducts, footbridges, and other structures. Brazilian Association of Technical Standards - ABNT.

NBR 8800 (2024). Design of steel and composite structures for buildings. Brazilian Association of Technical Standards - ABNT.

O'Sullivan, D., Caprani, C.C., Keogh, J. (2012). The response of a footbridge to pedestrians carrying additional mass. BCRI (Bridge and Concrete Research Ireland) Conference, Dublin.

Ohlsson, S. (1982). Floor vibrations and human discomfort [Ph.D. thesis], Chalmers University of Technology, Gothenburg, Sweden.

OptiTrack, OptiTrack Documentation, USA, 2022. Available online: https://docs.optitrack.com/markersets/full-body/conventional-39.

Pavic, A. Reynolds, P. (2002a). Vibration serviceability of long-span concrete building floors: Part 1—Review of background information. Shock and Vibration, v 34, p 191–211.

Pedersen, L. C. Frier, Sensitivity of footbridge vibrations to stochastic walking parameters, J. Sound Vib. 29 (2010) 2683–2701. https://doi.org/10.1016/j.jsv.2009.12.022.

Pernica, G. Dynamic load factors for pedestrian movements and rhythmic exercises. Canadian Acoustics, vol 18(2) pp. 3–18, 1990.

Pfeil, M. N. Costa, R. Pimentel, R. Vasconcelos, Analytic-numerical model for walking person-footbridge structure interaction, in: Proceedings of the 9th International Conference on Structural Dynamics (EURODYN 2014), Porto, Portugal, 2014, pp. 1079–1086.

Pfeil, M.S., Varela, W.D., Costa, N.P.A. Experimental calibration of a one degree of freedom biodynamic model to simulate human walking-structure interaction. Engineering Structures, vol 262, 114330, 2022.

Pimentel R.L., Waldron, P. (1996). Validation of the numerical analysis of a pedestrian bridge for vibration serviceability applications. In Proceedings of the International Conference on Identification in Engineering Systems, p 648–657, Swansea, UK.

Pimentel, R. Vibration performance of pedestrian bridges due to human-induced loads, Ph.D. thesis, University of Sheffield, Sheffield, UK, 1997.

Pirker, W., Katzenschlager, R. Gait disorders in adults and the elderly, Wiener klinische Wochenschrift, v. 129, pp. 81 - 95, 2017.

Pospíšil, S. Hračov, S. Urushadze, S. Jermoljev, D. (2013). Analysis and Mitigation of vibration of Steel Footbridge with Excessive Amplitudes. Topics in Dynamics of Bridges, v 3, p 27-35.

Pretlove, A.J., Rainer, J.H. (1995). Human response to vibrations, in: Vibration Problems in Structures: Practical Guidelines, Birkha" user, Basel, Appendix I.

Qin, J.W. Law, S.S. Yang, Q.S. Yang, N. (2013). Pedestrian-bridge dynamic interaction, including human participation. Journal of Sound and Vibration, v 332(4), p 1107–1124.

Qin, J.W. Law, S.S. Yang, Q.S., Yang, N. (2014). Finite element analysis of pedestrian-bridge dynamic interaction. Journal of Applied Mechanics, v 81(4), p 1-14.

Qualisys, Qualisys Track Manager, Version 2021, Qualisys AB, Gothenburg, Sweden, 2021.

Racic V. Brownjohn, J.M.W. (2011). Stochastic model of near periodic vertical loads due to humans walking. Advanced Engineering Informatics, v 25(2), p 259–275.

Racic, V., Pavic, A., Brownjohn, J.M.W. (2009). Experimental identification and analytical modelling of human walking forces: Literature review. Journal of Sound and Vibration, v 326, p 1–49.

Rainer, J.H., Pernica, G., Allen, D.E. (1988). Dynamic Loading and Response of Footbridges. Canadian Journal of Civil Engineering, v 15(1), p 66–71.

- Ruiz, D. C. Magluta, N. Roitman, Analysis of vertical loads induced by pedestrians on footbridges through biodynamic models, in: Proceedings of the XXXVIII Iberian Latin-American Congress on Computational Methods in Engineering, Florianópolis, Brazil, 2017.
- Ruiz, D., Magluta, C., Roitman, N. (2021). Modeling Human-Induced Loads Through a Calibrated Bipedal Walking Model. Structural Engineering International. https://doi.org/10.1080/10168664.2021.1982661.
- Ruiz, D., Magluta, C., Roitman, N. (2023). Experimentally estimated bipedal model parameters to simulate human induced vibrations on footbridges. Proceedings of the XLIV Ibero-Latin-American Congress on Computational Methods in Engineering, ABMEC, Porto, Portugal, November 13-16, 2023.
- Ruiz, D., Magluta, C., Roitman, N. Experimental verification of biomechanical model of bipedal walking to simulate vertical loads induced by humans. Mech. Syst. Signal Process, vol 167, ID 108513, 2022.
- Ruiz, D.V. (2021). Verificação experimental de modelo de caminhada bípede para a simulação de cargas verticais induzidas por Humanos [PhD thesis]. Coppe UFRJ. Rio de Janeiro.
- Sachse, R. Pavic, A. Reynolds, P. (2003). Human-structure dynamic interaction in civil engineering dynamics: a literature review. Shock and Vibration, v 35(1), p 3–18.
- Sahnaci, C., Kasperski, M. (2005). A refined model for loads induced by walking. In 9th International Conference on Structural Safety and Reability ICOSSAR, Itália.
- Salyards, K.A., Hua, Y. (2015). Assessment of dynamic properties of a crowd model for human–structure interaction modelling. Engineering Structures, v 89, p 103–110.
- SCI P354 (2009). Smith, A.L., Hicks S.J., Devine, P.J. Design of Floors for Vibration: (2nd Edition). Steel Construction Institute (SCI): Berkshire, UK.
- Sétra (2006). Footbridges: assessment of vibrational behaviour of footbridges under pedestrian loading, Technical Guide 0611, Technical Department for Transport, Roads and Bridges Engineering, and Road Safety/French Association of Civil Engineering SETRA/AFGC, Paris, France.
- Shahabpoor, E. A. Pavic, Estimation of tri-axial walking ground reaction forces of left and right foot from total forces in real-life environments, Sensors (Basel) 18 (6) (2018) 1966.
- Shahabpoor, E. A. Pavic, J. Brownjohn, S. Billings, L. Guo, M. Bocian, Real-life measurement of tri-axial walking ground reaction forces using optimal network of wearable inertial measurement units, IEEE Trans. Neural Syst. Rehabil. Eng. 26 (2018) 1243–1253. https://doi.org/10.1109/TNSRE.2018.2830976.
- Shahabpoor, E., Pavic, A., Racic, V. (2015). Identification of mass spring damper model of walking humans. In Proceedings of the Structures Congress, p 912–923, Portland, Ore, USA.

- Shahabpoor, E., Pavic, A., Racic, V. (2016a). Interaction between walking Humans and Structures in Vertical Direction: A Literature Review. Shock and Vibration, Article ID 3430285.
- Shahabpoor, E., Pavic, A., Racic, V. (2016b). Identification of mass–spring–damper model of walking humans. Structures, v 5, p 233–246.
- Shahabpoor, E., Pavic, A., Racic, V. (2017). Structural vibration serviceability: New design framework featuring human-structure interaction. Engineering Structures, v 136, p 295–311.
- Silva F.T., Pimentel R.L. Biodynamic walking model for vibration serviceability of footbridges in vertical direction. In Proceeding of the 8th International Conference on Structural Dynamics (EURODYN '11), pp. 1090–1096, Leuven, Belgium, 2011.
- Silva, F. T. (2011). Footbridge vibrations in vertical direction considering walking biodynamic models [Ph.D. thesis]. Postgraduate Programme in Mechanical Engineering. Federal University of Paraiba, João Pessoa, Paraíba, Brazil.
- Silva, F.T., Brito, H.M.B.F., Pimentel, R.L. (2013). Modelling of crowd load in vertical direction using biodynamic model for pedestrians crossing footbridges. Canadian Journal of Civil Engineering. v 40, p 1196–1204.
- Silva, R. R. Pimentel, A. Pavic, P. Hawryszków, Influence of the ground reaction force prediction on the human-structure interaction phenomenon: An application of a bipedal model, in: Proceedings of IMAC XLII, Orlando, USA, 2024. https://doi.org/10.1007/978-3-031-68889-8 6.
- Silva, R. Pimentel, A. Pavic, Performance of biodynamic models to represent the action of a pedestrian in the vertical direction, in: Proceedings of the 11th International Conference on Structural Dynamics (EURODYN 2020), Athens, Greece, 2020, pp. 1824–1834.
- Smith, A. S. Hicks, P. Devine, Design of Floors for Vibrations: A New Approach, SCI Publication P354, Ascot, 2007.
- Smith, M. P. Leveridge, G. Massey, J. Tyrrell, M. Hilton, G. Williams, Investigating the Effect of Motion Capture Suits on the Test–Retest Reliability of Gait Parameters, Applied Sciences 14 (2024) 8570. https://doi.org/10.3390/app14188570.
- Strogatz, S.H, Abrams D.M, McRobie A, Eckhardt B, Ott E. Theoretical mechanics: crowd synchrony on the Millennium Bridge. Nature. 2005 Nov 3;438(7064):43-4. doi: 10.1038/43843a. PMID: 16267545.
- Thomson, W.T. (1973). Theory of Vibration with Applications. Ed. Prentice Hall Inc., Englewood Cliffs, New Jersey, USA.
- Toso, M.A., Gomes, H.M., Silva, F.T., Pimentel, R.L. (2016). Experimentally fitted biodynamic models for pedestrian-structure interaction in walking situations. Mechanical Systems and Signal Processing, v 72–73, p 590–606.

Toso, M.A., Gomes. H.M. (2018). A coupled biodynamic model for crowd-footbridge interaction. Engineering Structures, v 177, p 47-60.

UK NA to BS (2008). British Standards Institution (BSI), UK national annex to Eurocode 1: Actions on structures. Part 2: Traffic loads on bridges, NA to BS EN 1991-2:2003, London.

Van Nimmen, K., Maes, K., Živanović, S., Lombaert, G., De Roeck, G., Van den Broeck P. (2015). Identification and modelling of vertical human-structure interaction. In Proceedings of the 33rd Conference and Exposition on Balancing Simulation and Testing (IMAC '15), p 319–330.

Venuti, F., Racic, V., Corbetta, A. (2016). Modelling framework for dynamic interaction between multiple pedestrians and vertical vibrations of footbridge. Journal of Sound and Vibration, v 379, p 245–263.

VSimulators. (n.d.). University of Exeter. Available in https://www.exeter.ac.uk/research/facilities/vsimulators/. Access in April 2025.

Wheeler, J.E. Prediction and control of pedestrian induced vibration in footbridges, ASCE Journal of the Structural Division, vol 108 (ST9), p. 2045–2065, 1982.

Whittington B.R., Thelen, D.G. (2009). A simple mass-spring model with roller feet can induce the ground reactions observed in human walking. Journal of Biomechanical Engineering, v 131(1), Article ID 011013.

Wikipedia (2025). Passerelle Léopold-Sédar-Senghor. Available in Passerelle Léopold-Sédar-Senghor - Wikipedia. Access in April 2025.

Winter, D. H. Sidwall, D. Hobson, Measurement and reduction of noise in kinematics of locomotion, J. Biomech. 7 (1974) 157–159. https://doi.org/10.1016/0021-9290(74)90056-6.

Yoneda, M. A simplified method to evaluate pedestrian-induced maximum response of cable-supported pedestrian bridges. In Proceedings of the International Conference on the Design and Dynamic Behaviour of Footbridges, Paris, France, November 20–22, 2002.

Young, P. Improved Floor Vibration Prediction Methodologies, Vibration Seminar by Arup, London, October, 2001.

Zhang, M. Georgakis, C.T., Qu, W., Chen, J. SMD model parameters of pedestrians for vertical human-structure interaction. In Proceedings of the 33rd Conference and Exposition on Balancing Simulation and Testing (IMAC '15), p 311–317.

Zhang, M., Geogarkis, C., Chen. J. (2016). Biomechanically Excited SMD Model of a Walking Pedestrian. Journal of Bridge Engineering, v 21(8) Article ID C4016003.

Zhou, X., Li, J., Liu, J. (2015). Vibration of prestressed cable RC truss floor system due to human activity. Journal of Structural Engineering, v 142, p 1–10.

Živanović, A. Pavic. S., (2011). Quantification of dynamic excitation potential of pedestrian population crossing footbridges, Shock and Vibration, Vol. 18, No 4, pp. 563-577, doi:10.3233/SAV-2010-0562

Živanović, S. (2015). Modelling human actions on lightweight structures: experimental and numerical developments. In MATECWeb of Conferences, v 24, Article ID 01005.

Zivanovic, S. Benchmark footbridge for vibration serviceability assessment under the vertical component of pedestrian load, J. Struct. Eng. 138 (2012) 1193–1202.

Živanović, S. M. Diaz, A. Pavic, Influence of walking and standing crowds on structural dynamic properties, in: Proceedings of IMAC-XXVII, Orlando, USA, 2009.

Živanović, S. Modelling human actions on lightweight structures: Experimental and numerical developments, MATEC Web of Conferences 24 (2015) 01005. https://doi.org/10.1051/matecconf/20152401005.

Živanović, S., Lin, B., Vu Dang, H., Zhang, S., Ćosić, M., Caprani, C., Zhang, Q. Evaluation of Inverted-Pendulum-with-Rigid-Legs Walking Locomotion Models for Civil Engineering Applications. Buildings, vol 12, pp.1216, 2022.

Živanović, S., M. Diaz, A. Pavic, Influence of walking and standing crowds on structural dynamic properties, in: Proceedings of IMAC-XXVII, Orlando, USA, 2009.

Živanović, S., Pavic, A., Reynolds, P. (2005a). Vibration serviceability of footbridges under human-induced excitation: a literature review, Journal of Sound and Vibration, v 279 (12), p 1–74.

Živanović, S., Pavic, A., Reynolds, P. (2005b). Human–structure dynamic interaction in footbridges. Bridge Engineering, v 158 (4), p 165–177.

APPENDIX A

Table A.1 – Gait and DBIP model parameters extracted from experimental measurements and from simulations before calibration for TS1

Walking	Cross	Exper	imental						BM_1						BM_2							
Scenario		f_s	ν	DLF_1	L_p	k_{leg}	E_0	θ_0	٤	θ_0	$\dot{z}(0)$	DLF_1		Max	ξ -	E_0	θ_0	$\dot{x}(0)$	$\dot{z}(0)$	DLF_1		Max
		(Hz)	(m/s)	Value	(m)	(kN/m)	(J)	(°)	(%)	(°)	(m/s)	value	(%)	Force(N)	(%)	(J)	(°)	(m/s)	(m/s)	value	(%)	Force(N)
Slow	1	1.73	1.13	0.22	1.16	19.12	864.77	65.28	3	70.07	-0.21	0.31	38%	766.02	3	842.00	70.04	1.28	-0.15	0.32	41%	841.89
	2	1.59	1.13	0.20	1.17	16.50	854.99	65.71	3	68.54	-0.20	0.31	57%	779.10	3	845.50	68.56	1.32	-0.13	0.32	62%	876.68
	3	1.64	1.08	0.19	1.16	19.99	848.85	66.81	3	70.24	-0.16	0.28	45%	806.87	4	837.10	70.52	1.28	-0.07	0.28	50%	949.65
	4	1.61	1.13	0.19	1.16	18.38	848.78	66.50	3	69.11	-0.17	0.31	68%	829.80	3	843.20	69.38	1.35	-0.07	0.32	71%	967.41
	5	1.58	1.07	0.17	1.16	18.60	846.96	66.51	3	69.80	-0.17	0.26	57%	795.68	5	838.30	70.17	1.27	-0.08	0.27	62%	954.09
	6	1.64	1.14	0.19	1.17	17.99	853.79	66.51	3	69.24	-0.19	0.32	63%	813.76	8	845.00	69.59	1.34	-0.14	0.33	69%	967.63
	7	1.58	1.08	0.16	1.16	19.39	849.11	66.59	3	69.69	-0.13	0.28	69%	852.30	8	838.50	70.37	1.31	-0.12	0.29	75%	1056.59
	8	1.61	1.08	0.15	1.16	18.66	840.50	67.48	3	69.85	-0.18	0.27	73%	777.56	8	838.30	70.22	1.26	-0.13	0.28	79%	928.90
Normal	1	1.83	1.47	0.33	1.17	16.22	881.17	64.16	5	65.65	-0.43	0.73	123%	994.22	13	880.00	66.13	1.68	-0.42	0.73	124%	1212.96
	2	1.75	1.33	0.28	1.16	17.20	865.81	65.77	5	67.14	-0.30	0.52	87%	909.81	13	860.00	67.53	1.54	-0.28	0.52	88%	1101.13
	3	1.75	1.33	0.27	1.16	17.11	868.34	64.65	5	66.97	-0.32	0.53	97%	900.64	13	860.00	67.34	1.54	-0.31	0.53	97%	1084.37
	4	1.79	1.38	0.29	1.17	15.87	881.23	64.36	3	66.46	-0.37	0.60	107%	897.99	13	870.00	66.92	1.58	-0.36	0.60	109%	1109.42
	5	1.83	1.34	0.30	1.16	17.41	878.51	64.63	3	67.70	-0.32	0.53	76%	870.35	13	860.50	68.08	1.51	-0.31	0.54	78%	1064.64
	6	1.87	1.37	0.30	1.16	17.26	874.15	65.07	3	67.59	-0.34	0.58	97%	891.61	13	865.20	68.02	1.55	-0.33	0.59	98%	1090.10
	7	1.84	1.30	0.25	1.16	18.49	865.79	65.98	3	68.58	-0.27	0.48	89%	857.19	13	853.50	68.95	1.47	-0.26	0.49	92%	1048.42
	8	1.83	1.33	0.27	1.16	18.02	865.24	65.92	3	67.86	-0.30	0.53	92%	878.32	13	858.50	68.30	1.52	-0.29	0.53	94%	1077.49
Free	1	1.80	1.37	0.31	1.17	16.50	874.82	64.19	5	66.88	-0.37	0.58	88%	908.16	8	866.50	66.92	1.55	-0.32	0.59	91%	1020.90
	2	1.72	1.28	0.25	1.16	17.15	868.84	64.72	5	67.55	-0.28	0.47	83%	876.47	8	855.50	67.76	1.48	-0.23	0.47	84%	997.25
	3	1.74	1.28	0.29	1.16	17.32	873.75	64.41	3	67.68	-0.27	0.46	59%	854.18	8	855.20	67.89	1.48	-0.23	0.47	62%	991.90
	4	1.71	1.26	0.26	1.17	16.84	868.40	65.22	3	67.76	-0.27	0.44	71%	839.82	8	854.10	68.00	1.45	-0.22	0.44	72%	980.41
	5	1.71	1.24	0.24	1.16	18.24	860.20	65.47	3	68.21	-0.22	0.42	76%	860.85	8	849.50	68.56	1.44	-0.18	0.42	79%	1014.51
	6	1.73	1.22	0.24	1.16	17.99	860.91	66.30	3	68.70	-0.24	0.39	60%	823.65	8	848.00	68.94	1.40	-0.19	0.40	64%	955.25
	7	1.72	1.26	0.24	1.17	16.78	867.13	65.31	5	67.90	-0.28	0.43	79%	850.60	8	854.10	68.06	1.45	-0.23	0.44	82%	963.68
	8	1.71	1.25	0.26	1.16	17.56	861.18	65.31	3	68.09	-0.24	0.42	65%	853.13	8	852.00	68.37	1.45	-0.19	0.43	69%	1000.70
Fast	1	2.04	1.64	0.42	1.15	24.43	883.62	66.98	13	67.00	-0.36	0.88	110%	1395.15	13	897.00	67.39	1.93	-0.33	0.87	108%	1530.77
	2	2.03	1.60	0.36	1.16	21.97	890.72	66.47	13	67.36	-0.38	0.84	137%	1307.73	13	895.50	67.60	1.85	-0.35	0.83	134%	1426.35
	3	2.02	1.60	0.38	1.16	23.20	903.83	65.36	3	66.80	-0.27	0.85	121%	1126.59	13	894.00	67.50	1.87	-0.34	0.84	118%	1451.72
	4	2.09	1.67	0.39	1.16	22.97	869.69	68.14	3	66.07	-0.43	1.03	161%	1157.62	13	905.00	66.87	1.92	-0.47	1.00	154%	1477.19
	5	2.13	1.72	0.38	1.16	21.76	903.82	67.61	3	65.88	-0.46	1.09	189%	1186.88	13	915.00	66.67	1.95	-0.48	1.09	188%	1535.60
	6	1.98	1.60	0.36	1.16	22.87	905.63	65.10	13	66.98	-0.35	0.83	131%	1359.90	13	894.70	67.31	1.89	-0.32	0.82	128%	1502.62
	7	2.11	1.64	0.35	1.16	22.68	896.13	66.66	13	67.38	-0.43	0.93	169%	1338.72	13	901.00	67.54	1.88	-0.39	0.93	168%	1448.77
	8	2.01	1.50	0.35	1.16	20.94	897.81	64.89	13	68.08	-0.39	0.74	113%	1159.98	13	884.50	68.19	1.70	-0.35	0.74	113%	1252.67
	9	2.09	1.56	0.37	1.16	21.42	878.45	67.16	13	67.98	-0.45	0.86	132%	1226.21	13	892.50	68.02	1.75	-0.40	0.85	130%	1312.41
	10	2.05	1.58	0.38	1.16	22.04	895.64	65.82	13	67.38	-0.45	0.87	128%	1246.72	13	893.00	67.50	1.79	-0.42	0.87	127%	1344.10

Table A. 2 - Gait and DBIP model parameters extracted from experimental measurements and from simulations before calibration for TS2

Walking	Cross	Experi	imental						BM ₁						BM_2							
Scenario		f_s	ν	DLF_1	L_p	k_{leg}	E_0	θ_0	ξ	θ_0	$\dot{z}(0)$	DLF_1		Max	ξ	E_0	θ_0	$\dot{x}(0)$	$\dot{z}(0)$	DLF_1		Max
		(Hz)	(m/s)	value	(m)	(kN/m)	(J)	(°)	(%)	(°)	(m/s)	value	(%)	Force(N)	(%)	(J)	(°)	(m/s)	(m/s)	value	(%)	Force(N)
Slow	1	1.61	0.99	0.20	1.20	17.11	925.51	67.32	13	71.13	-0.20	0.17	-11%	700.23	13	909.00	71.06	1.08	-0.18	0.18	-9%	758.80
	2	1.62	1.06	0.20	1.19	17.87	920.81	67.39	8	70.55	-0.21	0.23	19%	773.37	13	912.50	70.67	1.20	-0.18	0.24	24%	887.74
	3	1.63	1.05	0.24	1.19	17.70	929.20	66.61	13	70.64	-0.22	0.23	-5%	771.36	13	912.00	70.63	1.17	-0.18	0.23	-2%	850.45
	4	1.64	1.03	0.21	1.19	17.81	919.11	67.69	13	71.01	-0.21	0.21	-1%	750.79	8	910.50	70.96	1.15	-0.17	0.22	1%	802.59
	5	1.61	0.99	0.19	1.19	17.93	926.32	67.41	13	71.30	-0.20	0.19	-1%	727.83	8	907.50	71.23	1.10	-0.16	0.19	0%	782.97
	6	1.62	1.07	0.21	1.20	16.90	929.66	66.82	3	70.22	-0.22	0.23	14%	748.47	8	916.30	70.23	1.20	-0.17	0.25	19%	849.85
Normal	1	1.92	1.11	0.31	1.18	22.17	910.65	69.37	8	72.35	-0.22	0.27	-15%	766.42	3	907.00	72.22	1.19	-0.19	0.27	-14%	784.08
	2	1.93	1.14	0.33	1.18	20.94	912.62	68.82	3	72.08	-0.22	0.30	-9%	774.93	13	912.80	72.19	1.24	-0.20	0.31	-6%	888.30
	3	1.89	1.08	0.28	1.17	22.97	899.26	70.33	13	72.66	-0.20	0.25	-11%	800.03	3	904.00	72.51	1.18	-0.16	0.25	-11%	807.37
	4	1.81	1.12	0.29	1.18	20.39	923.69	67.58	14	71.30	-0.23	0.29	-1%	823.22	3	910.00	71.09	1.23	-0.19	0.29	-1%	817.53
	5	1.87	1.12	0.28	1.18	22.32	913.41	69.10	3	71.88	-0.20	0.28	1%	781.36	3	908.00	71.85	1.23	-0.17	0.29	4%	839.11
	6	1.89	1.14	0.28	1.18	19.32	925.71	67.41	3	71.50	-0.24	0.29	5%	753.43	10	914.50	71.48	1.23	-0.22	0.30	9%	834.24
Free	1	1.71	1.05	0.22	1.18	20.50	917.23	68.50	5	71.65	-0.19	0.23	5%	763.56	3	907.00	71.61	1.17	-0.14	0.23	8%	834.71
	2	1.72	1.15	0.26	1.19	18.61	924.18	67.68	4	69.81	-0.25	0.31	19%	789.97	8	918.00	69.82	1.28	-0.21	0.32	21%	878.45
	3	1.79	1.14	0.28	1.20	17.27	924.46	66.50	4	70.30	-0.26	0.30	9%	753.50	8	921.00	70.27	1.24	-0.24	0.31	11%	815.74
	4	1.71	1.10	0.24	1.19	18.83	919.66	67.71	3	70.74	-0.21	0.26	10%	770.59	8	914.40	70.80	1.23	-0.17	0.27	13%	870.18
	5	1.75	1.08	0.23	1.18	20.38	914.90	68.66	3	71.56	-0.20	0.25	6%	762.58	8	909.80	71.60	1.20	-0.16	0.26	9%	859.87
	6	1.74	1.16	0.25	1.19	19.28	922.90	67.67	3	70.16	-0.22	0.32	31%	819.02	10	919.00	70.33	1.31	-0.19	0.33	34%	950.87
	7	1.71	1.09	0.23	1.19	19.21	921.90	68.13	3	70.87	-0.21	0.26	11%	766.42	10	912.80	70.93	1.22	-0.18	0.27	15%	878.34
	8	1.74	1.11	0.24	1.19	17.92	923.92	67.27	3	70.69	-0.23	0.27	10%	750.05	10	917.20	70.68	1.22	-0.21	0.28	14%	841.62
Fast	1	2.13	1.31	0.36	1.18	23.76	942.80	69.74	4	71.43	-0.28	0.49	35%	884.03	13	933.00	71.60	1.42	-0.28	0.49	37%	1028.08
	2	2.17	1.40	0.37	1.18	23.93	941.34	69.12	13	71.09	-0.32	0.59	61%	1073.92	13	942.90	71.11	1.53	-0.30	0.59	62%	1138.87
	3	2.14	1.35	0.39	1.18	24.10	950.37	69.64	13	71.44	-0.30	0.53	36%	1027.04	13	936.80	71.48	1.47	-0.28	0.53	36%	1088.55
	4	2.14	1.34	0.39	1.18	25.63	933.66	70.04	13	71.62	-0.28	0.51	32%	1024.45	13	933.00	71.61	1.46	-0.26	0.51	32%	1087.71
	5	2.14	1.33	0.39	1.18	26.07	944.00	69.06	3	71.41	-0.26	0.50	28%	910.64	13	931.70	71.65	1.46	-0.26	0.51	30%	1083.37
	6	2.11	1.28	0.39	1.18	25.33	950.64	71.80	3	71.74	-0.25	0.44	15%	864.71	13	927.20	71.93	1.39	-0.25	0.45	17%	1015.44
	7	2.10	1.27	0.35	1.18	25.81	941.77	69.70	13	72.23	-0.24	0.43	22%	967.68	13	925.50	72.27	1.39	-0.22	0.43	22%	1031.96
	8	2.13	1.35	0.38	1.18	24.02	935.89	70.05	13	71.24	-0.32	0.54	40%	1014.41	13	936.40	71.22	1.47	-0.30	0.54	41%	1070.84

Table A. 3 - Gait and DBIP model parameters extracted from experimental measurements and from simulations before calibration for TS3

Walking	Cross	Experi	mental						BM_1						BM ₂							
Scenario		f_s	v	DLF_1	L_p	k_{leg}	E_0	θ_0	ξ	θ_0	$\dot{z}(0)$	DLF_1		Max	ξ -	E_0	θ_0	$\dot{x}(0)$	$\dot{z}(0)$	DLF_1		Max
		(Hz)	(m/s)	value	(m)	(kN/m)	(J)	(°)	(%)	(°)	(m/s)	value	(%)	Force(N)	(%)	(J)	(°)	(m/s)	(m/s)	value	(%)	Force(N)
Slow	1	1.58	0.98	0.17	1.14	19.70	792.44	67.90	3	71.07	-0.14	0.21	26%	755.11	8	790.80	71.77	1.18	-0.12	0.22	32%	954.79
	2	1.63	1.02	0.17	1.14	19.08	794.39	68.17	5	70.90	-0.18	0.23	32%	727.61	8	793.50	71.14	1.18	-0.12	0.24	38%	857.88
	3	1.57	1.03	0.17	1.14	19.46	792.10	67.98	3	70.28	-0.12	0.24	43%	805.04	8	794.30	71.04	1.25	-0.12	0.26	49%	1012.34
	4	1.65	1.11	0.19	1.14	18.97	799.91	67.27	3	69.63	-0.16	0.30	58%	796.79	8	800.50	70.07	1.32	-0.10	0.32	68%	1000.44
	5	1.60	1.04	0.17	1.14	20.00	792.18	67.64	3	70.34	-0.13	0.26	52%	808.84	8	794.30	71.09	1.26	-0.12	0.26	56%	1011.86
	6	1.61	1.05	0.17	1.14	19.71	792.85	68.46	3	70.35	-0.13	0.26	51%	807.99	8	795.50	71.00	1.26	-0.11	0.27	57%	998.97
Normal	1	1.84	1.23	0.22	1.14	19.02	803.34	67.70	10	69.62	-0.25	0.42	92%	865.97	13	806.00	69.78	1.40	-0.22	0.42	92%	976.20
	2	1.82	1.26	0.23	1.14	16.90	806.29	67.24	10	68.00	-0.38	0.49	113%	826.53	13	809.50	68.03	1.39	-0.36	0.50	116%	908.13
	3*	-	-	-	-	-	-	-	-	-	-	-	-	_	-	-	-	_	-	-	-	-
	4	1.85	1.19	0.20	1.13	22.31	795.03	69.35	3	70.39	-0.16	0.37	90%	839.39	13	798.00	70.87	1.37	-0.19	0.38	94%	1029.34
	5	1.89	1.19	0.19	1.14	17.12	794.81	69.11	3	70.14	-0.26	0.37	101%	734.31	13	806.00	70.31	1.31	-0.25	0.39	108%	858.29
	6	1.87	1.13	0.20	1.13	21.78	793.25	69.34	3	71.28	-0.19	0.31	54%	754.51	13	793.50	71.57	1.27	-0.18	0.32	59%	897.25
	7	1.82	1.13	0.19	1.13	20.98	795.54	69.13	3	70.90	-0.19	0.31	62%	760.96	13	794.50	71.23	1.28	-0.18	0.32	65%	912.33
	8	1.91	1.07	0.20	1.13	20.71	792.75	69.22	3	72.31	-0.19	0.26	28%	687.11	13	791.60	72.37	1.17	-0.18	0.27	34%	788.39
Free	1	1.70	1.07	0.19	1.14	19.21	794.76	67.63	10	70.62	-0.20	0.27	44%	762.09	3	792.20	70.51	1.22	-0.12	0.27	46%	816.01
	2	1.74	1.16	0.19	1.15	16.36	795.77	67.75	10	69.26	-0.26	0.35	86%	779.31	3	804.50	69.06	1.30	-0.20	0.35	86%	796.83
	3	1.71	1.13	0.19	1.14	17.42	789.46	68.15	3	69.55	-0.21	0.32	62%	748.03	3	800.50	69.52	1.29	-0.15	0.32	67%	826.79
	4	1.73	1.16	0.19	1.14	18.50	797.63	67.42	3	69.50	-0.20	0.34	78%	787.09	3	800.70	69.55	1.33	-0.12	0.35	81%	880.65
	5	1.69	1.11	0.19	1.14	18.76	797.50	67.45	3	69.79	-0.18	0.30	57%	773.24	3	796.60	69.90	1.29	-0.10	0.31	61%	878.42
	6	1.63	1.14	0.17	1.14	18.79	792.75	67.44	3	68.83	-0.17	0.33	89%	817.37	3	798.00	69.06	1.36	-0.07	0.34	95%	948.77
	7	1.68	1.10	0.18	1.14	18.86	792.08	67.82	3	69.83	-0.19	0.29	64%	765.98	3	795.50	69.90	1.28	-0.11	0.31	70%	862.26
	8	1.65	1.10	0.17	1.14	18.87	789.62	68.05	3	69.70	-0.16	0.30	71%	790.49	3	795.50	69.90	1.30	-0.07	0.30	76%	918.37
Fast	1	2.16	1.34	0.28	1.12	30.37	809.49	71.15	13	71.84	-0.20	0.52	82%	1109.47	13	810.50	72.08	1.52	-0.20	0.52	82%	1218.84
	2	2.18	1.26	0.28	1.12	28.12	798.29	72.43	13	72.85	-0.20	0.44	54%	970.36	13	805.50	72.98	1.39	-0.18	0.44	54%	1053.45
	3	2.21	1.30	0.26	1.12	30.93	797.62	71.32	3	72.11	-0.18	0.48	80%	878.13	13	805.50	72.44	1.44	-0.20	0.49	84%	1060.25
	4	2.22	1.37	0.26	1.12	31.96	802.67	71.73	3	71.57	-0.13	0.56	113%	999.00	13	812.00	72.13	1.55	-0.20	0.55	111%	1229.66
	5	2.20	1.39	0.28	1.12	31.36	797.55	70.65	3	71.34	-0.12	0.57	105%	1023.83	13	814.50	71.87	1.58	-0.21	0.57	105%	1267.68
	6	2.22	1.26	0.24	1.12	32.84	801.47	71.12	3	73.04	-0.10	0.44	82%	946.78	13	801.00	73.49	1.41	-0.17	0.44	81%	1144.73
	7	2.19	1.27	0.25	1.12	31.27	795.21	71.14	3	72.42	-0.14	0.45	85%	901.03	13	803.40	72.86	1.43	-0.18	0.46	87%	1093.54
	8	2.19	1.31	0.26	1.12	28.33	811.70	70.54	3	71.85	-0.17	0.50	90%	898.97	13	810.00	72.25	1.46	-0.20	0.50	89%	1091.47

^{*} No valid footfall forces detected to extract the models' parameters

Table A.4 – Calibrated DBIP models' parameters targeting step frequency f_s and DLF₁ pair for TS1

Walk	Cross	Target		Experi	nental	BM1					BM2						
Scenario		f_s	DLF_1	L_p	k_{leg}	v	ξ	$ heta_0$	ż(0)	Max. Force	v	ξ	$ heta_0$	$\dot{z}(0)$	$\dot{x}(0)$	E_0	Max Force
		(Hz)	value	(m)	(kN/m)	(m/s)	(%)	(°)	(m/s)	(N)	(m/s)	(%)	(°)	(m/s)	(m/s)	(J)	(N)
Slow	1	1.73	0.22	1.16	19.11	1.04	4.01	71.53	-0.20	699.31	1.02	6.63	71.75	-0.17	1.13	834.00	759.23
	2	1.59	0.20	1.17	17.25	1.00	13.60	70.79	-0.22	720.92	0.98	8.39	70.93	-0.17	1.11	834.45	775.48
	3	1.64	0.19	1.16	19.98	0.98	12.92	71.86	-0.21	724.58	0.97	9.83	72.05	-0.16	1.09	828.94	802.75
	4	1.61	0.19	1.16	18.37	0.98	8.77	71.36	-0.21	697.42	0.97	8.27	71.55	-0.16	1.09	831.48	768.93
	5	1.59	0.17	1.16	18.60	0.96	6.24	71.53	-0.20	678.41	0.94	10.65	71.78	-0.17	1.06	829.57	769.51
	6	1.64	0.19	1.17	17.98	0.99	4.63	71.36	-0.21	677.47	0.98	6.74	71.45	-0.17	1.10	833.34	747.41
	7	1.58	0.16	1.16	19.39	0.94	4.91	71.77	-0.19	672.55	0.92	6.33	72.16	-0.13	1.04	826.76	764.38
	8	1.61	0.15	1.16	18.66	0.93	12.65	72.10	-0.20	658.93	0.92	8.90	72.21	-0.16	1.02	828.13	720.24
Normal	1	1.83	0.33	1.17	16.22	1.16	12.90	70.22	-0.27	775.64	1.14	12.57	70.57	-0.26	1.24	846.50	808.66
	2	1.75	0.28	1.16	17.20	1.09	13.28	71.56	-0.37	770.16	1.09	9.82	70.62	-0.21	1.21	839.49	794.87
	3	1.75	0.27	1.16	17.11	1.10	9.46	70.67	-0.24	735.08	1.09	9.22	70.63	-0.20	1.20	839.05	778.90
	4	1.79	0.29	1.17	15.87	1.13	6.90	70.27	-0.25	720.33	1.11	5.60	70.42	-0.23	1.21	844.74	745.71
	5	1.83	0.30	1.16	17.41	1.13	13.50	70.89	-0.25	767.11	1.12	7.40	70.74	-0.22	1.23	841.50	779.62
	6	1.87	0.30	1.16	17.26	1.14	5.08	70.95	-0.25	718.62	1.13	5.17	70.85	-0.22	1.22	842.43	752.05
	7	1.84	0.25	1.16	18.49	1.08	8.83	71.59	-0.21	711.89	1.07	10.34	71.36	-0.21	1.21	834.53	758.14
	8	1.83	0.27	1.16	18.02	1.10	13.27	71.31	-0.23	743.19	1.09	11.92	71.39	-0.20	1.18	836.86	777.30
Free	1	1.79	0.31	1.17	16.50	1.14	13.67	70.41	-0.26	772.54	1.11	6.04	70.19	-0.23	1.24	844.92	778.06
	2	1.72	0.25	1.16	17.15	1.08	4.18	70.59	-0.22	706.12	1.07	10.19	70.27	-0.27	1.29	837.75	778.05
	3	1.73	0.29	1.16	17.32	1.13	13.80	68.65	-0.21	768.06	1.10	8.83	70.35	-0.21	1.23	840.37	813.60
	4	1.71	0.26	1.17	16.84	1.09	6.49	70.35	-0.23	721.88	1.08	5.62	70.32	-0.19	1.19	839.44	768.12
	5	1.71	0.24	1.16	18.24	1.06	7.99	70.88	-0.20	726.60	1.12	6.48	71.09	-0.17	1.16	833.53	774.53
	6	1.73	0.24	1.16	17.99	1.06	11.85	71.16	-0.22	731.57	1.05	11.60	71.21	-0.19	1.16	834.94	787.17
	7	1.72	0.24	1.17	16.78	1.07	6.56	70.70	-0.23	702.99	1.04	10.61	70.93	-0.19	1.15	837.62	757.31
	8	1.71	0.26	1.16	17.56	1.08	14.00	70.70	-0.24	762.57	1.07	7.81	70.73	-0.19	1.19	836.79	790.45
Fast	1	2.03	0.42	1.15	24.43	1.26	4.67	71.43	-0.22	858.80	1.25	6.60	71.60	-0.18	1.39	851.94	938.95
	2	2.03	0.36	1.16	21.97	1.20	6.33	72.00	-0.24	785.67	1.19	5.44	72.03	-0.21	1.29	850.38	818.17
	3	2.02	0.38	1.16	23.20	1.22	6.73	71.79	-0.23	824.29	1.20	9.78	72.08	-0.22	1.32	849.50	892.13
	4	2.11	0.39	1.16	22.97	1.23	4.68	72.16	-0.24	789.75	1.21	9.47	72.48	-0.23	1.31	851.20	858.58
	5	2.13	0.38	1.16	21.76	1.22	5.74	72.37	-0.26	773.25	1.20	12.26	72.68	-0.25	1.29	852.20	846.16
	6	1.98	0.36	1.16	22.87	1.20	6.83	71.80	-0.23	817.02	1.19	9.34	71.94	-0.20	1.31	848.46	890.33
	7	2.11	0.35	1.16	22.68	1.19	7.87	72.70	-0.24	777.53	1.17	13.51	72.86	-0.22	1.26	848.36	842.37
	8	2.01	0.35	1.16	20.94	1.19	10.98	71.77	-0.24	795.88	1.18	5.22	71.91	-0.22	1.28	851.10	798.47
	9	2.09	0.37	1.16	21.42	1.21	6.58	72.18	-0.25	773.24	1.20	10.30	72.31	-0.24	1.29	852.39	835.47
	10	2.05	0.38	1.16	22.04	1.22	5.63	71.94	-0.25	792.29	1.20	7.76	72.09	-0.23	1.31	851.91	843.29

Table A.5 – Calibrated DBIP models' parameters targeting step frequency f_s and DLF₁ pair for TS2

Walk	Cross	Target		Experi	mental	BM1					BM2						
Scenario		f_s	DLF_1	L_p	k_{leg}	v	ξ	$ heta_0$	ż(0)	Max. Force	ν	ξ	$ heta_0$	$\dot{z}(0)$	$\dot{x}(0)$	E_0	Max Force
		(Hz)	value	(m)	(kN/m)	(m/s)	(%)	(°)	(m/s)	(N)	(m/s)	(%)	(°)	(m/s)	(m/s)	(J)	(N)
Slow	1	1.61	0.20	1.20	17.11	1.02	8.70	70.83	-0.22	729.02	1.01	13.25	70.82	-0.17	1.13	911.49	806.79
	2	1.62	0.20	1.19	17.87	1.01	9.81	71.06	-0.20	733.79	1.00	13.34	71.24	-0.17	1.11	908.34	806.38
	3	1.63	0.24	1.19	17.70	1.06	8.68	70.41	-0.22	770.40	1.05	9.16	70.53	-0.17	1.18	912.60	836.44
	4	1.64	0.21	1.19	17.81	1.03	8.74	70.97	-0.22	741.80	1.03	10.73	70.27	-0.43	1.36	910.50	808.10
	5	1.62	0.19	1.19	17.93	1.00	9.56	71.30	-0.22	722.39	0.99	8.00	71.26	-0.16	1.10	907.41	782.11
	6	1.61	0.21	1.20	16.90	1.03	8.48	70.68	-0.23	735.45	1.03	13.77	70.55	-0.16	1.14	912.92	816.69
Normal	1	1.92	0.31	1.18	22.17	1.14	9.04	72.08	-0.23	815.95	1.14	12.15	72.12	-0.21	1.24	910.20	891.55
	2	1.93	0.33	1.18	20.94	1.16	9.44	71.71	-0.24	817.72	1.16	13.60	71.71	-0.22	1.26	914.24	895.11
	3	1.88	0.28	1.17	22.97	1.11	9.32	72.30	-0.21	812.76	1.10	8.73	72.26	-0.15	1.21	905.57	862.27
	4	1.81	0.29	1.18	20.39	1.12	9.95	71.35	-0.23	818.91	1.11	10.11	71.41	-0.20	1.23	910.41	874.65
	5	1.87	0.28	1.18	22.32	1.10	9.60	72.18	-0.22	804.87	1.10	13.65	72.26	-0.19	1.21	906.71	884.73
Free	6	1.89	0.28	1.18	19.32	1.13	8.33	71.71	-0.23	768.34	1.12	5.91	71.65	-0.21	1.21	912.84	793.46
	1	1.71	0.22	1.18	20.50	1.04	8.74	71.80	-0.21	766.36	1.04	4.62	71.67	-0.14	1.15	905.93	820.14
	2	1.72	0.26	1.19	18.61	1.10	8.36	70.84	-0.22	779.65	1.09	13.86	70.82	-0.18	1.21	914.10	872.45
	3	1.79	0.28	1.20	17.27	1.13	8.96	70.80	-0.25	769.04	1.13	7.45	70.57	-0.21	1.21	919.87	801.49
	4	1.71	0.24	1.19	18.83	1.07	9.18	71.22	-0.23	767.76	1.07	10.41	71.15	-0.17	1.18	911.57	835.20
	5	1.75	0.23	1.18	20.38	1.05	8.77	71.86	-0.21	763.20	1.05	10.53	71.95	-0.17	1.15	907.14	828.04
	6	1.74	0.25	1.19	19.28	1.08	8.50	71.33	-0.23	773.86	1.08	11.29	71.22	-0.17	1.19	911.96	845.55
	7	1.71	0.23	1.19	19.21	1.05	9.23	71.42	-0.22	760.13	1.05	13.34	71.34	-0.15	1.16	909.82	841.46
	8	1.74	0.24	1.19	17.92	1.08	9.46	71.21	-0.22	749.92	1.07	4.83	71.11	-0.19	1.16	913.99	775.85
Fast	1	2.13	0.36	1.18	23.76	1.20	9.04	72.90	-0.24	828.01	1.19	11.92	73.11	-0.23	1.27	921.50	882.10
	2	2.16	0.37	1.18	23.93	1.21	8.44	73.04	-0.25	831.40	1.22	5.53	72.30	-0.35	1.41	923.24	840.64
	3	2.14	0.39	1.18	24.10	1.23	9.26	72.66	-0.25	853.99	1.22	7.92	72.73	-0.23	1.31	923.80	879.99
	4	2.14	0.39	1.18	25.63	1.23	9.05	72.70	-0.24	875.94	1.23	6.61	72.58	-0.20	1.33	922.39	899.04
	5	2.14	0.39	1.18	26.07	1.23	9.72	72.81	-0.24	890.37	1.23	4.37	71.88	-0.37	1.48	921.77	883.29
	6	2.11	0.39	1.18	25.33	1.23	8.70	72.61	-0.23	874.02	1.24	9.29	72.37	-0.20	1.33	922.74	930.97
	7	2.10	0.35	1.18	25.81	1.20	8.09	72.92	-0.22	846.22	1.19	8.90	73.05	-0.21	1.28	918.00	896.49
	8	2.13	0.38	1.18	24.02	1.22	9.37	72.70	-0.25	849.96	1.21	7.97	72.62	-0.22	1.30	923.15	873.90

Table A.6 – Calibrated DBIP models' parameters targeting step frequency f_s and DLF₁ pair for TS3.

Walk	Cross	Target		Experin	nental	BM1					BM2						
Scenario		f_s	DLF_1	L_p	k_{leg}	v	ξ	$ heta_0$	ż(0)	Max. Force	ν	ξ	$ heta_0$	$\dot{z}(0)$	$\dot{x}(0)$	E_0	Max Force
		(Hz)	value	(m)	(kN/m)	(m/s)	(%)	(°)	(m/s)	(N)	(m/s)	(%)	(°)	(m/s)	(m/s)	(J)	(N)
Slow	1	1.58	0.17	1.14	19.70	0.92	9.58	71.96	-0.18	673.32	0.91	5.89	72.23	-0.11	1.06	786.32	790.64
	2	1.63	0.17	1.14	19.08	0.94	8.66	72.01	-0.20	652.53	0.93	4.65	72.05	-0.11	1.05	788.18	732.49
	3	1.57	0.17	1.14	19.46	0.92	8.88	71.77	-0.20	670.66	0.92	9.54	72.14	-0.14	1.06	786.50	799.85
	4	1.64	0.19	1.14	18.97	0.97	9.72	71.77	-0.18	676.95	0.96	12.40	72.00	-0.16	1.08	789.91	763.66
	5	1.60	0.17	1.14	20.00	0.92	9.76	72.12	-0.18	670.00	0.91	12.08	72.40	-0.16	1.04	785.57	778.47
	6	1.61	0.17	1.14	19.71	0.93	8.00	72.02	-0.19	663.26	0.92	7.75	72.26	-0.13	1.06	786.80	769.68
Normal	1	1.84	0.22	1.14	19.02	1.03	9.41	72.30	-0.21	671.35	1.02	7.44	72.34	-0.18	1.11	790.06	701.44
	2	1.82	0.23	1.14	16.90	1.05	8.93	71.56	-0.21	661.98	1.04	4.61	71.52	-0.19	1.12	794.30	682.14
	3*	-	-	-	-	-	-	-	-	-	-	-	-	-	-	-	-
	4	1.85	0.20	1.13	22.31	0.98	8.42	73.21	-0.17	669.82	0.97	9.41	73.27	-0.14	1.07	782.56	727.09
	5	1.89	0.19	1.14	17.12	1.01	9.60	72.47	-0.18	623.65	1.00	11.75	72.64	-0.18	1.07	792.20	656.35
	6	1.87	0.20	1.13	21.78	0.99	8.23	73.20	-0.17	661.05	0.98	10.51	73.26	-0.16	1.07	784.02	722.01
	7	1.82	0.19	1.13	20.98	0.97	8.66	73.08	-0.19	652.85	0.97	13.97	73.11	-0.17	1.06	784.00	723.45
E.	8	1.91	0.20	1.13	20.71	1.00	9.50	73.31	-0.19	649.20	0.99	5.89	73.23	-0.16	1.07	786.63	678.24
Free	1	1.70	0.19	1.14	19.21	0.97	9.48	72.13	-0.20	663.20	0.97	5.84	71.95	-0.14	1.08	786.15	730.47
	2	1.74	0.19	1.15	16.36	0.99	8.73	71.64	-0.20	632.32	0.99	4.93	71.48	-0.17	1.08	793.09	667.58
	3	1.71	0.19	1.14	17.42	0.98	9.37	71.71	-0.21	649.36	0.98	5.57	71.55	-0.15	1.08	790.32	691.46
	4	1.73	0.19	1.14	18.50	0.98	9.58	72.13	-0.20	652.80	0.98	4.63	71.96	-0.15	1.08	788.07	698.41
	5	1.69	0.19	1.14	18.76	0.97	8.22	71.91	-0.18	657.05	0.96	6.21	71.95	-0.14	1.07	786.59	716.55
	6	1.63	0.17	1.14	18.79	0.93	8.58	71.94	-0.20	645.38	0.93	11.19	72.02	-0.16	1.05	784.49	738.65
	7	1.68	0.18	1.14	18.86	0.95	9.93	72.10	-0.20	652.14	0.95	12.04	72.08	-0.16	1.07	785.90	734.52
	8	1.65	0.17	1.14	18.87	0.94	9.39	72.11	-0.20	643.85	0.93	13.13	72.20	-0.17	1.04	784.30	727.65
Fast	1	2.16	0.28	1.12	30.37	1.08	8.87	74.51	-0.17	772.17	1.08	12.14	74.62	-0.16	1.18	788.80	848.52
	2	2.18	0.28	1.12	28.12	1.10	8.22	74.30	-0.18	739.02	1.09	11.52	74.36	-0.15	1.17	791.35	792.73
	3	2.21	0.26	1.12	30.93	1.06	8.90	75.04	-0.15	735.10	1.06	6.15	75.01	-0.13	1.14	786.62	769.10
	4	2.22	0.26	1.12	31.96	1.06	8.12	75.18	-0.16	737.94	1.06	11.95	75.24	-0.15	1.15	785.94	816.45
	5	2.20	0.28	1.12	31.36	1.09	9.55	74.79	-0.17	776.10	1.08	8.42	74.79	-0.12	1.17	787.80	821.95
	6	2.22	0.24	1.12	32.84	1.03	8.85	75.44	-0.14	729.35	1.03	13.05	75.56	-0.12	1.11	782.72	799.53
	7	2.19	0.25	1.12	31.27	1.05	9.45	75.11	-0.17	741.11	1.05	11.51	75.17	-0.15	1.13	785.70	806.37
	8	2.19	0.26	1.12	28.33	1.06	8.22	74.79	-0.18	710.39	1.06	13.32	74.84	-0.16	1.14	789.28	775.56

^{*} No valid footfall forces detected to extract the models' parameters

APPENDIX B

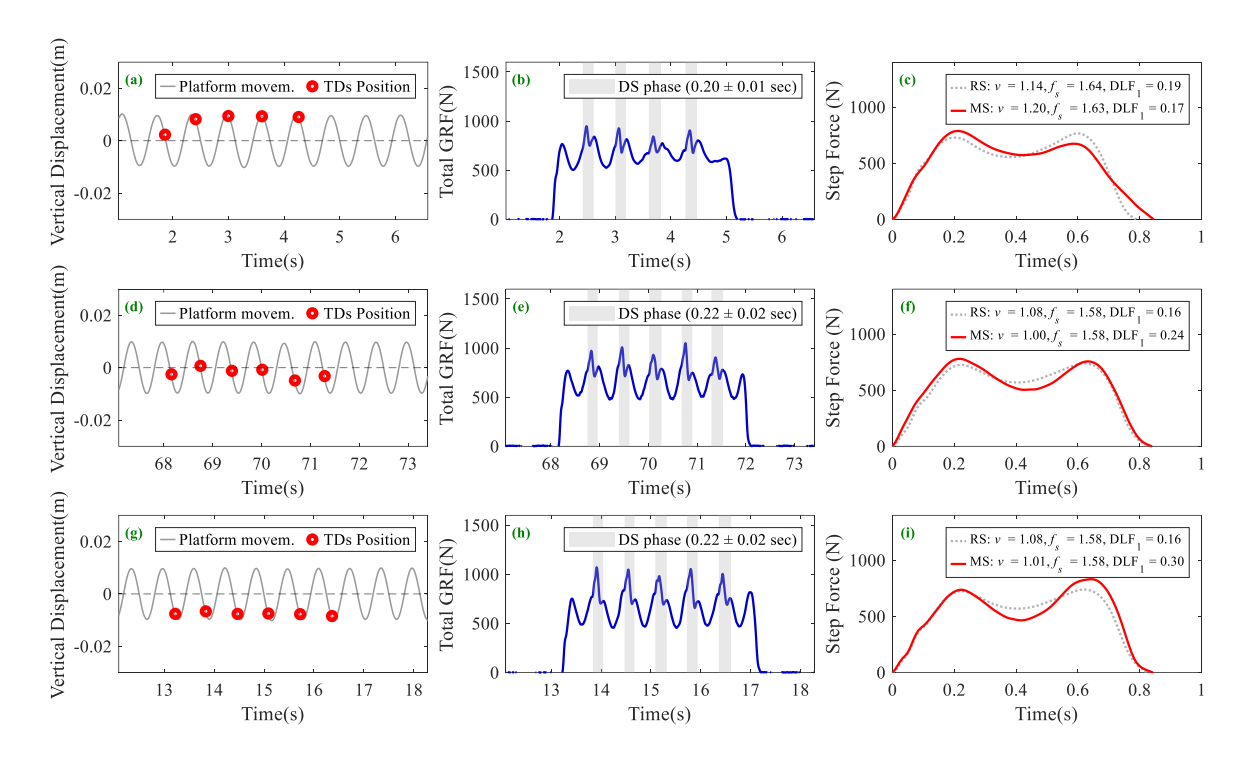


Figure B.1 - TD vertical positions at the platform, GRFs and single footfall force for TS1, slow walking, moving surface scenario (frequency of 1.6Hz and 1.0m/s²): (a), (b) and (c) phase case 2; (d), (e) and (f) phase case 3; and (g), (h) and (i) phase case 4.

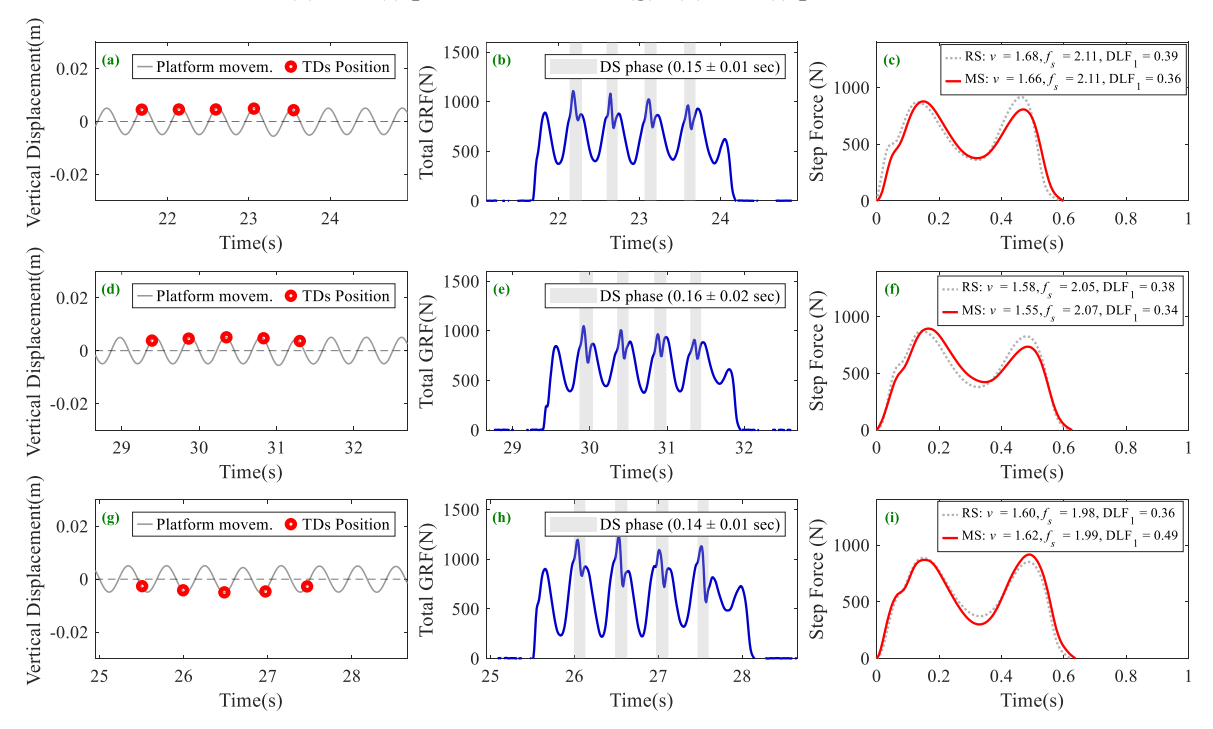


Figure B.2 – TD vertical positions at the platform, GRFs and single footfall force for TS1, fast walking, moving surface scenario (frequency of 2.2Hz and 1.0m/s²): (a), (b) and (c) phase case 2; (d), (e) and (f) phase case 2; and (g), (h) and (i) phase case 4.

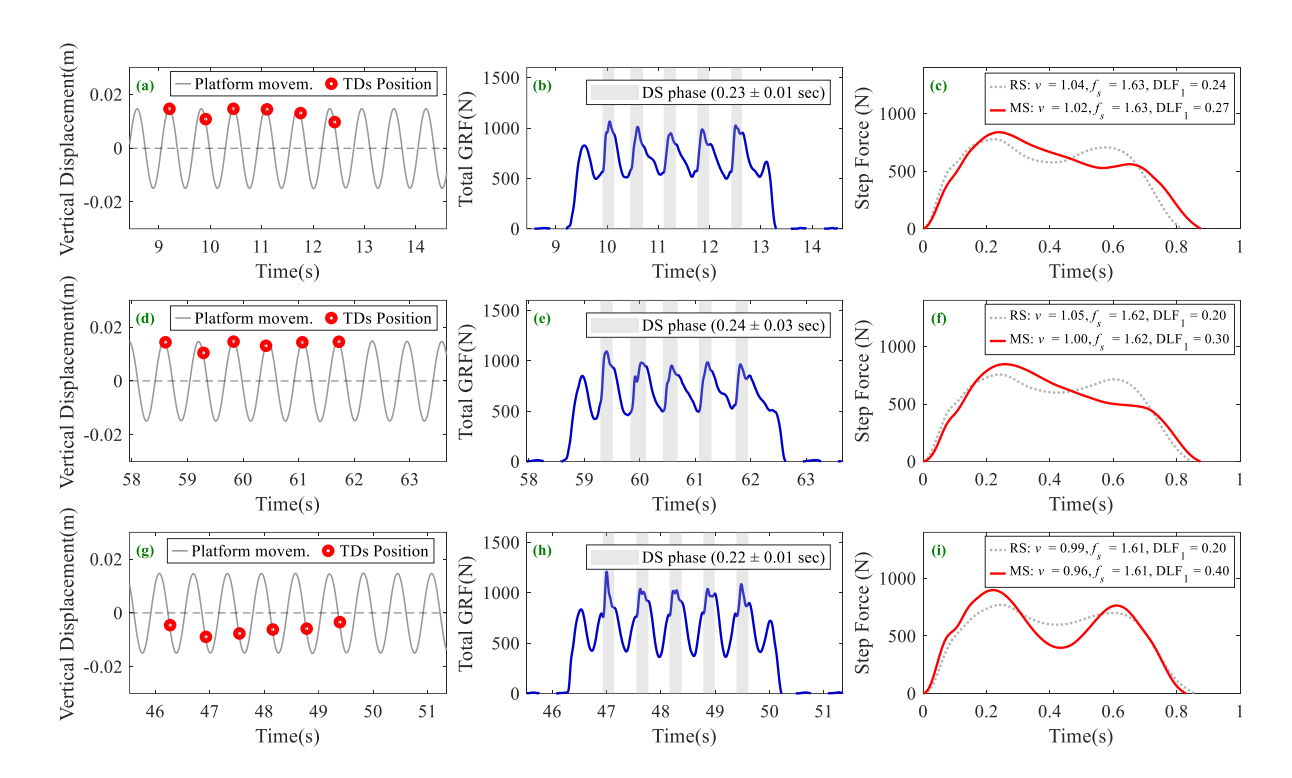


Figure B.3 – TD vertical positions at the platform, GRFs and single footfall force for TS2, slow walking, moving surface scenario (frequency of 1.6Hz and 1.5m/s²): (a), (b) and (c) phase case 2; (d), (e) and (f) phase case 2; and (g), (h) and (i) intermediate phase case.

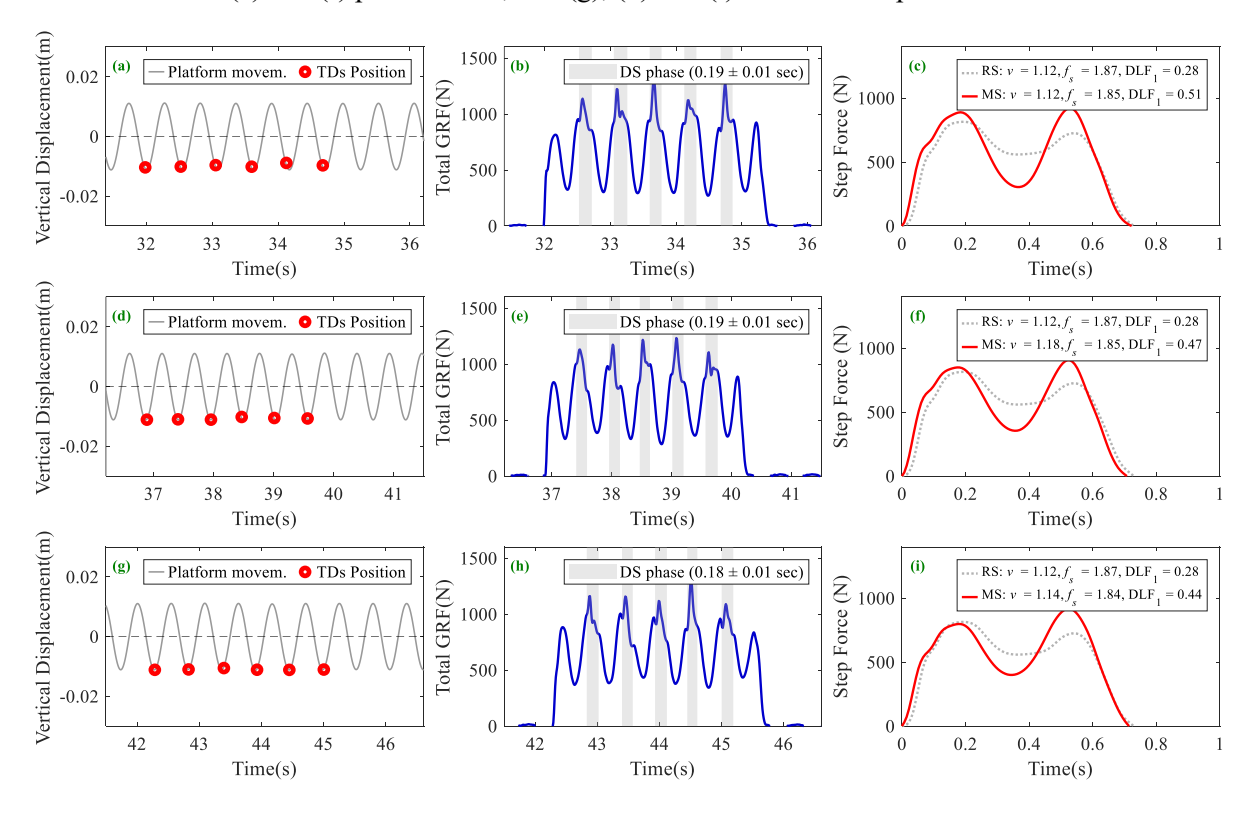


Figure B.4 – TD vertical positions at the platform, GRFs and single footfall force for TS2, normal walking, moving surface scenario (frequency of 1.85Hz and 1.5m/s²): (a), (b) and (c) phase case 4; (d), (e) and (f) phase case 4; and (g), (h) and (i) phase case 4.

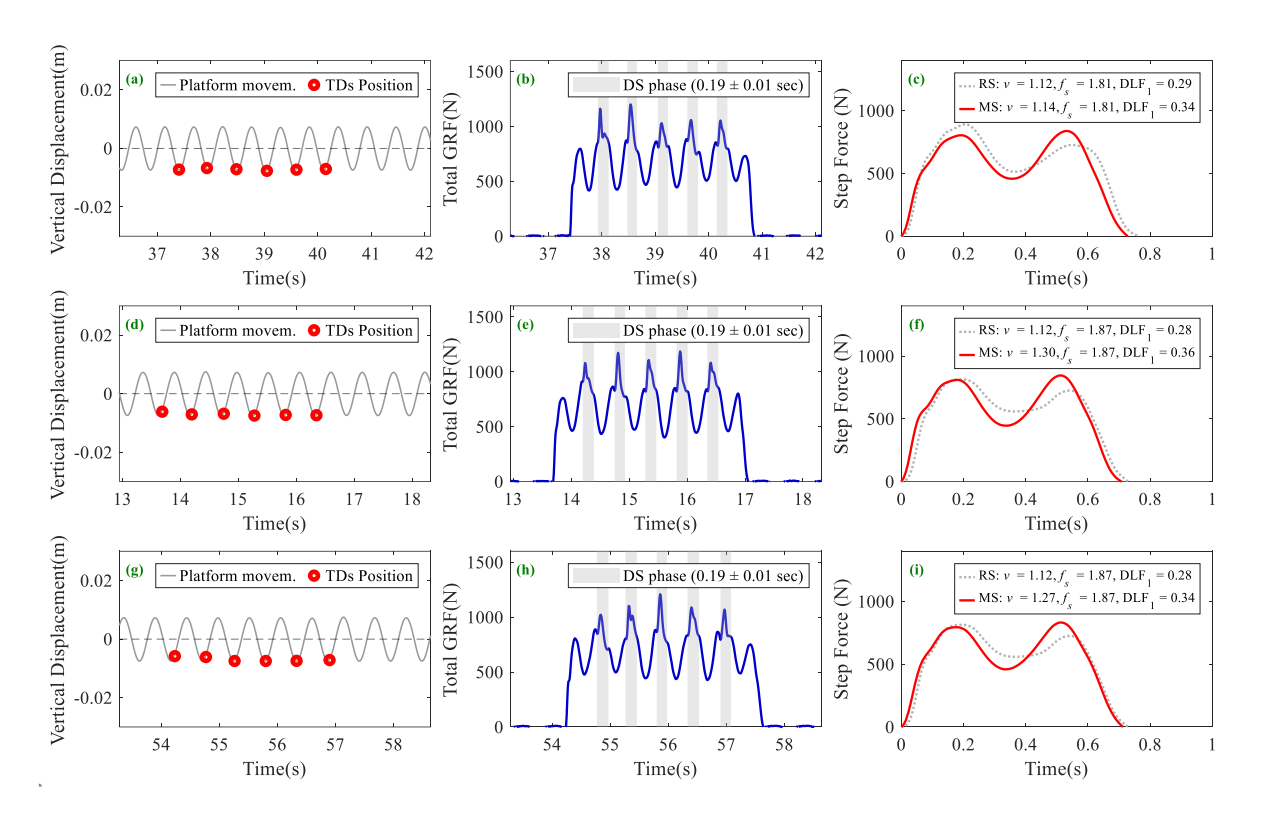


Figure B.5 – TD vertical positions at the platform, GRFs and single footfall force for TS2, normal walking, moving surface scenario (frequency of 1.85Hz and 1.0m/s²): (a), (b) and (c) phase case 4; (d), (e) and (f) phase case 4; and (g), (h) and (i) phase case 4.

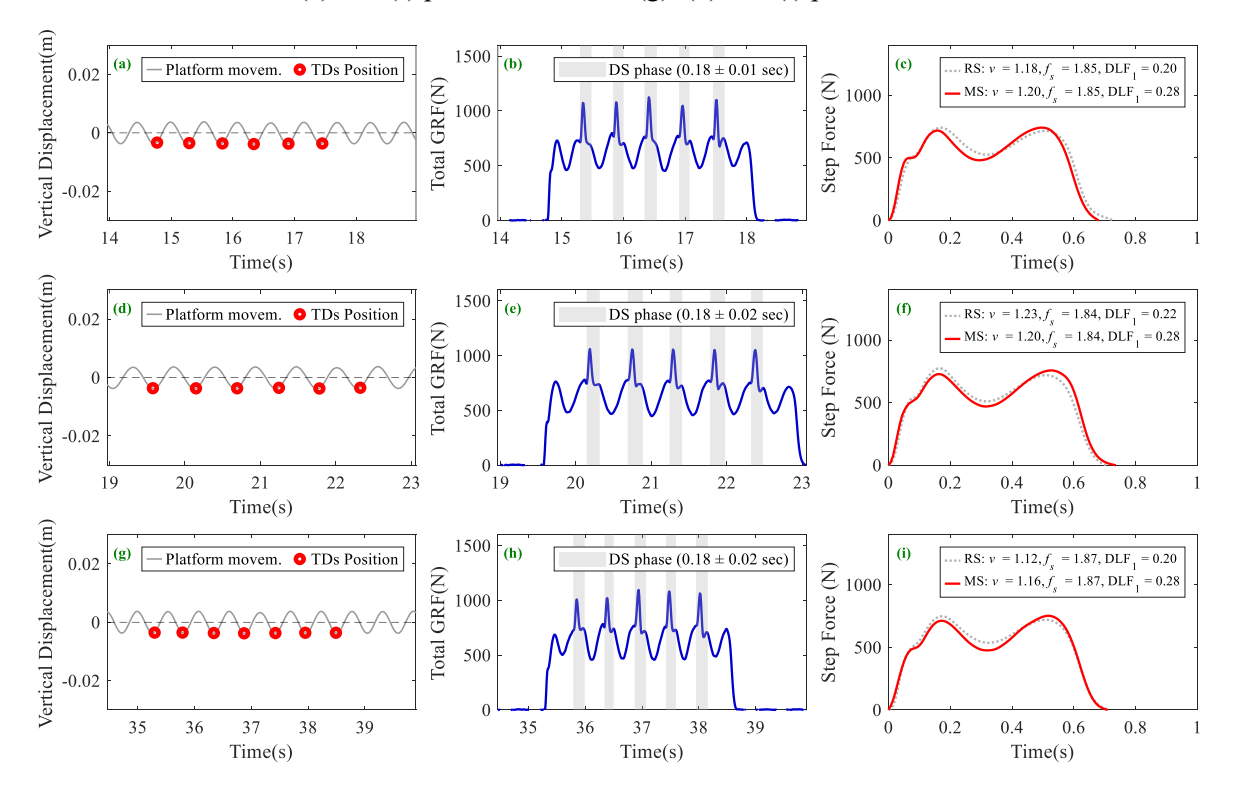


Figure B.6 – TD vertical positions at the platform, GRFs and single footfall force for TS3, normal walking, moving surface scenario (frequency of 1.85Hz and 0.5m/s²): (a), (b) and (c) phase case 4; (d), (e) and (f) phase case 4; and (g), (h) and (i) phase case 4.

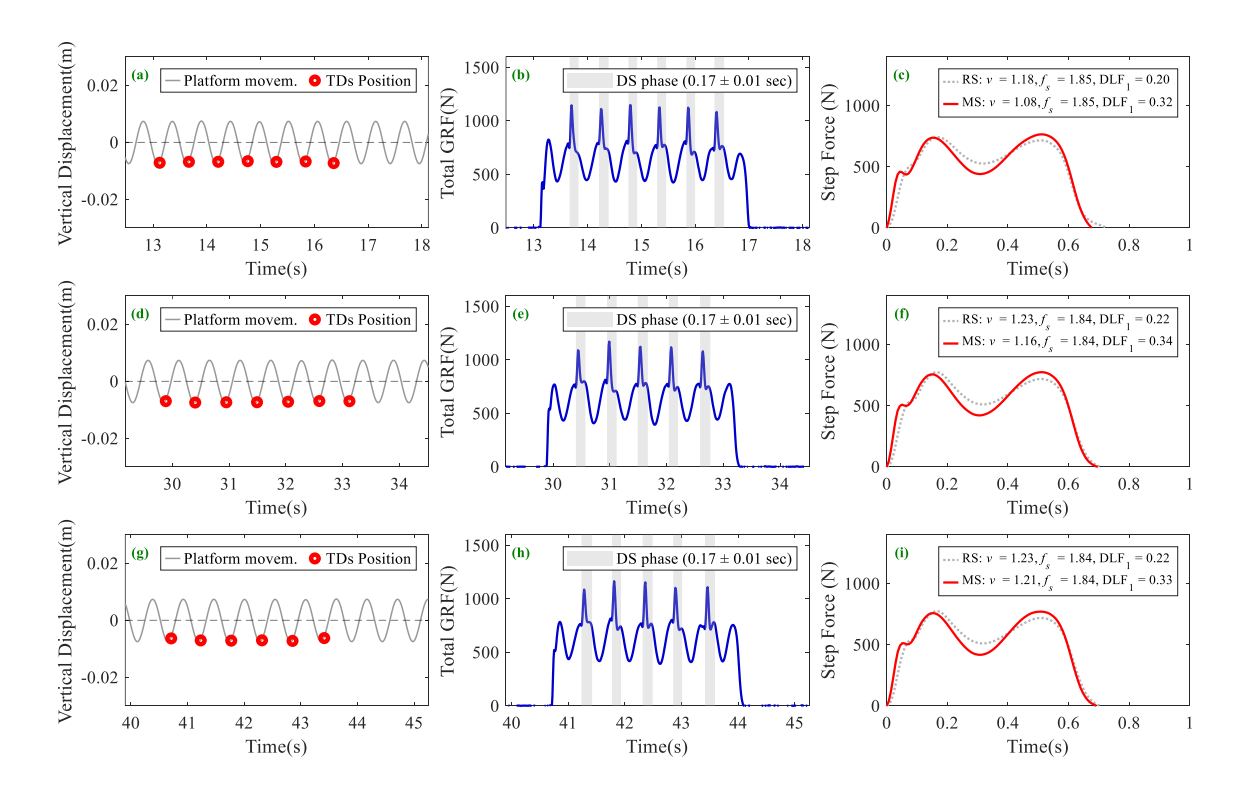


Figure B.7 – TD vertical positions at the platform, GRFs and single footfall force for TS3, normal walking, moving surface scenario (frequency of 1.85Hz and 1.0m/s²): (a), (b) and (c) phase case 4; (d), (e) and (f) phase case 4; and (g), (h) and (i) phase case 4.

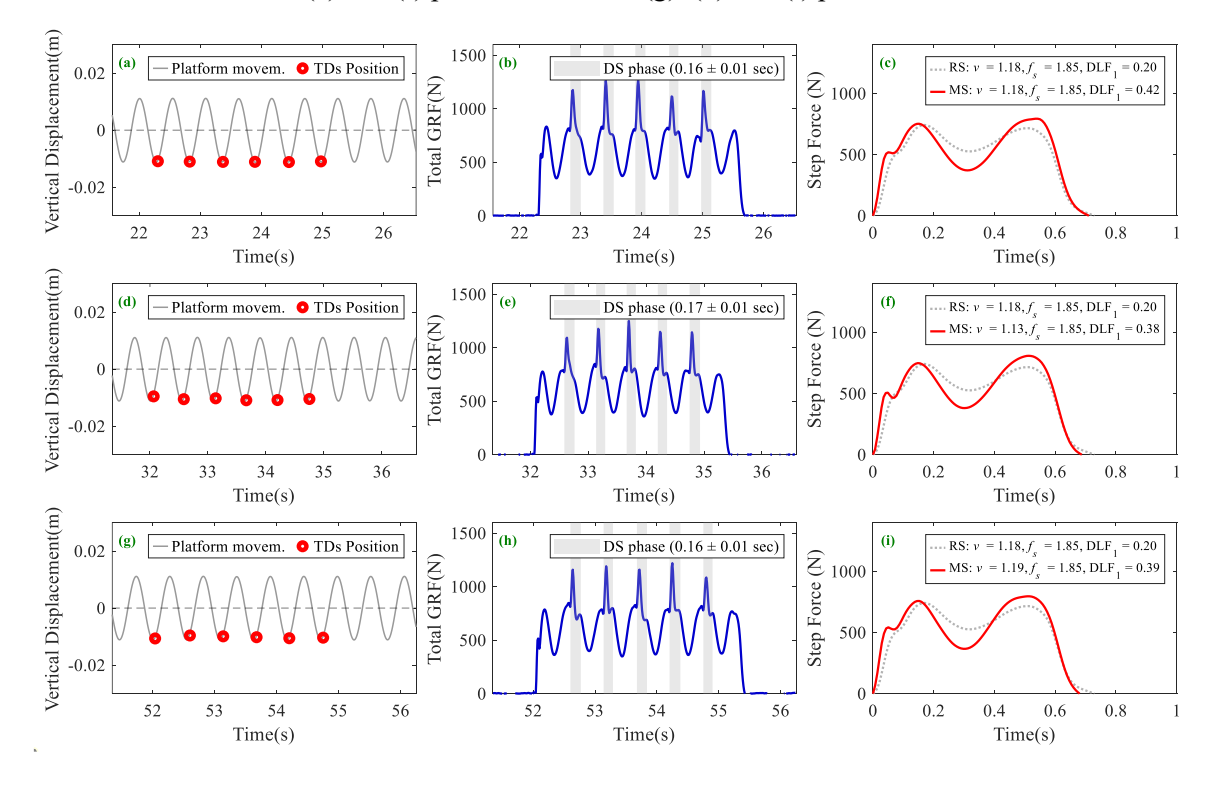


Figure B.8 – TD vertical positions at the platform, GRFs and single footfall force for TS3, normal walking, moving surface scenario (frequency of 1.85Hz and 1.5m/s²): (a), (b) and (c) phase case 4; (d), (e) and (f) phase case 4; and (g), (h) and (i) phase case 4.